



저작자표시-비영리-변경금지 2.0 대한민국

이용자는 아래의 조건을 따르는 경우에 한하여 자유롭게

- 이 저작물을 복제, 배포, 전송, 전시, 공연 및 방송할 수 있습니다.

다음과 같은 조건을 따라야 합니다:



저작자표시. 귀하는 원저작자를 표시하여야 합니다.



비영리. 귀하는 이 저작물을 영리 목적으로 이용할 수 없습니다.



변경금지. 귀하는 이 저작물을 개작, 변형 또는 가공할 수 없습니다.

- 귀하는, 이 저작물의 재이용이나 배포의 경우, 이 저작물에 적용된 이용허락조건을 명확하게 나타내어야 합니다.
- 저작권자로부터 별도의 허가를 받으면 이러한 조건들은 적용되지 않습니다.

저작권법에 따른 이용자의 권리는 위의 내용에 의하여 영향을 받지 않습니다.

이것은 [이용허락규약\(Legal Code\)](#)을 이해하기 쉽게 요약한 것입니다.

[Disclaimer](#)

A Thesis for the Degree of Doctor of Philosophy

**Assessment and Optimal Management  
of Surface Water Resources in the  
Source of Upper Blue Nile River under  
Development and Climate Change  
Scenarios**

개발과 기후변화 시나리오에 따른  
블루나일강 상류의 지표수 영향 평가  
및 최적 관리 방안 도출

By

**Getachew Tegegne Damtew**

**February 2017**

**Graduate School of Seoul National University**

**Department of Civil and Environmental Engineering**



# **Assessment and Optimal Management of Surface Water Resources in the Source of Upper Blue Nile River under Development and Climate Change Scenarios**

Advisor: Professor Kim, Young-Oh

A dissertation submitted in partial fulfillment of the requirement  
for the Degree of Doctor of Philosophy

December 2016

**Graduate School of Seoul National University**  
**Department of Civil and Environmental Engineering**  
**Getachew Tegegne Damtew**

December 2016

## **Supervisory Committee:**

Chairman: \_\_\_\_\_

Vice Chairman: \_\_\_\_\_

Member: \_\_\_\_\_

Member: \_\_\_\_\_

Member: \_\_\_\_\_

## **Abstract**

# **Assessment and Optimal Management of Surface Water Resources in the Source of Upper Blue Nile River under Development and Climate Change Scenarios**

By

Getachew Tegegne Damtew

Department of Civil and Environmental Engineering

College of Engineering

Graduate School of Seoul National University

Advisor: Professor Kim, Young-Oh

The objective of this study focuses on the assessment and management of surface water resources of Lake Tana Basin under development and climate change scenarios. Good hydrologic models are needed to manage water resources of the Lake Tana Basin, but model comparison studies have not been carried out for this area. In this study, the daily streamflows were simulated by applying two simple conceptual models and one physically-based, semi-distributed model for four major gauged catchments of the study area and compared their performances in both time and quantile domains. The best model in the time-domain can be applied for management and real-time operation, whereas the best model in the quantile-domain can be implemented for planning and climate change impact assessment. The calibrated parameters of the selected hydrological model were then

transposed to the ungauged catchments by using the arithmetic mean, the physical similarity, the spatial proximity, and the catchment runoff-response similarity approaches. The catchment runoff-response similarity approach proposed by this study performed best for estimation of the surface water resources in the ungauged catchments. Furthermore, understanding the hydrological processes under changing climate is also crucial for future water resources planning and management in the study area, and thus this study inputted the three Representative Concentration Pathways (i.e. RCP 2.6, RCP 4.5, and RCP 8.5) to the selected hydrologic model with an appropriate statistical downscaling procedure. Lastly, this study developed an optimization model with a multi-objective genetic algorithm for optimally allocating the surface water resources to ongoing and planned water resources projects in the Lake Tana Basin. The model resulted in releases of more than 90% of the irrigation and hydropower demands for all baseline and future inflow scenarios. The optimization result also revealed that the Lake Tana water levels exceed the minimum Lake level (i.e. 1785 m) that required for navigation under all climate change scenarios.

Keywords: Climate Change, Lake Tana Basin, Reservoir Operation,  
Ungauged Catchment Modeling, Water Resources Assessment

Student Number: 2013-31302

# Table of Contents

ABSTRACT .....	I
LIST OF FIGURES .....	VII
LIST OF TABLES .....	XII
LIST OF SYMBOLS .....	XV
<b>CHAPTER ONE .....</b>	<b>1</b>
1. INTRODUCTION .....	1
<i>1.1. Problem Statement</i> .....	<i>1</i>
<i>1.2. Research Objectives</i> .....	<i>3</i>
<i>1.3. Research Procedures</i> .....	<i>3</i>
<i>1.4. Outline</i> .....	<i>6</i>
<b>CHAPTER TWO .....</b>	<b>7</b>
2. DATA AND STUDY AREA DESCRIPTION .....	7
<i>2.1. Location</i> .....	<i>7</i>
<i>2.2. Topography</i> .....	<i>9</i>
<i>2.3. Climate and Hydrology</i> .....	<i>11</i>
<i>2.4. Land Use and Soil Use</i> .....	<i>14</i>
<i>2.5. Water Resource Development</i> .....	<i>18</i>
<b>CHAPTER THREE .....</b>	<b>21</b>
3. LITERATURE REVIEW .....	21

3.1. <i>Previous Studies for the Lake Tana Basin</i> .....	21
3.2. <i>Hydrological Models for the Lake Tana Basin</i> .....	25
3.3. <i>Climate Change Impact Assessment</i> .....	51
3.4. <i>Multi-objective Optimization of the Multi-reservoir System</i> .....	61
<b>CHAPTER FOUR</b> .....	<b>66</b>
4. SELECTION OF HYDROLOGIC MODELING APPROACHES FOR ASSESSMENT OF WATER RESOURCES IN THE LAKE TANA BASIN .....	66
4.1. <i>Introduction</i> .....	67
4.2. <i>Methodology</i> .....	69
4.3. <i>Application</i> .....	83
4.4. <i>Conclusions</i> .....	106
<b>CHAPTER FIVE</b> .....	<b>109</b>
5. SURFACE WATER RESOURCES ASSESSMENT IN THE UNGAUGED CATCHMENTS OF LAKE TANA BASIN.....	109
5.1. <i>Introduction</i> .....	110
5.2. <i>Methodology</i> .....	119
5.3. <i>Application</i> .....	123
5.4. <i>Conclusions</i> .....	137
<b>CHAPTER SIX</b> .....	<b>139</b>
6. POTENTIAL IMPACTS OF CLIMATE CHANGE ON THE WATER BALANCE COMPONENTS OF THE LAKE TANA BASIN.....	139

6.1. <i>Introduction</i> .....	140
6.2. <i>Methodology</i> .....	144
6.3. <i>Application</i> .....	153
6.4. <i>Conclusions</i> .....	174
<b>CHAPTER SEVEN</b> .....	<b>177</b>
7. REFLECTING UNCERTAINTY IN THE DEVELOPMENT OF A RESERVOIR OPERATION RULE WITH GENETIC PROGRAMMING .....	177
7.1. <i>Introduction</i> .....	178
7.2. <i>Methodology</i> .....	180
7.3. <i>Application</i> .....	196
7.4. <i>Conclusions</i> .....	212
<b>CHAPTER EIGHT</b> .....	<b>213</b>
8. CONCLUSIONS AND FUTURE STUDY .....	213
8.1. <i>Conclusions</i> .....	213
8.2. <i>Future Study</i> .....	216
REFERENCES .....	217
APPENDICES .....	252
Appendix A. <i>Hydrological Models</i> .....	252
Appendix B. <i>List of Figures</i> .....	275
Appendix C. <i>List of Tables</i> .....	282
ABSTRACT IN KOREAN .....	287



## List of Figures

<i>Figure 1.1. General framework of the study .....</i>	<i>5</i>
<i>Figure 2.1. Location map of the LTB .....</i>	<i>8</i>
<i>Figure 2.2. Map showing elevation of the LTB .....</i>	<i>10</i>
<i>Figure 2.3. Monthly average of maximum temperature for the LTB .....</i>	<i>12</i>
<i>Figure 2.4. Monthly average of minimum temperature for the LTB .....</i>	<i>12</i>
<i>Figure 2.5. Monthly average rainfall in the LTB .....</i>	<i>13</i>
<i>Figure 2.6. Land use classification of the LTB.....</i>	<i>15</i>
<i>Figure 2.7. Soil use classification of the LTB.....</i>	<i>17</i>
<i>Figure 2.8. Existed &amp; proposed irrigation and hydropower projects in the LTB .....</i>	<i>19</i>
<i>Figure 3.1. Schematic representation of the hydrological cycle used in SWAT model .....</i>	<i>36</i>
<i>Figure 3.2. Conceptual layout of the IHACRES-CMD model.....</i>	<i>36</i>
<i>Figure 3.3. Schematic diagram of the GR4J rainfall-runoff model .....</i>	<i>37</i>
<i>Figure 3.4. The general procedure for the assessment of the climate change impact on the water resources of the LTB.....</i>	<i>59</i>
<i>Figure 3.5. Flowchart of the multiobjective genetic algorithm.....</i>	<i>65</i>
<i>Figure 4.1. Schematic diagram of the artificial neural network.....</i>	<i>82</i>
<i>Figure 4.2. The most sensitive parameters distribution for each watershed. The red dots represents the optimal values of the objective function (NSE). .....</i>	<i>86</i>

<i>Figure 4.3. Observed flow, best-simulated flow, and the 95% uncertainty interval.....</i>	<i>88</i>
<i>Figure 4.4. The average performance values of all folds for the simple conceptual models for each watershed.....</i>	<i>91</i>
<i>Figure 4.5. Box plots of model performance variation of all three models for all watersheds for the four folds. ....</i>	<i>95</i>
<i>Figure 4.6. Flow duration curve for each flow category .....</i>	<i>98</i>
<i>Figure 4.7. Performance of models in each watersheds .....</i>	<i>105</i>
<i>Figure 5.1. Thiessen polygon for the estimation of areal rainfall in the Lake Tana .....</i>	<i>122</i>
<i>Figure 5.2. Elevation-volume and area-volume relationship of the Lake Tana .....</i>	<i>122</i>
<i>Figure 5.3. Map shows the clustered of similar units based on a) spatial proximity approach and b) catchment runoff-response similarity approach .....</i>	<i>129</i>
<i>Figure 5.4. Simulation of the Lake Tana water level .....</i>	<i>132</i>
<i>Figure 5.5. The Monthly average Lake Tana Water level (1995-2012).....</i>	<i>132</i>
<i>Figure 5.6. Total surface water inflow hydrograph into the Lake Tana....</i>	<i>135</i>
<i>Figure 5.7. Monthly water balance components of the Lake Tana (1995-2008).....</i>	<i>135</i>
<i>Figure 5.8. Average annual simulated water balance for the baseline scenario (1995-2012) .....</i>	<i>136</i>

<i>Figure 6.1. The percent error reduction in bias-corrected precipitation in relative to the raw downscaled precipitation .....</i>	<i>157</i>
<i>Figure 6.2. The boxplot of observed, modeled, and bias-corrected precipitation. (In each station (shown in the box), from left to right shows the observed, modeled, bias-corrected in quantile domain, and bias-corrected in the time domain, respectively).....</i>	<i>158</i>
<i>Figure 6.3. Future changes in annual precipitation after bias correction at Bahirdar weather station.....</i>	<i>162</i>
<i>Figure 6.4. Comparison of future changes in temperature in relative to the baseline.....</i>	<i>166</i>
<i>Figure 6.5. Time series plot of a 6-month standard precipitation index in Bahirdar weather station under RCP2.6, RCP4.5, and RCP8.5.....</i>	<i>166</i>
<i>Figure 6.6. Frequency of time (%) in each dry or wet category of SPI-6 in all weather stations for the period of 2006–2100.....</i>	<i>168</i>
<i>Figure 6.7. Mean annual inflow into the Lake Tana by using the bias-corrected precipitation in time-domain.....</i>	<i>169</i>
<i>Figure 6.8. Mean annual inflow into the Lake Tana by using the bias-corrected precipitation in quantile-domain.....</i>	<i>169</i>
<i>Figure 6.9. Monthly water balance components of the Lake Tana for future scenario .....</i>	<i>172</i>
<i>Figure 6.10. Average annual simulated water balance components for the future scenario under RCP2.6 in time-domain (2011-2100).....</i>	<i>172</i>

*Figure 6.11. Average annual simulated water balance components for the future scenario under RCP4.5 in time-domain (2011-2100).....173*

*Figure 6.12. Average annual simulated water balance components for the future scenario under RCP8.5 in time-domain (2011-2100).....173*

*Figure 7.1. Schematic diagram of the Lake Tana Basin’s reservoir model configuration .....182*

*Figure 7.2. Elevation-Area & Elevation-Volume relationship of the Lake Tana reservoir .....182*

*Figure 7.3. Method of reflecting the uncertainty of inflows in the reservoir operating rule where  $I_i(t)$  is the reservoir inflow,  $R_i(t)$  is the reservoir release, and  $S_i(t)$  is the reservoir active storage .....189*

*Figure 7.4. Monthly inflow, areal rainfall, and evaporation of the Lake Tana for the four clustered scenarios. (C1: cluster-I, C2: cluster-II, C3: cluster-III, and C4: cluster-IV).....189*

*Figure 7.5. Autocorrelation function (acf) of the monthly inflow to the Lake Tana. The dotted horizontal line indicates a confidence interval for the acf value.....194*

*Figure 7.6. Pareto front, where the goal is to maximize both objectives: objective-I (irrigation) and objective-II (hydropower). .....200*

*Figure 7.7. Reservoir release policies for each irrigation projects .....203*

*Figure 7.8. Reservoir release policies for Tana-Beles hydropower project .....203*

<i>Figure 7.9. Individual reservoir storage curve under optimal reservoir policy .....</i>	<i>204</i>
<i>Figure 7.10. Volumetric reliability (%) of water resources projects in the LTB .....</i>	<i>204</i>
<i>Figure 7.11. Monthly inflow series into the Lake Tana.....</i>	<i>206</i>
<i>Figure 7.12. Plot of the forecasted inflow, actual inflow, 80% and 95% confidence interval .....</i>	<i>206</i>
<i>Figure 7.13. Plot of model residual.....</i>	<i>206</i>
<i>Figure 7.14. Autocorrelation function of the forecasting model.....</i>	<i>209</i>
<i>Figure 7.15. Correlation matrix between the possible reservoir releases .</i>	<i>209</i>
<i>Figure 7.16. The monthly Lake level for the baseline scenario .....</i>	<i>210</i>
<i>Figure 7.17. The monthly Lake level for future inflow scenarios.....</i>	<i>210</i>
<i>Figure 7.18. Downstream release from the basin for future inflow scenarios under climate change.....</i>	<i>211</i>

## List of Tables

<i>Table 2.1. Land use classification of the LTB</i> .....	16
<i>Table 2.2. Major soil types of the LTB</i> .....	16
<i>Table 2.3. Water resource projects in the study basin (Source: MoFED, 2006)</i> .....	20
<i>Table 3.1. Hydrological models selected for review</i> .....	30
<i>Table 3.2. Description and ranges of the rainfall-runoff model's parameters</i> .....	38
<i>Table 3.3. Model performance indicators for each model comparison criterion</i> .....	50
<i>Table 3.4. Advantages, disadvantages, and requirements of dynamical and statistical downscaling</i> .....	60
<i>Table 4.1. Description of the key flow parameters for the SWAT model</i> .....	75
<i>Table 4.2. Model comparison methods</i> .....	75
<i>Table 4.3. SWAT model flow parameter t-statistics and P-values</i> .....	85
<i>Table 4.4. NSE values of the SWAT model for the calibration and validation periods</i> .....	85
<i>Table 4.5. Average performance measure values of all folds for each model</i> .....	94
<i>Table 4.6. The performance of the three models for the estimation of 7Q10 low flow</i> .....	101

<i>Table 4.7. Trend statistics of the annual maximum simulated and observed discharges.....</i>	<i>101</i>
<i>Table 4.8. Performance of models in reproducing the amounts of annual maximum flow.....</i>	<i>102</i>
<i>Table 4.9. Correlations between model errors.....</i>	<i>104</i>
<i>Table 4.10. The performance of ANN model in the training, validation &amp; test dataset.....</i>	<i>104</i>
<i>Table 5.1. Catchment attributes used in physical similarity .....</i>	<i>126</i>
<i>Table 5.2. Physically similar hydrologic response units.....</i>	<i>127</i>
<i>Table 5.3. Performance measure of the Lake Tana water level simulations .....</i>	<i>131</i>
<i>Table 5.4. Monthly water balance components of the Lake Tana (1995-2008).....</i>	<i>134</i>
<i>Table 5.5. Comparison of this study result with the previous studies findings .....</i>	<i>134</i>
<i>Table 6.1. Description of predictor variables .....</i>	<i>147</i>
<i>Table 6.2. Standard Precipitation Index (SPI) classification.....</i>	<i>152</i>
<i>Table 6.3. % increase in mean annual bias-corrected precipitation in quantile and time domain in relative to the precipitation in the baseline period.....</i>	<i>161</i>
<i>Table 6.4. Mann-Kendall trend test and Sen’s nonparametric trend slope</i>	<i>163</i>
<i>Table 6.5. <math>\Delta^{\circ}\text{C}</math> in future mean temperature in relative to the baseline .....</i>	<i>163</i>

<i>Table 6.6. Water balance components of the Lake Tana under climate change.....</i>	<i>170</i>
<i>Table 6.7. Mann-Kendall trend test.....</i>	<i>170</i>
<i>Table 7.1. Planned irrigation development in the Lake Tana Basin (Source: BCEOM 1998).....</i>	<i>183</i>
<i>Table 7.2. Recommended flow over the Tis Issat Falls from the Chara-Chara Weir (Source: Bellier et al., 1997).....</i>	<i>183</i>
<i>Table 7.3. Coefficient values of the regression equation with their performance for the baseline inflow scenarios.....</i>	<i>208</i>
<i>Table 7.4. Performance indices of the reservoir release rule for each cluster .....</i>	<i>208</i>
<i>Table 7.5. Correlation coefficients between the possible pairs of release.</i>	<i>208</i>
<i>Table 7.6. Coefficient values &amp; performance of the regression equation for the future inflow scenarios .....</i>	<i>208</i>

## List of Symbols

### *Latin Uppercase*

$B$	<i>Backward shift operator</i>
$D$	<i>Order of seasonal differencing</i>
$D_{n,t}$	<i>Required demand for each irrigation site at period <math>t</math></i>
$DR_{n,t}^{\min}$	<i>Minimum flow required by downstream users</i>
$DR_{n,t}$	<i>Downstream release from reservoir <math>n</math> during period <math>t</math></i>
$D_{g,t}$	<i>Required demand to generate hydropower during period <math>t</math></i>
$E_{n,t}$	<i>Evaporation losses from reservoir <math>n</math> during period <math>t</math></i>
$I_{n,t}$	<i>Inflow to reservoir <math>n</math> at period <math>t</math></i>
$L$	<i>Maximum value of the likelihood function</i>
$O_i$	<i>Measured value</i>
$\bar{O}$	<i>Average measured value</i>
$O_{n,t}$	<i>Overflow from reservoir <math>n</math> during period <math>t</math></i>
$P$	<i>Order of seasonal autoregressive term</i>
$\bar{P}_{BSIM}$	<i>Mean of downscaled daily time series of precipitation</i>
$P_{cor}$	<i>Corrected (de-biased) future daily time series of precipitation</i>
$P_{FSIM}$	<i>Downscaled daily time series of precipitation</i>
$P_i$	<i>Simulated value</i>

$P_{n,t}$	<i>Areal rainfall in each reservoir</i>
$P$ -value	<i>Probability of obtaining an effect at least as extreme as the one in your sample data, assuming the truth of the null hypothesis</i>
$Q$	<i>Order of seasonal moving average term</i>
$Q_{LB}$	<i>Ljung-Box test statistic</i>
$\bar{P}_{OBS}$	<i>Long -term mean monthly observed values of precipitation</i>
$R_{n,t}$	<i>Irrigation release for each demand site at period <math>t</math></i>
$R_{8,t}$	<i>Release for hydropower at time <math>t</math></i>
$R_{9,t}$	<i>Downstream release from Lake Tana reservoir</i>
$S_{n,t}$	<i>Initial storage volumes of reservoir <math>n</math> at period <math>t</math></i>
$S_{n,(t+1)}$	<i>Initial storage volumes of reservoir <math>n</math> at period <math>t+1</math></i>
$S_n^{min}$	<i>Minimum active storage of reservoir <math>n</math></i>
$S_n^{max}$	<i>Maximum active storage of reservoir <math>n</math></i>
$\bar{T}_{BSIM}$	<i>Mean of downscaled daily time series of temperature</i>
$T_{cor}$	<i>Corrected (de-biased) future daily time series of temperature</i>
$T_{FSIM}$	<i>Downscaled daily time series of temperature</i>
$\bar{T}_{OBS}$	<i>Long -term mean monthly observed values of temperature</i>

$V_d$	<i>Volume of water demanded</i>
$V_{max}$	<i>Maximum vulnerability</i>
$V_s$	<i>Volume of water supplied</i>
$X_1$	<i>Maximum capacity of the production store</i>
$X_2$	<i>Groundwater exchange coefficient</i>
$X_3$	<i>One day ahead maximum capacity of the routing store</i>
$X_4$	<i>Time base of unit hydrograph</i>

***Latin Lowercase***

$d$	<i>Order of nonseasonal differencing</i>
$d$	<i>CMD threshold for producing flow</i>
$e$	<i>Temperature to potential evapotranspiration conversion factor</i>
$f$	<i>CMD stress threshold as a proportion of <math>d</math></i>
$f_{1,i}$	<i>Value of efficient solution in iteration <math>i</math> for objective 1</i>
$f_{2,i}$	<i>Value of efficient solution in iteration <math>i</math> for objective 2</i>
$f_{1,i}^{std}$	<i>Standardized value of efficient solutions in objective 1</i>
$f_{2,i}^{std}$	<i>Standardized value of efficient solutions in objective 2</i>
$f_{1+2,i}^{std}$	<i>Summation of standardized values of efficient solutions in objective 1 &amp; 2</i>
$k$	<i>Number of estimated parameters in the model</i>
$n$	<i>Sample size</i>

$p$	<i>Order of nonseasonal autoregressive term</i>
$q$	<i>Order of nonseasonal moving average term</i>
$r_v$	<i>Volumetric reliability</i>
$S$	<i>Seasonal length</i>
$t$	<i>Time</i>
$v_j$	<i>Maximum irrigation water deficit among all the continuous failure</i>

### ***Greek Uppercase***

$\Phi(B)$	<i>Seasonal autoregressive operator</i>
$\Theta(B)$	<i>Seasonal moving average operator</i>

### ***Greek Lowercase***

$\tau_s$	<i>Time constant for slow flow store</i>
$\tau_q$	<i>Time constant for quick flow store</i>
$v_s$	<i>Fractional volume for slow flow</i>
$\alpha$	<i>Level of Significance</i>
$\phi(B)$	<i>Nonseasonal autoregressive operator</i>
$\theta(B)$	<i>Nonseasonal moving average operator</i>
$\varepsilon_t$	<i>Residuals (white noise series)</i>
$\rho(j)$	<i>Autocorrelation at lag <math>j</math></i>
$\emptyset$	<i>Empty</i>

## ***Abbreviation***

<i>ABS</i>	<i>Absolute of the standardized values</i>
<i>AGRC</i>	<i>Agro-Pastoral Land Use</i>
<i>AGRL</i>	<i>Agricultural Land Use</i>
<i>AIC</i>	<i>Akaike Information Criterion</i>
<i>ALh</i>	<i>Haplic Alisols Soil Use</i>
<i>ALPHA_BF</i>	<i>Base Flow Alfa Factor</i>
<i>ALPHA_BNK</i>	<i>Base flow alpha factor for bank storage</i>
<i>AM</i>	<i>Arithmetic Mean</i>
<i>ARIMA</i>	<i>Autoregressive Integrated Moving Average</i>
<i>AR5</i>	<i>Fifth Assessment Report</i>
<i>BCEOM</i>	<i>Bureau Central d'Etude Pour les Equipements d'Outre Mer (Central Office for the Buildings of Facilities Overseas)</i>
<i>CH_K2</i>	<i>Effective Hydraulic Conductivity in Main Channel Alluvium</i>
<i>CH_N2</i>	<i>Manning's "n" Value for the Main Channel</i>
<i>CMD</i>	<i>Catchment Moisture Deficit</i>
<i>CMe</i>	<i>Eutric Cambisols Soil Use</i>
<i>CMIP5</i>	<i>Coupled Model Intercomparison Project phase 5</i>
<i>CN2</i>	<i>SCS Runoff Curve Number</i>
<i>CRRS</i>	<i>Catchment Runoff-Response Similarity</i>

<i>DEM</i>	<i>Digital Elevation Model</i>
<i>ESCO</i>	<i>Soil Evaporation Compensation Factor</i>
<i>ET</i>	<i>Evapotranspiration</i>
<i>FLe</i>	<i>Eutric Fluvisols Soil Use</i>
<i>FRSD</i>	<i>Agro-Sylvicultural Land Use</i>
<i>FRSE</i>	<i>Sylvicultural Land Use</i>
<i>GAs</i>	<i>Genetic Algorithms</i>
<i>GCM</i>	<i>General Circulation Model</i>
<i>GHG</i>	<i>Greenhouse gas</i>
<i>GUI</i>	<i>Graphical user interface</i>
<i>GR4J</i>	<i>Mode'le du Ge'nie Rural a' 4 Parame'tres Journalier</i>
<i>GW_DELAY</i>	<i>Groundwater delay time</i>
<i>GWQMN</i>	<i>Threshold depth of water in shallow aquifer required for return flow</i>
<i>GW_REVAP</i>	<i>Groundwater "revap" coefficient</i>
<i>HRU</i>	<i>Hydrological Response Unit</i>
<i>IHACRES</i>	<i>Identification of Unit Hydrographs And Component flows from Rainfall, Evaporation, and Streamflow</i>
<i>IPCC</i>	<i>Intergovernmental Panel on Climate Change</i>
<i>LTB</i>	<i>Lake Tana Basin</i>
<i>Lpe</i>	<i>Eutric Leptosols Soil Use</i>
<i>LVh</i>	<i>Haplic Luvisols Soil Use</i>

<i>LVx</i>	<i>Chromic Luvisols Soil Use</i>
<i>Masl</i>	<i>Meters above sea level</i>
<i>MoFED</i>	<i>Ministry of Finance and Economic Development</i>
<i>MOGA</i>	<i>Multiobjective Genetic Algorithm</i>
<i>NCEP/NCAR</i>	<i>National Centers for Environmental Prediction/National Center for Atmospheric Research</i>
<i>NSGA-II</i>	<i>Non-dominated Sorting Genetic Algorithm-II</i>
<i>NSE</i>	<i>Nash-Sutcliffe efficiency</i>
<i>NTh</i>	<i>Haplic Nitisols Soil Use</i>
<i>PAST</i>	<i>Pastoral Land Use</i>
<i>PBIAS</i>	<i>Percent Bias</i>
<i>PET</i>	<i>Potential Evapotranspiration</i>
<i>PS</i>	<i>Physical Similarity</i>
<i>PSO</i>	<i>Particle Swarm Optimization</i>
<i>P-factor</i>	<i>Relative Width of 95% Probability Band</i>
<i>RCP</i>	<i>Representative Concentration Pathways</i>
<i>RGe</i>	<i>Eutric Regosols Soil Use</i>
<i>RMSE</i>	<i>Root Mean Square Error</i>
<i>RNGB</i>	<i>Sylivo-Pastoral Land Use</i>
<i>RSR</i>	<i>Root Mean Square Error to the Standard Deviation of Measured Data</i>
<i>r-factor</i>	<i>Percentage of Observation Covered by the 95PPU</i>

<i>SARIMA</i>	<i>Seasonal Autoregressive Integrated Moving Average</i>
<i>SCE</i>	<i>Shuffled Complex Evolution</i>
<i>SCS-CN</i>	<i>Soil Conservation Service-Curve Number</i>
<i>SDSM</i>	<i>Statistical Downscaling Model</i>
<i>SMEC</i>	<i>Snowy Mountains Engineering Corporation</i>
<i>SOL_AWC</i>	<i>Available water capacity of the soil layer</i>
<i>SOL_BD</i>	<i>Moist bulk density</i>
<i>SOL_K</i>	<i>Saturated hydraulic conductivity</i>
<i>SP</i>	<i>Spatial Proximity</i>
<i>SPI</i>	<i>Standard Precipitation Index</i>
<i>SWAT</i>	<i>Soil and Water Assessment Tool</i>
<i>SWAT-CUP</i>	<i>Soil and Water Assessment Tool-Calibration Uncertainty Program</i>
<i>UNESCO</i>	<i>United Nations Educational, Scientific and Cultural Organization</i>
<i>URLD</i>	<i>Urban Land Use</i>
<i>USBR</i>	<i>United States Bureau of Reclamation</i>
<i>VRe</i>	<i>Eutric Vertisols Soil Use</i>
<i>WETL</i>	<i>Marsh Land Use</i>
<i>WMO</i>	<i>World Meteorological Organization</i>
<i>7Q10</i>	<i>10-Year 7-day Low Flow</i>
<i>95PPU</i>	<i>95 Percent Prediction Uncertainty</i>

# CHAPTER ONE

## 1. Introduction

### 1.1. Problem Statement

The Nile River obtains about 85% of its total flow from the Blue Nile River that originates in the Ethiopian highlands, while the majority of the Nile River's water is used in Sudan and Egypt. The Ethiopian Government has identified the Lake Tana Basin (LTB) as a region for irrigation and hydropower development, which are vital for food security and economic growth in Ethiopia (MoFED, 2006). Because of this basin's significant water resources potential, some irrigation and hydropower projects are planned for the near future in the LTB. However, there is no detailed study concerning the future water allocation in the basin. Therefore, the optimal operation of the ongoing and proposed reservoirs in the LTB is significant for the efficient use of the available surface water resources. Besides, accurate estimation and forecasting of water supply and demand as well as obtaining a balance between them still lack in the study area. In more than a decade, few water balance studies have been conducted in this basin (e.g. Conway, 1997; Kebede *et al.*, 2006; SMEC, 2007; Wale *et al.*, 2009). Most of these previous studies estimated the water balance within the basin but produced notably heterogeneous results. The reasons for these differences

remain unclear, however, because each study has used different models and parameter estimation schemes to simulate the hydrological processes of the ungauged catchments. A commonly used approach to overcome this problem is to identify a good hydrologic modeling approach for the gauged and ungauged catchments, but no comparative studies have been conducted for the LTB. Furthermore, more than 60% of the Lake Tana Basin is ungauged. In many hydrologic analysis studies, handling ungauged catchments has become a major obstacle to be first solved and various versions of regionalization, a process of transferring hydrological information from gauged to ungauged catchments, have been developed for last several decades. However, no study correctly estimated the surface water from the ungauged catchments. Agriculture in Ethiopia is mostly small-scale, rainfall dependent, and traditional. The heavy reliance of the Ethiopian economy on rain-fed agriculture makes it particularly vulnerable to hydrological variability. Climate change can affect multiple features of the hydrology, and it can significantly influence the sustainability of the water resources projects in the basin, but have not received attention in planning for future water management. Moreover, the previous studies primarily focused on the early experiments of the Intergovernmental Panel on Climate Change (IPCC). However, policymakers need the latest information on the likely future impacts of the climate change to reconcile human society with natural systems. Therefore, evaluation and application

of the updated generation of the Fifth Assessment Report (AR5) of IPCC in Ethiopia are needed.

## **1.2. Research Objectives**

General objectives

- ✓ To accurately assess the surface water resources potential of the basin,
- ✓ To efficiently manage the surface water resources of the basin.

Specific objectives

- ✓ To suggest a good hydrological model for the estimation of the surface water resources of the basin.
- ✓ To propose a new parameter transfer technique for the estimation of the surface water resources of the ungauged catchments.
- ✓ To assess the upstream development and climate change impact on the Lake Tana water level.
- ✓ To develop the optimal management strategy for the surface water resource allocation.

## **1.3. Research Procedures**

Figure 1.1 is the general flowchart that indicates the overall framework of the methodology of this study.

First, all the required data that used to setup the three hydrological models in the four major gauged catchments of the study basin were collected and analyzed. The observed weather data from the 13 weather gauging stations were collected from the Ethiopian National Metrological Agency, whereas the spatial input data, and observed streamflow data were provided by the Ministry of Water, Irrigation & Energy of Ethiopia. The three rainfall–runoff models were compared based on their performances both in time and quantile domains. Then, the best model among the three hydrological models was used to model the ungauged catchments of the study area. For this, the selected model parameters were transposed to the ungauged catchments by using the arithmetic mean, the physical similarity, the spatial proximity, and the catchment runoff-response similarity approaches. Besides, the performance of the parameter transfer schemes were also compared to identify the robust methodology of obtaining the selected model parameters for use in modeling the ungauged catchments. After the estimation of the surface water resources from the gauged and ungauged catchments, we explore the impacts of climate change in the water resources of the study basin for the future periods by statistical downscaling the coarse spatial resolution of the general circulation models output. Finally, a multi-objective model was formulated to optimally allocate the surface water resources of the basin to multiple users.

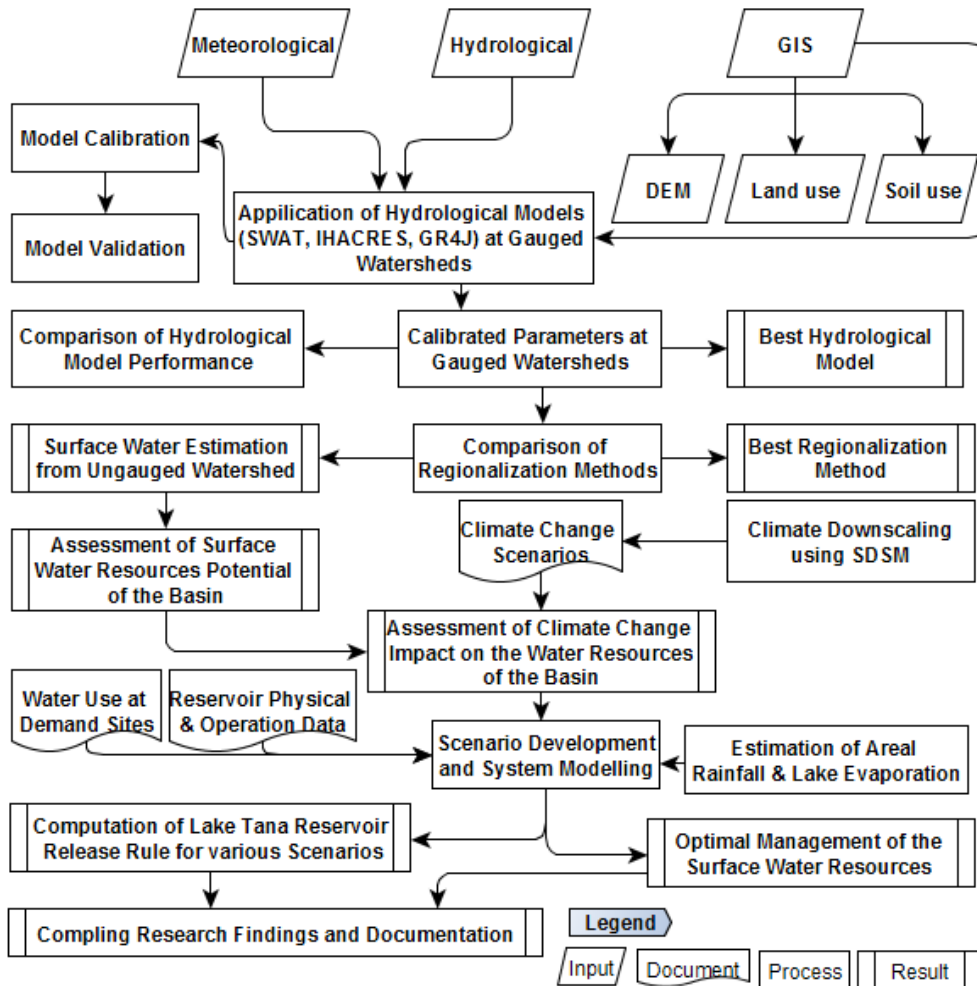


Figure 1.1. General framework of the study

## **1.4. Outline**

This research is organized into eight chapters. The first chapter is an introduction that includes a statement of the problem, objectives and the procedure of the study as well as the overall report outline. Chapter two gives a general description of the study area and data. The third chapter covers the review of the main related facts from references and review of earlier studies in the basin. The various studies conducted in specific parts of the entire study area are well described. The Hydrological models used in this study are also discussed. The fourth chapter presents the methodology for the selection of the best hydrological models for the assessment of surface water resources in the study basin. The performance of lumped and physically-based semi-distributed hydrological models are also reported. The fifth chapter presents the surface water resources potential of the ungauged catchments in the study basin. This chapter also discussed different parameter transfer approaches. Moreover, the methodology of the newly proposed parameter transfer scheme is also reported. Chapter six discusses the detailed assessment of the potential impacts of climate change on the water balance components of the study basin. Chapter seven presents the allocation surface water resources to multiple water users. This chapter also discussed the method of reflecting the uncertainty of reservoir inflows in the development of a reservoir operation rule with genetic programming. Finally, the conclusions and future study are provided in chapter eight.

## CHAPTER TWO

### 2. Data and Study Area Description

#### 2.1. Location

The Lake Tana is the sources of the Blue Nile River; its natural drainage area is about 15,114 km<sup>2</sup>. The Lake Tana Basin is found in the northwest part of Ethiopia in the Amhara administrative region. It covers eight Woredas (smaller administrative units); Dembia and Gondar Zuria in the north of the basin, Libo Kemkem, Fogera, Farta and Dera in the eastern part of the basin, Achefer and Alefa-Bechigne in the west and with Bahirdar Zuria in the south of the basin. Geographically, it extends between 10.95 °N to 12.78 °N latitude and from 36.89 °E to 38.25 °E longitudes. Gilgelabay, Ribb, Gummera, and Megech catchments are the major gauged catchments of the study area (see Figure 2.1). The only surface outflow from the basin is the Blue Nile River, which comprises 7% of the Blue Nile flow at the Ethio-Sudanese border (Shahin, 1988).

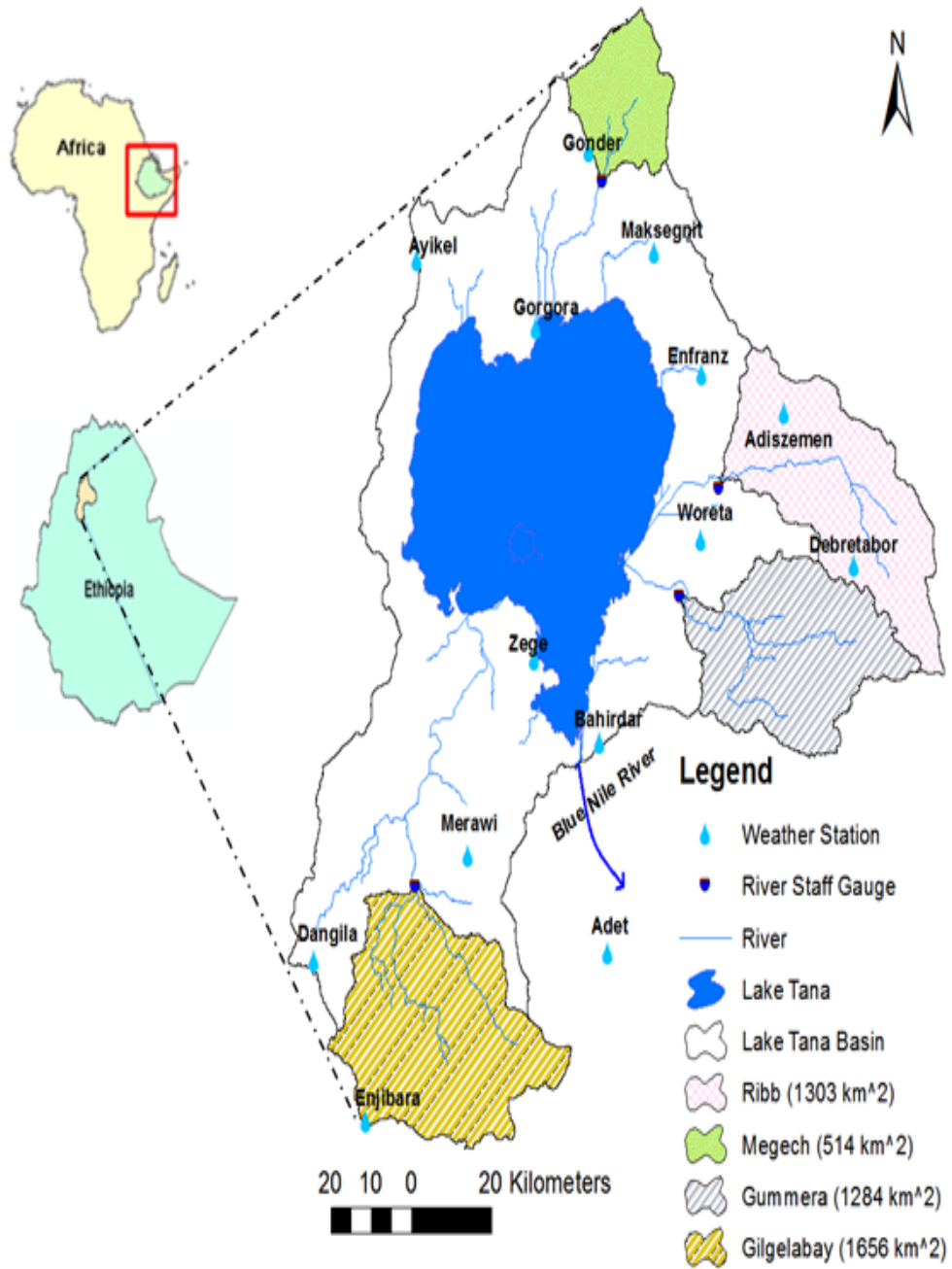


Figure 2.1. Location map of the LTB

## **2.2. Topography**

The elevation of the Lake Tana Basin ranges between 914 m to 4096 m above mean sea level (Figure 2.2), which is extracted from DEM (90\*90) m resolution. The basin is characterized by a large flat to very gently sloping plain bordering the lake on the North and East and an extensive area of gently rolling to hilly uplands on the South. Hurst *et al.*, 1959 explained that the Lakeshore is broken by the rocky Gorgora which separates two marshy stretches. East of the Gorgora lies the Dembia plain which has been formed by alluvium sediments brought down by Megech, Dirma, and other streams. The northeast part of the Lake Tana lies down on the foothills and south of them are the Fogera plains which are broad plains forming a great bay in the hills. These hills to the east of this plain are drained by Gummera and Ribb streams which pour into the Lake Tana. The highland mountains continue to the south of the Lake, and the Blue Nile River flows out of the Lake lies in the deep gorges on its way to the Sudan. The southern mountains rise to a height of about 4000 m, and the western slopes fall towards the Gilgelabbay. The Lake Tana Basin is also known by the most densely populated area with a population density of over 250 people per square kilometer of land area.

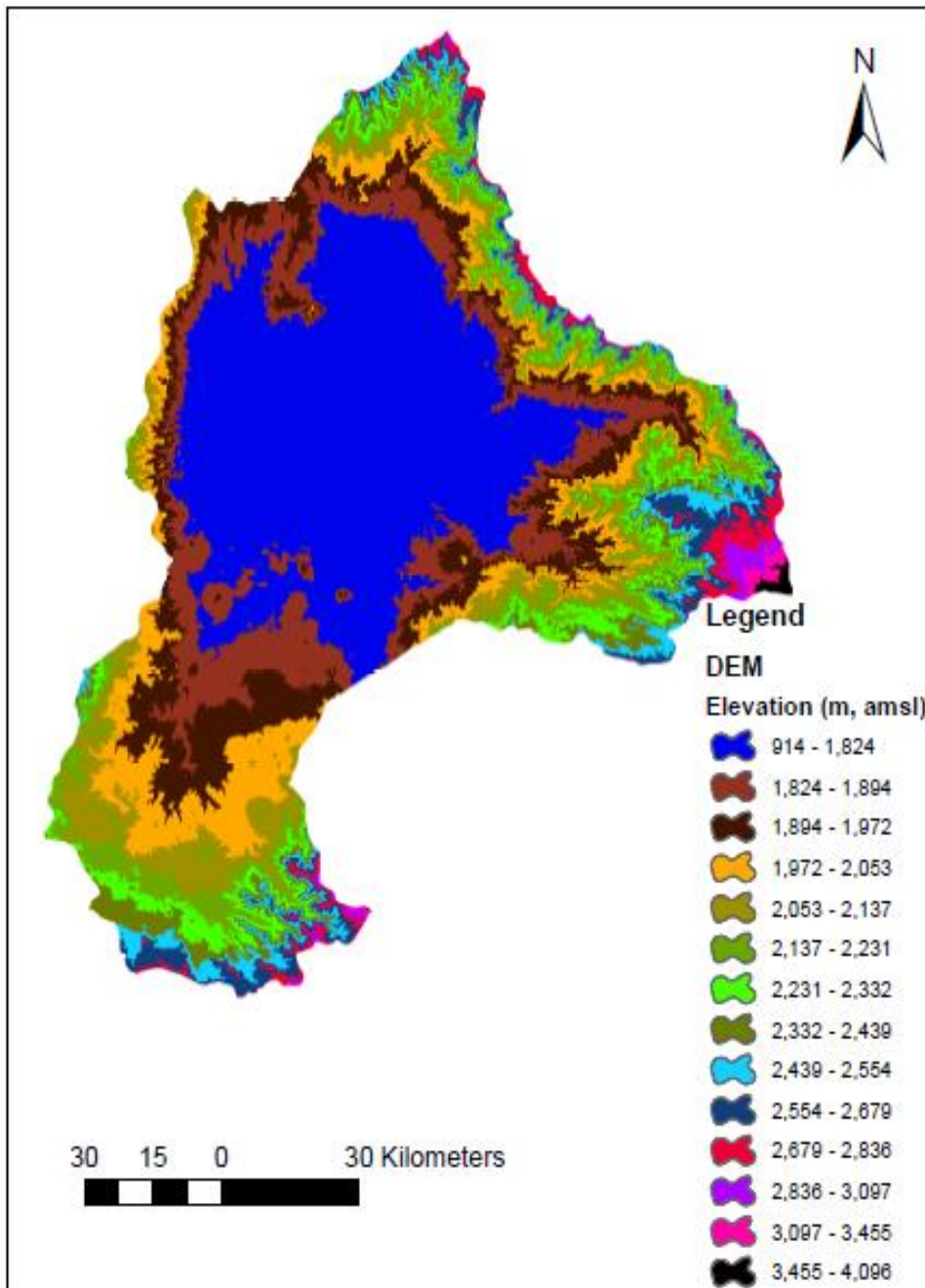


Figure 2.2. Map showing elevation of the LTB

### **2.3. Climate and Hydrology**

Like most of the central highlands, the elevated position of the Lake Tana area makes for a temperate, subtropical, and an equable climate despite its proximity to the equator. There are two seasons called rainy and dry. The rainy season has two periods: the little rains, during April and May; and the big rains, which last from June to August. The rainfall distribution in the basin is found to be a mono-modal pattern (i.e. one peak value observed during the rainy season). Considering the 13 rainfall stations (see Figure 2.1) in the basin for 1995-2014, a mean annual rainfall amount ranges between 955.20 mm in Enfranz and 2364.55 mm in Enjibara. Similarly, a minimum and a maximum temperature range between 8.84 °C in Merawi and 28.09 °C in Enfranz, respectively. Figure 2.3, 2.4, and 2.5 presents the maximum temperature, minimum temperature, and monthly average rainfall variations of the Lake Tana Basin, respectively. There are four major rivers in the basin (i.e. Gilgelabay, Gummera, Megech, and Ribb). The Gilgelabbay River is the largest River in the basin, which enters the Lake at its southwestern corner.

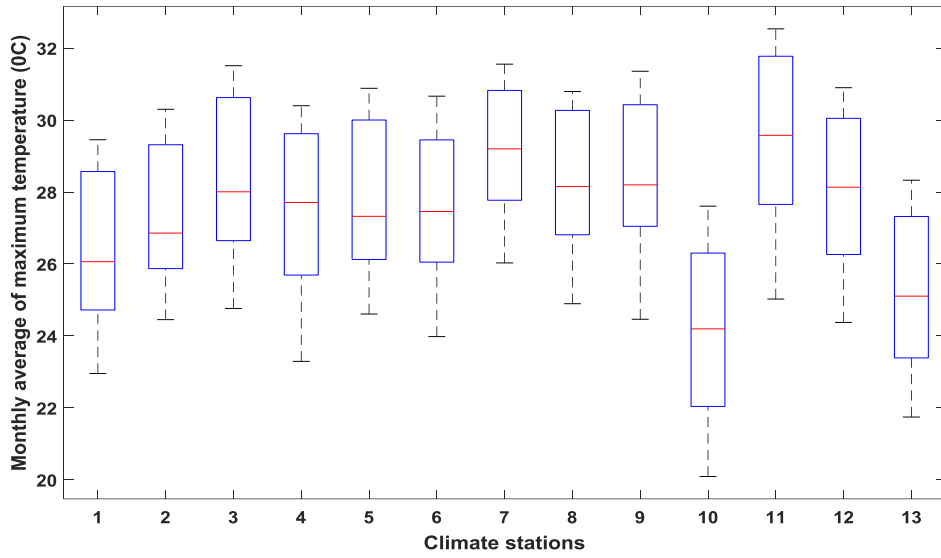


Figure 2.3. Monthly average of maximum temperature for the LTB

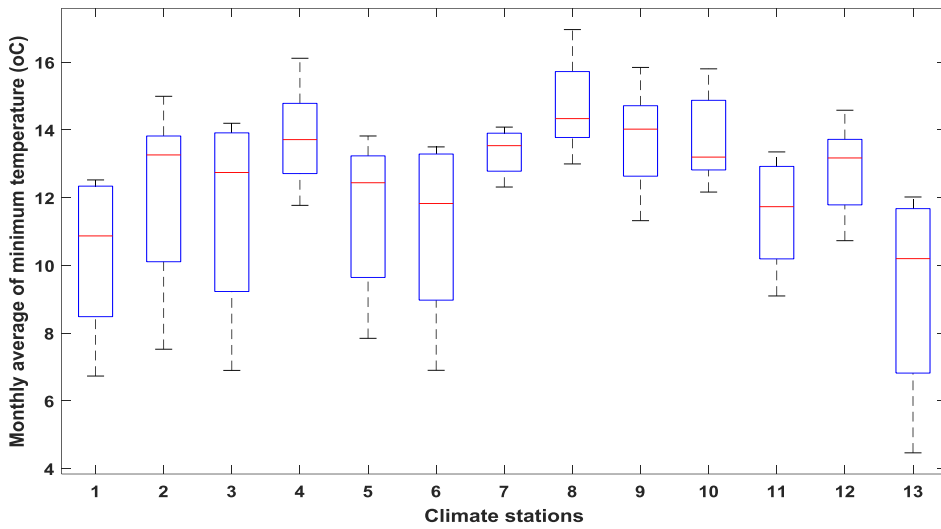


Figure 2.4. Monthly average of minimum temperature for the LTB

(1-Adet, 2-Baahirdar new, 3-Bahirdar airport, 4-Gonder, 5-Zege, 6-Merawi, 7-Gonder, 8-Enfranz, 9-Maksegnit, 10-Ayikel, 11-Addiszemen, 12-Woreta, 13-Dangila)

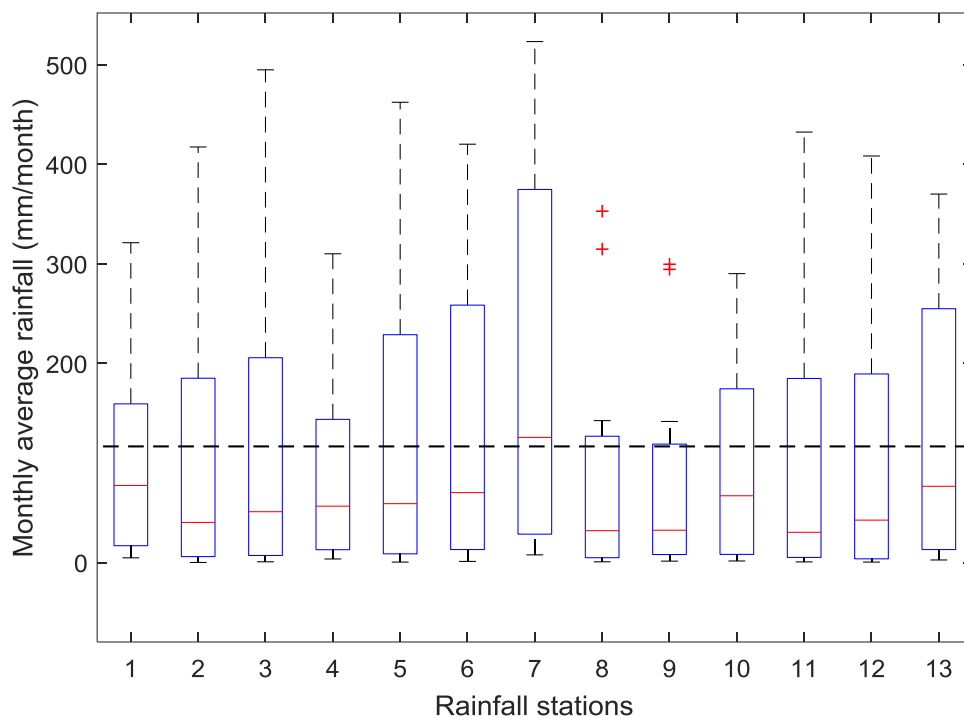


Figure 2.5. Monthly average rainfall in the LTB

(1-Adet, 2-Baahirdar new, 3-Bahirdar airport, 4-Gonder, 5-Zege, 6-Merawi, 7-Enjibara, 8-Enfranz, 9-Maksegnit, 10-Ayikel, 11-Addiszemen, 12-Woreta, 13-Dangila). The horizontal dash line represents the overall monthly average rainfall in the study basin.

## **2.4. Land Use and Soil Use**

The Land use data was collected from the Ministry of Water and Energy Metadata section. Land use of the study area was classified based on the Abay River master plan study conducted by BCEOM, in 1996-1999. About 51.37% of the basin area is covered by Agriculture, 21.94% by Agro-pastoral, 20.41% by Lake Tana, 0.39% by Agro-sylvicultural, 0.13% by wetland, 5.47% by Pastoral, 0.15% by sylvicultural, 0.03% by sylvo-pastoral and 0.11% by Urban.

The soil classification of the study area was also adopted from the Abay River master plan study conducted by BCEOM in 1996-1999. Based on the soil classification, Halpic Luvisols which covers about 20.68% of the basin area is found to be the major dominant soil in the study area.

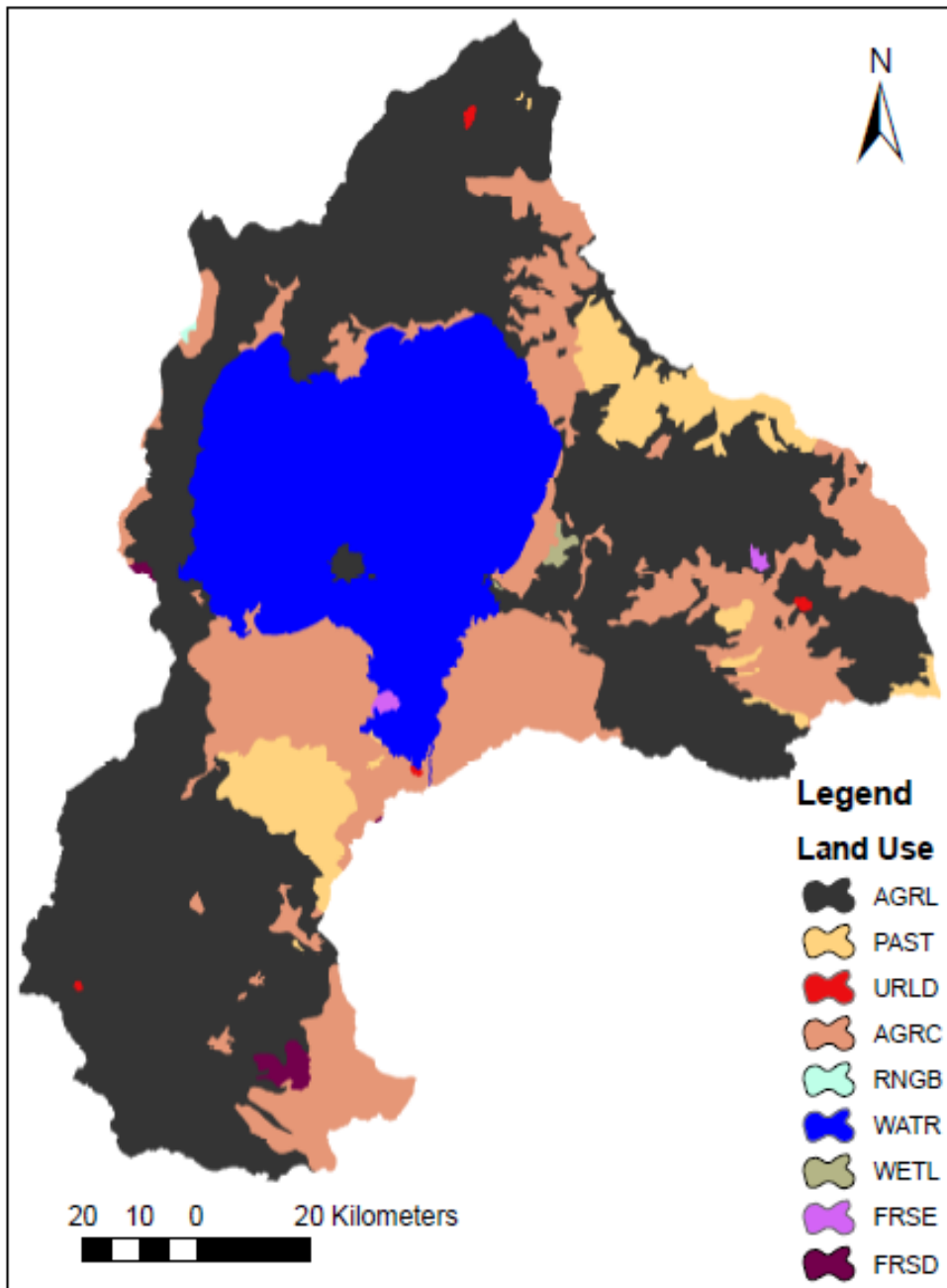


Figure 2.6. Land use classification of the LTB

Table 2.1. Land use classification of the LTB

<b>Land use</b>	<b>Symbol</b>	<b>Area (ha)</b>	<b>% Watershed area</b>
Agriculture	AGRL	776406.18	51.37
Agro-Pastoral	AGRC	331601.16	21.94
Agro-Sylvicultural	FRSD	5894.46	0.39
Marsh	WETL	1964.82	0.13
Pastoral	PAST	82673.58	5.47
Sylvicultural	FRSE	2267.10	0.15
Sylivo-Pastoral	RNGB	453.42	0.03
Urban	URLD	1662.54	0.11
Water	WATR	308476.74	20.41
<b>Total</b>		<b>1,511,400</b>	<b>100</b>

Table 2.2. Major soil types of the LTB

<b>Soil type</b>	<b>Symbol</b>	<b>Area (ha)</b>	<b>% Watershed area</b>
Chromic Luvisols	LVx	238498.92	15.78
Eutric Cambisols	CMe	302.28	0.02
Eutric Fluvisols	FLe	149024.04	9.86
Eutric Leptosols	Lpe	184088.52	12.18
Eutric Regosols	RGe	4080.78	0.27
Eutric Vertisols	VRe	178798.62	11.82
Haplic Alisols	ALh	71489.22	7.62
Haplic Luvisols	LVh	312557.52	20.68
Haplic Nitisols	NTh	18892.50	1.25
Urban	URLD	1511.40	0.11
Water	WATR	308476.74	20.41
<b>Total</b>		<b>1,511,400</b>	<b>100</b>

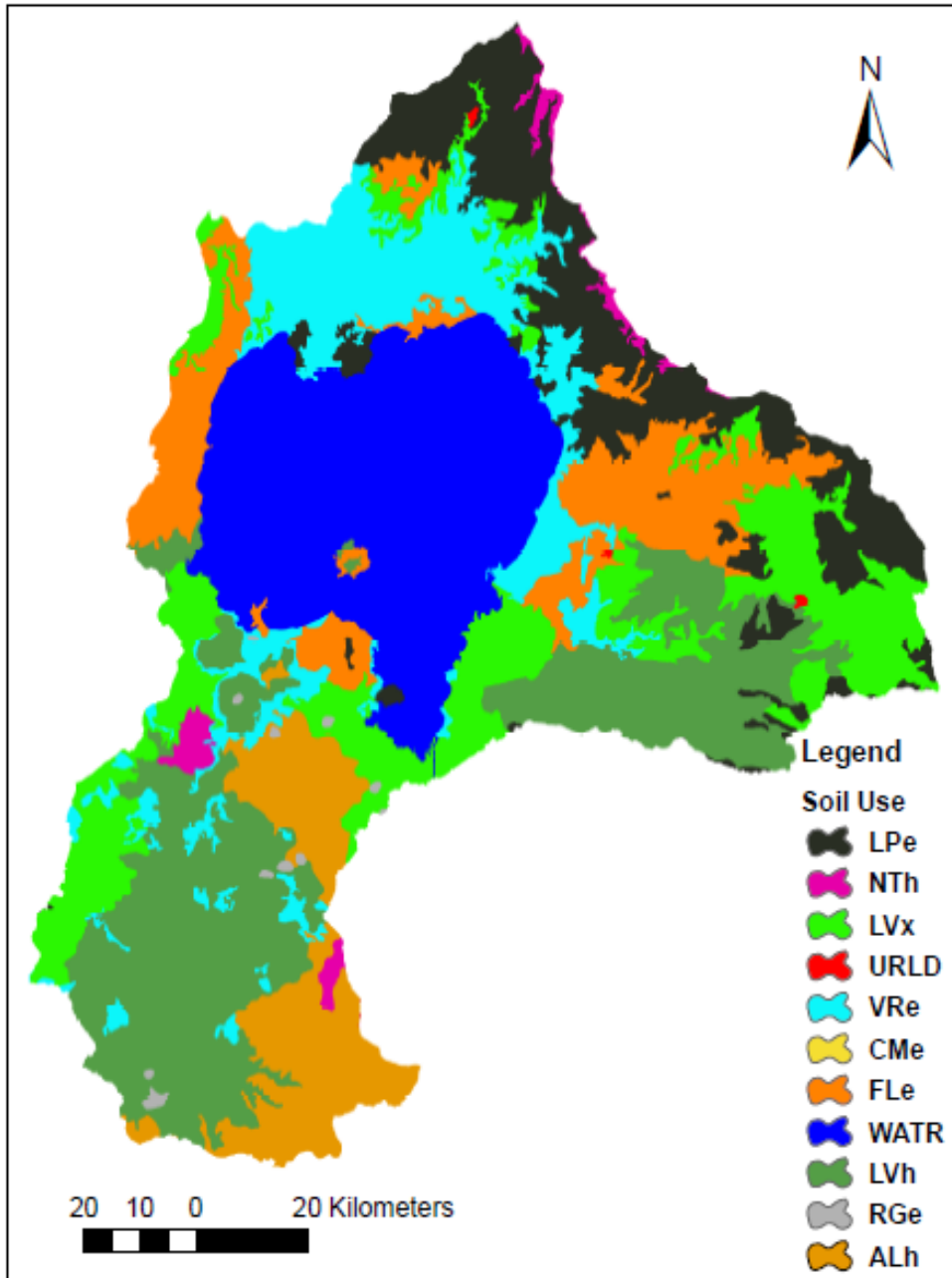


Figure 2.7. Soil use classification of the LTB

## **2.5. Water Resource Development**

The Lake Tana has a surface area of about 3050 km<sup>2</sup> with a length of 74 km, maximum depth of 14 m, mean depth of 9 m and width of 68 km. The Lake Tana Basin is at the center of Ethiopia's plans for water resource development owing to its immense water resource potential. Some water resources projects are under construction, and lots of reservoirs are scheduled for the future. Of these, Tana-Beles multipurpose project, which integrated hydropower and irrigation development, has been completed. This scheme involves the transfer of water from the Lake Tana, with an average supply rate of 77 m<sup>3</sup>/s (SMEC, 2008), to the Beles River via a 12 km long, 7.1 m diameter tunnel (Salini and Mid-day 2006). The hydropower project has an installed capacity of 460 MW of power production (which enable more electricity to be generated than is previously produced in the Tis Abbay power stations). The irrigation project is designed to irrigate 175,000 ha of land. As well the Tana-Beles multipurpose project, the Koga Irrigation Project (6,000 ha) is currently under function. Several of the other water resources projects detailed feasibility studies have been undertaken, and planning is at an advanced stage. It is anticipated that the construction of several of the dams and irrigation projects will commence shortly. Due to the planned and functional water resources projects, the management of Lake Tana water resources needs a comprehensive operational management that balances the water requirement by the upstream and downstream users.

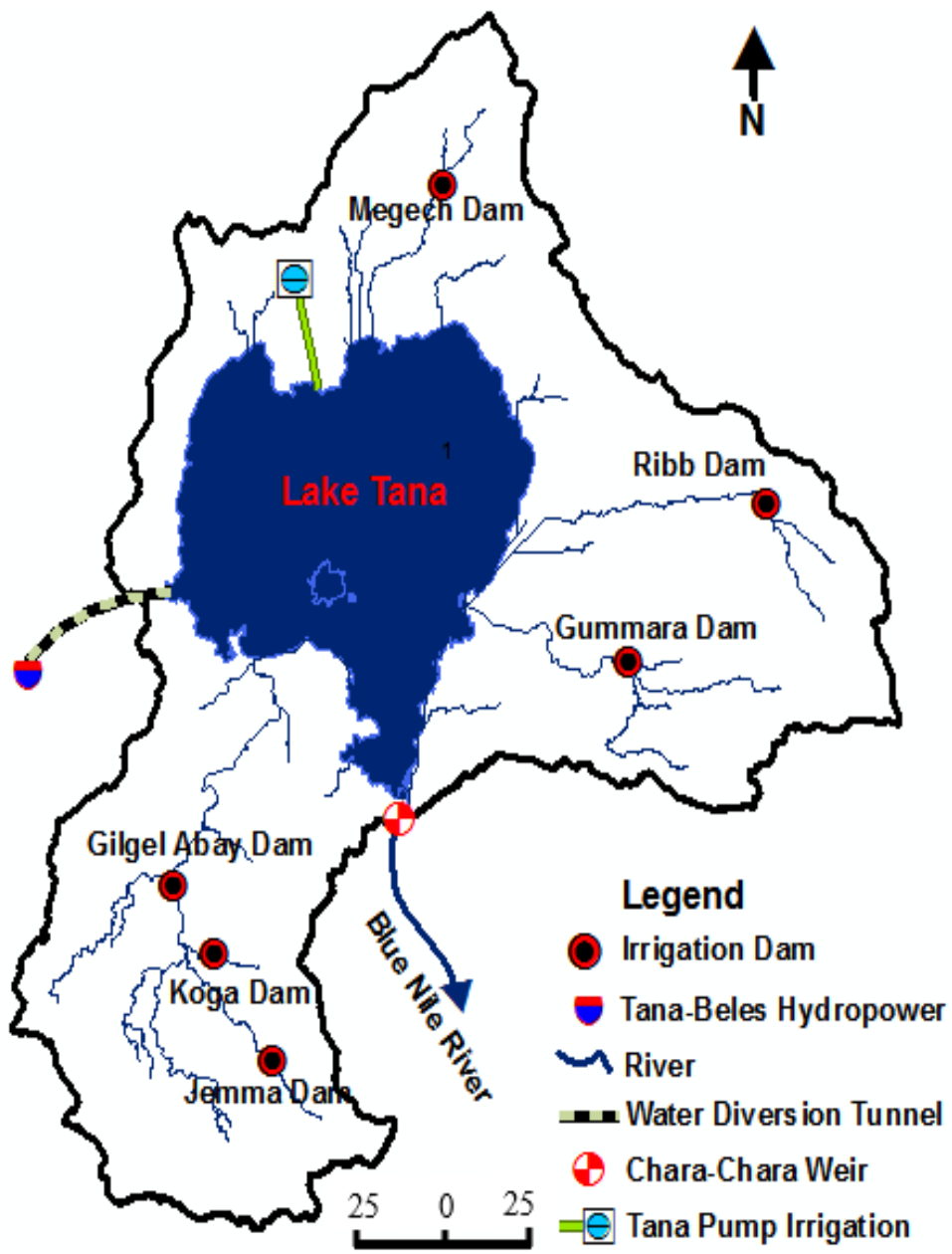


Figure 2.8. Existed & proposed irrigation and hydropower projects in the LTB

Table 2.3. Water resource projects in the study basin (Source: MoFED, 2006)

<b>Sr. No</b>	<b>Scheme name</b>	<b>Scheme type</b>	<b>Project</b>	<b>Project status</b>
1	Koga	Dam/Reservoir	Irrigation Project	Start operation
2	Gilgelabbay	Dam/Reservoir	Irrigation Project	Feasibility study completed
3	Gummera	Dam/Reservoir	Irrigation Project	Feasibility study completed
4	Megech	Dam/Reservoir	Irrigation Project	Feasibility study completed
5	Ribb	Dam/Reservoir	Irrigation Project	Under Construction
6	Lake Tana Pump Irrigation	Water abstraction from the Lake Tana	Irrigation Project	Identified
7	Tana-Beles Hydropower	Water transfer from the Lake Tana	Hydropower Project	Start operation

# CHAPTER THREE

## 3. Literature Review

### 3.1. Previous Studies for the Lake Tana Basin

#### 3.1.1. Water Resources Planning and Development

**USBR (1964):** The study conducted by the USBR in 1964 was a study of land and water resources of the Blue Nile Basin. The study was carried out at reconnaissance level and have identified significant sites, both for irrigation and hydropower in the Tana and Beles subbasins. This reconnaissance study has identified six major irrigation sites (Megech, Ribb, Gummera, West Megech pump, East Megech pump, and Northeast Tana pump) in the Tana Basin. The USBR studies have also proposed a regulation dam for the Lake Tana at Chara-Chara with the objective of diverting the Lake water to the upper Beles hydropower plant, which is in operation currently. The Lake Tana reservoir is planned to be operated between the water surface levels of 1783 m and 1787 m in which the spillway crest level is fixed at 1787 m above mean sea level.

**BCEOM (1998/99):** The study by BCEOM was carried out over a three-year period between 1996 and 1999 and comprised three phases: Inception, Inventory & Analysis, and finally, Master Planning. The consultant has established different scenarios while effecting Master Plan of

the water resources development in the Abbay River Basin. These scenarios were developed based on the idea that planning is primarily the function of finance and implementation capacity of the country. In assessing the implementation capacity of the country, the consultant has given due emphasis on the involvement of the public and private sectors in the development of water resources in the basin within the planning horizon. According to the study of the consultant, the Abay River Basin has the potential of 526,000 ha irrigable land that includes large and medium scale irrigation schemes.

### **3.1.2. Water Balance Assessment**

**Kebede *et al.* (2006):** The study by Kebede *et al.* (2006) focused on the estimation of the water balance of the Lake Tana Basin and concluded that the four major catchments (Gilgelabay, Gummera, Ribb, and Megech) contribute 93% of the inflow to the Lake Tana.

**Wale *et al.* (2008):** The study by Wale *et al.* (2008) estimated the water balance of the Lake Tana by using the HBV hydrologic model. They concluded that 58% of the inflow to the Lake Tana was from the gauged catchments and 42% of the inflow was from the ungauged catchments.

**SMEC (2008):** The study by SMEC (2008) focused on the hydrological study of the Tana-Beles Basin. The study used the river basin simulation model MIKE BASIN to simulate different development scenarios in the

basin. According to this study, total River inflow to the Lake Tana was estimated to be 1.403 times the inflow from the major gauged catchments. The inflow from the ungauged catchment was computed by subtracting the inflow from gauged catchments to the total river inflow into the Lake Tana, which means 71% of the Lake inflows was from gauged catchments and 29% of the Lake inflows was from ungauged catchments.

**Setegn *et al.* (2009):** The study by Setegn *et al.* (2009) tested the performance of SWAT model in the four major gauged catchments of the Lake Tana basin. The study has shown that the SWAT model can produce reliable estimates of the water balance components of the study basin.

**Rientjes *et al.* (2011):** The study by Rientjes *et al.* (2011) used regression approach to transfer the information from gauged to ungauged catchments of the basin and concluded that 29.5% of the inflow to the Lake Tana was from ungauged catchments while the area of ungauged catchments covers nearly 62% of the total basin area.

Most of these previous studies estimated the water balance within the basin but produced notably heterogeneous results. For example, Kebede *et al.* (2006) concluded that the four major catchments contribute 93% of the inflow into Lake Tana, whereas SMEC (2007) and Wale *et al.* (2009) reported values of 71% and 58%, respectively, for the same four catchments. The reasons for these differences remain unclear, however,

because each study has used different methodology to simulate the hydrological processes.

### **3.1.3. Climate Change Impact on the Water Resources**

**Setegn *et al.* (2011):** The study by Setegn *et al.* (2011) investigated the sensitivity of hydrological components to climate change for the LTB. The SRES emission scenarios (A1B, B1, and A2) were used for the climate change projection and concluded that the sensitivity of hydrological components to the climate change in the Lake Tana Basin have the potential to cause a significant agricultural drought unless there is ample water available for irrigation.

**Nigatu *et al.* (2016):** The study by Nigatu *et al.* (2016) assessed the impact of climate change on the Lake Tana's water balance. The HadCM3 output for the A2a and B2a emission scenarios were used to statistically downscale the weather variables using the Statistical Downscaling Model (SDSM). The SDSM outputs were used as an input to the HBV hydrological model to assess the climate change impact on the water balance of the Lake Tana. This study concluded that the Lake Tana storage would increase for both emission scenarios (A2, and B2).

### **3.2. Hydrological Models for the Lake Tana Basin**

Models have long been used in water resources management to guide decision making and to improve understanding of the system. Hydrologic models can be classified in numbers of criteria, mainly how to act processes (black box, conceptual, and physically based model), the time step they use (fixed time scale and variable time scale), spatial resolution (Lumped and distributed model), and method of solution addressing (numerical, analytical, and analogue). In general, deterministic hydrologic models can be classified into three broad categories: Lumped models, semi-distributed models, and distributed models. In regards to lumped models, the parameters do not vary spatially within the basin, and thus, basin response is evaluated only at the outlet, without explicitly accounting for the response of individual subbasins. Parameters of lumped models often do not represent physical features of hydrologic processes and involve some level of empiricism. If the interest is primarily in the discharge prediction only, then these models can provide just as good simulations as complex physically based models (Beven, 2000a). The parameters of semi-distributed models are partially allowed to vary in space by dividing the basin into some smaller subbasins. Distributed model's parameters are fully allowed to vary in space at a resolution usually chosen by the user. Hydrologic models can be further divided into event-driven models and continuous-process models based on the hydrologic processes modeled. Event driven models are

designed to simulate individual precipitation-runoff events, and their objective is for the evaluation of direct runoff. They have no provision for moisture recovery between storm events and, therefore, are not suited for the simulation of dry weather flows. Continuous process models are designed to simulate both short-term and continuous events. They are suited for the simulation of daily, monthly or seasonal streamflow, usually for long-term runoff-volume forecasting and estimates of water yield (Ponce, 1989).

According to Maidment (1993), the accuracy of model results is a function of the quality of the input data and the degree to which the model structure correctly represents the hydrological process appropriate to the problem. The complex model requires complex data, and if the required data can be roughly estimated, it may be better to use a model whose input data are in tune with available data resources. This review is intended to provide the information necessary for choosing the best model; a model which would be the most appropriate hydrologic modeling tool for the Lake Tana Basin in terms of various criteria. At the initial screening, a large number of existing hydrologic models are reviewed, and a subset of 20 models is identified (Table 3.1). The selected 20 models are then ranked according to several evaluation criteria. There are numerous criteria which can be used for choosing the best hydrologic model. These criteria are usually project-dependent (Cunderlik, 2003) since every project has its specific

requirements and some more criteria are user-dependent (e.g., Graphical user interface (GUI), and computer operation system (OS)). In general, the best model that is going to be selected for this study must answer the following questions:

- Does the model simulate the variables required by this research?
- Does the model capable of simulating a continuous process?
- Can all the inputs required by the model be provided within time and cost constraints of the study?
- Is the model available freely?
- How is the model performance in the previous studies?

The selected candidate models are grouped into the following categories:

*(i) Lumped hydrologic model*

The selection of lumped hydrologic models is due to their simple structure, minimum data requirements, fast setup, calibration, and easy use. The hydrologic process in the lumped models is usually very simplified; however, they can provide just as good simulation as complex physically based models (Beven, 2000a). None of the models selected from this categories is capable of representing all the hydrologic processes fully. The models do not simulate especially reservoir routing. However, they can efficiently solve partial research objectives such as modeling the gauged catchments and analyzing the potential impact of climate change on the

water resources. Therefore, the two lumped hydrologic models (IHACRES, & GR4J) are selected from this group for modeling the watersheds.

*(ii) Semi-distributed hydrologic models:*

All the selected models can be successfully used for simulating all hydrologic processes required by this research. The main advantage of semi-distributed models is that their structure is more physically based than the structure of lumped models and that they are less demanding on input data than fully distributed models. Under this category, ten models are evaluated based on the primary selection criteria's, and out of them, the Soil and Water Assessment Tool (SWAT) model was ranked first. The SWAT model has been used extensively worldwide for hydrology and water quality modeling. For example, the SWAT model has been incorporated into the United States Environmental Protection Agency (USEPA) Better Assessment Science Integrating Point & Nonpoint Sources (BASINS) software package. It is also used by the United States Department of Agriculture (USDA) for the Conservation Effects Assessment Project (CEAP) (Gassman *et al.*, 2007). Over 2400 peer-reviewed published articles have reported the SWAT applications, reviews of SWAT components, or other research that include SWAT (see SWAT database). As a semi-distributed model, SWAT is attractive for its computational efficiency as it offers some compromise between the constraints imposed by the other model types such as lumped, conceptual or fully distributed, physically

based models (Watson *et al.*, 2003). Recently, after 2015, SWAT has been used successfully in North America (Rajib, M.A. and V. Merwade, 2015; Gabriel *et al.*, 2015; Stewart *et al.*, 2015; Goldstein, J.C. and A. Tarhule, 2015; Mekonnen *et al.*, 2016; Rajib *et al.*, 2016), in South America (Monteiro *et al.*, 2015; Niraula *et al.*, 2015), in Asia (Zhang *et al.*, 2015; Tian *et al.*, 2015; Zhuang *et al.*, 2015; Ahn *et al.*, 2015; Devkota *et al.*, 2015; Wang *et al.*, 2015; Neupane *et al.*, 2015; Uniyal *et al.*, 2015; Azari *et al.*, 2016), in Europe (Guse *et al.*, 2015; Grusson *et al.*, 2015; Me *et al.*, 2015; Santos *et al.*, 2015; Dams *et al.*, 2015; Hesse *et al.*, 2015; Malagò *et al.*, 2015; Markovic *et al.*, 2015; Karlsson *et al.*, 2016), in Africa (Mechal *et al.*, 2015; Wambura *et al.*, 2015; Duku *et al.*, 2015; Sellami *et al.*, 2015; Seyoum *et al.*, 2015), in Australia (Githui *et al.*, 2015). Furthermore, the SWAT model performed best in the previous studies (Setegn *et al.*, 2009).

### ***(iii) Distributed hydrologic models***

Parameters of these models are fully spatially varied at a given resolution and therefore require considerably more input data (often unavailable) than semi-distributed models, but they can provide the highest accuracy in the modeling of the rainfall-runoff process. Under this category, eight models are selected for screening, and none of them is chosen for this study due to the preselection criteria.

Table 3.1. Hydrological models selected for review

<b>Rank</b>	<b>Model</b>	<b>Reference</b>	<b>Model type</b>
1	SWAT (Soil and Water Assessment Tool)	Arnold <i>et al.</i> (1998)	Semi-distributed
2	GR4J (mode'le du Ge'nie Rural a' 4 parame'tres Journalier)	Perrin <i>et al.</i> (2003)	Lumped
3	IHACRES (Identification of Unit Hydrographs And Component flows from Rainfall, Evaporation, and Streamflow)	Jakeman & Hornberger, (1993)	Lumped
4	HBV-96 (Hydrologiska Byrans Vattenbalansavdelning)	Lindstriom <i>et al.</i> (1997)	Semi-distributed
5	HEC-HMS (Hydrologic Engineering Center-Hydrologic Model System)	US-ACE (2002)	Semi-distributed
6	SWMM (Storm Water Management Model)	Huber & Dickinson (1988)	Semi-distributed
7	HSPF (Hydrologic Simulation Program-Fortran)	Bicknell <i>et al.</i> (1997)	Semi-distributed
8	TOPMODEL (Topography based hydrological model)	Beven (1997)	Semi-distributed
9	WATBAL	Knudsen <i>et al.</i> (1986)	Semi-distributed
10	SLURP (Semi-distributed Land Use-based Runoff processes)	Kite (1995)	Semi-distributed
11	HRCDHM (Hydrologic Research Center Distributed Hydrologic Model)	Carpenter & Georgakos (2001)	Semi-distributed
12	VIC (variable infiltration capacity model)	Liang <i>et al.</i> (1994)	Semi-distributed
13	MIKE SHE	Refsgaard and Storm (1995)	Fully-distributed
14	WATFLOOD (Waterloo Flood Forecasting Model)	Kouwen (1988)	Fully-distributed
15	WetSpa (Water and Energy Transfer between Soil, Plants, and Atmosphere)	Wang <i>et al.</i> (1997)	Fully-distributed
16	PAWS (Process-based Adaptive Watershed Simulator)	Shen and Phanikumar (2010)	Fully-distributed
17	ISBA (Interaction Soil Biosphere-Atmosphere)	Nolihan and Planton (1989)	Fully-distributed
18	CREST (The Coupled Routing and Excess storage)	Wang <i>et al.</i> (2011)	Fully-distributed
19	IHDM (Institute of Hydrology Distributed Model)	Beven <i>et al.</i> (1987)	Fully-distributed
20	GAWSER (Guelph All Weather Sequential Event Runoff)	Fortin <i>et al.</i> (2001)	Fully-distributed

### 3.2.1. Selected Hydrological Models

To assess the hydrologic processes in selected gauged catchments of the upper Blue Nile River Basin, three structurally different rainfall–runoff models, GR4J (Perrin *et al.*, 2003); IHACRES (Jakeman and Hornberger, 1993); and SWAT (Arnold *et al.*, 1998), were selected from the large variety of available models (see Table 3.1) based on the hydrologic processes modelled, their documentation, complexity, expertise, popularity, data availability, operating systems, applicability, cost effectiveness, and performances in the previous studies.

Simulation of the hydrology of a watershed in SWAT is separated into two major divisions. The first division is the land phase of the hydrological cycle as depicted in (Figure 3.1) which controls the amount of water, sediment, nutrient and pesticide loadings to the main channel in each subbasin. The hydrological balance is calculated based on equation 3.1.

$$SW_t = SW_0 + \sum_{i=1}^t (R_{day} - Q_{surf} - E_a - W_{seep} - Q_{gw}) \quad (3.1)$$

where  $SW_t$  is the final water content,  $SW_0$  is the initial soil water content on day  $i$ ,  $t$  is time,  $R_{day}$  is the amount of precipitation on day  $i$  (mm H<sub>2</sub>O),  $Q_{surf}$  is the amount of surface runoff on day  $i$ ,  $E_a$  is the amount of evapotranspiration on day  $i$ ,  $W_{seep}$  is the amount of water entering the vadose zone from the Soil profile on day  $i$ ,  $Q_{gw}$  is the amount of groundwater flow on day  $i$ .

The second division is the water or routing phase of the hydrological cycle which is the movement of water, nutrients, sediment and pesticides through the channel network of the watershed into the outlet. SWAT requires daily values of precipitation, maximum and minimum temperature, solar radiation, relative humidity and wind speed. These climatic variables are central to the determination of the hydrological cycle of the drainage basin beside DEM, land use, soil and management practices inputs. Estimation of evapotranspiration is vital in the assessment of water resources and the impact of climate. The difference between precipitation and evapotranspiration is the water available for human use and management (Neitsch *et al.*, 2005). SWAT incorporated three methods to estimate potential evapotranspiration (PET): the Penman-Monteith method (Monteith, 1965), the Priestly-Taylor method (Priestly and Taylor, 1972) and the Hargreaves method (Hargreaves *et al.*, 1985). The Penman-Monteith method requires solar radiation, air temperature, relative humidity, and wind speed, whereas the Priestly-Taylor method requires solar radiation, air temperature, and relative humidity. The Hargreaves method requires air temperature only. The Penman-Monteith method is recommended for the computation of the potential evapotranspiration when the standard meteorological variables are available (Allen, 1998). Therefore, the Penman-Monteith method was selected for the estimation of potential

evapotranspiration for this study. The detailed report can be found in the SWAT theoretical manual (Neitsch *et al.*, 2005).

The IHACRES model operates at a catchment scale and has been used to model catchments that range from 490 m<sup>2</sup> to 10,000 km<sup>2</sup> and with time-steps from six minutes time step (e.g. Hansen *et al.*, 1996) to one month in the Thames catchment (Littlewood and Marsh, 1996). The IHACRES model has been used in numerous applications (e.g. Hansen *et al.*, 1996; Post and Jakeman, 1996; Dye and Croke, 2003; Croke *et al.*, 2004) and there are many different versions of the model (Ye *et al.*, 1997; Croke and Jakeman, 2004). This study uses the IHACRES-CMD version as described in Croke and Jakeman (2004). The conceptual layout of the model is shown in Figure 3.2, in which the box on the left represents a non-linear loss module that converts rainfall,  $P$ , into effective rainfall,  $U$ . Effective rainfall is the portion of rainfall that will eventually leave the catchment as runoff. Effective rainfall is routed through two parallel stores to produce Streamflow. The non-linear loss module uses a catchment moisture deficit (CMD) accounting scheme, which partitions rainfall into drainage (effective rainfall), evapotranspiration (ET) and changes in catchment moisture. The configuration of stores is identified from the time series of rainfall and discharge but is typically either one store only, representing ephemeral streams, or two in parallel, allowing baseflow or slow flow to be represented as well as quick flow. The module uses temperature and rainfall data to

estimate the relative catchment moisture index, which indicates the proportion of rainfall that becomes effective rainfall. The second component is a linear unit hydrograph (UH) module that links effective rainfall to streamflow with the parameters  $\tau_q$ , the quick flow response decay time constant (in days);  $\tau_s$ , the slow flow response decay time constant (in days); and  $v_s$ , the proportional volumetric contribution of slow streamflow. The detailed description of the IHACRES-CMD version can be found in Croke and Jakeman (2004). Figure 3.2 shows a schematic diagram of the IHACRES model.

The GR4J modeling approach is mainly empirical (Michel *et al.*, 2006), and consists of searching data for the most efficient model structures, with the objective of getting a general, efficient and good model. The result being a parsimonious hydrological model, with successively improved versions. The GR4J model has been used in different studies (e.g. Payan *et al.*, 2008; Oudin *et al.*, 2008; Andréassian *et al.*, 2009). The main stages of the GR4J model development were: 3-parameter version proposed by Edijatno *et al.* (1999). This provided the groundwork for further model development through testing and refinement; 4-parameter version proposed by Nascimento (1995) and detailed by Edijatno *et al.* (1999) (with one fixed parameter); 4-parameter version proposed by Perrin (2000) and detailed by Perrin *et al.* (2003); 5-parameter version proposed by Le Moine (2008).

For this study, the 4-parameter version proposed by Perrin *et al.* (2003) is used. This model requires daily rainfall and potential evapotranspiration data as input data, two stores, and two unit hydrographs. The production store, for storage in the surface of the soil, has to process for storing rainfall, evapotranspiration, and percolation. The routing store has one effective rainfall as input that is routed by a unit hydrograph. One unit hydrograph routes 90% of effective rainfall (slow flow that infiltrates into the ground), and the other unit hydrograph routes the remaining 10% of effective rainfall (quick flow that flows on the surface of the soil) (Perrin *et al.*, 2003). Figure 3.3 shows a schematic diagram of the GR4J model.

The parameters descriptions and ranges of the three rainfall-runoff models are given in Table 3.2. The dominant flow parameters of SWAT model (i.e. 12 parameters) were used (e.g., Anna Malagò *et al.*, 2014). The mathematical details of the three selected hydrological models are provided in Appendix A.

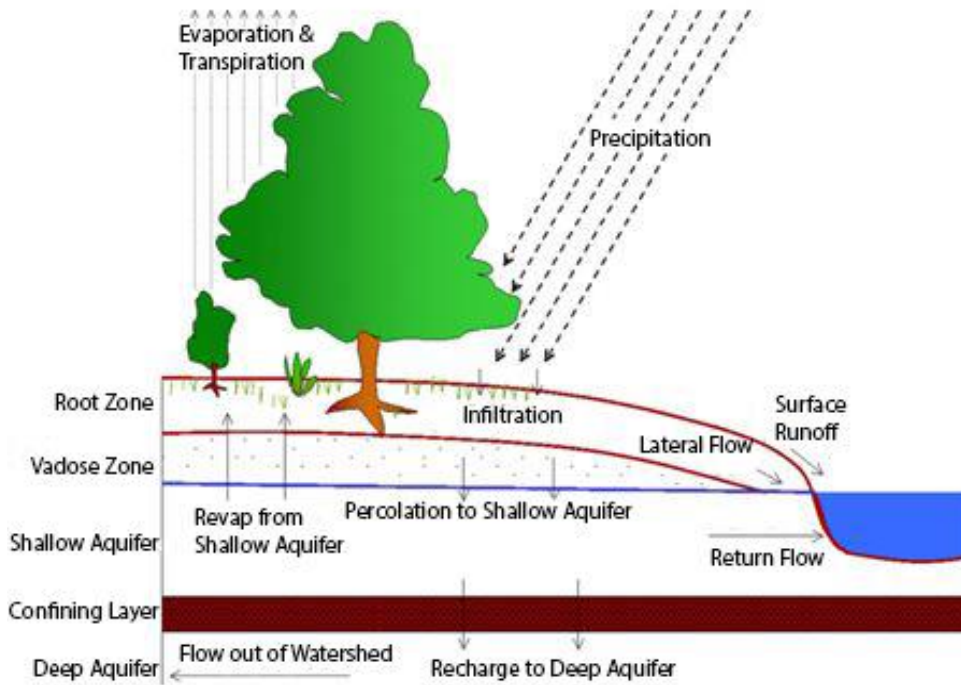


Figure 3.1. Schematic representation of the hydrological cycle used in SWAT model

(Source: Neitsch *et al.*, 2005)

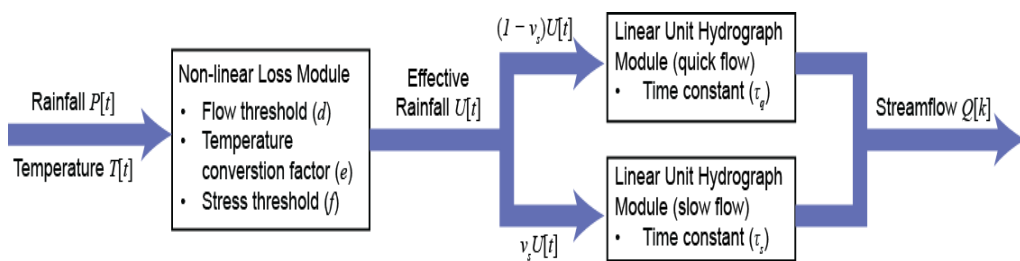


Figure 3.2. Conceptual layout of the IHACRES-CMD model

(Source: Croke and Jakeman, 2004)

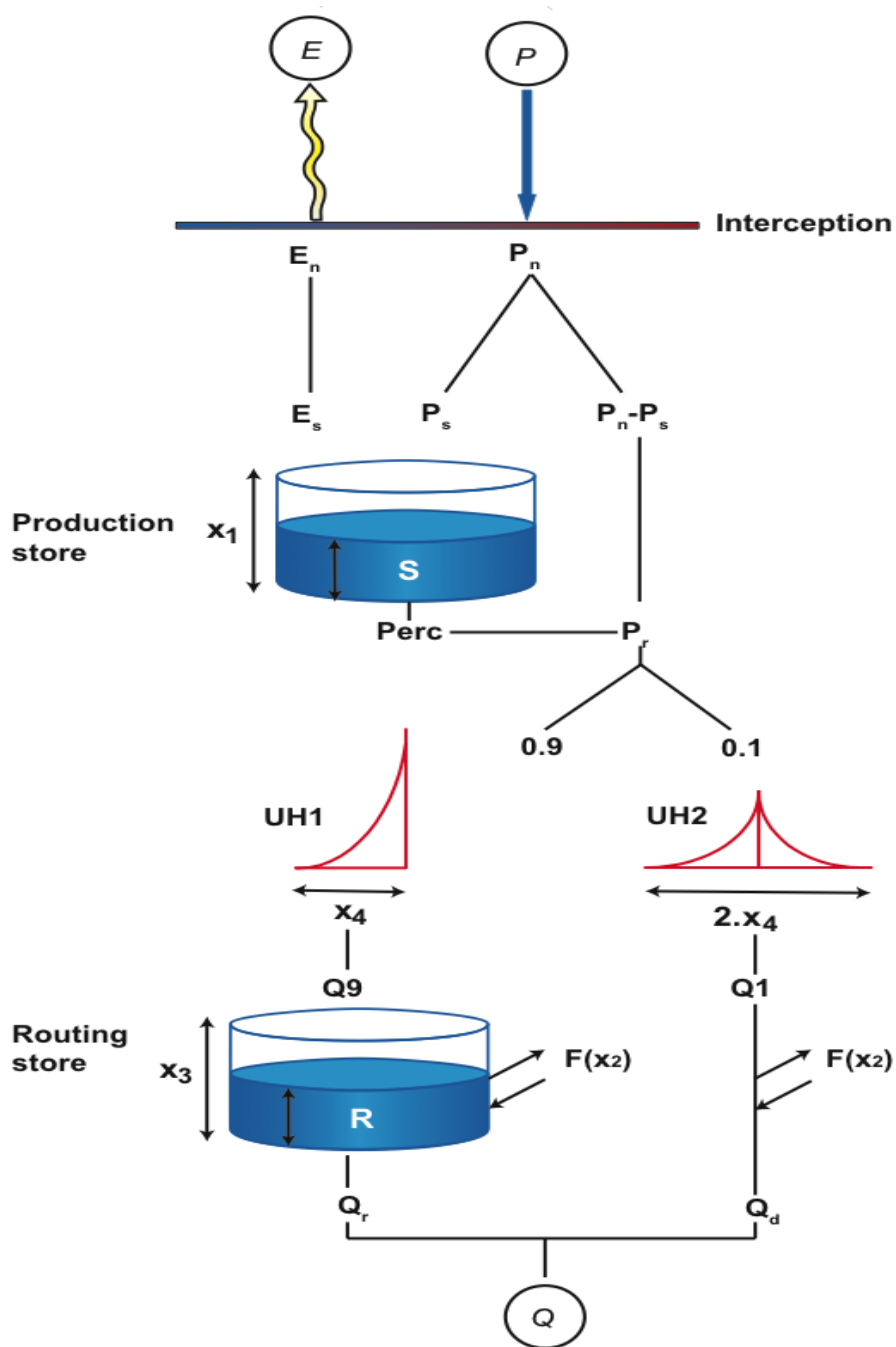


Figure 3.3. Schematic diagram of the GR4J rainfall-runoff model

(Source: Perrin *et al.*, 2003)

Table 3.2. Description and ranges of the rainfall-runoff model's parameters

<b>Model</b>	<b>Name</b>	<b>Description</b>	<b>Range</b>	<b>Unit</b>
<b>SWAT</b>	<i>CH_K2</i>	Effective hydraulic conductivity in the main channel alluvium	5.0 – 130	[mm/hr]
	<i>ALPHA_BNK</i>	Base flow alpha factor for bank storage	0.0 – 1.0	[day]
	<i>SOL_BD</i>	Moist bulk density	-0.5 – 0.6	[g/cm <sup>3</sup> ]
	<i>SOL_K</i>	Saturated hydraulic conductivity	-0.8 – 0.8	[mm/hr]
	<i>ALPHA_BF</i>	Base flow alfa factor	0.0 – 1.0	[day]
	<i>CN2</i>	SCS runoff curve number	-0.2 – 0.2	[-]
	<i>CH_N2</i>	Manning's "n" value for the main channel	0.0 – 0.3	[-]
	<i>SOL_AWC</i>	Available water capacity of the soil layer	-0.2 – 0.4	[-]
	<i>GW_DELAY</i>	Groundwater delay time	30 – 450	[day]
	<i>GW_REVAP</i>	Groundwater "revap" coefficient	0.0 – 0.2	[-]
	<i>ESCO</i>	Soil evaporation compensation factor	0.8 – 1.0	[-]
	<i>GWQMN</i>	Threshold depth of water in shallow aquifer required for return flow	0.0 – 2.0	[mm]
	<b>IHACRES-CMD</b>	<i>f</i>	CMD stress threshold as a proportion of d	0.5 - 1.3
<i>e</i>		Temperature to potential evapotranspiration conversion factor	1(fixed)	[-]
<i>d</i>		CMD threshold for producing flow	200(fixed)	[mm]
<i>ts</i>		Time constant for slow flow store	10-500	[day]
<i>τq</i>		Time constant for quick flow store	0 - 10	[day]
<i>vs</i>		Fractional volume for slow flow	0 - 1	[-]
<b>GR4J</b>	<i>X1</i>	Maximum capacity of the production store	50 - 5000	[mm]
	<i>X2</i>	Groundwater exchange coefficient	(-15) - 4	[mm]
	<i>X3</i>	One day ahead maximum capacity of the routing store	10 - 1300	[mm]
	<i>X4</i>	Time base of unit hydrograph	0.5 - 5	[day]

### 3.2.2. Model Parameter Estimation

The successful application of a hydrologic model depends on how well the model is calibrated (Duan *et al.*, 1992). The parameters of the hydrological models need to be estimated by automatic calibration so that the observed and predicted output values are in agreement. Before the availability of high-speed computers, hydrologic practitioners utilized knowledge of the watershed and experience with the model to adjust the parameters through a manual trial and error procedure (Gupta *et al.*, 1999). This kind of calibration is labor intensive. Global optimization algorithms can efficiently search optimum parameter solutions that can minimize (or maximize) objective functions which represent the agreement between observations and model outputs. In hydrologic models, for example, Duan *et al.* (1992) developed the shuffled complex evolution algorithm (SCE-UA), which is proved to be consistent and efficient for searching global optimum parameter values of hydrologic models (Vrugt *et al.*, 2003).

For optimizing the parameters of the rainfall-runoff models, we used an open software environment for hydrological model assessment and development called ‘Hydromad’ for the two simple conceptual rainfall-runoff models (IHACRES, and GR4J) and the SWAT-Calibration and Uncertainty program (SWAT-CUP) for the more complex physically based rainfall-runoff model (SWAT). The available evolutionary algorithms in hydromad R-based software package (Andrews *et al.*, 2011) are Shuffled

Complex Evolution (SCE-UA), Differential Evolution (DE), Differential Evolution Adaptive Metropolis (DREAM), Covariance matrix adapting evolutionary strategy (CMA-ES), Dynamically Dimensioned Search (DDS), and the Non-dominated Sorting Genetic Algorithm II (NSGA2). On the other hand, the available optimization algorithms in SWAT-CUP are Particle Swarm Optimization (PSO), Sequential Uncertainty Fitting (SUFI-2), Generalized Uncertainty Likelihood Estimation (GLUE), Parameter Solution (ParaSol), and Markov Chain Monte Carlo (MCMC) algorithms. Other optimization algorithms (i.e. harmony search (HS) algorithms and simulated annealing (SA) can also be used for automatic calibration of parameters in hydrologic models.

Several studies have been conducted to evaluate the performance of different algorithms. For example, Zhang *et al.* (2008) compared the performance of genetic algorithm (GA), shuffled complex evolution (SCE), particle swarm optimization (PSO), differential evolution (DE), and artificial immune system (AIS) methods for SWAT model. They concluded that genetic algorithm (GA) outperforms the other four algorithms given model evaluation numbers larger than 2000, while particle swarm optimization (PSO) can obtain better parameter solutions than other algorithms given a fewer number of model runs (less than 2000). Given limited computational time, the PSO algorithm is preferred, while GA should be chosen given plenty of computational resources (Zhang *et al.*,

2008). When applying GA and PSO for parameter optimization of SWAT, small population size should be chosen (Zhang *et al.*, 2008). As the time and computational resources did not allow for a vast number of model runs with SWAT, then the PSO method was selected for calibrating the SWAT flow parameters. Cooper *et al.* (1997) investigated the performance of three optimization techniques for calibrating the Tank model. These methods were the SCE-UA, genetic algorithms (GA) and simulated annealing (SA) methods. They found that out of the three global optimization methods, SCE-UA provided better estimates of the optimal solution than GA and SA methods. The SCE-UA algorithm has become a popular algorithm in the automatic calibration of rainfall-runoff models and has been extensively used for the calibration of various rainfall-runoff models. These include the Sacramento model (Yapo *et al.*, 1996; Ajami *et al.*, 2004), and the Xinanjiang model (Gan and Biftu, 1996; Cheng *et al.*, 2006). For this study, the SCE-UA method was selected for calibration of the simple conceptual rainfall-runoff models parameters. Therefore, two well-known evolutionary algorithms (EAs) are chosen to optimize the three rainfall-runoff model parameters. The Shuffled Complex Evolution (SCE) algorithm was used to optimize the parameters of the simple conceptual models. On the other hand, the Particle Swarm Optimization (PSO) algorithm was used to optimize the SWAT flow parameters. The description of the two algorithms is given as follows:

- ***The Particle Swarm Optimization (PSO) Algorithm***

The PSO was developed by Kennedy and Eberhart (1995). PSO is initialized with a group of random particles (trial solutions), which are assigned with random positions and velocities. The algorithm then searches for optima through a series of iterations where the particles are moved through the hyperspace searching for potential solutions. These particles “learn” over time in response to their experience and those of other particles in their group. Each particle keeps track of its best fitness position in hyperspace that it has achieved so far. This best position value is called personal best or “pbest”. The overall best value obtained by any particle so far in the population is called global best or “gbest”. During each iteration, every particle is accelerated towards its own “pbest” as well as in the direction of the “gbest” position that achieved by calculating a new velocity term for each particle based on the distance from its “pbest” as well as its distance from the “gbest” position. These two “pbest” and “gbest” velocities are then randomly weighted to produce the new velocity value for this particle, which will affect the next position of the particle.

- ***The Shuffled Complex Evolution (SCE) Algorithm***

The SCE method was originally developed by Qingyun Duan as part of his doctoral dissertation work at the Department of Hydrology and Water Resources, University of Arizona, USA. The dissertation is entitled as "A Global Optimization Strategy for Efficient and Effective Calibration of

Hydrologic Models." The SCE method is a global optimization algorithm which is based on a synthesis of four concepts that have proved to be effective automatic calibration tool for optimization problems (Duan *et al.*, 1992). These four concepts are a) combination of random and deterministic approaches, b) the concept of clustering, c) the concept of a systematic evolution of a complex of points spanning the space, d) the concept of competitive evolution. The combination of these concepts made the SCE known as a powerful, effective and flexible method. SCE method consists of two parts, SCE and competitive complex evolution (CCE). For SCE method, the search within the feasible region is conducted by first dividing the set of currently feasible trial solutions into several complexes, each containing an equal number of trial solutions. Concurrent and independent searches within each complex are conducted until each converges to its local optimal value. For each of the complex, which is now defined by new trial solutions is collated into a common pool, shuffled by ranking according to their objective function value and then further divided into new complexes. The procedure is terminated when none of the local optima found among the complexes can improve on the best current local optimum.

### **3.2.3. Performance Measures**

The three rainfall–runoff models were applied to reproduce the streamflow in the time domain and the quantile domain (see Chapter 4 for detail). The

model performance metrics that used to evaluate the three hydrological models were Nash-Sutcliffe efficiency (NSE), percent bias (PBIAS), a coefficient of determination ( $R^2$ ), and root mean square error to the standard deviation of measured data (RSR).

- *Nash-Sutcliffe efficiency (NSE)*

The NSE is a normalized statistic that determines the relative magnitude of the residual variance (“noise”) compared to the measured data variance (“information”) (Nash and Sutcliffe, 1970). NSE indicates how well the plot of observed versus simulated data fits the 1:1 line. NSE ranges between  $-\infty$  and 1.0, with  $NSE = 1$  being the optimal value. This performance indicator has been widely used to evaluate the hydrological model performance (e.g., Sevati and Dezetter, 1991; ASCE, 1993; and Legates and McCabe, 1999).

- *Root mean square error to the standard deviation of measured data (RSR)*

The RSR is a commonly used error index statistics (Chu and Shirmohammadi, 2004; Singh *et al.*, 2005; Vazquez-Amábile and Engel, 2005). The RSR standardizes the root mean square error (RMSE) using the observation-based standard deviation. The RSR varies from the optimal value of zero to a large positive value. This value is calculated as the ratio of the RMSE and the standard deviation of measured data, as shown in equation 3.2.

$$RSR = \frac{RMSE}{STDEV_{obs}} = \frac{\left[ \sqrt{\sum_{i=1}^n (O_i - P_i)^2} \right]}{\left[ \sqrt{\sum_{i=1}^n (O_i - \bar{O})^2} \right]} \quad (3.2)$$

where  $P_i$  is the simulated value,  $O_i$  is the measured value, and  $\bar{O}$  is the average measured value.

- **Percent bias (PBIAS)**

The PBIAS measures the normal tendency of the simulated data to be larger or smaller than their observed counterparts (Gupta *et al.*, 1999). The PBIAS can clearly indicate poor model performance (Gupta *et al.*, 1999). The optimal value of PBIAS is zero, with low-magnitude values indicating accurate model simulation. Positive values indicate model underestimation bias, whereas negative values indicate model overestimation bias (Gupta *et al.*, 1999). PBIAS is calculated with equation 3.3.

$$PBIAS = \left[ \frac{\sum_{i=1}^n (O_i - P_i)}{\sum_{i=1}^n O_i} * 100 \right] \quad (3.3)$$

where PBIAS is the deviation of the evaluated data, expressed as a percentage,  $P_i$  is the simulated value, and  $O_i$  is the measured value.

- **10-Year 7-day Low Flow**

It is the lowest average discharge over a period of one week with a recurrence interval of 10 years. There is a 90% probability that the flow

will be greater than the 7Q10 value. 7Q10 is one of the most widely used low flow indices (Caruso, 2000; Smakhtin, 2001).

#### ***- Annual maximum discharges***

Floods are of great concern in many areas of the world. Bahir Dar City, which is located near Lake Tana, is vulnerable to flooding because of its location. Almost 99.73% of the LTB is at a higher elevation than the average elevation of Bahir Dar, which is approximately 1800 m. Therefore, we analyzed the trends in annual maximum simulated discharge output of the three rainfall–runoff models and the resulting trend statistics were compared with the observed annual maximum discharge trend statistics to determine the inter-annual variability of annual maximum flow. For trend analysis, we used the non-parametric Mann–Kendall test and Sen’s slope estimator. The purpose of the Mann–Kendall test (Mann, 1945; Kendall, 1975; Gilbert, 1987) is to statistically assess whether there is a monotonic upward or downward trend in the variable of interest over time. The Sen’s nonparametric method is used to estimate the true slope of an existing trend (e.g. the change per year).

#### ***- Mann-Kendall test***

The Mann-Kendall test is applicable in cases when the data values  $x_i$  of a time series can be assumed to obey the model

$$x_i = f(t_i) + \varepsilon_i \tag{3.4}$$

where  $f(t)$  is a continuous monotonic increasing or decreasing function of time and the residuals  $\varepsilon_i$  can be assumed to be from the same distribution with zero mean.

It is therefore assumed that the variance of the distribution is constant in time. We want to test the null hypothesis of no trend,  $H_0$ , i.e. the observations  $x_i$  are randomly ordered in time, against the alternative hypothesis,  $H_1$ , where there is an increasing or decreasing monotonic trend. For time series with less than 10 data points the  $S$  test is used, and for time series with 10 or more data points the normal approximation is used. For this study, we have 12 data points. Therefore, the normal approximation ( $Z$  statistics) was used to test the trend. The procedures are given as follows: First, the Mann-Kendall test statistic  $S$  is calculated using equation 3.5.

$$S = \sum_{k=1}^{n-1} \sum_{j=k+1}^n \text{sgn}(X_j - X_k) \quad (3.5)$$

where  $n$  is the number of years,  $j$  is the time after time  $k$ , and  $X_j$  &  $X_k$  are the annual values in years  $j$  and  $k$ , respectively.

$$\text{sgn}(X_j - X_k) = \begin{cases} 1 & \text{if } X_j - X_k > 0 \\ 0 & \text{if } X_j - X_k = 0 \\ -1 & \text{if } X_j - X_k < 0 \end{cases} \quad (3.6)$$

Then, the variance of  $S$  was computed by the following equation which takes into account that ties may be present:

$$VAR(S) = \frac{1}{18} \left[ n(n-1)(2n+5) - \sum_{p=1}^q t_p(t_p-1)(2t_p+5) \right] \quad (3.7)$$

where  $q$  is the number of tied (equal value) groups,  $t_p$  is the number of data values in the  $p^{\text{th}}$  group.

The values of  $S$  and  $VAR(S)$  are used to compute the test statistic  $Z$  as follows:

$$Z = \begin{cases} \frac{S-1}{\sqrt{VAR(S)}} & \text{if } S > 0 \\ 0 & \text{if } S = 0 \\ \frac{S+1}{\sqrt{VAR(S)}} & \text{if } S < 0 \end{cases} \quad (3.8)$$

The presence of a statistically significant trend is evaluated using the  $Z$  value. A positive (negative) value of  $Z$  indicates an upward (downward) trend. The statistic  $Z$  has a normal distribution. To test for either an upward or downward monotonic trend a two-tailed test at  $\alpha$  level of significance was used.  $H_0$  is rejected if the absolute value of  $Z$  is greater than  $Z_{1-\alpha/2}$ , where  $Z_{1-\alpha/2}$  is obtained from the standard normal cumulative distribution tables.

### ***- Sen's Slope Method***

To estimate the true slope of an existing trend (as change per year) the Sen's nonparametric method was used.

$$f(t) = Qt + B \quad (3.9)$$

where  $Q$  is the slope,  $t$  is the time, and  $B$  is a constant.

To get the slope estimate  $Q$ , we first calculate the slopes of all data value pairs.  $Q_i$  values for each data pair were calculated, and the median value was taken as a final slope of the trend.

$$Q_i = \frac{x_j - x_k}{j - k} \quad (3.10)$$

where  $j$  is time after time  $k$ ,  $X_j$  &  $X_k$  constitute the pairs of observations identified by a place in the series.

In addition to the trend statistics, we have also evaluated the three hydrological models performance in terms of their capability of reproducing the amount of annual maximum flow by using two performance measures (i.e. PBIAS, and RSR). In general, the model performance metrics that we used to evaluate the three hydrological models are given in Table 3.3.

Table 3.3. Model performance indicators for each model comparison criterion

<b>Performance indicator</b>	<b>Model comparison criteria</b>			
	<b>Time-domain</b>	<b>Quantile-domain</b>	<b>Annual Maximum Flow</b>	<b>7Q10 Low Flow</b>
Nash-Sutcliffe efficiency (NSE)	√	√		
Root mean square error to the standard deviation of measured data (RSR)	√	√	√	
Percent bias (PBIAS)	√	√	√	√
Coefficient of determination ( $R^2$ )	√	√		
Trend statistics			√	

√ marks the performance indicators used for the corresponding model comparison criteria

### **3.3. Climate Change Impact Assessment**

The first step in the assessment of climate change impact on the water resources is the selection of Representative Concentration Pathways (RCPs) and a general circulation model. The general circulation model used in this study is the second generation Canadian Earth System Model (CanESM2) developed by the Canadian Centre for Climate Modeling and Analysis (CCCma) of Environment Canada. Three RCPs (i.e. RCP2.6, RCP4.5, and RCP8.5) of the CanESM2 outputs were used for this study and the weather events corresponding to these three RCPs were downscaled with the help of the statistical downscaling model. Then, the bias correction techniques are introduced to the downscaled climate data to obtain the unbiased data of the future climate. Finally, the future changes in meteorological variables and surface runoff were analyzed with respect to the observed data in the baseline period (1975-2005). The climate of a particular region in the world is defined as the average statistical characteristics of the meteorological parameters such as temperature, precipitation, humidity and wind speed over an extended period, in which the World Meteorological Organization (WMO) is set as 30 years (IPCC, 2007). Therefore, the climate change impact on the water resources of the study basin was assessed by grouping the future climate scenarios into three periods (2011-2040), (2041-2070), and (2071-2099). The general procedures of this study to analyze the climate change impact assessment is given in Figure 3.4.

### **3.3.1. Emission Scenarios and General Circulation Models**

Global circulation models (GCMs) simulate the Earth's climate via mathematical equations that describe atmospheric, oceanic, and biotic processes, interactions, and feedbacks. They are the primary tools that provide reasonably accurate global, hemispheric, and continental-scale climate information and are used to understand present climate and future climate scenarios under increased greenhouse gas concentrations. Usually, in any climate change related study, GCMs are the starting point, as these provide the necessary data for such an investigation. Typically, current GCMs have a horizontal resolution (spacing between the grid points) in the order of hundreds of kilometers, 10 to 20 vertical layers in the atmosphere and up to 30 layers in the oceans (IPCC, 2011). For this study, the Canadian Centre for Climate Modeling and Analysis dataset of the Coupled Model Intercomparison Project phase 5 (CMIP5) that referenced in the Intergovernmental Panel on Climate Change Fifth (IPCC5) Assessment Report was considered for the analysis of the climate change impact in the study area. However, for assessing the hydrological impacts of climate change at the watershed and the regional scale, this GCM outputs cannot be used directly due to the mismatch in the spatial resolution between the GCMs and hydrological models. In principle, hydrological models run at a very fine spatial resolution (in the order of tens of kilometers, or even less) while the spatial resolution of GCMs is quite coarse, with a grid size of

about 100–500 kilometers. Each modeled grid cell is homogeneous, (i.e. within the cell there is one value for a given variable). Downscaling is simply a process of converting the coarse spatial resolution of the GCM output into a fine resolution which can involve generating point/station data of a specific area by using the GCM climatic output variables. In a climate change simulation using GCM, the driving forces of greenhouse gas (GHG) emissions are set to vary with time on the basis of an emission scenario. Initial conditions are set according to the current or ‘baseline’ climate, and the GCM is run. Changes in the key climatic variables are then investigated by their comparison between simulated present and future climates. The Representative Concentration Pathways (RCPs) is the latest generation of scenarios that provide input to climate models. Scenarios have long been used by planners and decision makers to analyze situations in which outcomes are uncertain. In climate research, emissions scenarios are used to explore how much humans could contribute to future climate change uncertainties in factors such as population growth, economic development, and development of new technologies. The purpose of using scenarios is not to predict the future, but to explore both the scientific and real-world implications of different plausible futures. Over time, different approaches of climate change scenarios have been used in hydrological uncertainty research; from stylized representations of annual percentage increases in global average concentrations of greenhouse gases to advanced

representations of emissions of many gases and particles affecting climate and derived from specific socioeconomic and technology assumptions. The scenarios reported by the Intergovernmental Panel on climate change were SA90, IS92, a special report on emission and scenarios (SRES), and representative concentration pathways (RCP) in 1<sup>st</sup> (1990), 2<sup>nd</sup> (1992), 3<sup>rd</sup> & 4<sup>th</sup> (2000), and 5<sup>th</sup> (2009) assessment report, respectively.

The new approach was built around the concept of Representative Concentration Pathways (RCPs). RCPs are time and space dependent trajectories of concentrations of greenhouse gases and pollutants resulting from human activities, including changes in land use (Van Vuuren *et al.*, 2011). RCPs provide a quantitative description of concentrations of the climate change pollutants in the atmosphere over time, as well as their radiative forcing in 2100 (for example, RCP 6 achieves an overall impact of 6 watts per square meter by 2100). The word “representative” signifies that each RCP provides only one of many possible scenarios that would lead to the specific radiative forcing pathway. Radiative forcing is a measure of the additional energy taken up by the Earth system due to increases in climate change pollution.

A key difference between the new RCPs and the previous scenarios is that there are no fixed sets of assumptions related to population growth, economic development, or technology associated with any RCP (Van Vuuren *et al.*, 2011). Many different socio-economic futures are possible

leading to the same level of radiative forcing. In previous scenarios, for example, the SRES, analysis started with a socio-economic storyline from which emission trajectories and climate impacts were assessed. Another key difference is that the RCPs are spatially explicit and provide information a global grid at a resolution of approximately 60 kilometers (Van Vuuren *et al.*, 2011).

**- RCP 2.6 – Low emissions**

The RCP2.6 was developed by PBL Netherlands Environmental Assessment Agency. Here radiative forcing reaches 3.1 W/m<sup>2</sup> before it returns to 2.6 W/m<sup>2</sup> by 2100. Ambitious greenhouse gas emissions reductions would be required over time to reach such forcing levels. The future would require: declining use of oil, low energy intensity, a world population of 9 billion by the year 2100, use of croplands increase due to bio-energy production, more intensive animal husbandry, methane emissions reduced by 40 percent, CO<sub>2</sub> emissions stay at today's level until 2020, then decline and become negative in 2100, and CO<sub>2</sub> concentrations peak around 2050, followed by a modest decline to around 400 ppm by 2100 (Van Vuuren *et al.*, 2011).

**- RCP 4.5 – Intermediate emissions**

The RCP4.5 was developed by the Pacific Northwest National Laboratory in the US. Here radiative forcing is stabilized shortly after the year 2100, consistent with a future with relatively ambitious emissions reductions. The

future is in conformity with lower energy intensity, active reforestation programs, decreasing use of croplands and grasslands due to yield increases and dietary changes, stringent climate policies, stable methane emissions, CO<sub>2</sub> emissions increase only slightly before decline commences around 2040 (Van Vuuren *et al.*, 2011)

- ***RCP 6 – Intermediate emissions***

The RCP6 was developed by the National Institute for Environmental Studies in Japan. Radiative forcing is stabilized shortly after the year 2100, which is consistent with the application of a range of technologies and strategies for reducing greenhouse gas emissions. The future is in line with heavy reliance on fossil fuels, intermediate energy intensity, increasing use of croplands and declining use of grasslands, stable methane emissions, and CO<sub>2</sub> emissions peak in 2060 at 75 percent above today's levels, then decline to 25 per cent above today (Van Vuuren *et al.*, 2011).

- ***RCP 8.5 – High emissions***

The RCP8.5 is consistent with a future with no policy changes to reduce emissions. It was developed by the International Institute for Applied System Analysis in Austria. It is characterized by increasing greenhouse gas emissions that lead to high greenhouse gas concentrations over time. The future is consistent with three times today's CO<sub>2</sub> emissions by 2100, rapid increase in methane emissions, increased use of croplands and grassland

which is driven by an increase in population, a world population of 12 billion by 2100, lower rate of technology development, heavy reliance on fossil fuels, high energy intensity, no implementation of climate policies (Van Vuuren *et al.*, 2011).

The RCP2.6, RCP4.5, and RCP8.5 emission scenarios were considered for this study to analyze the climate change impact on the water resources of the Lake Tana Basin.

### **3.3.2. Statistical Downscaling Models**

Various methods have been developed to bridge the gap between what GCMs can deliver and what society/businesses/stakeholders require for decision making. In broad terms, downscaling techniques can be classified as dynamical downscaling and statistical downscaling. Dynamical downscaling relies on the use of a regional climate model (RCM), similar to a GCM in its principles but with high resolution. RCMs take the large-scale atmospheric information supplied by GCM output at the lateral boundaries and incorporate more complex topography, the land-sea contrast, surface heterogeneities, and detailed descriptions of physical processes to generate realistic climate information at a spatial resolution of approximately 10–50 kilometers. RCMs models cannot meet the needs of spatially explicit models of hydrological systems. Hence there remains the need to downscale the results from such models to individual sites or localities for impact studies

(Xu, 1999). Statistical downscaling requires quantitative relationships between large-scale atmospheric variables/ GCM outputs (predictors), and local scale observed variables (predictands) (Wilby *et al.*, 2006). Mathematically, this relationship can be written as:

$$Y = f(X) \tag{3.11}$$

where  $Y$  is the predictand,  $X$  is the predictor, and  $f$  is the transfer function which has to be determined empirically from historical observations.

Once a relationship has been determined and validated, future atmospheric variables that GCMs project are used to predict future local climate variables. Statistical downscaling can produce site-specific climate projections, which RCMs cannot provide. Several statistical models have been developed over the last few decades, such as the Weather GENERator (WGEN) (Richardson, 1981), the CLimate GENERator (CLIGEN) (Nicks and Gander, 1994), the Statistical Downscaling Model (SDSM) (Wilby, 2002), and the Long Ashton Research Station-Weather Generator (LARSWG) (Semenov and Barrow, 2002). This study used the widely used statistical downscaling model (SDSM) (Wilby *et al.*, 2002) for generating the local-scale meteorological variables from the large-scale model outputs. The mathematical details of the SDSM are provided in the study by Wilby *et al.* (1999).

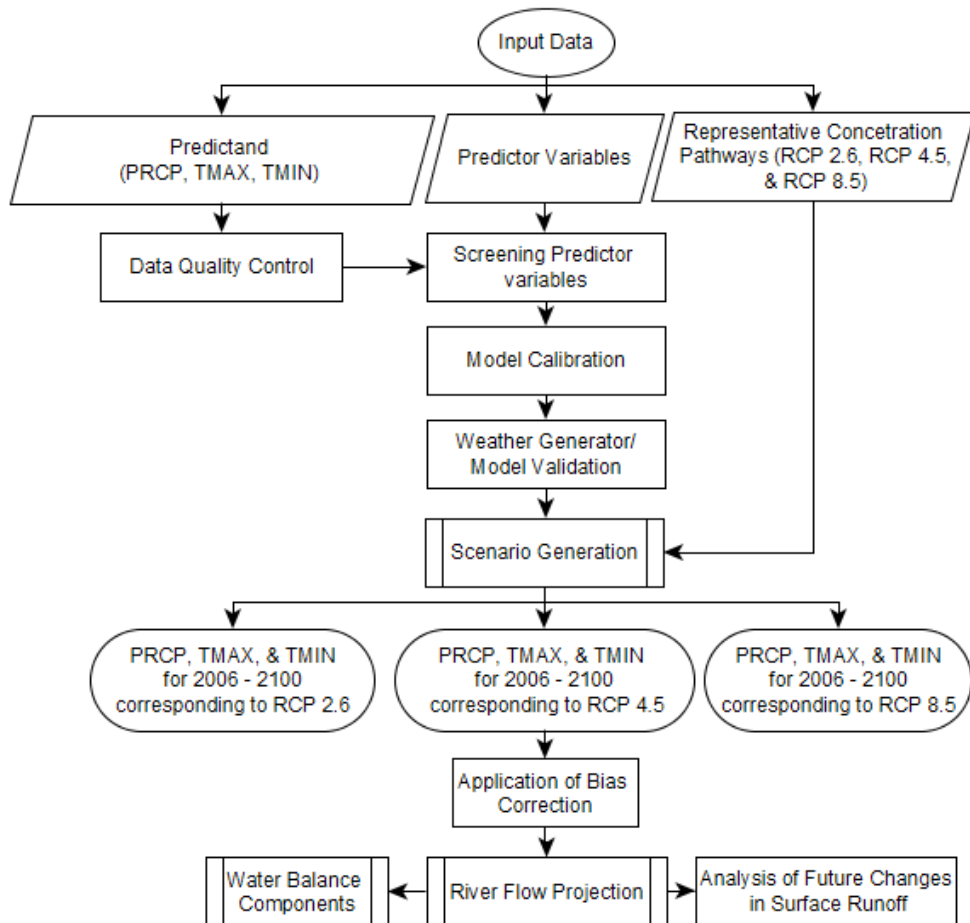


Figure 3.4. The general procedure for the assessment of the climate change impact on the water resources of the LTB

Table 3.4. Advantages, disadvantages, and requirements of dynamical and statistical downscaling

<b>Criteria</b>	<b>Dynamical downscaling</b>	<b>Statistical downscaling</b>
Requires	High computational resources and expertise, high volume of data inputs, and reliable GCM simulations	Medium/low computational resources, Medium/low volume of data inputs, sufficient amount of good quality observational data, and reliable GCM simulations
Advantages	Resolves atmospheric and surface process occurring at sub GCM grid scale, Based on consistent, physical mechanism, and not constrained by historical record so that novel scenarios can be simulated	Computationally inexpensive and efficient relies on the observed climate as a basis for driving future projections, can provide point-scale climate variables for GCM-Scale output, tools are freely available and easy to implement and interpret
Disadvantage	Computationally intensive, limited number of RCMs available freely, may require further downscaling and bias correction of RCM outputs, results depend on RCM assumptions, and affected by bias of driving GCM	Assumptions of the relationships between large and local-scale processes will remain the same in the future (stationary assumption), and high quality observed data might be unavailable for many areas or variables

### **3.4. Multi-objective Optimization of the Multi-reservoir System**

Reservoir operation management can be defined as a balancing of available water resources and demand, such as energy production and irrigation. The balanced operation is a complex task that requires a reservoir operation policy since each reservoir has different limitations and requirements. In reservoir operation, some factors need to be considered including inflow, outflow, reservoir elevation, and evaporation. Therefore, the decision for reservoir releases has to consider the restrictions due to physical and environmental constraints. Moreover, the multi-objective reservoir operation system requires the consideration of conflicting multiple objectives in an efficient way. For this, it is more convincing to find ‘Pareto-optimal’ solutions than a single optimal solution.

Multi-objective optimization techniques have been used for managing and operating complex reservoir systems (Cai *et al.*, 2001; Chang and Chang, 2001; Huang *et al.*, 2002; Huang and Yuan, 2004; Chang *et al.*, 2005; Kim *et al.*, 2006; Reddy and Kumar, 2006; Chen *et al.*, 2007; Chiu *et al.*, 2007; Yang *et al.*, 2007; Chang, 2008; Chen and Chang, 2009). A genetic algorithm was the widely used method in those previous studies.

Genetic Algorithm (GA) is a search procedure based on the mechanics of natural selection and natural genetics that combine artificial survival of the fittest with genetic operators abstracted from nature. A population of starting chromosomes that are randomly generated to represent the

problem's initial solutions goes through the process of the GA. Searching for an optimal design from a population of possible designs instead of a single design allows the GA to maintain a multipoint perspective on many regions of the solution space at the same time, resulting in a high probability of locating the global optimum (Goldberg, 1989).

This study focused on the application of Multi-objective Genetic Algorithm (MOGA) to the ongoing and proposed multi-reservoir systems in the Lake Tana Basin. The solutions of MOGA yield a trade-off relationships between the various objectives by identifying a population of points that define optimal solutions of the formulated problem. In this case, the goal of the search algorithm becomes the identification of a set of solutions which are non-dominated by any others.

The main idea of multi-objective optimization is the notion of Pareto dominance, in which a solution is said to be Pareto dominate another if the first is not inferior to the second in the objective space. There is no single solution to this multi-objective problem. Therefore, the goal of the multi-objective genetic algorithm is to find a set of efficient solutions for the formulated model. The set of these efficient solutions is also known as a Pareto front along which all solutions are optimal.

For solving the multi-objective optimization problems, a number of evolutionary algorithms were suggested during the last two decades, such as: the Strength-Pareto Evolutionary Algorithm (Zitzler and Thiele, 1999),

Non-dominated Sorting Genetic Algorithm (Srinivas and Deb, 1994), Niche Pareto Genetic Algorithm (Horn *et al.*, 1994), Particle Swarm Optimization (Kennedy and Eberhart, 1995), Pareto-Archived Evolution Strategy (Knowles and Corne, 2000), and Non-dominated Sorting Genetic Algorithm-II (Deb *et al.*, 2002). Deb *et al.* (2002) compared various multi-objective evolutionary algorithms. They showed that the Non-dominated Sorting Genetic Algorithm-II (NSGA-II) outperforms Pareto-Archived Evolution Strategy and Strength-Pareto Evolutionary Algorithm in converging nearer to the true Pareto-optimal set. Therefore, this study applied the NSGA-II principle to solve the multi-objective reservoir operation problem in the Lake Tana Basin. This algorithm uses elitism to preserve the best solutions and to speed up the convergence, in which the combination of parents and offspring population are grouped into different fronts and the best individuals selected for the next generation (Reddy and Kumar, 2006).

The algorithm first initializes the population within the specified decision variables range, and then different alternatives are generated and classified into different fronts based on the non-dominated sorting principle. The population was then selected for the next generation based on their fitness value rank. The crowding distance assignment operator (Deb *et al.*, 2002) helps to measure the concentration of population and keeps the most-fit population down to the specified fraction to maintain a diverse

population by using the Pareto front population fraction. The crossover and mutation operations were performed, in which the mutation make a small random change in the individuals of the population that provides genetic diversity to enable the genetic algorithm to search a broader space, and the crossover combines two individuals to form a new individual for the next generation. The heuristic approach was also used for this study to perform the crossover in which the best individuals from one subpopulation replace the worst individuals in another subpopulation. The general flowchart of the NSGA-II is provided in Figure 3.4.

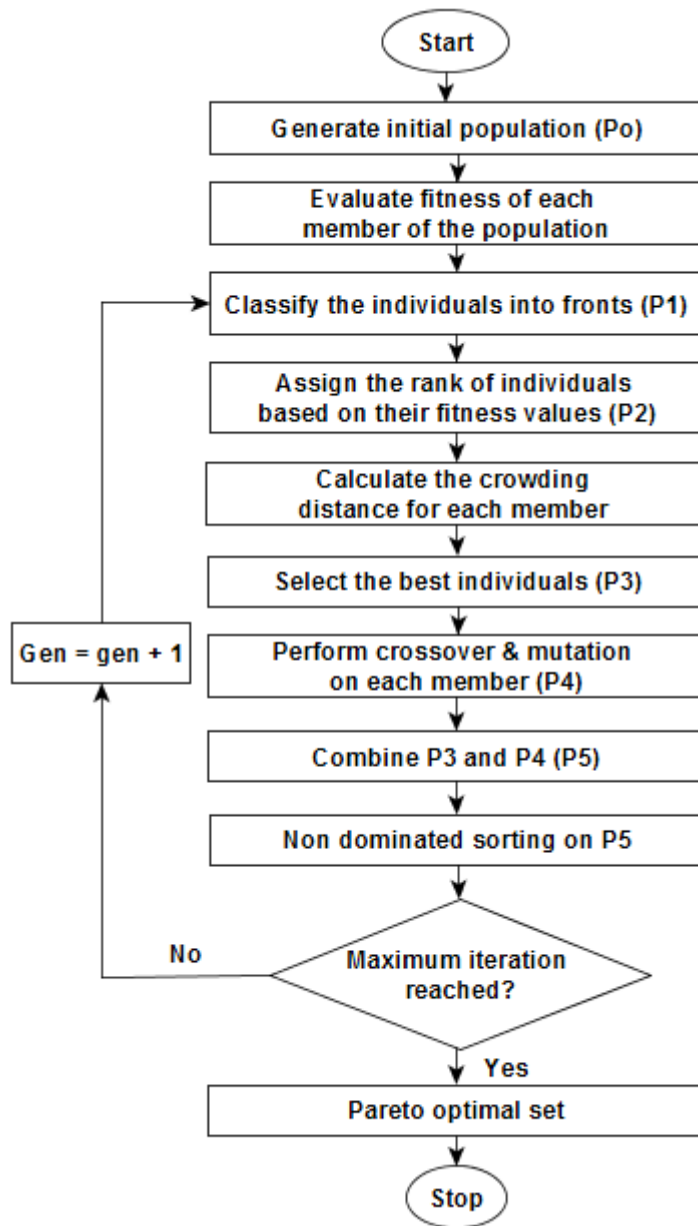


Figure 3.5. Flowchart of the multiobjective genetic algorithm

## CHAPTER FOUR

### 4. Selection of Hydrologic Modeling Approaches for

#### Assessment of Water Resources in the Lake Tana Basin

**Summary:** Good hydrologic models are needed to manage water resources of the Lake Tana Basin, but model comparison studies have not been carried out for this area. In this chapter, the daily streamflows were simulated by applying two simple conceptual models and one physically-based, semi-distributed model for four major gauged catchments of the study area and compared their performances in both time and quantile domains. The best model in the time domain can be applied for management and real-time operation, whereas the best model in the quantile domain can be implemented for planning and climate change impact assessment. Six performance measures were used: the Nash–Sutcliffe efficiency, percent bias, the coefficient of determination, drought indices, flood indices, and ratio of the root-mean-square error to the standard deviation of measured data. Global sensitivity analysis was performed for the complex model to reduce the number of flow parameters; effective hydraulic conductivity in main channel alluvium was the most sensitive parameter, followed by the curve number. The optimal number of partitioned subbasins for this model was also evaluated. For reproducing observed streamflow in the time domain, the simple conceptual models performed best for smaller gauged

watersheds, whereas the complex model performed best for the largest gauged catchment. For reproducing observed streamflow in the quantile domain, the simple conceptual models performed best for simulation of high, moist, mid-range, and dry flows in the Gilgelabay watershed; of dry and low-flows in the Gummera and Megech watersheds; and of high flows in the Ribb watershed. For the remaining flow ranges of each watershed, the complex model performed better. In general, our results do not indicate that any particular hydrologic model of those evaluated is superior. Therefore, integrating these three rainfall-runoff models may be suitable for assessment, planning, and management of water resources in the Lake Tana Basin.

#### **4.1. Introduction**

The Ethiopian government has identified the Lake Tana Basin (LTB) as a region for irrigation and hydropower development, which are vital for food security and economic growth in Ethiopia (MoFED, 2006). Because of this basin's significant water resources potential, some irrigation and hydropower projects are planned for the near future in the LTB. However, in more than a decade, few water balance studies have been conducted in this basin (e.g. Conway, 1997; Kebede *et al.*, 2006; SMEC, 2007; Wale *et al.*, 2009). Most of these previous studies estimated the water balance within the basin but produced notably different results. For example, Kebede *et al.* (2006) concluded that the four major watersheds (Gilgelabay, Gummera,

Ribb, and Megech) contribute 93% of the inflow into Lake Tana, whereas SMEC (2007) and Wale *et al.* (2009) reported values of 71% and 58%, respectively, for the same four watersheds. The reasons for these differences remain unclear, however, because each study has used different models and parameter estimation schemes to simulate hydrological processes. A commonly used approach to overcome this problem is to perform a model intercomparison study, but no comparative studies have been conducted for the LTB. For this study, two lumped models, IHACRES (the Identification of Unit Hydrographs And Component flows from Rainfall, Evaporation, and Streamflow data model (Croke and Jakeman, 2004)), and GR4J (modèle du Génie Rural à 4 paramètres Journalier (Perrin *et al.*, 2003)), and one semi-distributed model, SWAT (Soil and Water Assessment Tool (Arnold *et al.*, 1998; Arnold and Fohrer, 2005)), were applied for the four major gauged catchments of the LTB, and the capabilities of these models in reproducing the observed discharge frequency distributions, as well as the observed hydrographs, were compared.

Various investigations of distributed and lumped hydrologic models have been conducted (e.g. Krajewski *et al.*, 1991; Refsgaard and Knudsen, 1996; Shah *et al.*, 1996; Refsgaard, 1997; Bergstrom and Graham, 1998; Boyle *et al.*, 2001; Koren *et al.*, 2004; Reed *et al.*, 2004; Smith *et al.*, 2004; Zhang *et al.*, 2004; Modrick and Georgakakos, 2006). In a case study by Krajewski *et al.* (1991), the lumped model tended to underestimate flood

peaks compared to the distributed model. However, most of these studies have reported that distributed models may or may not provide any improvement over lumped models (e.g. Refsgaard, 1997; Reed *et al.*, 2004). This study mainly addresses the performance comparison of lumped and physically-based semi-distributed hydrological models for assessment of the surface water resources of the LTB. Furthermore, we evaluate the effects of the number of partitioned subbasins on the performance of the physically-based semi-distributed model.

## **4.2. Methodology**

### **4.2.1. Hydrological Model Calibration Methods**

For the SWAT model, observed daily weather data recorded over 32 years, from 1983 to 2014, collected from 13 weather gauging stations (the Adet, Addiszemen, Ayikel, Bahir Dar, Dangila, Enfranze, Enjibara, Gonder, Gorgora, Maksegnit, Merawi, Woreta, and Zege stations) were input. To use the same input data for SWAT as well as the two simple conceptual models, areal rainfall data generated with the Thiessen polygon method (Thiessen, 1911) and potential evapotranspiration data generated with the Penman–Monteith method (Monteith, 1965) in the SWAT model were used as the input data for the IHACRES and GR4J models. Observed flow time series from 1995 to 2009 for the Ribb catchments and from 1998 to 2012 for the Gilgelabay, Gummera, and Megech catchments were used for model fitting.

The observed weather data from the 13 weather gauging stations were retrieved from the Ethiopian National Metrological Agency, whereas the spatial input data (digital elevation model (DEM), land use, and soil data), and observed streamflow data were provided by the Ministry of Water, Irrigation & Energy of Ethiopia.

In the study area, there is a great deal of observational data missing for metrological conditions and flow before 1998 for the Gilgelabay, Gummera, and Megech catchments, and prior to 1995 for the Ribb catchment. Therefore, only more recent flow data from the Gilgelabay, Gummera, and Megech catchment (1998–2012) and the Ribb catchment (1995–2009) were used to evaluate the capabilities of these three hydrological models in reproducing the observed discharge frequency distributions and hydrographs. For the three hydrological models, we used a k-fold cross-validation with  $k = 4$  folds, 9 years for calibration, and 3 years for validation. The main reasons for using cross-validation instead of the conventional validation method (e.g. partitioning the dataset into two sets of 70% for training and 30% for testing) is that the error (e.g. the root-mean-square error (RMSE)) for the training dataset in the conventional validation is not a useful estimator of model performance, and therefore the error measure calculated for the testing dataset does not suitably represent model performance (Grossman *et al.*, 2010). The reason for this limitation is that there are insufficient data available to be partitioned into training and testing sets for

the conventional validation method. In these cases, an appropriate way to estimate model prediction performance is to use cross-validation, which is a powerful general technique (Grossman *et al.*, 2010). Multiple rounds of cross-validation were performed using different partitions to reduce variability, and the validation results were averaged across these rounds.

We used the Shuffled Complex Evolution (SCE) algorithm (Duan *et al.*, 1993), an optimization algorithm in the Hydromad R package (Andrews *et al.*, 2011), to optimize the parameters of the simple conceptual models. However, the Particle Swarm Optimization (PSO) algorithm, one of the optimization programs integrated with SWAT-CUP (SWAT Calibration and Uncertainty Programs), was used to optimize the SWAT flow parameters. The PSO algorithm is a population-based stochastic optimization technique developed by Eberhart and Kennedy (1995), who were inspired by the social behavior of flocking birds and schooling fish. The objective function applied for estimation of parameters for all three rainfall–runoff models was the well-known Nash–Sutcliffe efficiency method (Nash and Sutcliffe, 1970), as given below:

$$NSE = 1 - \frac{\sum_{i=1}^n (O_i - P_i)^2}{\sum_{i=1}^n (O_i - \bar{O})^2} \quad (4.1)$$

where  $P_i$  is the simulated value,  $O_i$  is the measured value, and  $\bar{O}$  is the average measured value.

#### 4.2.2. Model Sensitivity and Uncertainty Analysis

Over-parameterization is a well-known and frequent problem with hydrological models (Box and Jenkins, 1976), mainly distributed models (Beven, 1989). Sensitivity analysis methods designed to reduce the number of parameters that require fitting with input–output data are common (e.g. Spear and Hornberger, 1980). Therefore, for this study, parameter sensitivity and uncertainty analyses were carried out for the most complex of the three models (SWAT). Sensitivity analyses are often referred to as either "local" or "global". A local analysis addresses sensitivity relative to point estimates of parameter values, whereas a global analysis determines sensitivity with regard to the entire distribution of a parameter. Global sampling methods randomly or systemically scan the entire range of possible parameter values and sets. The sampled parameter sets can give the user a good idea of the importance of each parameter. These, in turn, can be used to quantify the global parameter sensitivity and the uncertainty of parameters and outputs. The sampling strategy is essential to this method (Van Griensven *et al.*, 2006). One sampling strategy is using Latin Hypercube (LH) simulations. The concept of LH simulation (McKay *et al.*, 1979; Iman and Conover, 1980; McKay, 1988) is based on Monte Carlo simulation, but a stratified sampling approach is used that allows efficient estimation of the output statistics. The distribution of each parameter is subdivided into  $N$  strata with a probability of occurrence equal to  $1/N$ .

In this study, SWAT-CUP was used for the global sensitivity and uncertainty analyses, and parameter sensitivities were determined by calculating the multiple regression systems that regress the Latin-hypercube-generated parameters against the objective function values. A t-test was then used to identify the relative significance of each parameter. A description of the SWAT flow parameters used for this study is provided in Table 4.1.

For a given parameter value, the model defines an input–output map that maps some specific set of allowed model inputs to model outputs. The uncertainties of parameters, expressed as ranges, account for all sources of uncertainty, such as the uncertainty in deriving variables (e.g. rainfall and temperature), the model structure, parameters, and measured data (Abbaspour, 2012). Propagation of the uncertainties in the parameters leads to uncertainties in the model output variables, which are expressed as the 95 % Prediction Uncertainty (95PPU). These uncertainties are calculated at the 2.5% and 97.5% levels of the cumulative distribution (disallowing the worst 5% of the simulations) of the output variables generated by the propagation of parametric uncertainties using LH sampling (Abbaspour, 2012). We have used the percentage of observations covered by the 95PPU (P-factor) and the relative width of the 95PPU (r-factor) to quantify the fit between simulation results expressed as 95PPU and observational data expressed as a single signal. A P-factor of one and an r-factor of zero represent a simulation that exactly corresponds to the measured data. In the

SWAT-CUP manual, it is suggested that a P-factor value of greater than 0.7 and r-factor of around one is recommended.

#### **4.2.3. Model Comparison Methods**

The three rainfall–runoff models were compared based on their performances in the time domain and the quantile domain. The time-domain approaches compare the simulated and the observed flow series at every unit time while the quantile domain approach does so at specified quantiles. The first has been commonly employed but the second is more reasonable for the planning purpose of climate change assessment where the macroscopic water balance match is more meaningful than the microscopic hydrological process simulation (Table 4.2). In this study, we used two approaches but compare the simulated and the observed flows with respect to five flow zones: high flows (0–10%), moist flows (10–40%), mid-range flows (40–60%), dry conditions (60–90%), and low flows (90–100%) in a flow duration curve (Kannan and Jeong, 2011).

Table 4.1. Description of the key flow parameters for the SWAT model

<b>Parameters</b>	<b>Description</b>	<b>Parameter range</b>
CH_K2	Effective hydraulic conductivity in main channel alluvium	5.0 – 130.0
ALPHA_BNK	Base flow alpha factor for bank storage	0.0 – 1.0
SOL_BD	Moist bulk density	-0.5 – 0.6
SOL_K	Saturated hydraulic conductivity	-0.8 – 0.8
ALPHA_BF	Base flow alfa factor	0.0 – 1.0
CN2	SCS runoff curve number	-0.2 – 0.2
CH_N2	Manning's "n" value for the main channel	0.0 – 0.3
SOL_AWC	Available water capacity of the soil layer	-0.2 – 0.4
GW_DELAY	Groundwater delay time	30.0 – 450.0
GW_REVAP	Groundwater "revap" coefficient	0.0 – 0.2
ESCO	Soil evaporation compensation factor	0.8 – 1.0
GWQMN	Threshold depth of water in shallow aquifer required for return flow	0.0 – 2.0

Table 4.2. Model comparison methods

<b>Validation</b>	<b>Time-domain</b>	<b>Quantile-domain</b>
Unit time	Short	Long
Management	Operation	Planning
Process	Microscopic	Macroscopic
Application	Real-time forecasting	Climate change assessment

#### 4.2.4. Combination of Rainfall-Runoff Model Outputs

Hydrologists often have available two or more alternative hydrological models for the assessment of the surface water resources. One possibility is to select a single hydrological model, either on subjective grounds or past performance of the hydrological model. An alternative strategy is to assess the performance of a combined model output to improve the performance of the individual models. The combining concept has been widely used in economic forecasting; it has received almost no attention in hydrologic forecasting or simulation studies (Kim, *et al.*, 2006). The main idea of weighting model outputs that provide unique information is to combine two or more model outputs that incorporate diverse information like the model outputs from the complex and the simple rainfall-runoff model. The underlying idea is that the systematic and random errors of individual model outputs are more likely to cancel out in the aggregate if the individual models draw on different information, and are thus likely uncorrelated. The following methods were used for combining the three model outputs (Kim, *et al.*, 2006; Jeong and Kim, 2009).

##### - *The simple average method (SAM)*

The simple average method is the simplest method of combining the outputs of different individual models. Considering  $K$  model outputs  $F_{t,i}$  available at

time  $t$ , the simple average method to estimate the combined output  $F_{t,c}$  can be expressed as:

$$F_{t,c} = \frac{1}{K} \sum_{i=1}^K F_{t,i} \quad (4.2)$$

- *The weighted average method (WAM)*

The use of the simple average method for combination of model outputs can be quite inefficient when some of the individual models selected for combination appear to be consistently more accurate than others (Armstrong, 1989). In this case, the use of a weighted average would be considered.

The weighted average method for combining the outputs  $K$  rainfall-runoff models may be expressed as:

$$F_{t,c} = \sum_{i=1}^K w_i F_{t,i} \quad (4.3)$$

where  $F_{t,i}$  is the rainfall-runoff model outputs of each model,  $w_i$  is the weights assigned to the  $i^{\text{th}}$  model outputs  $F_{t,i}$ .

The main reason of constraining the sum of the weights to one is to ensure that if the individual model outputs are unbiased, the combination of model outputs will also be unbiased (Jeong and Kim, 2009).

Let  $F_{t,i}$  ( $i = 1, \dots, K, t = 1, \dots, n$ ) be model outputs of  $Q_t$ ; then we will have observed the model output errors

$$e_{t,i} = Q_t - F_{t,i} \quad (4.4)$$

where  $e_{t,i}$  is the errors with zero means, individual variances  $\sigma_i^2$  and covariance  $\sigma_{ij}^2$ .

In the case of combining two model outputs, the weight that gives the minimum error variance (Granger and Newbold, 1977) can be obtained by

$$w_1 = \frac{\sigma_2^2 - \sigma_{12}}{\sigma_1^2 + \sigma_2^2 - 2\sigma_{12}} \quad (4.5)$$

$$w_2 = \frac{\sigma_1^2 - \sigma_{12}}{\sigma_1^2 + \sigma_2^2 - 2\sigma_{12}} \quad (4.6)$$

If  $K$  model outputs are available to combine, their weights is given by

$$w_i = \left( \sum_{t=1}^n e_{t,i}^2 \right)^{-1} / \sum_{j=1}^K \left( \sum_{t=1}^n e_{t,j}^2 \right)^{-1} \quad (4.7)$$

Bates and Granger (1969) named this approach the variance-covariance method.

**- The sum of squared error method (SSEM)**

The sum of squared error method is a special case of the weighted average method where the errors in the individual model outputs are not correlated (Jeong and Kim, 2009). For combining two model outputs, the weights are given by:

$$w_1 = \frac{1/\sigma_1^2}{1/\sigma_1^2 + 1/\sigma_2^2} = \frac{\sigma_2^2}{\sigma_1^2 + \sigma_2^2} \quad (4.8)$$

$$w_2 = \frac{1/\sigma_2^2}{1/\sigma_1^2 + 1/\sigma_2^2} = \frac{\sigma_1^2}{\sigma_1^2 + \sigma_2^2} \quad (4.9)$$

If  $K$  model outputs are going to be combined, the weights can be obtained using equation 4.10.

$$w_i = \frac{1/\sigma_i^2}{\sum_{j=1}^K 1/\sigma_j^2} \quad (4.10)$$

- *Time-varying weights*

The usage of time-varying weights is often preferred when the properties of the model output errors vary in time. Granger and Newbold (1977) have made several suggestions for obtaining the time-varying weights.

$$\sigma_{t,i}^2 = \sum_{s=t-v}^{t-1} (e_{s,i})^2 / v \quad (4.11)$$

$$w_{t,i} = \frac{1/\sigma_{t,i}^2}{\sum_{j=1}^K 1/\sigma_{t,j}^2} \quad (4.12)$$

where  $v$  is the number of previous model output errors employed to calculate the weight.

- *The artificial neural network method (ANN)*

The artificial neural network method provides an alternative to the simple average and weighted average methods for combining the outputs of different models. The ANN is applied in the context of providing a non-

linear function mapping of a set of inputs into the network output. Figure 4.1 shows a schematic diagram of the one hidden layer and the three-layer feed forward neural network that used for combining the outputs of the three rainfall-runoff models.

The mathematical form of the artificial neural network, as described in the study by Jeong and Kim (2009), for  $K$  model outputs, is given by equation 4.13.

$$F_{t,c} = g_2 \left( \sum_{j=1}^J w_{1j} g_1 \left( \sum_{i=0}^K w_{ji} F_{t,i} \right) \right) \quad (4.13)$$

where  $F_{t,i}$  is the  $i^{\text{th}}$  constituent model output at time  $t$ . This set of signals is called the input layer of the network. The input layer signals are combined into  $J$  different weighted sums, which are fed into a non-linear activation function  $g_1$ . The output layer is the result of feeding a weighted sum of the hidden layer signals into a second activation function  $g_2$ . The weights  $w_{ji}$  control the strength of the connection between the input nodes and the hidden nodes, and the weights  $w_{1j}$  controls the strength of the connections between the hidden nodes and the output node.

In ANN modeling, we typically partition the dataset into three parts: a training set, a validation set, and a test set. The network was trained with the training set to adjust the weights of the neural network. The validation set can be used to minimize overfitting without adjusting the weights of the network. Finally, the accuracy of the model on the test data gives a realistic

estimate of the performance of the model on completely unseen data and to confirm the actual predictive power of the network. For this study, the data was partitioned into 70 %, 15 %, and 15 % for training, validation, and testing, respectively.

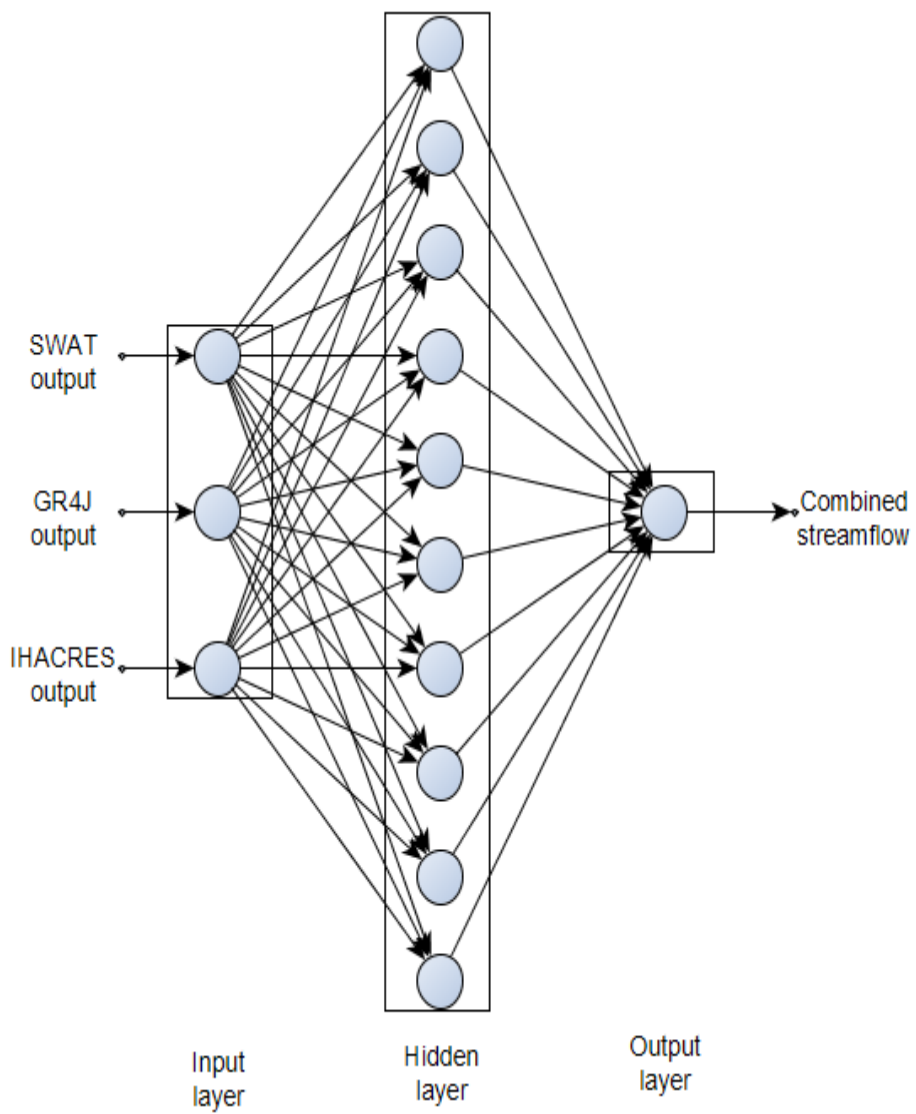


Figure 4.1. Schematic diagram of the artificial neural network

## **4.3. Application**

### **4.3.1. Application of the Physically Based Semi-distributed Model,**

#### **SWAT**

From the sensitivity analysis, the effective hydraulic conductivity in the main channel alluvium (CH\_K2) was found to be the most sensitive parameter for the Gilgelabay, Gummera, and Megech catchments, whereas the SCS runoff curve number (CN2) was found to be the most sensitive parameter for the Ribb catchment. On average, the effective hydraulic conductivity in the main channel alluvium (CH\_K2) was found to be the most sensitive flow parameter for the study basin (see Table 4.3) and eight flow parameters (i.e. CH\_K2, CN2, CH\_N2, ALPHA\_BNK, SOL\_K, ESCO, ALPHA\_BF, GW\_DELAY) showed significant impacts on the streamflow, which therefore would be estimated very carefully in this study. For the other non-sensitive parameters, the default values were used.

#### **- *SWAT Model Performances***

The values of the objective function (NSE) for the SWAT model are given in Table 4.4; these values show that the sensitivity of the model's performance is based on the number of partitioned subbasins. The model parameters were calibrated several times by varying the numbers of partitioned subbasins in the gauged catchments to determine the sensitivity of the model. The numbers of partitioned subbasins that found to generate

the best performance with the SWAT model were 45, 25, 45, and 3 for the Gilgelabay, Gummera, Megech, and Ribb catchments, respectively. In the Gilgelabay catchment, in particular, the performance of the model was improved when the number of partitioned subbasins was increased, which indicates that a fully distributed model would be valuable because of its physical heterogeneity. Figure 4.2 illustrates the objective function (NSE) as a function of the most sensitive parameter for each watershed. The main purpose of this graph is to show the distribution of the sampling points and to demonstrate the concept of parameter sensitivity.

Table 4.3. SWAT model flow parameter t-statistics and P-values

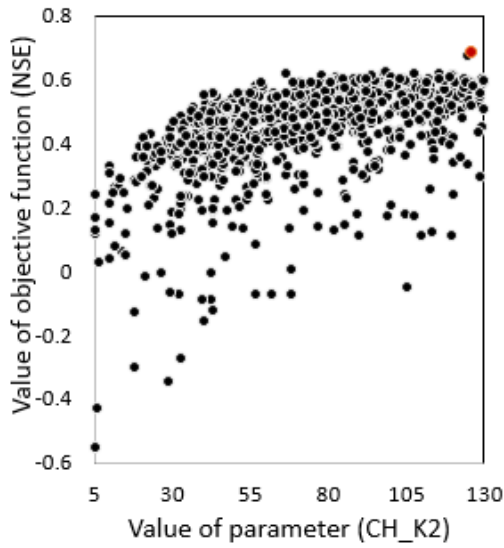
Rank	Parameter	Gilgelabay		Gummera		Rib		Megech		Average	
		t-Stat	P-Value	t-Stat	P-Value	t-Stat	P-Value	t-Stat	P-Value	t-stat	P-Value
1	CH_K2.rte	<b>17.30</b>	0.00	<b>26.45</b>	0.00	9.21	0.00	<b>21.12</b>	0.00	<b>18.52</b>	0.00
2	CN2.mgt	5.82	0.00	6.82	0.00	<b>-39.46</b>	0.00	-10.55	0.00	-9.34	0.00
3	CH_N2.rte	5.26	0.00	5.34	0.00	15.98	0.00	6.53	0.00	8.28	0.00
4	ALPHA_BNK.rte	-0.24	0.81	-2.71	0.01	-18.16	0.00	-8.27	0.00	-7.35	0.21
5	SOL_K.sol	0.74	0.46	-0.17	0.87	13.00	0.00	1.90	0.06	3.87	0.35
6	ESCO.hru	-3.15	0.00	-2.26	0.02	-5.77	0.00	-2.09	0.04	-3.32	0.02
7	ALPHA_BF.gw	1.02	0.31	2.85	0.00	-16.37	0.00	-0.04	0.97	-3.14	0.32
8	GW_DELAY.gw	-1.83	0.07	-11.2	0.00	8.33	0.00	-2.70	0.01	-1.85	0.02
9	GW_REVAP.gw	-1.40	0.16	1.84	0.07	1.97	0.05	1.59	0.11	1.00	0.09
12	GWQMN.gw	-0.59	0.56	-0.93	0.35	-0.48	0.63	-0.88	0.38	-0.72	0.48
11	SOL_AWC.sol	-1.14	0.25	-1.47	0.14	0.79	0.43	-0.31	0.75	-0.53	0.39
12	SOL_BD.sol	1.17	0.24	-1.95	0.05	0.15	0.88	-0.61	0.54	-0.31	0.43

Note: A larger absolute t-statistic values indicate higher sensitivity, and P-value close to zero indicates greater significance.

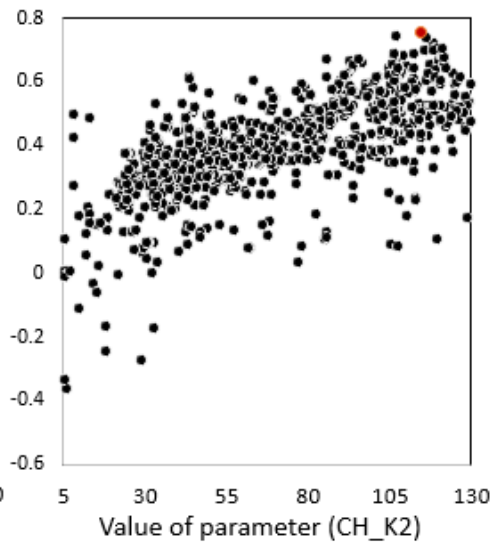
Table 4.4. NSE values of the SWAT model for the calibration and validation periods

Catchment	No. of Partitioned Subbasins	NSE Values									
		Fold-I		Fold-II		Fold-III		Fold-IV		Average	
		Calib	Valid	Calib	Valid	Calib	Valid	Calib	Valid	Calib	Valid
Gilgelabay	3	0.58	0.62	0.61	0.45	0.56	0.64	0.59	0.58	0.59	0.57
	17	0.62	0.63	0.64	0.52	0.61	0.66	0.61	0.65	0.62	0.62
	25	0.71	0.56	0.67	0.67	0.66	0.66	0.65	0.73	0.67	0.66
	45*	0.72	0.58	0.69	0.67	0.67	0.71	0.66	0.75	<b>0.69</b>	<b>0.68</b>
Gummera	3	0.66	0.70	0.66	0.67	0.69	0.56	0.66	0.70	0.67	0.66
	9	0.72	0.71	0.75	0.66	0.74	0.70	0.69	0.81	0.73	0.72
	25*	0.75	0.78	0.76	0.73	0.77	0.70	0.74	0.81	<b>0.76</b>	<b>0.76</b>
	45	0.71	0.77	0.73	0.70	0.72	0.70	0.73	0.71	0.72	0.72
Megech	3	0.27	0.26	0.21	0.56	0.30	0.17	0.35	-0.54	0.28	0.11
	11	0.32	0.18	0.21	0.49	0.26	0.27	0.30	-0.23	0.27	0.18
	25	0.32	0.18	0.21	0.49	0.26	0.29	0.30	-0.19	0.27	<b>0.19</b>
	45*	0.31	0.20	0.21	0.50	0.27	0.29	0.31	-0.27	<b>0.28</b>	0.18
Ribb	3*	0.51	0.41	0.40	0.73	0.50	0.31	0.52	0.40	<b>0.48</b>	<b>0.46</b>
	11	0.44	0.50	0.43	0.53	0.43	0.49	0.52	0.29	0.46	0.45
	25	0.44	0.36	0.34	0.66	0.41	0.40	0.50	0.25	0.42	0.42
	45	0.43	0.57	0.45	0.54	0.48	0.38	0.53	0.34	0.47	0.46

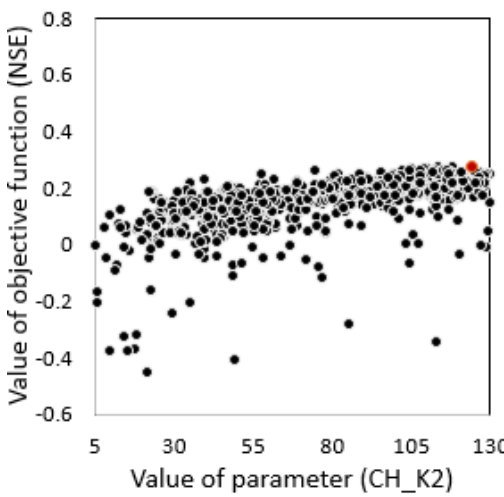
\*indicates the number of partitioned subbasins that yields optimal NSE value for the corresponding watershed



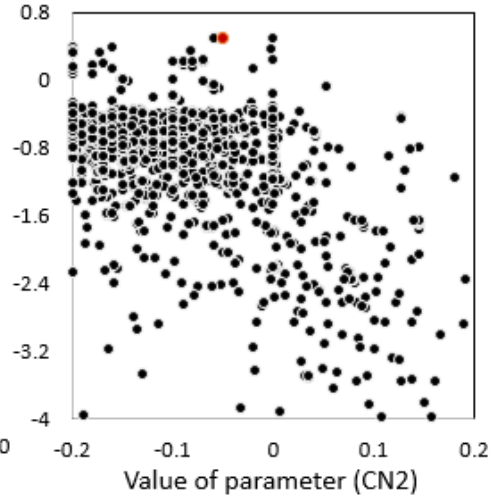
a) Scatter plot for the Gilgelabay



b) Scatter plot for the Gummera



c) Scatter plot for the Megech

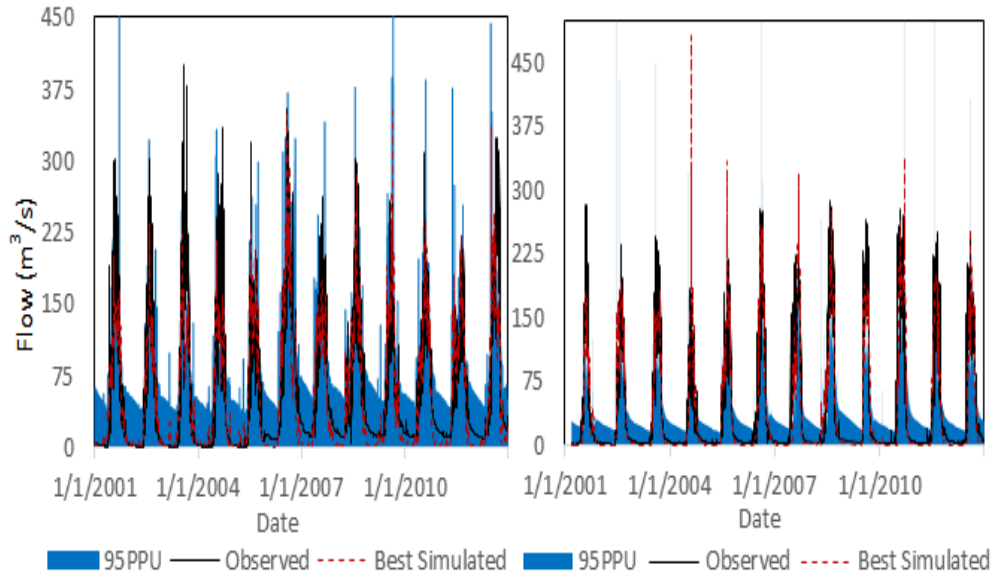


d) Scatter plot for the Ribb

Figure 4.2. The most sensitive parameters distribution for each watershed. The red dots represents the optimal values of the objective function (NSE).

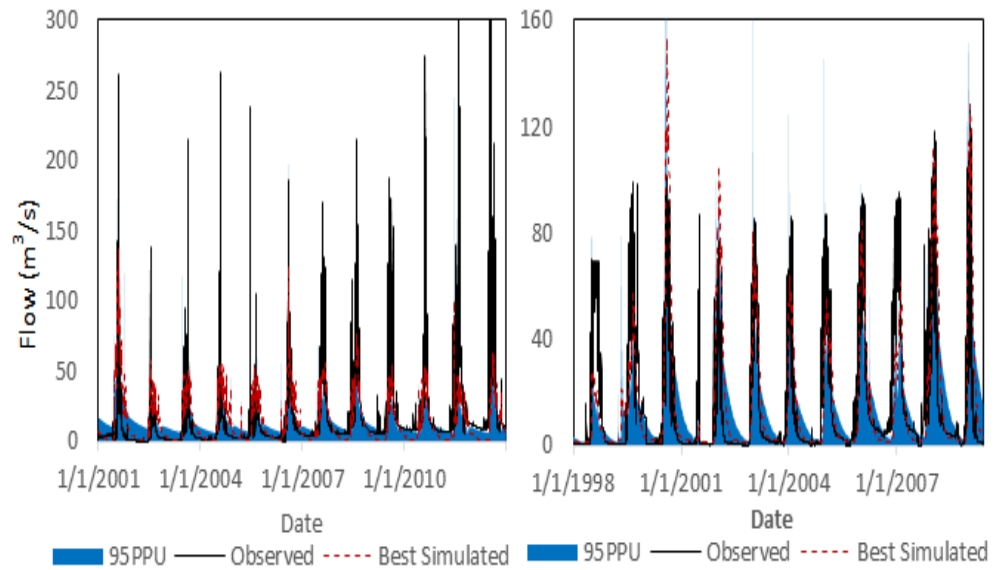
- *SWAT Model Uncertainty*

Figure 4.3 presents the 95% uncertainty band (which comprises all uncertainties in the model), observed streamflow, and the best-simulated streamflow plot. As mentioned before, we used the percentage of observations within the 95PPU (*P*-factor) and the relative width of the 95% probability band (*r*-factor) as performance indicators for the model in the estimation of uncertainty. Figure 4.3. shows *P*-factors of 0.64, 0.85, 0.74, and 0.44 and *r*-factors of 1.1, 0.78, 0.59, and 0.70 for the Gilgelabay, Gummera, Megech, and Ribb catchments, respectively. The *P*-factor and *r*-factor values for the Gilgelabay, Gummera, and Megech catchments were acceptable, but the *P*-factor value for the Ribb catchments was not within the acceptable limits, which indicates that the parameter uncertainties were not within the desired ranges for this catchment.



a) Gilgelabay catchment

b) Gummera catchment



c) Megech catchment

d) Ribb catchment

Figure 4.3. Observed flow, best-simulated flow, and the 95% uncertainty interval

### **4.3.2. Application of Simple Conceptual Models, IHACRES & GR4J**

The performance measure values of the two simple conceptual models are given in Figure 4.4 and Table 4.5. On average, the values of the NSE coefficients obtained for all four folds using the GR4J model structure fall within the ranges of 0.54–0.60, 0.76–0.77, 0.21–0.39, and 0.52–0.63 for the Gilgelabay, Gummera, Megech, and Ribb catchments, respectively. The NSE coefficients obtained using the IHACRES model structure fall within the ranges of 0.58–0.64, 0.78–0.79, 0.23–0.42, and 0.06–0.29 for the Gilgelabay, Gummera, Megech and Ribb catchments, respectively. The highest NSE coefficient values for both simple conceptual models were obtained for the Gummera catchment. The performance results of the two models from the validation period show a similar pattern to those from the calibration period. The NSE coefficients for the simulation of daily discharge for the validation period using the GR4J model vary within 0.5–0.66, 0.70–0.80, 0.11–0.42, and 0.41–0.67, and using the IHACRES model vary within 0.53–0.69, 0.76–0.8, 0.12–0.45, and 0.14–0.54, for the Gilgelabay, Gummera, Megech, and Ribb catchments, respectively. In general, these two conceptual models have comparable performance results for the Gilgelabay, Gummera, and Megech catchments, but the performance of the IHACRES model was poor for the Ribb catchment with NSE values. Because of the inferior performance of the IHACRES model for the Ribb catchment, the GR4J model is considered a more robust model, even though

the IHACRES model performs optimally for the Gilgelabay, Gummera, and Megech catchments.

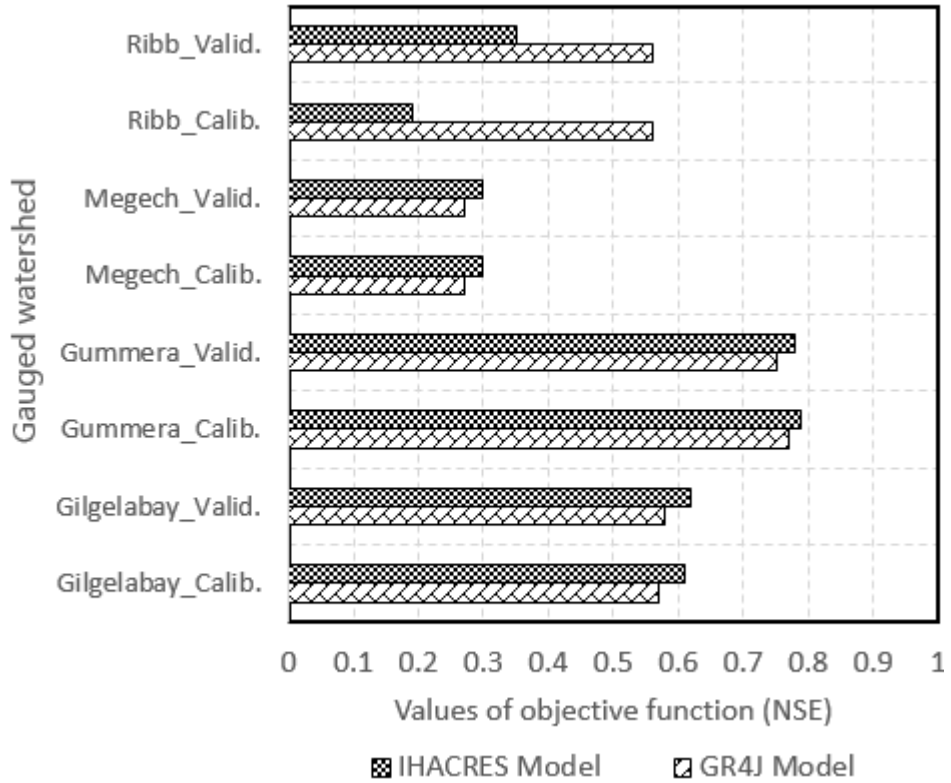


Figure 4.4. The average performance values of all folds for the simple conceptual models for each watershed.

“Calib.” and “Valid.” indicate the calibration and validation periods, respectively.

### **4.3.3. Comparison between the SWAT, IHACRES and GR4J Models**

#### ***- Model Comparison in the Time-domain***

The performance results based on the time-domain comparison of the three models are given in Table 4.5; these results concluded that the GR4J model yields better results for the Ribb catchment, that the SWAT model performed best for the Gilgelabay catchment, and that the IHACRES model produces better results for the Gummera and Megech catchments. The calibration of the three model parameters for the Megech catchments was found to be poor (see Table 4.5), which indicates that the three models did not effectively capture the hydrologic characteristics of the Megech catchment. Therefore, the simulation results of the models are unreliable, even worthless, for assessing hydrologic responses. For the SWAT model, this unfortunate result may be related to the insensitivity of the flow parameters (e.g. CH\_K2). In other words, CH\_K2 for the Megech catchment was not sensitive to the change in parameter values in terms of NSE (i.e. an almost horizontal line corresponding to parameter values), whereas it was very sensitive for the other catchments (Figure 4.2). In addition, the poor performances of the three models may be attributed by the models' capabilities of reproducing streamflow of mountainous areas, and to the quality of the measured data within and around the Megech catchment. For these reasons, the three models failed to reproduce streamflow of the Megech catchment. The IHACRES model showed extremely poor

performance for the Ribb catchment, whereas it did not perform worse for the other catchments. The poor result for the Ribb catchment was mainly caused by the model's failure to appropriately reproduce dry and low flows of the Ribb catchment (see Figure 4.6). For the three gauged catchments (Gilgelabay, Gummera, and Ribb), the GR4J and SWAT models captured the magnitudes and variabilities of observed streamflow at the corresponding gauged stations. The results do not indicate that any specific hydrologic model was superior or inferior to the others for regional water resources assessment and management, except the IHACRES model for the Ribb catchment. In general, the selected simple conceptual models (GR4J and IHACRES) performed comparably to a more complex model (SWAT) at a daily time step.

The box plots in Figure 4.5 present the variation of the three hydrological models' performances for each fold in terms of the values of the objective function (NSE) for all catchments. As shown by these box plots, the SWAT model produces better NSE values for the Gilgelabay catchment; the IHACRES model produces better NSE values for the Gummera and Megech catchments, and the GR4J model produces better NSE value for the Ribb catchment.

Table 4.5. Average performance measure values of all folds for each model

Watershed	Model	NSE		PBIAS		RSR		R <sup>2</sup>		Best model
		Calib	Valid	Calib	Valid	Calib	Valid	Calib	Valid	
Gilgelabay	GR4J	0.57	0.58	6.26	6.64	0.65	0.64	0.59	0.64	SWAT
	IHACRES	0.61	0.62	<b>0.95</b>	<b>1.06</b>	0.63	0.62	0.61	0.66	
	SWAT	<b>0.69</b>	<b>0.68</b>	4.79	4.87	<b>0.56</b>	<b>0.56</b>	<b>0.7</b>	<b>0.71</b>	
Gummera	GR4J	0.77	0.75	<b>-0.55</b>	<b>2.44</b>	0.48	0.50	0.77	0.77	IHACRES
	IHACRES	<b>0.79</b>	<b>0.78</b>	7.73	6.76	<b>0.46</b>	<b>0.47</b>	<b>0.79</b>	<b>0.8</b>	
	SWAT	0.76	0.76	7.34	7.29	0.50	0.50	0.77	0.78	
Megech	GR4J	0.27	0.27	30.60	13.20	0.85	0.85	0.32	0.42	IHACRES
	IHACRES	<b>0.30</b>	<b>0.30</b>	27.82	<b>9.12</b>	<b>0.84</b>	<b>0.83</b>	<b>0.34</b>	<b>0.44</b>	
	SWAT	0.28	0.18	<b>5.86</b>	-19.32	0.85	0.89	0.3	0.40	
Ribb	GR4J	<b>0.56</b>	<b>0.56</b>	7.40	<b>6.02</b>	<b>0.67</b>	<b>0.66</b>	0.57	0.60	GR4J
	IHACRES	0.19	0.35	-94.57	-60.44	0.90	0.80	<b>0.58</b>	<b>0.63</b>	
	SWAT	0.48	0.46	<b>-3.65</b>	-6.55	0.72	0.73	0.56	0.58	

Bold figures are best results

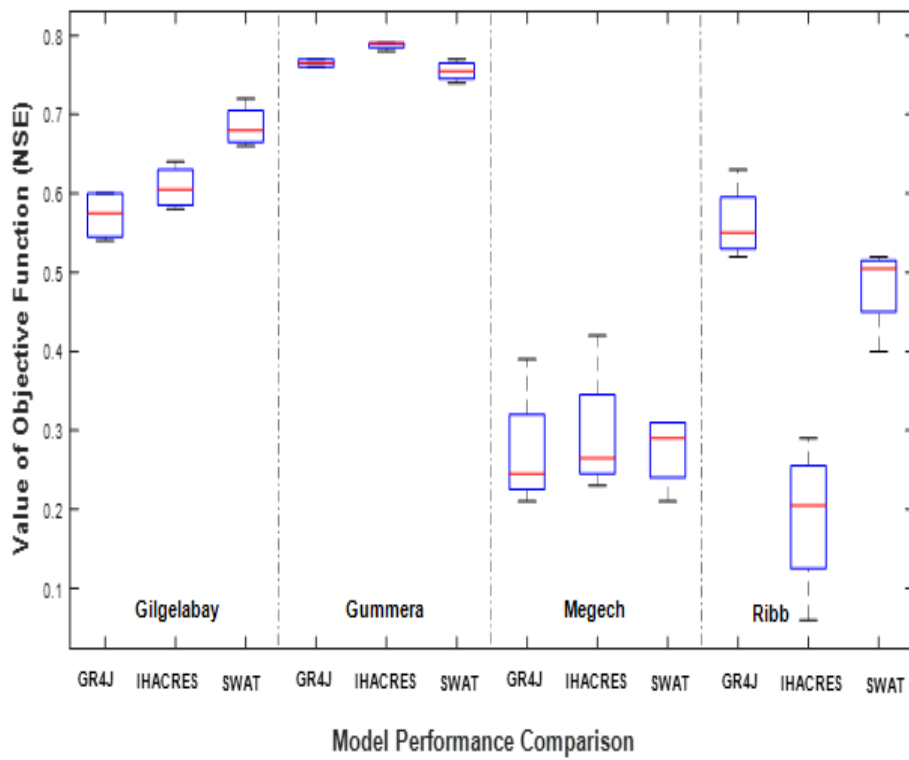


Figure 4.5. Box plots of model performance variation of all three models for all watersheds for the four folds.

- *Model Comparison in the Quantile-domain*

From the quantile domain-based model comparison results, the SWAT model performed better than did the simple conceptual models (GR4J and IHACRES) for the simulation of mid-range, dry, and low flows in the Ribb catchment; the simulation of high, moist, and mid-range flows in the Gummera catchment; the simulation of high and mid-range flows in the Megech catchment; and the simulation of low flows in the Gilgelabay catchment. GR4J performed best for the simulation of high, mid-range, and dry flows in the Gilgelabay catchment; the simulation of low flows in the Gummera catchment; and the simulation of moist and low flows in the Megech catchment. IHACRES yields the best performance for the simulation of mid-range flows in the Gilgelabay catchment; the simulation of dry flows in the Gummera and Megech catchments; and the simulation of high flows in the Ribb catchment. In general, all models performed good for the simulation of high and moist flows, but their performances were relatively poor for the simulation of mid-range, dry, and low flows. However, the results of this investigation of a particular study basin with day-to-day flow comparisons may not be applicable for the selection of a robust rainfall-runoff models for a climate change assessment study. Therefore, climate change impact in the study basin should be assessed with the simple conceptual and distributed models together. Figure 4.6 presents

the flow duration curve for each category of flow range based on the quantile-domain model comparison.

#### **4.3.4. Model Comparison with well-known Drought & Flood Indices**

##### **- *10-Year 7-day Low Flow***

The relative biases of the estimated 7Q10 low-flow values based on the observations are given in Table 4.6. The highest relative bias is found for the Ribb catchment with the IHACRES model. The results show that the SWAT model estimated the 7Q10 low flows close to the historic low flows for the Gilgelabay and Megech catchments, whereas the simple conceptual models highly overestimated the historic low flows of these two catchments, although the estimated low flows of these models were relatively close to the historic low flows for the Gummera and Ribb catchments.

##### **- *Annual Maximum Discharge***

Table 4.7 presents the trend statistics of the annual maximum values of the simulated and observed discharges of the four major gauged catchments of the study area. The observed annual maximum discharge of the Gilgelabay catchment showed a decreasing trend with a significance level greater than 10 % and an average rate of decrease per year of  $-5.23$ . The three rainfall-runoff models do not produce similar trends for the simulated annual maximum discharge of the Gilgelabay catchment.

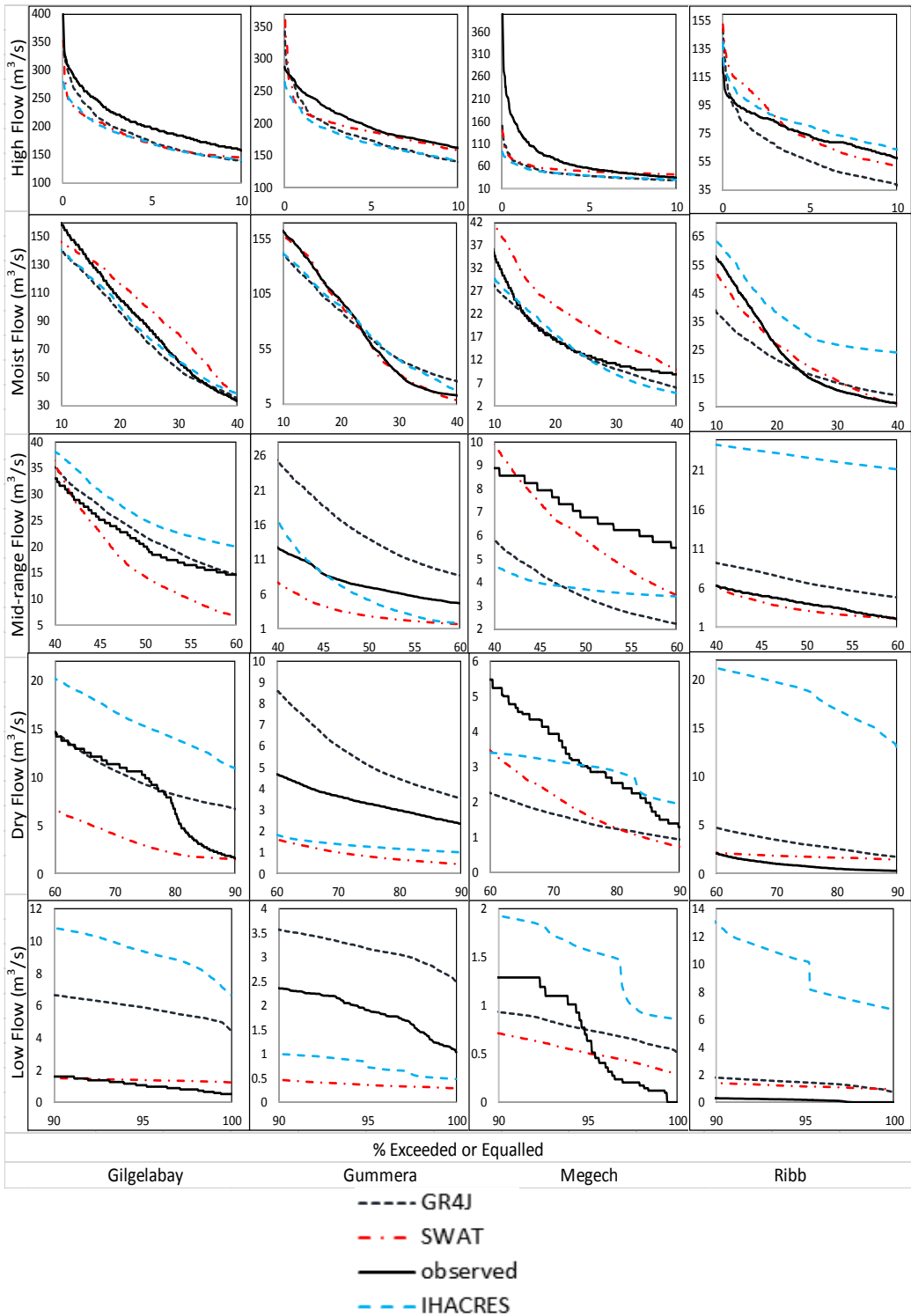


Figure 4.6. Flow duration curve for each flow category

For the Gummera catchment, the pattern of observed annual maximum discharge showed an increasing trend with a significance level greater than 10 % and an average rate of increase per year of 1.05. For the Megech catchment, the trend for the GR4J model was relatively close to the trend of the observed annual maximum discharge, which was an increasing trend with a significance level greater than 10 % and an average rate of increase per year of 10.35.

For the Ribb catchment, the trend of annual maximum observed discharge showed an increasing trend with a significance level of 5% and an average rate of increase per year of 2.95, and this trend was closely estimated by the SWAT model (see Table 4.7). In general, the SWAT model performed relatively well in flood analyses of the Gilgelabay, Gummera, and Ribb catchments, whereas the GR4J model performed well in flood analysis of the Megech catchment.

The trend test is used to determine the capability of hydrologic models to reproduce the inter-annual variability of annual maximum flow, not for the amount of annual maximum flow. Therefore, we used two more model performance measures (i.e. PBIAS and RSR) to evaluate the performances of the three models in reproducing the amounts of annual maximum flow. Table 4.8 presents the model performance measurements, which show that the SWAT model performed better than the two simple conceptual models in reproducing the annual maximum flow of the Gilgelabay and Megech

catchments, whereas the GR4J and IHACRES models were found to be better in the Gummera and Ribb catchments in terms of the PBIAS and RSR values.

#### **4.3.5. Model Error Correlation**

The correlation matrix (see Table 4.9) reveals the directions and strengths of the linear associations between the three hydrological models based on their errors. There are strong positive correlations between the errors of the two simple conceptual models (GR4J and IHACRES), whereas these two conceptual models correlate moderately to weakly with the more complex physically-based, semi-distributed model (SWAT). Therefore, we infer that it is good practice to perform model intercomparison between the simple and complex models. The results also indicate a possibility of combining the outputs of the simple conceptual and complex models to improve the performance of the individual models since the individual models draw on different information, in which the systematic and random errors of individual model outputs are more likely to cancel out in the aggregate.

Table 4.6. The performance of the three models for the estimation of 7Q10 low flow

Model	Relative bias			
	Gilgelabay	Gummera	Megech	Ribb
GR4J	-5.67	-1.17	-4.00	<b>-34.00</b>
IHACRES	-8.33	<b>0.56</b>	-16.5	-582.33
SWAT	<b>-0.53</b>	0.78	<b>-1.00</b>	-40.67

Table 4.7. Trend statistics of the annual maximum simulated and observed discharges

Watershed	Annual maximum discharge	Kendall trend		Sen slope estimate	
		Test Z	Significance level ( $\alpha$ )	Slope (Q)	Constant (B)
Gilgelabay	Observed	-0.89	> 0.1	-5.23	339.99
	GR4J	1.85	0.1	12.27	160.51
	IHACRES	1.99	0.05	7.79	166.00
	SWAT	<b>1.17</b>	<b>&gt; 0.1</b>	4.95	208.15
Gummera	Observed	0.75	> 0.1	1.05	242.33
	GR4J	-0.48	> 0.1	-3.04	277.69
	IHACRES	0.07	> 0.1	0.53	217.27
	SWAT	<b>0.62</b>	> 0.1	1.83	242.96
Megech	Observed	1.37	> 0.1	10.35	187.50
	GR4J	<b>0.21</b>	> 0.1	0.47	61.42
	IHACRES	-0.21	> 0.1	-0.53	55.94
	SWAT	-0.07	> 0.1	-0.02	56.75
Ribb	Observed	2.13	0.05	2.95	70.78
	GR4J	-0.34	> 0.1	-1.62	102.83
	IHACRES	-0.62	> 0.1	-1.25	113.99
	SWAT	<b>1.30</b>	> 0.1	5.65	46.05

Table 4.8. Performance of models in reproducing the amounts of annual maximum flow

Watershed	Model	Performance	
		PBIAS	RSR
Gilgelabay	GR4J	26.17	2.94
	IHACRES	36.11	3.14
	SWAT	<b>17.31</b>	<b>1.96</b>
Gummera	GR4J	<b>-0.52</b>	2.26
	IHACRES	12.30	<b>2.03</b>
	SWAT	-6.39	3.72
Megech	GR4J	70.94	2.09
	IHACRES	77.34	2.21
	SWAT	<b>70.50</b>	<b>2.03</b>
Ribb	GR4J	<b>6.99</b>	2.35
	IHACRES	-7.53	<b>2.07</b>
	SWAT	16.93	2.31

Bold figures in Table 4.6 & 4.8 indicate the best-performing models for the corresponding catchments

#### **4.3.6. Combination of Hydrological Model Outputs**

We have available three alternative hydrological models (i.e. SWAT, GR4J, IHACRES) for the assessment of surface water resources of the Lake Tana Basin. The simple average, weighted average, the sum of squared error, time-varying weight, and the artificial neural network methods were used to combine the outputs of the three hydrological models. The result revealed that the outputs of the artificial neural network method proved to be good for improving the individual model outputs (see Figure 4.7). Table 4.10 presents the performance of the artificial neural network for combining the three model outputs in the training, validation, and test datasets. The result showed that the combination of the three model outputs using the artificial neural network significantly reduced the root mean square error (RMSE) of the individual models by 11.98 %, 7.69%, and 28.58% for Gilgelabay, Gummera, and Ribb catchments, respectively, for the entire flow range in the time-domain (Figure 4.7). The combined output of the two simple conceptual model slightly improved the performance of the individual models by more than 1.26%. For the categorized flow range, the combined outputs of the SWAT and GR4J models reduced the RMSE significantly. Therefore, this study suggests for using the three hydrological models integrated by the artificial neural network to better estimate the surface water resources of the Lake Tana Basin. The result of this approach is provided in Appendix C, Table C.1.

Table 4.9. Correlations between model errors

Watershed	Model	SWAT	GR4J	IHACRES
Gilgelabay	SWAT	1.00	0.70	0.74
	GR4J	0.70	1.00	<b>0.96</b>
	IHACRES	0.74	<b>0.96</b>	1.00
Gummera	SWAT	1.00	0.82	0.86
	GR4J	0.82	1.00	<b>0.94</b>
	IHACRES	0.86	<b>0.94</b>	1.00
Megech	SWAT	1.00	0.96	0.96
	GR4J	0.96	1.00	<b>0.99</b>
	IHACRES	0.96	<b>0.99</b>	1.00
Ribb	SWAT	1.00	0.35	0.43
	GR4J	0.35	1.00	<b>0.88</b>
	IHACRES	0.43	<b>0.88</b>	1.00

Bold figures indicate relatively strong correlations between model outputs for each watershed

Table 4.10. The performance of ANN model in the training, validation & test dataset

Catchment	Dataset	No. of samples	Performance	
			R <sup>2</sup>	RMSE
Gilgelabay	Training	3054	0.76	32.24
	Validation	655	0.77	32.62
	Testing	655	0.72	36.56
Gummera	Training	3054	0.83	28.57
	Validation	655	0.83	28.88
	Testing	655	0.83	28.26
Megech	Training	3054	0.37	22.24
	Validation	655	0.34	21.18
	Testing	655	0.32	23.76
Ribb	Training	3054	0.77	11.12
	Validation	655	0.69	13.24
	Testing	655	0.72	12.37

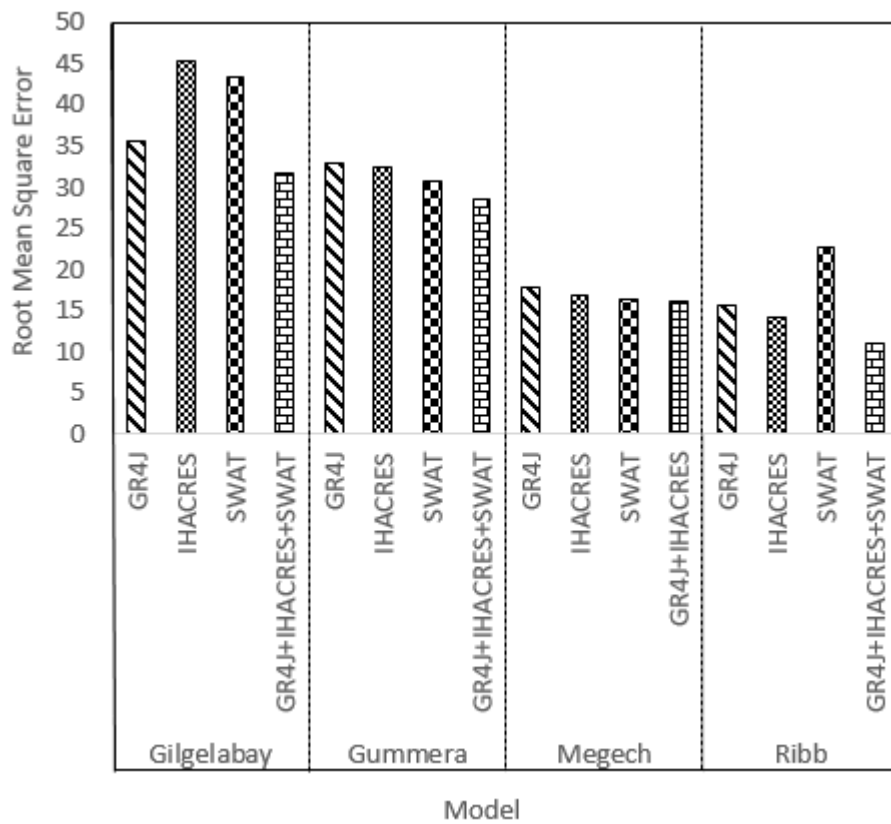


Figure 4.7. Performance of models in each watersheds

#### **4.4. Conclusions**

We have compared two conceptual rainfall–runoff models and one physically-based rainfall–runoff model in terms of time domain- and quantile domain-based model performance. The parameter sensitivity and uncertainty analyses were carried out for the most complex of the three hydrological models (SWAT), and from the sensitivity analysis result, the effective hydraulic conductivity in main channel alluvium (CH\_K2) was found to be the most sensitive parameter for the Gilgelabay, Gummera, and Megech catchments, whereas the SCS runoff curve number (CN2) was found to be the most sensitive parameter for the Ribb catchment. Furthermore, SWAT showed the sensitivity for the numbers of partitioned subbasins and the number of subbasins that generate the best performance with SWAT were 45, 25, 45, and 3 for the Gilgelabay, Gummera, Megech, and Ribb catchments, respectively. The time domain-based model comparison showed that GR4J produced a superior result for the Ribb catchment, that SWAT performed best for the Gilgelabay catchment, and that IHACRES performed best for the Gummera and Megech catchments. The assessment of model performance in the quantile domain revealed that SWAT was better than the simple conceptual models (GR4J and IHACRES) for the simulation of mid-range, dry, and low flows in the Ribb catchment; the simulation of high, moist, and mid-range flows in the Gummera catchment; the simulation of high and mid-range flows in the Megech

catchment; and the simulation of low flows in the Gilgelabay catchment. GR4J performed best for the simulation of high, mid-range, and dry flows in the Gilgelabay catchment; the simulation of low flows in the Gummera catchment; and the simulation of moist and low flows in the Megech catchment. IHACRES performed best for the simulation of mid-range flows in the Gilgelabay catchment; the simulation of dry flows in the Gummera and Megech catchments; and the simulation of high flows in the Ribb catchment. In general, all three models captured the magnitudes and variabilities of the observed streamflow for the four gauging stations, and our results do not indicate that any of these hydrologic models is superior to the others for all sites or all measures of model performance. Therefore, the selected simple conceptual models (GR4J and IHACRES) perform comparably to a more complex model (SWAT) at a daily time step. The sign of the correlation coefficient between the errors of the three models indicates a strong relationship between the simple conceptual models, perhaps because of their structural similarity. Therefore, our results suggest that a multi-model ensemble approach with SWAT and either GR4J or the IHACRES should be utilized for regional water resources assessment and management in the LTB. An alternative strategy to assess the water resources of the LTB is to combine either two or three of the model outputs. For this, the combined output of the three models by using the artificial neural network method significantly improved the individual model

performances by 11.98%, 7.69%, and 28.58% for Gilgelabay, Gummera, and Ribb catchments, respectively.

## CHAPTER FIVE

### 5. Surface Water Resources Assessment in the Ungauged Catchments of Lake Tana Basin

**Summary:** The Ethiopian Government has identified the Lake Tana Basin as a region for irrigation and hydropower development, which is vital for food security and economic growth. However, there is no reliable hydrological information available from more than 60 % of the Lake Tana Basin. Assessing water resources potential of the ungauged catchments is vital for the design of drainage infrastructure and flood protection as well as for water resources management tasks such as water allocation and climate impact analysis. Therefore, the objective of this chapter was mainly to estimate the surface water resources in the ungauged catchments of the Lake Tana Basin. The calibrated SWAT model parameters were transposed to the ungauged catchments by using the arithmetic mean, the physical similarity, the spatial proximity, and the catchment runoff-response similarity which is proposed by this study. The performance of these four parameter transfer schemes were compared to identify the best methodology for obtaining SWAT model parameters for use in modeling the ungauged catchments. The results revealed that the catchment runoff-response similarity approach slightly improved the performance achieved by the other three parameter transfer methods. The mean annual total surface water inflow into the Lake

Tana was found to be  $6.35 \text{ Bm}^3/\text{year}$  based on the analysis for the time periods of (1995-2010) by using the catchment runoff-response similarity approach. The mean annual surface water inflow from the four major gauged catchments was found to be  $3.74 \text{ Bm}^3/\text{year}$  making up 59 % of the total inflow, while the inflow from the ungauged catchments was found to be  $2.61 \text{ Bm}^3$ , which represents 41 % of the total inflow. The water balance closure error was estimated to be about  $0.443 \text{ Bm}^3/\text{year}$ , which indicates 6.9 % of the mean annual surface inflow to the Lake Tana. This error may be associated with the negligible assumption of the Lake groundwater in the water balance computation.

## **5.1. Introduction**

In spite of continuous research efforts and investments to accumulating the hydrologic data for the last century, the gauging sites are still sparse over the world, especially very sparse in developing countries. In Ethiopia, Africa, for example, only 454 operational gauging stations exist overall, and thus one single gauging station covers approximately only  $2432.4 \text{ km}^2$  on average. In many hydrologic analysis studies, therefore, handling ungauged catchments has become a major obstacle to be first solved and various versions of regionalization, a process of transferring hydrological information from gauged to ungauged catchments, have been developed for last several decades. The most common choices for regionalization includes

the spatial proximity, the regression-based, and the physical similarity approaches. More recently, Merz and Bloschl (2004) and Parajka *et al.* (2005) reported that the predictive performance of physical similarity and the spatial proximity approaches become similar when the density of stream gauges decreases to less than 60 gauges per 100,000 km<sup>2</sup>. Oudin *et al.*, (2008) compared these three regionalization approaches for runoff predictions of ungauged catchments using 913 gauged catchments in France and concluded that spatial proximity provides the best regionalization solution where a dense network of gauging stations is available, and the regression approach is the least satisfactory whereas the physical similarity approach is intermediary. They also reported that spatial proximity slightly outperformed the similarity method in regions with a dense stream gauge network.

The physical similarity approach uses some catchment attributes to group the similarity of catchment attributes. In other words, this approach finds a donor catchment that is most similar to an ungauged site regarding its catchment attributes and then transfers a complete parameter set from the donor to the corresponding ungauged catchments for the hydrologic modeling. The primary advantage of the physical similarity approach over the regression method is that it does employ the physical attributes but does not require the linearity assumption (Samuel *et al.*, 2011). The success of this approach depends on the choices of attributes for the similarity of

catchments. The attributes that determine homogeneous regions can be classified into geomorphological, meteorological, and hydrological attributes. Topography, land use, and soil type have been widely used as the geomorphological attributes (e.g., Merz and Blöschl, 2004; Heuvelmans *et al.*, 2006; Wagener *et al.*, 2007; Bastola *et al.*, 2008) while long-term precipitation characteristics, and potential evapotranspiration as the meteorological attributes (e.g., Wagener *et al.*, 2007, Bastola *et al.*, 2008).

The regression-based approach uses the catchment attributes as independent variables and the hydrological model parameters as dependent variables (Post and Jakeman 1996; Sefton and Howarth, 1998; Merz and Blöschl, 2004; Parajka *et al.*, 2005; Young 2006; Cheng *et al.*, 2006; Götzing and Bárdossy, 2007). The main concerns of this approach are the values of the estimated parameters depending on the specific conditions of the calibration period and the possible input errors and inadequacies (Oudin *et al.*, 2006; Samuel *et al.*, 2011). The identification of hydrologically relevant catchment descriptors for the regression technique and possible interactions between parameters are limitations of this approach (Oudin *et al.*, 2008).

The spatial proximity approach estimates the model parameters at ungauged catchments using an interpolation technique such as kriging (Merz and Blöschl, 2004; Parajka *et al.*, 2005). This approach assumes that the ungauged catchments are already located in a homogeneous or a

geographically similar region. One would expect that catchment attributes provide valuable hydrological information for flow predictions in ungauged basins (e.g., Young, 2006), but which is not considered in the spatial proximity approach.

The Ethiopian Government has identified the Lake Tana Basin for irrigation and hydropower development. However, few studies have been done in the past for the estimation of surface water resources in the ungauged catchments. For example, Kebede *et al.*, (2006) concluded that the four major catchments (Gilgelabay, Gummera, Ribb, Megech) contribute 93% of the inflow to Lake Tana while SMEC (2007) and Wale *et al.* (2009) reported 71% and 58% of the inflow to the Lake Tana, respectively, are originated from the four major catchments. The reasons for the differences, however, remain unclear since each study uses different parameter transfer schemes to simulate the hydrological processes in the ungauged catchment. A common approach to overcome this problem is to investigate the best parameter transfer approach. Therefore, due to the advantages discussed above and previous performance of the regionalization techniques, this study adopted the physical similarity, and the spatial proximity approaches to assess the surface water resources potential in the typical ungauged catchments of Ethiopia. Furthermore, this study proposes a new methodology for the parameter transfer which was based on the catchment runoff-response similarity. The attributes for this new parameter transfer

approach are derived from the observed meteorological data (rainfall, temperature, relative humidity, solar radiation, and wind speed) and spatial data (soil use, land use, topography). These meteorological and spatial data were used to set up the SWAT model, and the default output of the SWAT model was considered as the attribute of the new parameter transfer approach.

Another key issue for the parameter transfer scheme is to identify which gauged and ungauged subbasins play the role of donors and recipients, respectively, within a homogeneous region and to determine how to make a weighted average when multiple donors are considered. This study aims to identify the most appropriate parameter transfer scheme to reach its ultimate goal, i.e. quantification of surface water resources potential of the ungauged study catchment in a typical Basin of Ethiopia.

Razavi and Coulibaly (2013) concluded that the catchment descriptors are different across various studies and this seems that an initial hypothetical judgment is required to identify which potential catchment attributes would have an impact on the runoff responses of interests. Merz and Blöschl, (2004) used area, elevation, slope, porous aquifers, land covers, geologic units, soil types, river network density, lake index, mean annual precipitation, and maximum annual daily precipitation as the catchment attribute for identifying the similar catchments. Buttle and Eimer (2009)

used the physiographic characteristics like area, mean slope, drainage density, and a fraction of the basin area.

He *et al.* (2011), and Razavi & Coulibaly *et al.* (2013) have reviewed the methods that were used to estimate model parameters of the ungauged catchments. The study by He *et al.* (2011) classified the regionalization methods into distance-based (based on geographical and hydrological similarities) and regression-based methods. The study by Razavi and Coulibaly (2013) classified the regionalization approaches into hydrologic model-dependent (e.g. arithmetic mean, spatial proximity, physical similarity, scaling relationships, regression-based methods, hydrological similarity) and hydrologic model-independent (e.g. regression-based methods, time series model, scaling relationships) groups. The first regionalization methods transfer rainfall-runoff model parameters between basins. The second regionalization methods transfer the input-output equation structure instead of hydrologic model parameters.

This study used the arithmetic mean (Merz and Blöschl, 2004; Oudin *et al.*, 2008; Jin *et al.*, 2009); the physical similarity (Oudin *et al.*, 2008; Samaniego *et al.*, 2010; Samuel *et al.*, 2011); the spatial proximity (Merz and Blöschl, 2004; Parajka *et al.*, 2005; Oudin *et al.*, 2008; Li *et al.*, 2009); and the catchment runoff-response similarity approaches to transfer the calibrated parameters to the ungauged catchments.

In the arithmetic mean approach, each model parameters for the ungauged catchment is computed as the mean of the corresponding parameter from the gauged catchments. So, parameter values are the same for the overall ungauged catchments. The assumption in this technique is that all catchments within the study area are similar in their hydrological behavior and that all differences in parameter values arise from random factors (Kokkonen *et al.*, 2003).

The physical similarity approach is based on the assumption that catchment physiographic characteristics predetermine the hydrological behavior. The catchment attributes selected and used to define similarity are related to topography, land cover, and soil features. They are derived from the available data such as land use maps, soil maps, and digital elevation model. These catchment attributes are considered as the main drivers of the hydrological process in the literature (Merz and Blöschl, 2004) and are the most common ones used to define similarity between catchments in model parameter regionalization schemes. However, the selection of the appropriate catchment attributes also depends on the physical meaning of the selected model parameters, on the objective of the regionalization procedure, and on the knowledge about the key hydrological processes occurring within the catchment (Sellami *et al.*, 2014). For instance, in the SWAT model, the curve number parameter (CN2) depends on the soil and land use characteristics of the catchment. So, a concept of Hydrologic

Response Units (HRUs), in which the land use, soil use, and land slope were all unique, was introduced to facilitate the parameter transfer from gauged to ungauged catchments.

The spatial proximity approach is based on a spatial distance between catchment centroids by using interpolation technique as a function of the geographic location. The spatial interpolation techniques used in this study was the kriging (Samuel *et al.*, 2011). The kriging is an improvement over inverse distance weighting method because prediction estimates tend to be less bias since prediction accompany the standard prediction errors. The basic tool of kriging is the semivariogram which captures the spatial dependence between samples by plotting semivariance against separation distance.

The catchment runoff-response similarity (CRRS) approach assumes that all catchments within the region are similar in their hydrological behavior. The attributes of this technique were indirectly derived from the observed meteorological data (i.e. rainfall, temperature, relative humidity, wind speed, solar radiation) and spatial data (i.e. soil-use, land-use, topography). These data were used to set up the physically based semi-distributed hydrological model called SWAT in all the gauged and ungauged catchments. First, the Lake Tana Basin was divided into 75 smaller units using a Geographical Information Systems (GIS) by keeping track of flow direction in a Digital Elevation Model (DEM). Once the basin

is delineated, it can then be used to crop out data from each smaller units (e.g. area and runoff-response of each unit). The default outputs (i.e., streamflow without calibration) of the SWAT model for all the 75 sub-units were obtained and normalized by the corresponding subbasin area to group the similar units based on their runoff-response similarity. The default outputs of the model were used by expecting the model itself gives the acceptable output in all similar regions of the study area (at least for parameter regionalization techniques) since all the input data to the hydrological model were recorded and the deviation from the output of the model can be almost related to the model error.

The Euclidean distance ( $D_{(i,j)}$ ) was used for clustering the most similar units based on their runoff-response.

$$D_{i,j} = \left[ \sum_{k=1}^p (z_{i,k} - z_{j,k})^2 \right]^{\frac{1}{2}} \quad (5.2)$$

$$z_i = \frac{x_i - \bar{x}}{\sigma} \quad (5.3)$$

where  $z_{i,k}$  is a standardized value for variable  $k$  at site  $i$ .  $x_i$  is the runoff-response at site  $i$ ,  $\bar{x}$  is the mean value of runoff-response of all 75 units, and  $\sigma$  is the standard deviation of runoff-response values of all 75 units.

## 5.2. Methodology

### 5.2.1. The Lake Tana Water Balance

The Lake Tana water balance estimation is important for water management decision making by assessing the current status and trends in water resource availability. Therefore, the Lake Tana water balance was estimated by using the principle of conservation of mass. The general water balance equation is given by equation 5.1.

$$I + P + G_{inflow} - G_{outflow} - O - E \pm \Delta S = 0 \quad (5.1)$$

where  $I$  is the river inflow to the Lake Tana,  $P$  is the precipitation,  $E$  is the evaporation from the Lake Tana,  $G_{inflow}$  is the groundwater inflow to the Lake Tana,  $G_{outflow}$  is the groundwater outflow from the Lake Tana,  $O$  is the outflow from the Lake Tana, and  $\Delta S$  is a change in surface storage.

The study by SMEC (2007) mentioned that about 80 m thick clay layer underlies the Lake that significantly prevents inflow or outflow through the Lake bottom. Therefore, the groundwater flow component in the water balance computation was assumed to be negligible.

The daily Lake areal rainfall has been estimated by using the Thiessen polygons method. The Penman-Monteith method is recommended for determining potential evapotranspiration when the standard meteorological variables including air temperature, relative humidity and sunshine hours are

available (Allen *et al.*, 1998). Hence, the potential evapotranspiration was calculated using the Penman-Monteith equation through CROPWAT-8 software, and then an aridity correction factor was applied for the estimation of open water evaporation. According to FAO Irrigation and Drainage Paper 56 (Allen *et al.*, 1998), page 114, the conversion of potential evapotranspiration to evaporation of open water, with a depth higher than 5 m, clear of turbidity, in a temperate climate, would vary from 0.65 to 1.25. For Ethiopia, the aridity correction factor was estimated to be 1.25 based on the report in a feasibility study of the Lake Tana subbasin dam project.

The SWAT model was used to estimate the runoff from the ungauged catchments due to its performance at the gauged catchments and also due to its benefit concerning physical representation of the ungauged catchments. The optimized SWAT model parameters at the four gauged catchments were transferred to the ungauged catchments with the help of the four parameter transfer schemes (i.e. arithmetic mean, physical similarity, spatial proximity, and catchment runoff-response similarity).

The Blue Nile River is the only natural outflow from the basin. For the water balance estimation of the Lake Tana Basin, the observed outflow to the Blue Nile River for the period of 1995 – 2012 was used.

### 5.2.2. Performance Measures for Parameter Transfer Schemes

The performance of each parameter transfer scheme was evaluated by comparing the observed and the simulated Lake Tana water level for the time periods of 1995 – 2012. The Nash-Sutcliffe efficiency (NSE), percent bias (PBIAS), ratio of the root mean square error to the standard deviation of measured data (RSR) and coefficient of determination ( $R^2$ ) were used as the performance indicators to compare the performance of the parameter transfer schemes. The detailed description and equation of all performance measures are provided in chapter 3. The polynomial fitted elevation-volume (equation 5.4), and area-volume (equation 5.5) relations developed by Wale *et al.* (2009) were used for the computation of the Lake Tana water level (Figure 5.2). The Lake Datum was referenced at 1783.515 m above mean sea level.

$$E = 1.21 \times 10^{-13} \times V^3 - 1.02 \times 10^{-8} \times V^2 + 6.2 \times 10^{-4} \times V + 1774.63 \quad (5.4)$$

$$A = 7.93 \times 10^{-11} \times V^3 - 5.81 \times 10^{-6} \times V^2 + 1.65 \times 10^{-1} \times V + 1147.51 \quad (5.5)$$

where  $A$  is the Lake surface area in  $\text{km}^2$ ,  $V$  is the Lake volume in  $\text{Mm}^3$  and  $E$  is the Lake level in m above mean sea level.

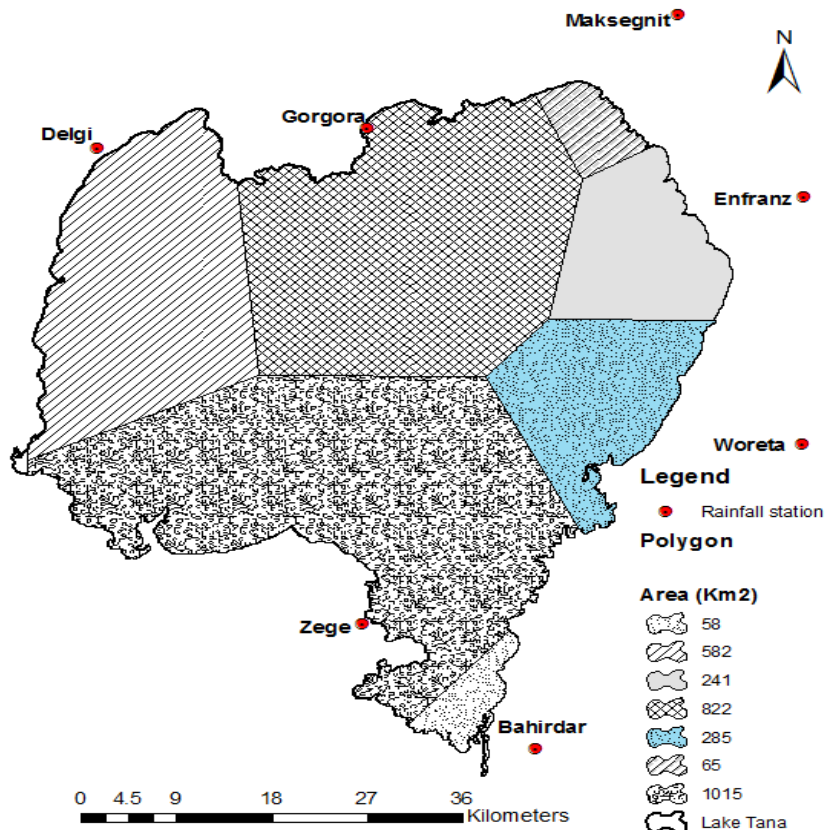


Figure 5.1. Thiessen polygon for the estimation of areal rainfall in the Lake Tana

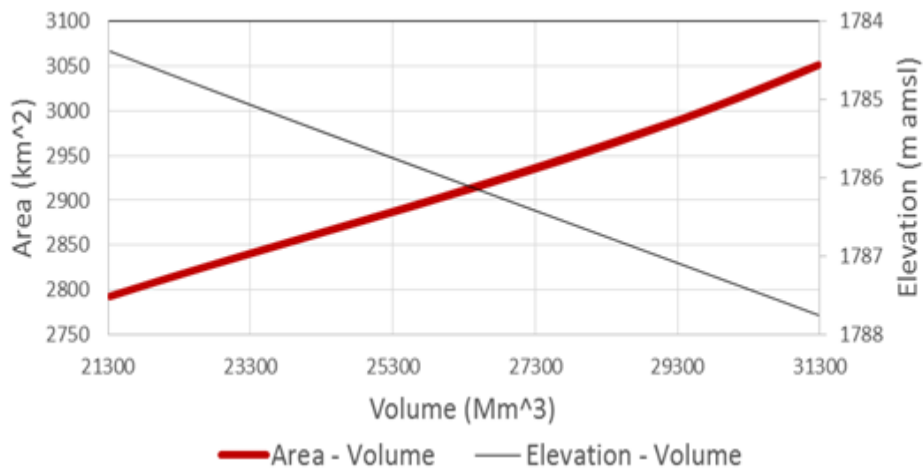


Figure 5.2. Elevation-volume and area-volume relationship of the Lake Tana

## **5.3. Application**

### **5.3.1. Performance of the Parameter Transfer Schemes**

#### **- *The arithmetic mean approach***

The consideration of poorly modeled gauged catchment (i.e. Megech) in the case of the arithmetic mean parameter transfer approach gives poor result compared to the result obtained by exempting the parameters from the Megech catchment. This result showed that the poorly modeled catchment yields highly uncertain model parameter values that could be the reason for the poor performance of the arithmetic mean parameter transfer approach. Therefore, the calibrated model parameters from the Megech catchment were not considered for the arithmetic mean approach. On the other hand, the consideration of the calibrated model parameters from the poorly modeled gauged Megech catchment for all other parameter transfer approaches gives better result in relative to the result obtained by exempting the parameter values. Therefore, the consideration of the poorly modeled catchment that introduced the diversity of catchment physical characteristics proved to be beneficial for modeling ungauged catchments by using the physical similarity, the spatial proximity, and the catchment runoff-response parameter transfer approach. These findings may not be warranted in other basins since this result will depend on the physical characteristics of the basin and the key attributes that used for identifying the similar units.

- ***The physical similarity approach***

Using the SWAT, the Lake Tana Basin was delineated into 75 smaller units, among which 16 were gauged while the rest were ungauged. By overlaying the soil use, land use, & slope of the basin, these 75 smaller units were clustered into 16 physically similar homogeneous groups called hydrological response units, in which the land use, soil use, and land slope were all unique. The key physical attributes (Table 5.1) were classified into three major land use classes (AGRL, AGRC, PAST), six major soil use classes (FLe, LVx, LPe, VRe, ALh, LVh), and three basin slope classes (0–8%, 8–16%, 16–9999%). Note that the dominant attributes for the study basin were the agriculture land use (AGRL, 51.33%) for the land use, Halpic luvisol (LVh, 20.70 %) for the soil use and 69.71% of the basin has the slope of 0 – 8%. Based on the physical similarity between the gauged and ungauged catchments, 37.15 % of the ungauged catchment will receive information from the gauged Gilgelabay catchment, whereas 33.30% from gauged Ribb, 25.38% from gauged Gummera, and 4.178% from gauged Megech catchment. Table 5.2 presents the cluster of subbasins based on the similarity of land use, soil use, and land slope.

- ***The spatial proximity approach***

Three homogeneous regions (see Figure 5.3 (a)) were identified based on the spatial proximity approach by using the well-known kriging technique. Therefore, gauged Gilgelabay catchment was identified as a donor for the

ungauged catchments in the region-III, both of the gauged Gummera & the gauged Rib catchments were considered as the donors for the ungauged catchments in the region-II, and finally gauged Megech catchment was identified as a donor for the ungauged catchment in the region-I. For the region-II, the areal average of two values of each parameter from gauged Gummera and Rib catchment were used to model the ungauged catchments in region-II.

- ***The catchment runoff-response similarity approach***

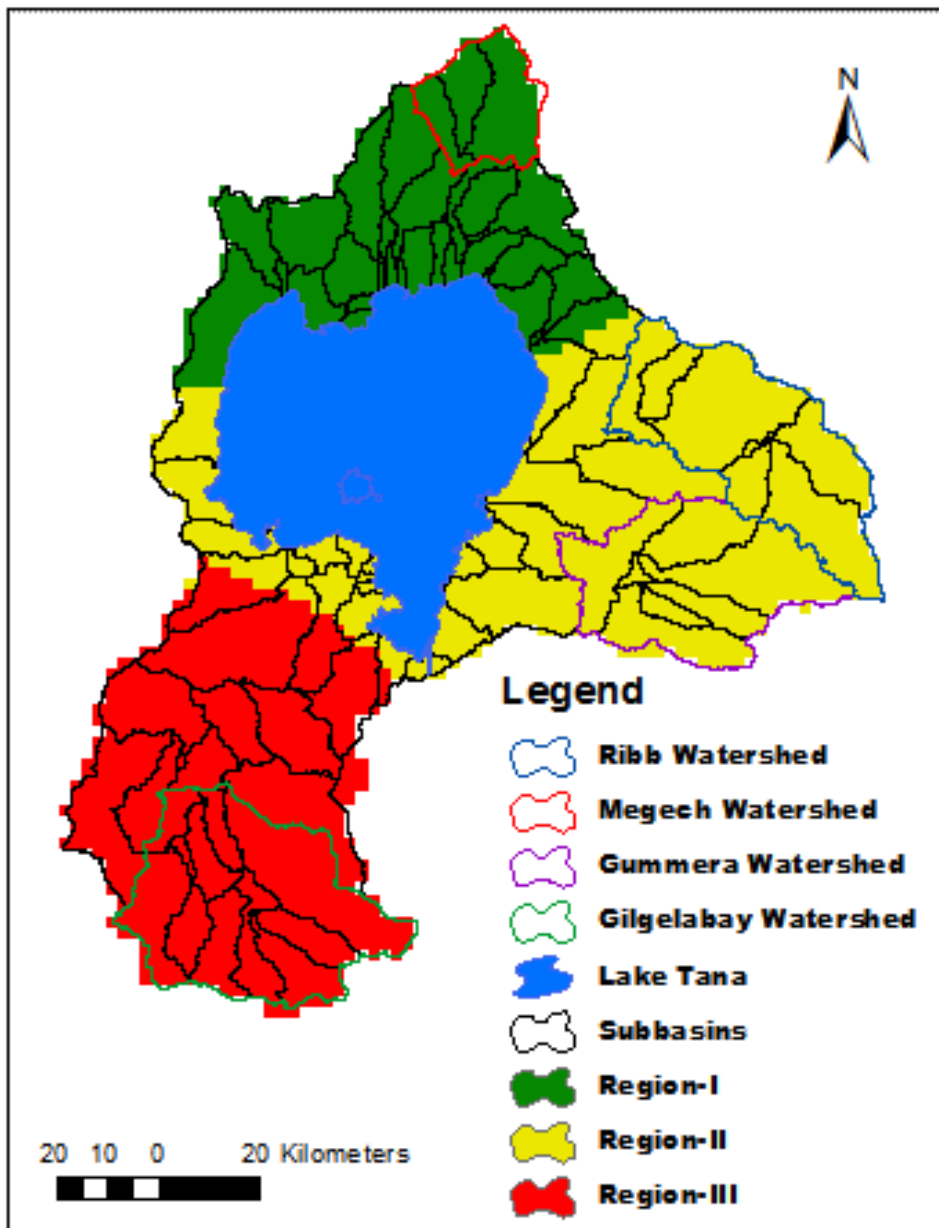
In regards to the CRRS approach, the default outputs (i.e. streamflow without calibration) of the SWAT model for all the 75 subbasins were obtained and normalized by the corresponding subbasin area to group the similar units based on their runoff-response similarity. Based on this approach, four hydrologically similar groups were identified as shown in Figure 5.3 (b). Therefore, gauged Megech, Ribb, Gummera, and Gilgelabay catchments were identified as a donor to model the ungauged catchments in the region-I, region-II, region-III, and region-IV, respectively. The performance result of the catchment runoff-response similarity approach outperforms the other three parameter transfer schemes (see Table 5.3). Therefore, this parameter transfer method was selected for the assessment of surface water resources in the ungauged catchments.

Table 5.1. Catchment attributes used in physical similarity

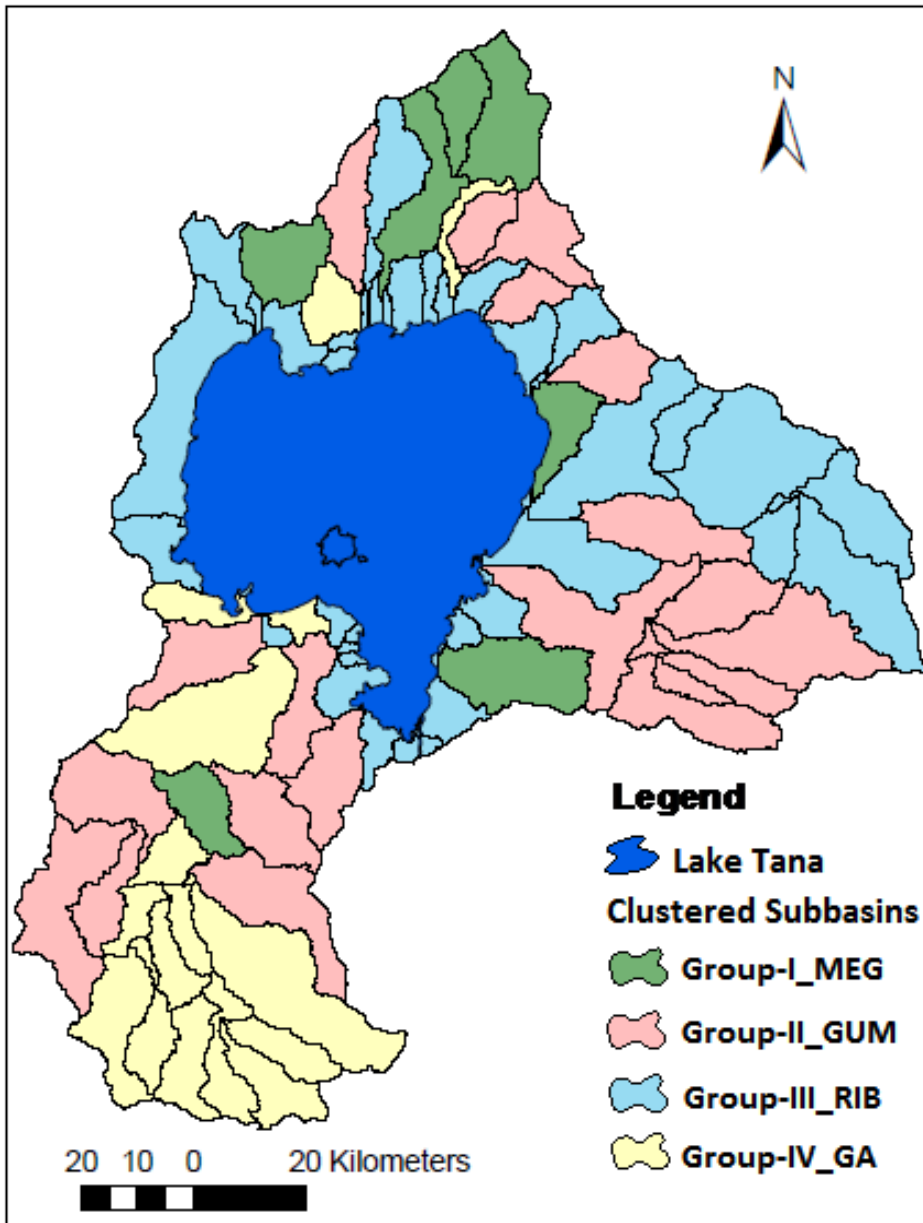
<b>Key physical attribute</b>	<b>Classification of attributes</b>	<b>% watershed area</b>	<b>Dominant attribute</b>
<b>Land use</b>	Agricultural Land-Generic (AGRL)	51.33	AGRL
	Pasture (PAST)	5.58	PAST
	Residential-Low Density (URLD)	0.11	
	Agricultural Land-Close-grown (AGRC)	21.81	AGRC
	Range-Brush (RNGB)	0.03	
	Water	20.47	
	Wetlands-Mixed (WETL)	0.13	
	Forest-Evergreen (FRSE)	0.15	
	Forest-Deciduous (FRSD)	0.39	
	<b>Soil use</b>	Halpic Alisols (ALh)	7.60
Eutric Cambisols (CMe)		0.01	
Eutric Fluvisols (FLe)		9.89	FLe
Eutric Leptosols (LPe)		12.22	LPe
Halpic Luvisols (LVh)		20.70	LVh
Chromic Luvisols (LVx)		15.70	LVx
Halpic Nitisols (NTh)		1.21	
Eutric Rigosols (RGe )		0.27	
Urban (URLD)		0.07	
Eutric Vertisols (VRe)		11.86	VRe
WATR		20.48	
<b>Slope</b>	0-8	69.71	0 - 8
	8-16	14.85	8 - 16
	16-9999	15.44	16 - 9999

Table 5.2. Physically similar hydrologic response units

<b>Cluster</b>	<b>Hydrologic response unit (land/soil/slope)</b>	<b>% catchment area</b>	<b>Donor gauged catchment</b>
<b>1</b>	AGRL/LPe/16-9999	4.18	Megech
<b>2</b>	AGRL/VRe/0-8	13.16	Gummera
<b>3</b>	AGRC/LPe/16-9999	5.25	Ribb
<b>4</b>	PAST/LPe/16-9999	2.68	Ribb
<b>5</b>	AGRL/FLe/0-8	18.54	Ribb
<b>6</b>	AGRL/LVx/8-16	4.56	Ribb
<b>7</b>	AGRC/LPe/0-8	0.07	Ribb
<b>8</b>	AGRC/VRe/0-8	1.91	Gummera
<b>9</b>	AGRL/LVx/0-8	1.88	Ribb
<b>10</b>	AGRC/LVh/16-9999	6.03	Gummera
<b>11</b>	AGRL/LVh/8-16	4.28	Gummera
<b>12</b>	AGRC/LVh/0-8	2.98	Gilgelabay
<b>13</b>	PAST/ALh/0-8	8.54	Gilgelabay
<b>14</b>	AGRC/LVx/0-8	0.32	Ribb
<b>15</b>	AGRL/LVh/0-8	17.97	Gilgelabay
<b>16</b>	AGRC/ALh/16-9999	7.65	Gilgelabay



a) Spatial proximity approach



b) Catchment runoff-response similarity

Figure 5.3. Map shows the clustered of similar units based on a) spatial proximity approach and b) catchment runoff-response similarity approach

### 5.3.2. Simulation of the Lake Tana Water Level

The four proposed parameter transfer schemes were used to simulate the Lake Tana water level, and their performance was evaluated by comparing the simulated and observed Lake Tana water level on a monthly basis from 1995 to 2012. Table 5.3 shows the performance of all proposed parameter transfer schemes. The catchment runoff-response similarity approach proved to be good for the simulation of the Lake Tana water level with the performance values of 0.93, 0.26, -0.001%, and 0.94 for the NSE, RSR, PBIAS, and  $R^2$ , respectively (see Table 5.3). It is noted that the parameter transfer approach developed by this study might be useful for other ungauged basins throughout the world. However, the conclusion of this study in regards to the parameter transfer approach is that the catchment runoff-response similarity method can be used as one of the best approaches to estimate the runoff in the ungauged catchments of the Upper Blue Nile River Basin. In Figure (5.4), and (5.5), the abbreviation *PS*, *AM*, *SP*, and *CRRS* represents Physical Similarity, Arithmetic Mean, Spatial Proximity, and Catchment Runoff-Response Similarity, respectively.

Table 5.3. Performance measure of the Lake Tana water level simulations

Parameter transfer schemes	NSE	R <sup>2</sup>	RSR	PBIAS
Physical similarity	0.90	0.92	0.32	-0.005
Spatial proximity	0.91	0.92	0.29	-0.002
Arithmetic mean	0.90	0.92	0.31	-0.005
Catchment runoff-response similarity	<b>0.93</b>	<b>0.94</b>	<b>0.26</b>	<b>-0.001</b>

Bold figures are the best results

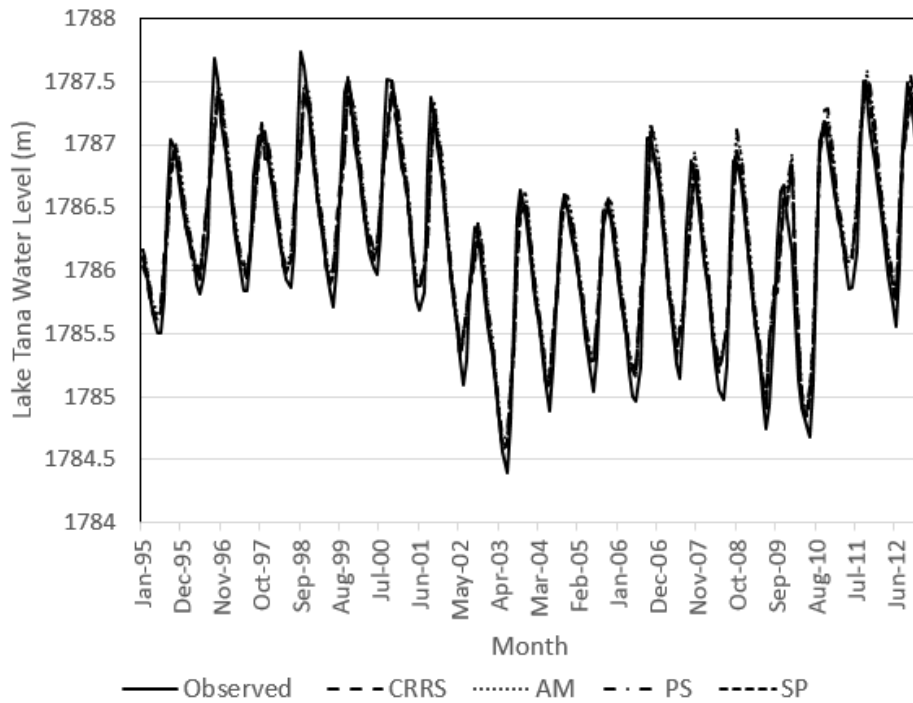


Figure 5.4. Simulation of the Lake Tana water level

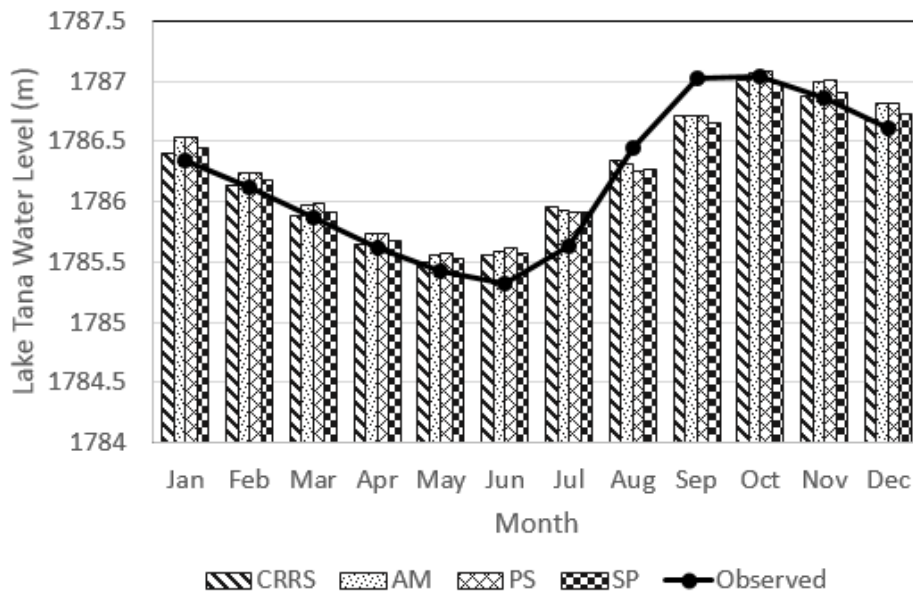


Figure 5.5. The Monthly average Lake Tana Water level (1995-2012)

### **5.3.3. Surface Water Resources Potential of the Lake Tana Basin**

The water resources potential of the Lake Tana Basin was quantified by estimating the total runoff from the gauged and ungauged catchments. Figure 5.6 presents the total surface water inflow hydrograph to the Lake Tana. The surface water inflow from the ungauged catchments was estimated by using the CRRS parameter transfer approach. The mean annual surface inflow to the Lake Tana was found to be 6.35 Bm<sup>3</sup>/year for (1995-2010). The surface inflow from the ungauged catchment represents 41 % of the total inflow to the Lake Tana with the catchment runoff-response similarity approach, whereas the four major gauged catchments contribute 59 % of the total mean annual surface inflow to the Lake. Figure 5.7 presents the monthly water balance components of the Lake Tana. The total water balance components of the basin is given in Appendix C, Table C.2. Figure 5.8 presents the average annual values of the hydrologic components (i.e. surface runoff, lateral runoff, groundwater contribution to streamflow, percolation, soil water storage, evapotranspiration, and water yield) that were obtained from SWAT outputs.

Table 5.4. Monthly water balance components of the Lake Tana (1995-2008)

<b>Month</b>	<b>Total inflow (Mm<sup>3</sup>/month)</b>	<b>Rainfall (Mm<sup>3</sup>/month)</b>	<b>Open water evaporation (Mm<sup>3</sup>/month)</b>	<b>Outflow (Mm<sup>3</sup>/month)</b>
Jan	62.88	8.06	437.22	275.16
Feb	38.95	1.66	464.75	221.06
Mar	43.77	32.01	554.65	240.37
Apr	50.21	72.22	557.63	239.02
May	149.21	216.51	529.14	205.78
Jun	503.39	584.64	420.35	192.01
Jul	1277.57	1103.08	348.82	279.77
Aug	1704.79	984.58	347.37	437.40
Sep	1342.11	529.86	398.70	797.79
Oct	769.92	212.91	439.31	644.24
Nov	284.09	26.64	414.81	472.05
Dec	128.66	6.15	415.32	358.05
Yearly (Mm <sup>3</sup> /yr)	6355.55	3778.29	5328.06	4362.69

Table 5.5. Comparison of this study result with the previous studies findings

<b>Water balance terms (Mm<sup>3</sup>/year)</b>	<b>This study</b>	<b>Wale <i>et al.</i> (2009)</b>	<b>Gieske <i>et al.</i> (2008)</b>	<b>SMEC (2007)</b>
Lake areal rainfall	3778	3784	3891	3906
River inflow	6355	6699	5487	5028
Lake evaporation	5328	5242	5180	5115
Blue Nile outflow	4362	4714	4179	3816
Closure terms	443	527	19	3

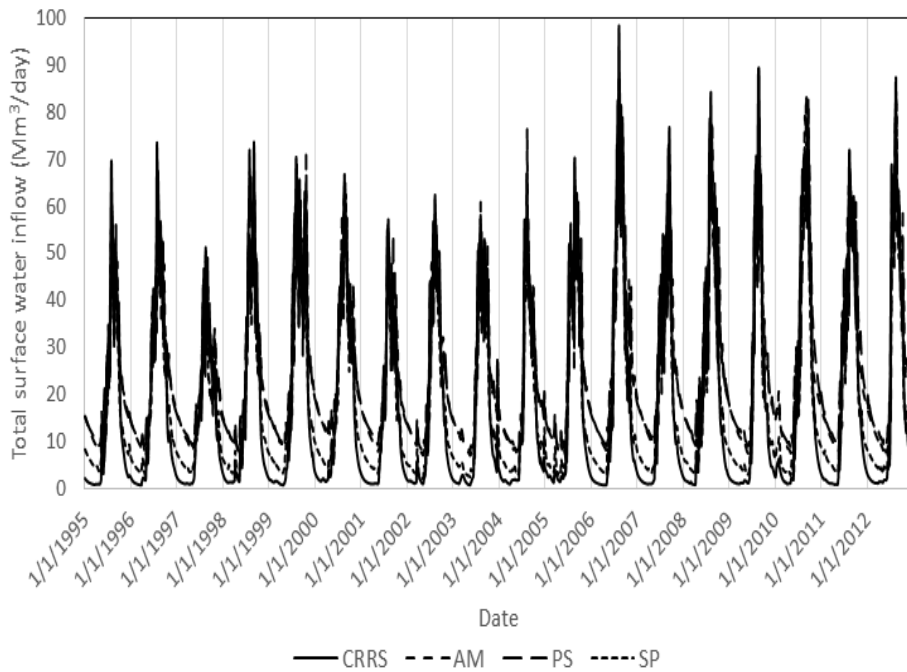


Figure 5.6. Total surface water inflow hydrograph into the Lake Tana

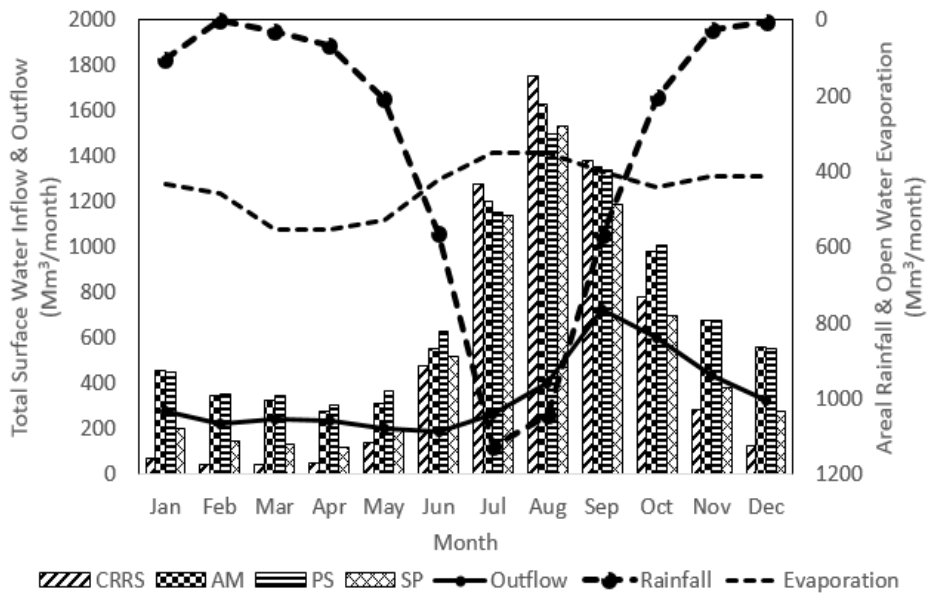


Figure 5.7. Monthly water balance components of the Lake Tana (1995-2008)

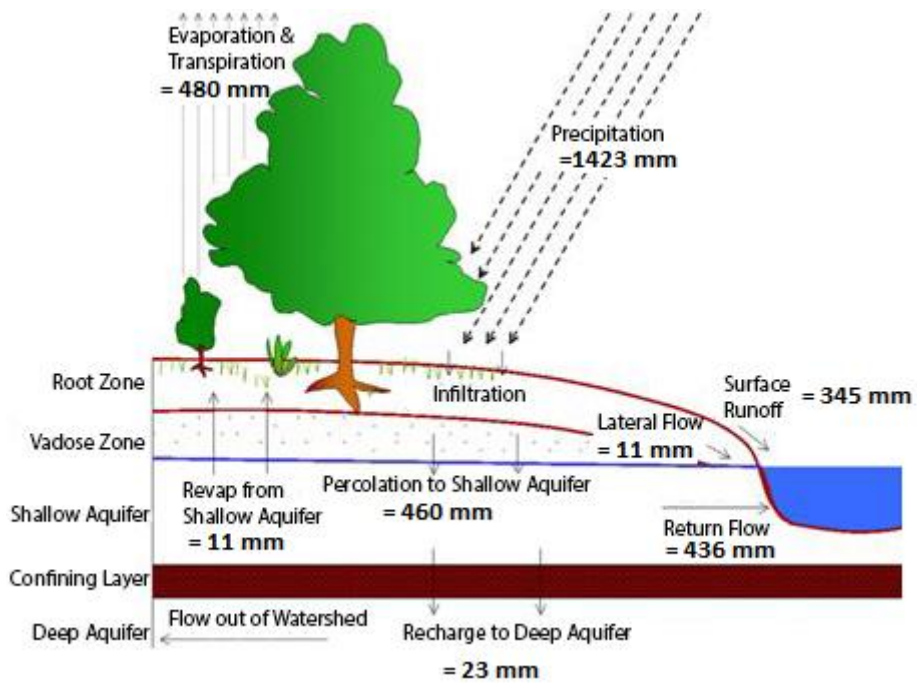


Figure 5.8. Average annual simulated water balance for the baseline scenario (1995-2012)

## 5.4. Conclusions

In the study basin, some water resources projects are planned to be implemented shortly. Hence, understanding of the hydrological processes and determination of the frequencies and magnitudes of streamflow is very crucial for the better management of the available water resources. One of the main challenging problems to accurately assess the water resources of the basin is that more than 60 % of the basin is ungauged. Therefore, the primary objective of this study was to accurately estimate the surface water resources in the ungauged catchments of the Lake Tana Basin. To achieve this objective, three commonly used parameter transfer techniques (i.e. arithmetic mean, physical similarity, and spatial proximity) with a new proposed method called catchment runoff-response similarity approach were used to transfer the calibrated model parameters from the gauged to ungauged catchments. The results showed that the catchment runoff-response similarity approach slightly improved the results obtained by the other three methods. Therefore, the parameter transfer method developed by this study could be useful for other ungauged basins throughout the world. However, the conclusion of this study in regards to the parameter transfer approach is that the catchment runoff-response similarity approach can be used as one of the best approaches to estimate the runoff in the ungauged catchments of the Upper Blue Nile River Basin. The mean annual total inflow to the Lake Tana was found to be 6.35 Bm<sup>3</sup>/year for (1995-2010).

The mean annual surface water inflow from the four major gauged catchments was found to be 3.74 Bm<sup>3</sup> making up 59 % of the total inflow, while the inflow from the ungauged catchments was found to be 2.61 Bm<sup>3</sup> which represents 41 % of the total inflow using the catchment runoff-response similarity parameter transfer method. The water balance closure error was estimated about 443 Mm<sup>3</sup>/year which indicates 6.9 % of the mean annual surface inflow to the Lake Tana. This error may be associated with the negligible assumption of the Lake-groundwater flow in the water balance computation.

## CHAPTER SIX

### 6. Potential Impacts of Climate Change on the Water

#### Balance Components of the Lake Tana Basin

**Summary:** This study is designed to assess the impact of climate change on the water balance components of the Lake Tana Basin, the source of the Blue Nile River. Understanding the hydrological processes under the changing climate is crucial for water resources planning and management. A statistical downscaling model was used to downscale the weather events associated to the three Representative Concentration Pathways (i.e., RCP 2.6, RCP 4.5, and RCP 8.5). The bias correction techniques were applied to the downscaled climate data to obtain a more realistic and unbiased data for the future climate. In the case of precipitation bias correction, we used two bias correction approaches (i.e. time-domain bias correction, and quantile-domain bias correction). The result revealed that the variability of the precipitation in all weather stations was significantly improved by applying the quantile-based bias correction. The Soil and Water Assessment Tool was used to simulate the river runoff for future time periods of the 2020s, 2050s, and 2080s. The potential impacts of climate change on the river runoff was assessed with respect to the baseline period (1995-2012). The mean annual rainfall and runoff showed increasing trend under all RCPs. Therefore, the inflow to the Lake Tana reservoir is expected to be remarkably higher

compared to the baseline period, and this can be beneficial to the improvement of agricultural productivity as well as to enhance the hydropower potential of the basin.

## **6.1. Introduction**

Global Climate Models (GCMs) indicate that rising concentrations of greenhouse gases will have significant implications for climate at global and regional scales (Wilby *et al.*, 2002). The GCMs are considered as the most advanced tools for estimating future climate change scenarios operating on a coarse scale. Statistical downscaling techniques are used to bridge the spatial and temporal resolution gaps between what climate modelers are currently able to provide (low resolution, coarse-scale data) and what impact assessors require. Even if global climate models in the future are run at high resolution, there will remain the need to ‘downscale’ the results from such models to individual sites or localities for impact studies (Wilby *et al.*, 2002).

The climate projections and their associated applications have become an important topic during recent decades to improve the understanding of the causes and consequences of global warming. Several research teams around the world develop models to simulate the current climate and its future evolution under different greenhouse gas and aerosol scenarios (Buser *et al.*, 2009). Global coupled Atmospheric-Ocean General

Circulation Models (coupled GCMs) are the modeling tools that are used in theoretical investigations of climatic change mechanisms (Covey *et al.*, 2003). By using GCMs, we can simulate the present and future climate changes under different scenarios to understand the climate variability and its impacts on the water resources. The GCMs simulations for the fifth assessment report (AR5) of the IPCC have recently become available (Taylor *et al.*, 2012). Comparing to the IPCC AR4, the GCMs in AR5 include a more diverse set of model types (i.e. climate/Earth system models with more interactive components such as atmospheric chemistry, aerosols, dynamic vegetation, ice sheets, and carbon cycle) (Liu *et al.*, 2013). Some improvements in the physics, numerical algorithms, and configurations are implemented in the IPCC AR5 models with a new set of scenarios called Representative Concentration Pathways (RCPs) used in the AR5 simulations (Moss *et al.*, 2010). The RCPs span a large range of stabilization, mitigation, and non-mitigation pathways. Consequently, the range of the temperature estimates is larger than that of the scenarios in the AR4, which only covers non-mitigation scenarios (Rogelj *et al.*, 2012). It is expected that some of the scientific questions that occur during the preparation of the IPCC AR4 will be addressed in the AR5 (Taylor *et al.*, 2012).

Agriculture in Ethiopia is mostly small-scale, rainfall dependent, and traditional. The heavy reliance of the Ethiopian economy on rain-fed agriculture makes it particularly vulnerable to hydrological variability.

Droughts are the greatest and most recurring climate hazards in Ethiopia, particularly for pastoral and agro-pastoral communities that inhabit drought-prone areas. In 2015, the country experienced one of the worst droughts in decades due to a powerful El Niño weather event. Due to these problems, the climate change in Ethiopia is a topic of great interest. For this, several studies have been conducted in the country, particularly in the Upper Blue Nile River Basin (e.g., Conway, 2005; Kim *et al.*, 2008; Beyene *et al.*, 2010; Setegn *et al.*, 2011; Nigatu *et al.*, 2016). However, the magnitude of the climate change impact in the previous studies varies due to differences in the study period, and the methods used for analyses. Conway (2005) concluded that there is no long-term trend in the precipitation. The study by Kim *et al.* (2008) found that the average changes in precipitation, temperature, potential evapotranspiration, and runoff, can be increased about 11%, 2.3 °C, 16%, and 4%, respectively. The study by Setegn *et al.* (2011) concluded that the sensitivity of the water resources to the climate change in the Lake Tana Basin has the potential to cause a significant agricultural drought. Nigatu *et al.* (2016) concluded that the Lake Tana storage would increase under emission scenarios of A2 and B2. The previous studies were primarily focused on the early experiments of the IPCC. Evaluation and application of the updated generation of the AR5 GCMs in Ethiopia are missing. Moreover, policymakers need the latest information on the likely future impacts of climate change to reconcile

human society with natural systems. In this case, the model used in this study was the second generation Canadian Earth System Model (CanESM2) developed by the Canadian Centre for Climate Modeling and Analysis (CCCma) of Environment Canada. The CanESM2 outputs were used for three different climate scenarios viz., Representative Concentration Pathway (RCP) 2.6, 4.5 and 8.5. This study employed the freely available Statistical Downscaling Model (SDSM) that facilitates the single-site scenarios of daily surface weather variables under present and future climate forcing for the Lake Tana Basin.

The aim of this study is to assess the impact of climate change on the weather events, and surface water resources of the Lake Tana Basin. Emphasis is also placed on analyzing trends and variability in the extreme events of the daily temperature and precipitation. The standard precipitation index (SPI) was used to analyze the metrological and hydrological drought within the next 100 years. The SPI was designed to quantify the precipitation deficit for multiple timescales or moving averaging windows. These timescales reflect the impacts of drought on different water resources needed by various decision-makers. Meteorological and soil moisture conditions (agriculture) respond to precipitation anomalies on relatively short timescales, for example, 1-6 months, whereas streamflow, reservoirs, and groundwater respond to longer-term precipitation anomalies of the order of 6 months up to 24 months or longer. So, for example, one may want to

look at a 1- or 2-month SPI for meteorological drought, anywhere from 1-month to 6-month SPI for agricultural drought, and something like 6-month up to 24-month SPI or more for hydrological drought analyses and applications (WMO-No. 1090, 2012). The SPI can be calculated from 1 month up to 72 months. Statistically, 1–24 months is the best practical range of application (Guttman, 1994, 1998).

## **6.2. Methodology**

### **6.2.1. The Statistical Downscaling Model (SDSM)**

The SDSM, developed by Wilby *et al.* (2002), has seven discrete steps: 1) quality control and data transformation; 2) screening of predictor variables; 3) model calibration; 4) weather generation (using observed predictors); 5) statistical analyses; 6) graphical model output; 7) scenario generation (using climate model predictors). The SDSM is a combination of Multiple Linear Regression (MLR) and the Stochastic Weather Generator (SWG). MLR generates statistical/empirical relationships between NCEP predictors and predictands during the screening process of predictors, and the calibration process of SDSM results in some regression parameters. Ordinary Least Squares (OLS) and Dual Simplex (DS) are two kinds of optimization methods available for SDSM. There are two types of sub-models, unconditional and conditional, which are used according to the requirement of the predictands. For example, the unconditional sub-model is used for an

independent variable like temperature, and the conditional is used for a conditional (dependent) variable like precipitation (Wilby et al., 2002).

The 26 predictors of NCEP/NCAR were obtained from the Canadian Centre for Climate Modeling and Analysis (CCCma) (available at <http://www.ccds-dscc.ec.gc.ca/?page=pred-canesm2>) for the periods of 1961–2005. The screening of large-scale variables is the most important process in all types of statistical downscaling (Wilby et al., 2002; Huang et al., 2011). Many indicators can be used in this process. For this study, the combinations of the partial correlation, correlation matrix, explained variance, P-value, histograms, and scatter plots were used to select some suitable predictors from a multitude of atmospheric predictors. First, a correlation matrix between each predictand and the NCEP predictors (26 in this case) is found out, and then highly correlating predictors are selected. These predictors must show a physical relation with the predictands. It can be seen in different studies (Wilby et al., 2002; Chu et al., 2010) that mostly 1 – 3 large scale variables are believed to be enough to capture the variation of a predictand during calibration. It is better to use a smaller number of predictors during calibration because as the number of predictors increases in the regression equation, the chances of multiple collinearities also increase. So, the fewer the predictors, the lower is the chance of multiple collinearities during calibration. The description of the predictor variables is provided in Table 6.1.

### **6.2.2. Calibration and Validation**

The most recent data sets (1975 – 2005) were selected for the calibration and validation of the SDSM. Then, 20 ensembles each for precipitation, maximum, and minimum temperature were simulated by the calibrated model. The mean values of these ensembles were used in this study. Four performance indicators were used to evaluate the performance of the SDSM: Nash-Sutcliffe efficiency (NSE), root mean square error to the standard deviation of measured data (RSR), the coefficient of determination ( $R^2$ ), and percent bias (PBIAS).

### **6.2.3. Bias Correction**

Climate models often provide biased representations of observed time series, requires correction procedures (Christensen *et al.*, 2008; Teutschbein and Seibert, 2010). The linear-scaling approach (Lenderink *et al.*, 2007) that operates with monthly correction values based on the differences between observed and present-day simulated values was used for this study. Most of the previous studies followed this technique to adjust the bias of the downscaled weather data (e.g. Salzmann *et al.*, 2007).

Table 6.1. Description of predictor variables

<b>S.No.</b>	<b>Predictor variables</b>	<b>Description of predictor variables</b>	<b>S.No.</b>	<b>Predictor variables</b>	<b>Description of predictor variables</b>
1	mslp <sub>gl</sub>	mean sea level pressure	14	p5zh <sub>gl</sub>	500 hPa divergence of true wind
2	p1_f <sub>gl</sub>	1000 hPa wind speed	15	p850 <sub>gl</sub>	850 hPa geopotential
3	p1_u <sub>gl</sub>	1000 hPa zonal wind component	16	p8_f <sub>gl</sub>	850 hPa wind speed
4	p1_v <sub>gl</sub>	1000 hPa meridional wind component	17	p8_u <sub>gl</sub>	850 hPa zonal wind component
5	p1_z <sub>gl</sub>	1000 hPa relative vorticity of wind	18	p8_v <sub>gl</sub>	850 hPa meridional wind component
6	p1th <sub>gl</sub>	1000 hPa wind direction	19	p8_z <sub>gl</sub>	850 hPa relative vorticity of wind
7	p1zh <sub>gl</sub>	1000 hPa divergence of true wind	20	p8th <sub>gl</sub>	850 hPa wind direction
8	p500 <sub>gl</sub>	500 hPa Geopotential	21	p8zh <sub>gl</sub>	850 hPa divergence of true wind
9	p5_f <sub>gl</sub>	500 hPa wind speed	22	prcp <sub>gl</sub>	total precipitation
10	p5_u <sub>gl</sub>	500 hPa zonal wind component	23	s500 <sub>gl</sub>	500 hPa specific humidity
11	p5_v <sub>gl</sub>	500 hPa meridional wind component	24	s850 <sub>gl</sub>	850 hPa specific humidity
12	p5_z <sub>gl</sub>	500hPa relative vorticity of wind	25	shum <sub>gl</sub>	1000 hPa specific humidity
13	p5th <sub>gl</sub>	500 hPa wind direction	26	temp <sub>gl</sub>	air temperature at 2m

hPa is atmospheric pressure in hectopascal

The precipitation was corrected with a factor based on the ratio of long-term monthly mean observed, and control run data (equation 6.1) whereas, the temperature was corrected with the help of an additive term based on the difference of long-term monthly mean observed and control run data (equation 6.2). Then, the biases were adjusted with future simulated daily time series according to their respective months. The assumption is that the applied correction factors were assumed to remain constant even for future conditions.

$$P_{cor} = P_{FSIM} \times (\bar{P}_{OBS} / \bar{P}_{BSIM}) \quad (6.1)$$

$$T_{cor} = T_{FSIM} - (\bar{T}_{BSIM} - \bar{T}_{OBS}) \quad (6.2)$$

where  $P_{cor}$  and  $T_{cor}$  are the corrected (de-biased) future daily time series of precipitation and temperature, respectively.  $P_{FSIM}$  and  $T_{FSIM}$  are the raw downscaled daily time series of precipitation and temperature data, respectively, for future periods (i.e. 2011-2040, 2041-2070, and 2071-2099).  $\bar{P}_{BSIM}$  and  $\bar{T}_{BSIM}$  are the long-term mean monthly simulated values of precipitation and temperature, respectively, for the baseline periods (1975-2005).  $\bar{P}_{OBS}$  and  $\bar{T}_{OBS}$  are the long-term mean monthly observed values of precipitation and temperature, respectively, for the control period (1975-2005).

The frequency and intensity of precipitation are the two most common factors affecting precipitation variability. For this, two methodologies were

considered to apply the linear scaling correction factor (i.e. time-domain time series matching, and quantile-domain time series matching).

***- Time-domain based time series matching***

Computations are carried out to match the day-to-day events. This method keeps track of the time to compute the correction factor and as well to apply it to the future time series data. The output of this result can be useful for process wise water resources operation.

***- Quantile-domain based time series matching***

In this technique, the bias correction factors were calculated by categorizing the whole time series control data into seven groups after arranging the whole time series in descending order. The categorized weather events were: extreme wet weather events (0-1%), severe wet weather events (1-5%), moderate wet weather events (5-10%), near normal weather events (10-20%), moderate weather events (20-30%), severe dry weather events (30-40%), and extreme dry weather events (40-100%). Then, the biases were introduced to the future weather events according to their respective frequency intervals. The surface runoff response from this input data can be used for adaptation and mitigation of climate change.

#### **6.2.4. Analysis of Future Changes in Meteorological Variables and Surface Runoff**

The SWAT model was used to simulate the river flow. The future changes in the weather events and surface runoff in relative to the baseline scenarios were analyzed by using Mann-Kendall and Sen's slope estimator statistical tests. The purpose of the Mann-Kendall test (Mann, 1945; Kendall, 1975; Gilbert, 1987) is to statistically assess if there is a monotonic upward or downward trend of the variable of interest over time. A monotonic upward (downward) trend means that the variable consistently increases (decreases) through time. We have also used the standard precipitation index (SPI) to analyze the meteorological and hydrological droughts that expected to happen in the next 100 years. The detailed description of Mann-Kendall and Sen's slope methods are provided in Chapter 3.

##### **- *Standardized Precipitation Index (SPI)***

The deficit of rainfall over a period at a specified location could lead to various degrees of drought conditions affecting water resources, agriculture, and socio-economic activities. Since rainfall varies significantly among different regions, the concept of drought may differ from place to place. As such, for more effective assessment of the drought phenomena, in 2010 the World Meteorological Organization (WMO) selected the SPI as a key meteorological drought indicator to be produced operationally by

meteorological services. McKee *et al.* (1993) developed the SPI to quantify the precipitation deficit for multiple time scales (see Table 6.2 to define drought intensities resulting from the SPI). These time scales reflect the impact of drought on the availability of different water resources. The key advantage of SPI is that it can be calculated for different time scales. Suppose we have a time series of monthly total precipitation  $P_t$ , the equations calculating the SPI for a chosen time scale  $m$  are as follows:

$$R_t = P_t + P_{t-1} + \dots + P_{t-m+1} \quad (6.3)$$

where  $R_t$  is the aggregated precipitation for the t-month time scale.

By aggregating the precipitation for the desired period, each month has a new value determined from the previous  $m$  months. Next, a two-parameter Gamma distribution is fitted to the  $R_t$ .

$$g\left(\frac{x}{\alpha}, \beta\right) = \frac{1}{\Gamma(\alpha)\beta^\alpha} x^{\alpha-1} e^{-\frac{x}{\beta}}, \quad 0 \leq x \leq \infty, \quad \alpha > 0, \quad \beta > 0 \quad (6.4)$$

After obtaining the estimated shape parameter  $\alpha$  and scale parameter  $\beta$ , we then standardized  $R_t$  data.

$$SPI_t = \frac{R_t - \bar{R}_t}{S_{R_t}} \quad (6.5)$$

where  $\bar{R}_t = \alpha\beta$  is the mean that estimated from the fitted gamma distribution;  $S_{R_t} = \sqrt{\alpha\beta^2}$  is the standard deviation that estimated from the fitted gamma distribution.

Table 6.2. Standard Precipitation Index (SPI) classification

<b>SPI value</b>	<b>Class</b>
$SPI \geq 2.00$	extremely wet
$1.50 \leq SPI < 2.00$	very wet
$1.00 \leq SPI < 1.50$	moderately wet
$-1.00 < SPI < 1.00$	near normal
$-1.50 < SPI \leq -1.00$	moderately dry
$-2.00 < SPI \leq -1.50$	severely dry
$SPI \leq -2.00$	extremely dry

(Source: McKee *et al.*, 1993)

## **6.3. Application**

### **6.3.1. Screening of Predictors**

The predictor variables available from NCEP/NCAR reanalysis data were chosen to put forth for calculating the correlation coefficient (partial  $r$ ) following the preliminary analysis of explained variance of all the predictor variables. The final set of predictor variables were selected after analyzing the correlation coefficient and checking the association of predictors and predictand via scatter-plot. The dominant predictor variables selected for simulating both maximum and minimum temperature for all stations were air temperature at 2m, specific humidity at 1000 hPa, Geopotential at 850 hPa, and relative vorticity of the wind at 500 hPa. Similarly, total precipitation, wind direction at 1000 hPa, specific humidity at 1000 hPa, and wind speed at 850 hPa were selected as the dominant predictor variables to simulate the precipitation at all stations.

### **6.3.2. Performance of the Statistical Downscaling Model, SDSM**

Four performance measures were used to evaluate the performance of SDSM during the calibration (1975 – 2000) and validation (2001 – 2005) period. Based on the outputs of SDSM on a monthly basis, the NSE value for the minimum and maximum temperature output, calculated in all stations during the calibration period, ranges from 0.04 to 0.84. Similarly,

the NSE value ranges from -1.82 to 0.89 for precipitation simulation. The results showed that the SDSM captured the variability and pattern of minimum and maximum temperature. In contrast, the SDSM did not capture the pattern and variation of the precipitation as similar to temperature. Therefore, a bias correction approach was introduced to the climate variables to obtain a more realistic and unbiased data of future climate.

### **6.3.3. Application of Bias Correction**

As the performance indicators simulated by SDSM were not satisfactory (typically for precipitation simulation), the bias correction factor was applied to minimize the biases between simulated and observed data. The performance measure values showed that the application of bias correction on the precipitation showed a significant improvement. The NSE values for the bias-corrected precipitation in time-domain varied from the relatively poor values of 0.71 in Maksegnit to the best values of 0.90 in Enjibara during the calibration period. For validation period, it ranges from the poor values of 0.80 in Gonder to the best values of 0.92 in both Bahirdar & Enjibara. Similarly, for the bias-corrected precipitation in quantile-domain, the NSE values varied from the relatively poor value of 0.96 in Gonder to the best values of 0.99 in both Dangila & Enjibara during the calibration period. For the validation period, the NSE value varied from 0.55 in Gonder to the best values of 0.99 in Dangila. The maximum error reduction (%) in

the precipitation was found in the Enjibara weather station, which was 86.5 % during the calibration period and 62.79 % during the validation period when the precipitation was corrected in the time-domain. The quantile-domain based bias-correction reduced 50 % error in Maksegnit during the calibration period and 94.36 % in Gonder weather station during the validation period (See Figure 6.1). In general, the two bias correction approaches reduced the error of the raw downscaled precipitation to some extent. However, the result showed that the quantile-domain based bias correction technique is more effective than the time-domain time series matching to improve the variability of the precipitation (see Figure 6.2). Figure 6.2 shows a box plot comparison of the observed, modeled, time-domain corrected, and quantile-domain corrected precipitation values.

It is clearly seen from Figure 6.2 that the variability of the precipitation is significantly improved in all weather stations with the quantile-domain based bias-correction. The quantile-domain based bias-correction improved most of the statistical characteristics and had the closest variability ranges with the observation. The bias-correction was also applied to adjust the downscaled maximum and minimum temperature based on equation 6.2 in time-domain. The result of the bias-corrected temperature also showed an improvement in the performance measures statistics. The NSE value varied from 0.52 at Maksegnit to 0.82 at Bahirdar weather station during the calibration period, and it ranges from 0.32 at Maksegnit to 0.92 at the

Ayikel weather station during the validation period. Similarly, for the minimum temperature, the NSE value ranges from 0.43 at Zege to 0.81 at Dangila weather station during the calibration period, whereas it ranges from 0.54 at Zege to 0.86 at Dangila weather station during the validation period.

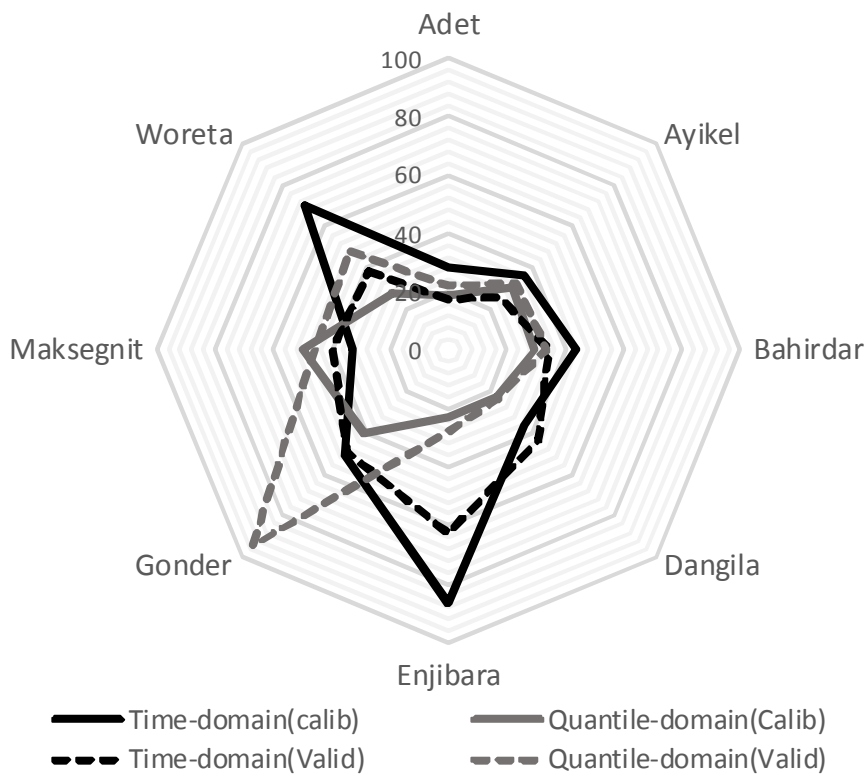


Figure 6.1. The percent error reduction in bias-corrected precipitation in relative to the raw downscaled precipitation

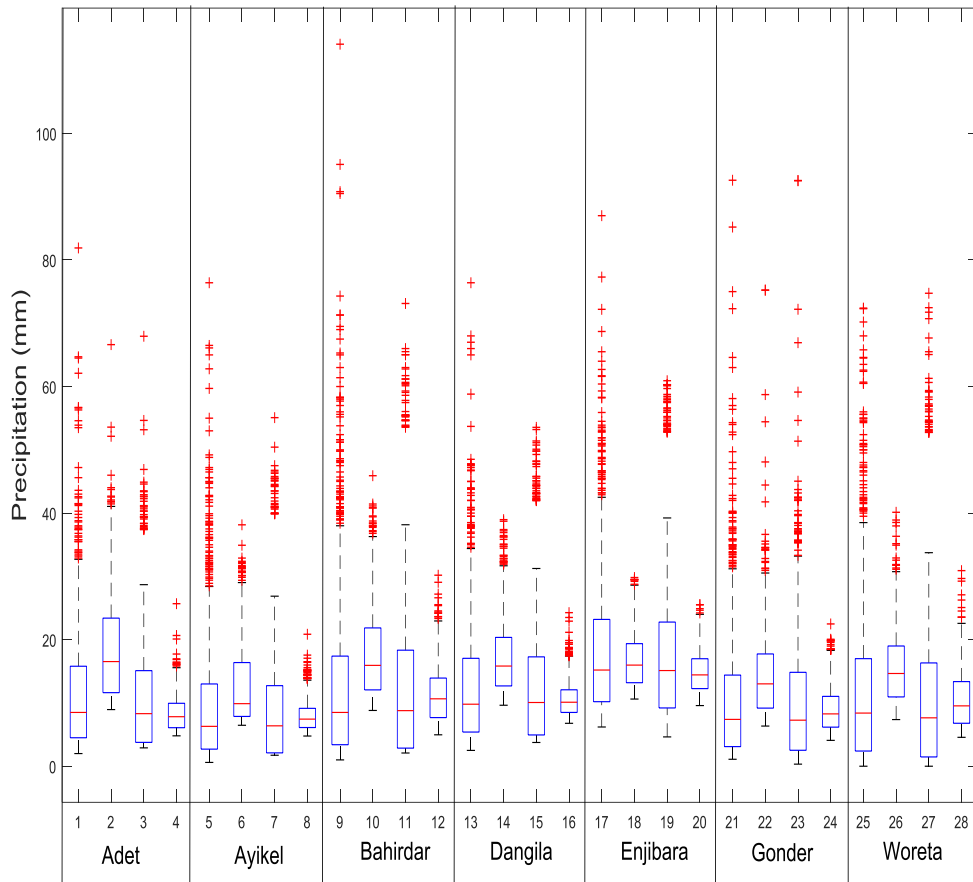


Figure 6.2. The boxplot of observed, modeled, and bias-corrected precipitation. (In each station (shown in the box), from left to right shows the observed, modeled, bias-corrected in quantile domain, and bias-corrected in the time domain, respectively)

### **6.3.4. Future Changes in Precipitation and Temperature**

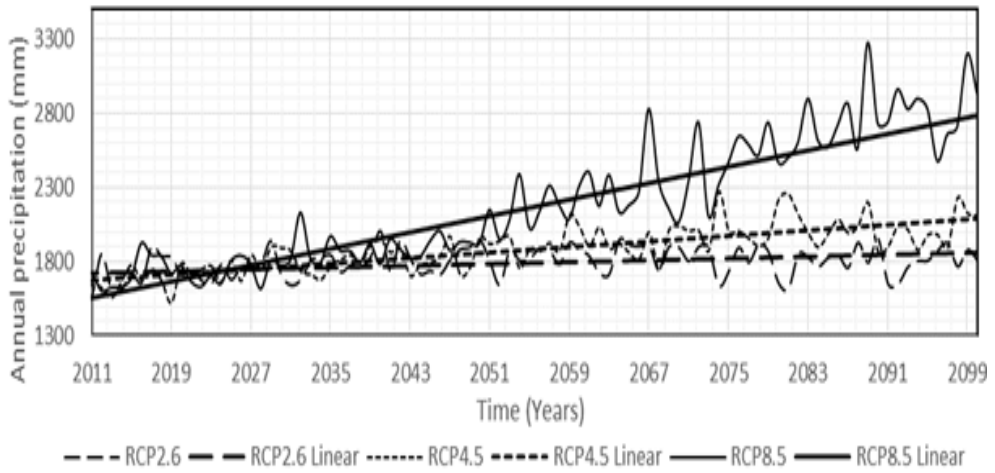
The overall results showed the increase in mean annual precipitation in all weather stations of the Lake Tana Basin for future periods (the 2020s, 2050s, and 2080s) compared to the precipitation in the baseline scenario. Based on the quantile-domain bias-corrected precipitation, the future mean annual precipitation relative to the precipitation in the baseline period showed a significant decrease in the 2020s by 0.87%, 5.54%, 20.21% under RCP2.6, RCP4.5, and RCP8.5, respectively, in the Gonder weather station. The future mean annual precipitation in the Ayikel station has also shown a significant decrease by 14.93% in the 2020s under RCP4.5. The mean annual precipitation in all other stations showed an increasing magnitude in all future time periods and RCPs (see Table 6.3). Similarly, the mean annual bias-corrected precipitation in time-domain showed an increasing in the amount in all weather stations and future time periods under all RCPs. Figure 6.3 presents the pattern of the annual bias-corrected precipitation in quantile and time-domain for the period of 2011-2100 in the Bahirdar weather station. The pattern of the bias-corrected annual precipitation for the other weather stations are provided in Appendix B.

The climate change signal was quantified by applying the Mann-Kendall trend test and Sen's nonparametric true trend slope estimate as well as the standard precipitation index (SPI). The Mann-Kendall trend test was used to analyze the inter-annual variability of precipitation amount in all

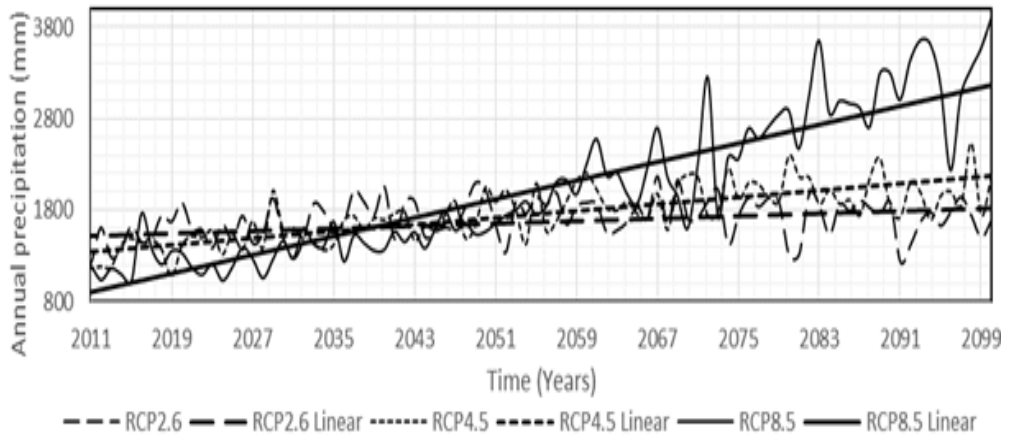
weather stations. The Mann-Kendall trend test and Sen's nonparametric true trend slope estimate on annual precipitation values resulting in the values reported in Table 6.4. The absolute value of  $Z$  is compared to the standard normal cumulative distribution to define if there is a trend or not at the selected level of significance. The Mann-Kendall trend test statistic indicated as there is an increasing precipitation trend for all RCPs scenarios in all weather stations of the Lake Tana Basin except the decrease in Ayikel, and Woreta weather stations under RCP2.6. For RCP8.5 in each station, the increasing trend has occurred at the significance level of 0.001. The RCP8.5 scenario has showed that the annual increase in precipitation by 49.86 mm, 8.49 mm, 13.81 mm, 17.45 mm, 13.22 mm, 7.82 mm and 6.70 mm in Adet, Ayikel, Bahirdar, Dangila, Enjibara, Gonder, and Woreta weather stations, respectively, with respect to the bias-corrected precipitation in the time-domain. The highest increase has occurred in Adet weather station with 49.86 mm increments per year under RCP8.5. In general, the result showed that there would be a probable high flood event in the study area and we infer that the result can be a warning for preparation to overcome the response of high weather events.

Table 6.3. % increase in mean annual bias-corrected precipitation in quantile and time domain in relative to the precipitation in the baseline period

Domain	Weather station	RCP2.6			RCP4.5			RCP8.5		
		2011-2040	2041-2070	2071-2100	2011-2040	2041-2070	2071-2100	2011-2040	2041-2070	2071-2100
Quantile domain	Adet	38.48	78.67	64.64	30.72	93.14	135.02	10.85	154.83	504.26
	Aykikel	-9.60	-11.62	-9.77	-14.93	-4.07	19.08	-25.84	42.30	860.45
	Bahirdar	12.52	23.39	20.21	3.37	27.17	40.22	-9.13	31.41	107.29
	Dangila	19.18	41.13	29.90	10.92	41.43	77.80	7.33	83.19	290.34
	Enjibara	7.96	14.21	16.28	3.64	17.01	23.66	-7.00	22.68	62.32
	Gonder	-0.87	5.71	4.91	-5.54	6.23	19.86	-20.21	13.60	77.81
	Woreta	12.51	19.39	13.04	0.65	23.67	38.74	-13.91	26.12	109.87
Time domain	Adet	54.32	77.86	68.77	57.47	95.98	119.57	60.93	157.66	382.70
	Aykikel	12.30	11.04	11.87	10.20	12.24	14.71	12.49	19.61	85.82
	Bahirdar	22.82	28.27	26.40	22.54	32.50	41.93	24.59	48.46	87.73
	Dangila	42.73	50.74	46.33	40.77	56.79	65.75	45.04	75.00	128.23
	Enjibara	27.91	31.53	31.17	26.93	35.57	39.83	27.76	45.79	65.17
	Gonder	19.50	23.68	21.89	19.32	27.48	32.18	19.41	38.07	62.00
	Woreta	27.00	28.70	26.43	25.49	31.57	35.89	27.73	41.04	61.52



a) Time-domain based bias-corrected precipitation



b) Quantile-domain based bias-corrected precipitation

Figure 6.3. Future changes in annual precipitation after bias correction at Bahirdar weather station

Table 6.4. Mann-Kendall trend test and Sen's nonparametric trend slope

Station	RCPs	Time-domain bias correction				Quantile-domain bias correction			
		Test Z	Trend sign level	Sen's slope	Sen's constant	Test Z	Trend sign level	Sen's slope	Sen's constant
Adet	RCP2.6	4.60	$\alpha = 0.001$	4.23	1839.23	5.18	$\alpha = 0.001$	7.46	1593.33
	RCP4.5	9.93	$\alpha = 0.001$	13.33	1698.59	9.90	$\alpha = 0.001$	21.64	1237.04
	RCP8.5	11.73	$\alpha = 0.001$	49.86	1054.18	11.88	$\alpha = 0.001$	75.97	-55.55
Ayikel	RCP2.6	-1.41	$\alpha > 0.1$	-0.38	1197.87	-1.31	$\alpha > 0.1$	-0.59	976.33
	RCP4.5	2.49	$\alpha = 0.05$	0.65	1152.92	4.14	$\alpha = 0.001$	3.37	830.27
	RCP8.5	9.64	$\alpha = 0.001$	8.49	992.39	10.86	$\alpha = 0.001$	70.95	-705.48
Bahirdar	RCP2.6	3.68	$\alpha = 0.001$	1.59	1715.73	3.65	$\alpha = 0.001$	3.51	1496.35
	RCP4.5	8.67	$\alpha = 0.001$	4.68	1648.38	8.39	$\alpha = 0.001$	9.29	1300.20
	RCP8.5	11.19	$\alpha = 0.001$	13.81	1486.82	11.39	$\alpha = 0.001$	25.42	777.56
Dangila	RCP2.6	2.82	$\alpha = 0.01$	1.13	2037.71	3.00	$\alpha = 0.01$	2.33	1677.96
	RCP4.5	9.40	$\alpha = 0.001$	6.00	1922.90	8.76	$\alpha = 0.001$	12.17	1351.56
	RCP8.5	12.07	$\alpha = 0.001$	17.45	1756.12	10.95	$\alpha = 0.001$	43.25	638.87
Enjibara	RCP2.6	3.42	$\alpha = 0.001$	1.83	2738.83	3.68	$\alpha = 0.001$	4.11	2194.26
	RCP4.5	7.88	$\alpha = 0.001$	4.87	2684.16	6.89	$\alpha = 0.001$	7.58	2098.27
	RCP8.5	12.10	$\alpha = 0.001$	13.22	2545.33	11.89	$\alpha = 0.001$	23.89	1549.26
Gonder	RCP2.6	2.56	$\alpha = 0.05$	0.77	1420.80	2.97	$\alpha = 0.01$	1.92	1129.90
	RCP4.5	7.47	$\alpha = 0.001$	2.67	1385.44	6.42	$\alpha = 0.001$	5.10	1029.37
	RCP8.5	11.16	$\alpha = 0.001$	7.82	1289.25	10.81	$\alpha = 0.001$	16.74	632.28
Woreta	RCP2.6	-0.19	$\alpha > 0.1$	-0.06	1644.94	-0.14	$\alpha > 0.1$	-0.17	1520.04
	RCP4.5	5.54	$\alpha = 0.001$	2.04	1584.35	6.85	$\alpha = 0.001$	6.87	1208.42
	RCP8.5	10.50	$\alpha = 0.001$	6.70	1506.10	10.79	$\alpha = 0.001$	23.27	603.32

Table 6.5.  $\Delta^0\text{C}$  in future mean temperature in relative to the baseline

Temperature	Weather station	RCP2.6			RCP4.5			RCP8.5		
		2011-2040	2041-2070	2071-2100	2011-2040	2041-2070	2071-2100	2011-2040	2041-2070	2071-2100
Maximum Temperature	Adet	1.17	1.19	1.20	1.17	1.22	1.24	1.19	1.27	1.33
	Ayikel	0.27	0.29	0.28	0.28	0.30	0.30	0.29	0.30	0.34
	Bahirdar	1.02	1.18	1.17	1.06	1.29	1.43	1.06	1.54	2.04
	Dangila	-0.12	0.01	0.02	-0.10	0.10	0.15	-0.08	0.23	0.56
	Enfranz	-0.01	0.14	0.14	0.01	0.30	0.39	0.05	0.50	1.09
	Woreta	0.85	0.94	0.94	0.89	1.04	1.10	0.92	1.13	1.38
	Zege	<b>4.79</b>	<b>5.23</b>	<b>5.10</b>	<b>4.77</b>	<b>5.56</b>	<b>5.94</b>	<b>4.87</b>	<b>6.26</b>	<b>7.94</b>
Minimum Temperature	Adet	-1.04	-0.95	-0.96	-1.03	-0.89	-0.78	-1.03	-0.74	-0.44
	Ayikel	0.21	0.30	0.25	0.21	0.34	0.41	0.22	0.48	0.75
	Bahirdar	<b>1.45</b>	<b>1.55</b>	<b>1.51</b>	<b>1.47</b>	<b>1.67</b>	<b>1.73</b>	<b>1.47</b>	<b>1.83</b>	<b>2.27</b>
	Dangila	-0.01	0.01	0.03	-0.05	0.04	0.09	-0.03	0.13	0.40
	Enfranz	-0.49	-0.13	-0.19	-0.47	0.09	0.42	-0.40	0.68	1.89
	Woreta	-0.51	-0.28	-0.32	-0.49	-0.03	0.20	-0.44	0.35	1.31
	Zege	0.72	0.94	0.86	0.74	1.06	1.26	0.74	1.43	2.12

It is of immense importance to discuss the ecological, economic, and social impacts that could result if increasing precipitation trends continue in the future. The vulnerability to storms might further be aggravated if extreme rainfall episodes continue in the future and consequently lead to inland flooding. Institutional changes and management goals have to be, therefore, adapted in a timely manner. Increased precipitation can influence the water quality and possibly result in the outbreak of waterborne diseases due to sewage overflows. On the other hand, the increasing trend of precipitation in this basin has a benefit of increasing agricultural productivity for the local farmers.

Figure 6.4 presents the future changes in the maximum and minimum temperature values in relative to the baseline temperature, which showed that the increase in minimum and maximum temperature. Table 6.5 presents the maximum and minimum temperature changes for all the future climate change scenarios. The overall average changes in the maximum temperature for the time periods of 2020s, 2050s, and 2080s, respectively, showed a value of 1.14 °C, 1.28 °C, and 1.26 °C under RCP2.6; 1.15 °C, 1.40 °C, and 1.50 °C under RCP4.5; 1.19 °C, 1.60 °C, and 2.10 °C under RCP8.5. Similarly, the overall average changes in the minimum temperature for the time periods of 2020s, 2050s, and 2080s, respectively, showed a value of 0.05 °C, 0.21 °C, and 0.17 °C under RCP2.6; 0.05 °C, 0.33 °C, and 0.44 °C under RCP4.5; 0.07 °C, 0.60 °C, and 1.19 °C under RCP8.5. The highest

increase of the minimum temperature was found to be 2.27 °C at Bahirdar weather station in the 2080s under RCP8.5 and the highest increase in the maximum temperature was found to be 7.94 °C at Zege weather station in the 2080s under RCP2.6.

Figure 6.5 presents the time series plot of the standard precipitation index (SPI) over a 6-month period. The 6-month SPI time series plot for the other weather stations are provided in Appendix B. The negative SPI values represent a rainfall deficit, whereas positive SPI values indicate rainfall surplus. The average values of a 6-month SPI indicated that 2.12% of the time for extremely wet, 4.4% of the time for very wet, 9.93% of the time for moderately wet, 66.81% of the time for near normal, 10.64% of the time for moderately drought, 4.33% of the time for severely drought, and 1.77% of the time for extreme drought. Since the SPI is standardized, these percentages are expected from a normal distribution of the SPI. The frequency of time in each dry or wet category expressed as the percentage of months in a given category is shown in Figure 6.6 for Adet, Ayikel, Bahirdar, Dangila, Enjibara, Gonder, and Woreta weather stations. It is apparent from these results that the SPI for each RCPs scenarios tends to have the same frequencies. From Figure 6.6, the maximum frequency of extremely wet event occurred in Ayikel station with 4.05%, whereas the maximum extremely drought occurred in Enjibara station with 3.70%.

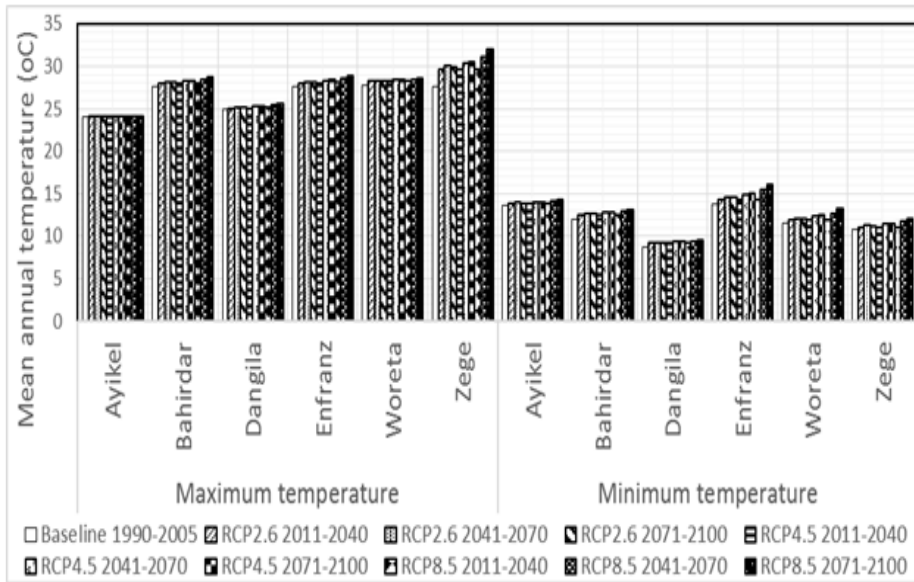


Figure 6.4. Comparison of future changes in temperature in relative to the baseline

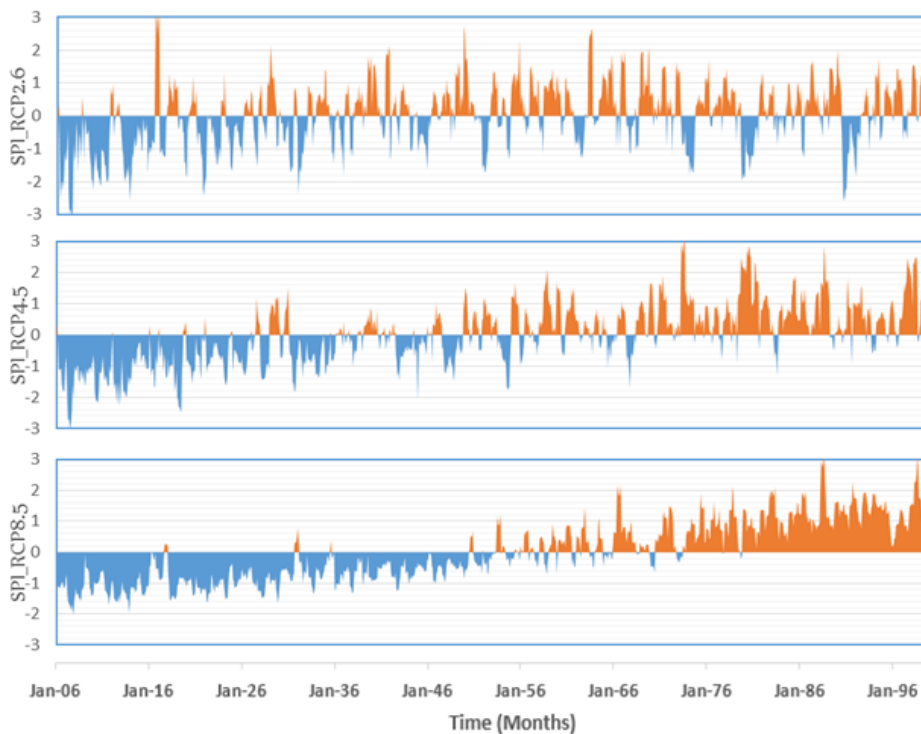


Figure 6.5. Time series plot of a 6-month standard precipitation index in Bahirdar weather station under RCP2.6, RCP4.5, and RCP8.5.

### **6.3.5. Future Changes in the Surface Runoff**

The simulated streamflow using SWAT model based on the three RCPs are presented in Figure 6.7 & 6.8. From these Figures, it can be easily seen that the mean annual streamflow showed the increasing trend almost under all scenarios and during all future periods. Therefore, the future inflow to the Lake Tana is expected to be remarkably higher compared to the baseline period (see Figure 6.9). The long-term mean annual inflow to the Lake Tana was found to be substantially high with 69%, 100%, and 206% compared to the mean annual streamflow, 6355 Mm<sup>3</sup>/year, in the baseline period when the bias-corrected precipitation in quantile-domain was used to simulate the runoff using SWAT model. These values were found to be 92%, 111%, and 165%, respectively, when the bias-corrected precipitation in time-domain was used to drive the SWAT model. Figure 6.9 presents the monthly water balance components of the Lake Tana for the time periods of (2011-2040), (2041-2070) and (2071-2100). The monthly water balance components showed that the increase in magnitude for the future periods in relative to the baseline periods. The total monthly average water balance component values of the basin under all climate change scenarios are given in Appendix C, from Table C.3 to Table C.8. The annual average water balance component values of the LTB is also given in Appendix C, Table C.9. Figure 6.10, 6.11, & 6.12 presents the annual average water balance components of the LTB for RCP2.6, RCP4.5 & RCP8.5, respectively.

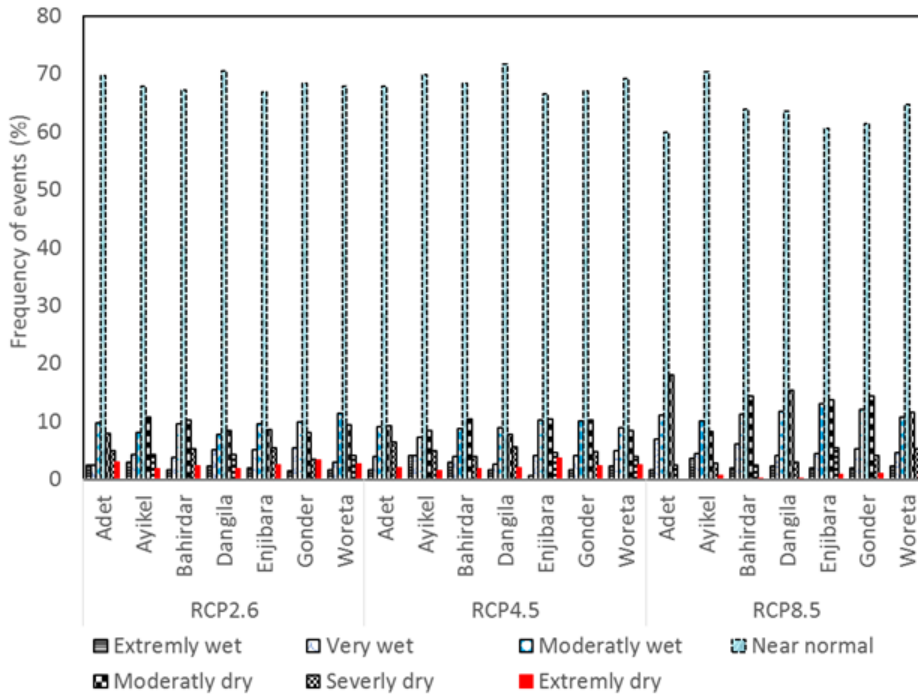


Figure 6.6. Frequency of time (%) in each dry or wet category of SPI-6 in all weather stations for the period of 2006–2100

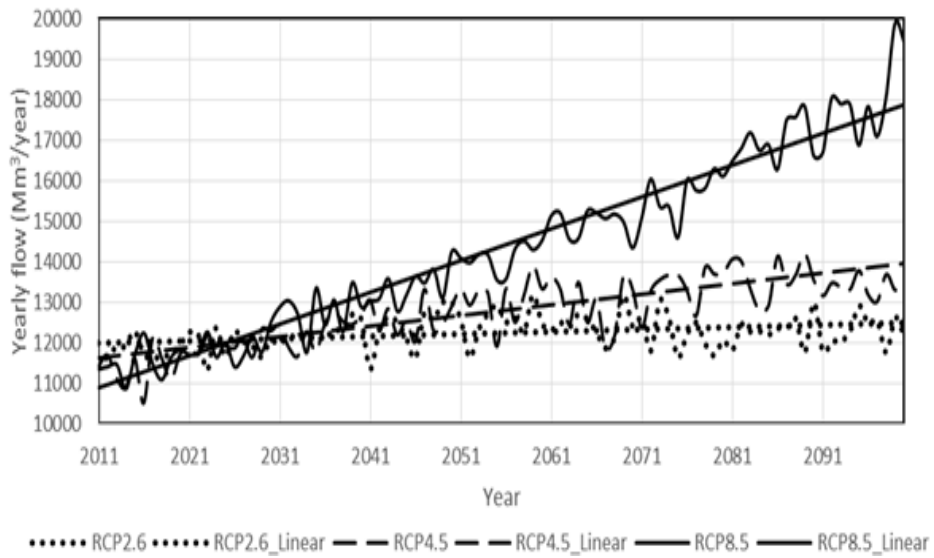


Figure 6.7. Mean annual inflow into the Lake Tana by using the bias-corrected precipitation in time-domain

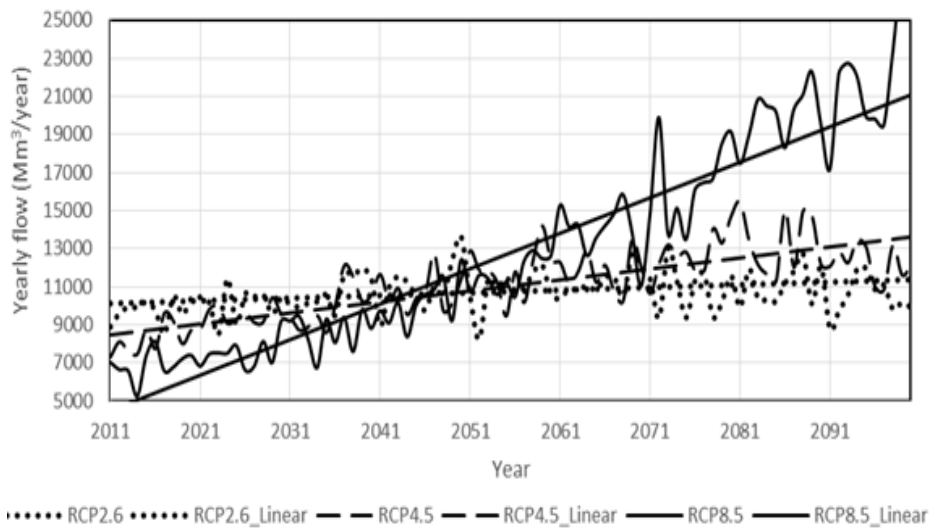


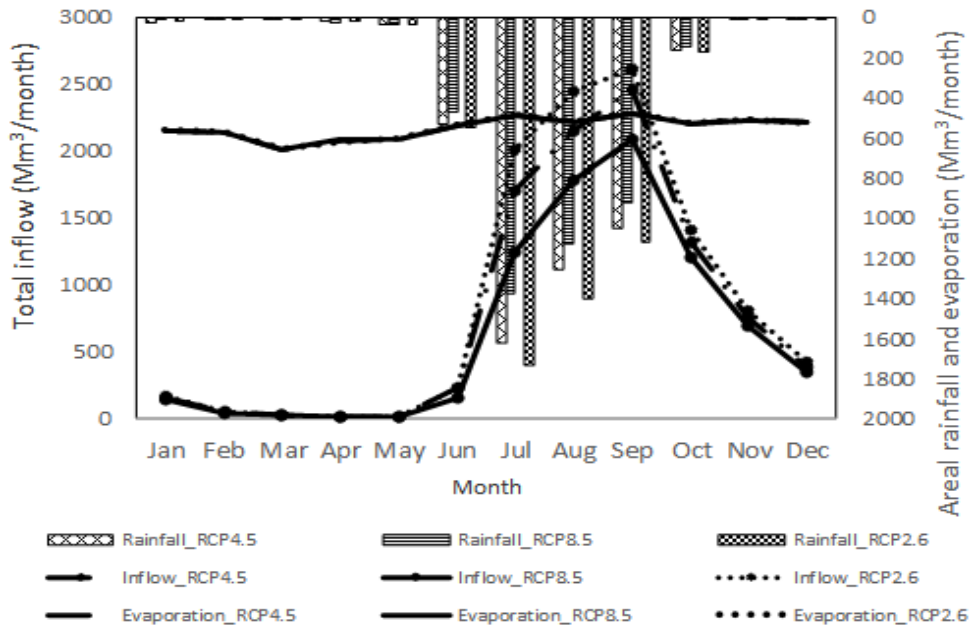
Figure 6.8. Mean annual inflow into the Lake Tana by using the bias-corrected precipitation in quantile-domain

Table 6.6. Water balance components of the Lake Tana under climate change

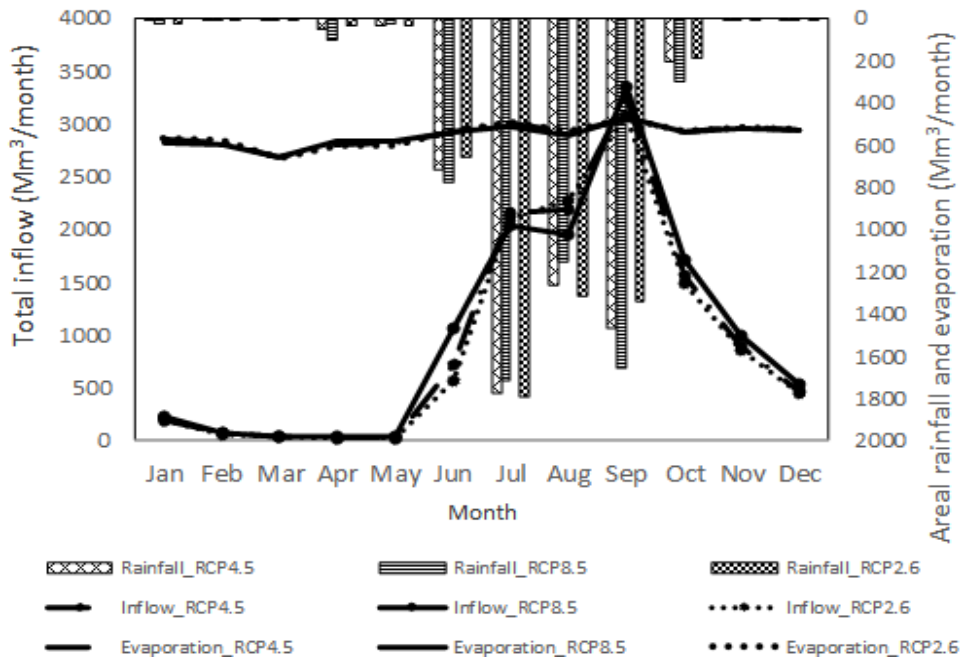
Periods	Scenarios	Rainfall (mm/year)		Evaporation (Mm/year)	Surface inflow (Mm <sup>3</sup> /year)	
		Time-domain	Quantile-domain	time-domain	Time-domain	Quantile-domain
2020s	RCP2.6	1528	1285	2155	12005	10181
	RCP4.5	1517	1176	2158	11886	9221
	RCP8.5	1532	1002	2159	12063	7688
2050s	RCP2.6	1564	1365	2166	12437	11051
	RCP4.5	1605	1402	2169	12873	11450
	RCP8.5	1729	1464	2185	14158	11941
2080s	RCP2.6	1539	1328	2167	12255	10803
	RCP4.5	1665	1577	2179	13451	12744
	RCP8.5	2008	2349	2206	16872	19507

Table 6.7. Mann-Kendall trend test

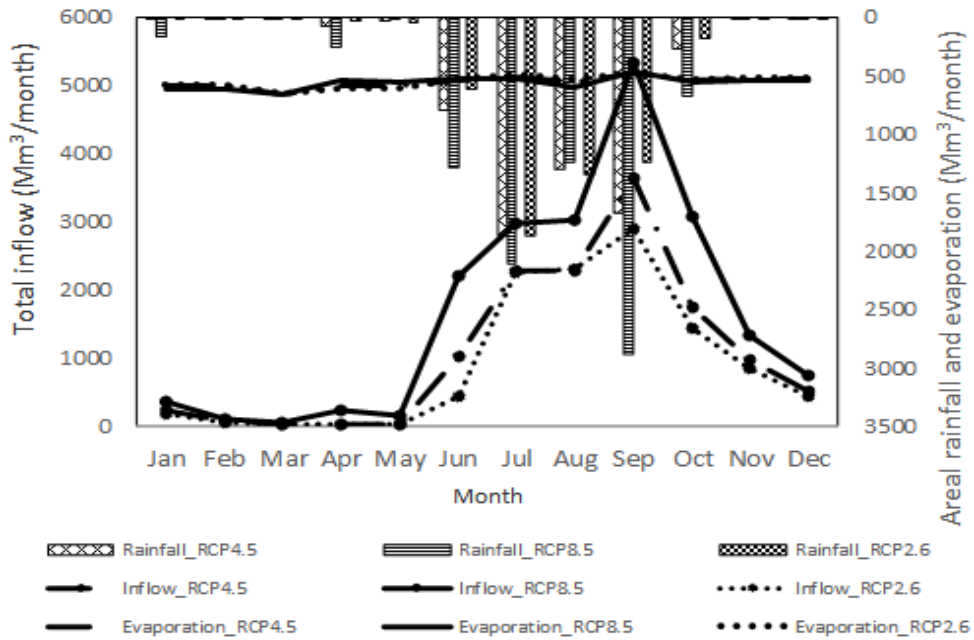
Domain	RCPs	Test z	Trend significance level ( $\alpha$ )
Quantile domain	RCP2.6	2.93	$\alpha = 0.01$
	RCP4.5	8.34	$\alpha = 0.001$
	RCP8.5	11.71	$\alpha = 0.001$
Time domain	RCP2.6	2.78	$\alpha = 0.01$
	RCP4.5	8.49	$\alpha = 0.001$
	RCP8.5	12.25	$\alpha = 0.001$



a) Monthly water balance components of Lake Tana for the time periods of (2011-2040)



b) Monthly water balance components of Lake Tana for the time periods of (2041-2070)



c) Monthly water balance components of Lake Tana for the time periods of (2071-2100)

Figure 6.9. Monthly water balance components of the Lake Tana for future scenario

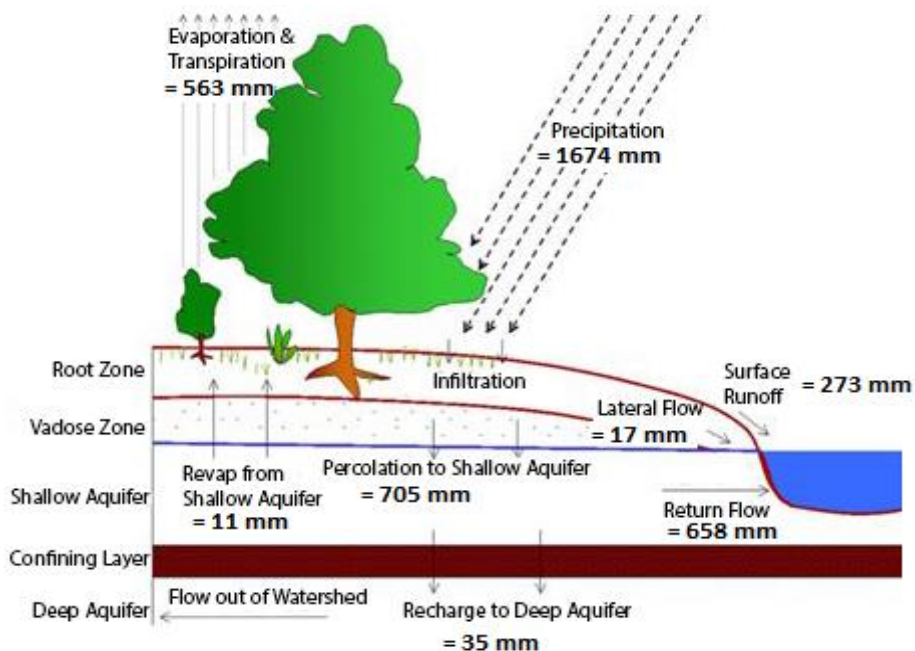


Figure 6.10. Average annual simulated water balance components for the future scenario under RCP2.6 in time-domain (2011-2100).

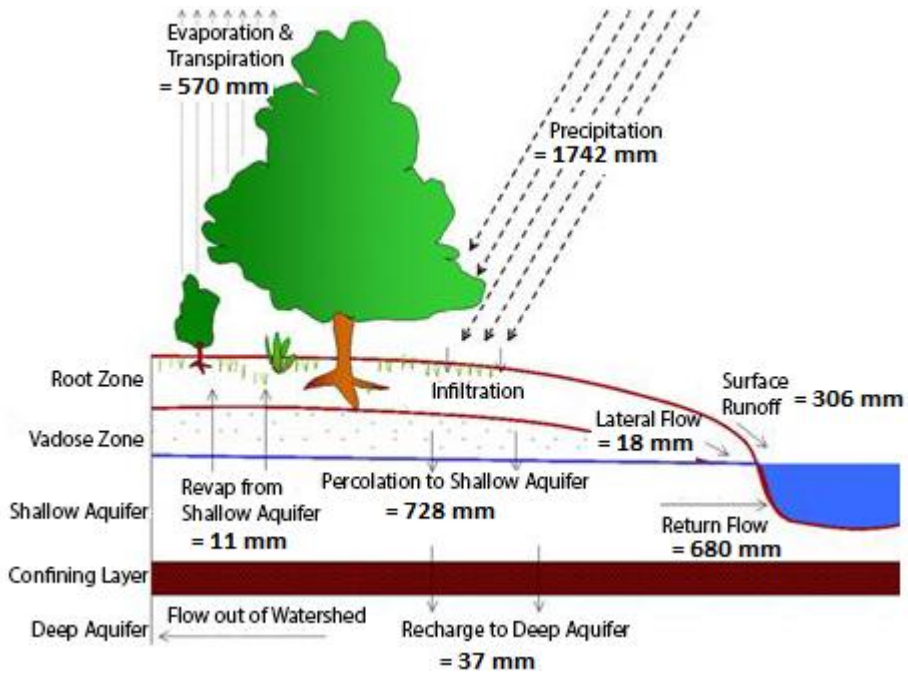


Figure 6.11. Average annual simulated water balance components for the future scenario under RCP4.5 in time-domain (2011-2100)

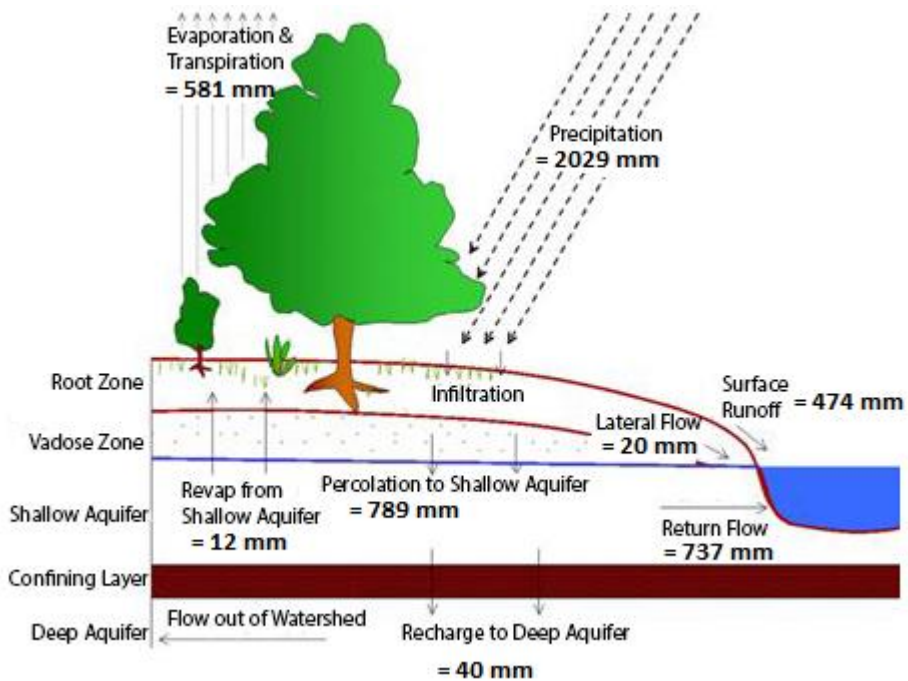


Figure 6.12. Average annual simulated water balance components for the future scenario under RCP8.5 in time-domain (2011-2100).

## 6.4. Conclusions

SDSM was successfully calibrated (1975– 2000) and validated (2001 – 2005) to explore future changes of temperature, and precipitation in the Lake Tana Basin for the future periods of 2011 – 2040, 2041– 2070, and 2071– 2100 under RCP2.6, RCP4.5, and RCP8.5, relative to the baseline period of 1995 – 2012. The precipitation output of SDSM was corrected for the bias in time and quantile-domain whereas the temperature was adjusted for the bias in time-domain only. The two bias correction approaches for precipitation can improve the raw downscaled data to some extent. The quantile-domain based bias correction performed much better than the time-domain based bias correction regarding correcting several statistical characteristics and concerning the variability range. It corrects most of the statistical characteristics and has the narrowest variability ranges. The main drawback of this method is that the same correction algorithm applies to both current and future climate conditions. To solve this kind of issues for future study, consideration of time-dependent bias corrections can be a good approach. In the 2020s, the quantile-based bias-corrected mean annual precipitation has shown a significant decrease by 14.93% at Ayikel station under RCP4.5; 0.87%, 5.54%, 20.21% in Gonder station under RCP2.6, RCP4.5, and RCP8.5, respectively, at Gonder weather station. The quantile-based bias-corrected mean annual precipitation in all other stations showed an increasing magnitude in all RCPs and future time periods. Similarly,

time-based bias-corrected mean annual precipitation showed an increasing in the amount in all weather stations and time periods under all RCPs. The overall average changes in the maximum and minimum temperature showed values of 1.40 °C and 0.35 °C, respectively. Increase in precipitation can influence the water quality and possibly result in the outbreak of waterborne diseases due to sewage overflows. Excess rainfall could also lead to soil saturation as well as to runoff and soil erosion problems. Increase in precipitation also has a benefit of increasing agricultural productivity for the local farmers. SWAT was used to simulate the streamflow in the basin for the future time periods. The model was cross-validated for the periods of 1998-2012, with three years for model warm-up, nine years for calibration, and three years for validation in 4 folds. The result showed that SWAT captured the magnitude and variability of observed streamflow at the four major gauged catchments (Gilgelabay, Gummera, Megech, and Ribb). The simulated streamflow using SWAT based on the three RCPs scenarios showed that an increasing trend in the mean annual streamflow under all scenarios. The highest and lowest total surface inflow to the Lake Tana were found to be 19507 Mm<sup>3</sup>/year (in the 2080s under RCP8.5) and 7688 Mm<sup>3</sup>/year (in the 2020s under RCP8.5), respectively, when the quantile-based bias-corrected precipitation is used to derive SWAT. On the other hand, the highest and lowest surface inflow to the Lake Tana that corresponding to the time-based bias-corrected precipitation were found to

be 16872 Mm<sup>3</sup>/year in the 2080s under RCP8.5 and 11886 Mm<sup>3</sup>/year in 2020s under RCP4.5, respectively. The increase in the mean annual runoff can be beneficial to the improvement of agricultural productivity as well as to enhance the hydropower potential of the basin. However, the increases in temperature will also have a significant impact on the water balance of the reservoir in which open water evaporation will be higher. Therefore, we highly recommend for evaluating the operation rule of the Lake Tana reservoir under climate change. For further studies in the basin, we also recommend the use of different GCMs so as to cover the range of uncertainties related to GCMs. The major limitation of this study can be that the land cover and soil properties were considered constant throughout the simulation period. However, such an assumption can affect the projections of streamflow in the basin.

## CHAPTER SEVEN

### 7. Reflecting Uncertainty in the Development of a Reservoir Operation Rule with Genetic Programming

**Summary:** Some irrigation and hydropower projects have been planned in the Upper Blue Nile River Basin of Ethiopia. These projects have likely been the sources of water conflict. However, no specific study developed a reservoir operation rule by maximizing the flow to the downstream users from the source of the Blue Nile River, Lake Tana Basin where seven reservoirs are located in parallel. Also, the projected climate change is expected to alter the hydrological patterns in the study basin. Therefore, this study is designed (1) to assess the impact of climate change in the operation of the proposed reservoirs based on three future climate scenarios of the 2020s, 2050s, and the 2080s and (2) to maximize the downstream water release by optimally allocating the surface water resources to all hydropower and irrigation projects. For this, a multi-objective genetic algorithm was employed, and a set of well distributed optimal solutions along the Pareto front were generated to offer many alternative policies. The uncertainty of inflow was considered by developing the operation rule for the most similar years that have been grouped by using a neural network clustering technique. A cross-validation technique was further implemented to improve the model's predictive performance. The obtained results

showed that the optimization technique proposed in this study is capable of solving the complex multi-reservoir system operation problems. More than 90% reliability was observed for all proposed projects in the Lake Tana Basin under all inflow scenarios.

## **7.1. Introduction**

The transboundary Nile River is the world's longest river and sustains the livelihoods of millions of people across ten countries in Africa (i.e., Rwanda, Burundi, the Democratic Republic of Congo, Tanzania, Kenya, Uganda, Ethiopia, South Sudan, Sudan, and Egypt). Due to the population growth in these countries, the food and water security situation is extremely vulnerable. Some water resources projects have been planned in the upstream riparian countries to balance the water demand. The developments of these water resources projects in these regions have likely become the sources of interstate water conflict among riparian countries. Unresolved political tensions over the use of the Nile River continue to emerge along with changing water needs in riparian states. These tensions constitute significant obstacles to the development of the upstream riparian countries.

The Nile River gets about 85 % of its total flow from the Blue Nile River that originates in the Ethiopian highlands, while the majority of the Nile River's water is used in Sudan and Egypt. Nowadays, the Ethiopian government started to implement some water resources projects in the

Upper Blue Nile River Basin to meet the growing demand for food and energy. Therefore, the optimal operation of the ongoing and proposed reservoirs in the Upper Blue Nile River Basin will be significant to maximize the water release to the downstream users (i.e. Egypt, and Sudan). However, accurate estimation and forecasting of water supply and demand as well as obtaining a balance between them still lack in the Upper Blue Nile River Basin. Allocating water to different competitive users has always been challenging. Finding an optimal water allocation by minimizing the water deficits in each sector is the aim of this research. For this, the study proposes a multi-objective water allocation problem. A number of efficient solutions are presented as a Pareto-optimal front in the case of multi-objective optimization approach, instead of a single optimal solution. To address the problems, many studies have used evolutionary algorithms that allow the discovery of a whole set of Pareto-optimal solutions in a single run of the algorithm (Cai *et al.*, 2001; Chang and Chang, 2001; Huang *et al.*, 2002; Huang and Yuan, 2004; Chang *et al.*, 2005; Kim *et al.*, 2006; Reddy and Kumar, 2006; Chen *et al.*, 2007; Chiu *et al.*, 2007; Yang *et al.*, 2007; Chang, 2008; and Chen and Chang, 2009). A genetic algorithm is a widely used method in those previous studies, and it is one of the most promising of evolutionary algorithms in water resources system optimization (Tung *et al.*, 2003; Fi-John *et al.*, 2005; Hejazi and Borah, 2008). A genetic algorithm (Goldberg, 1989) is a search procedure based on the mechanics of natural

selection and natural genetics that combine artificial survival of the fittest with genetic operators abstracted from nature (Chang *et al.*, 2013). Searching for an optimal design from a population of possible designs instead of a single design allows the genetic algorithms to maintain a multipoint perspective on many regions of the solution space at the same time, resulting in a high probability of locating the global optimum (Goldberg, 1989; Chang *et al.*, 2013). Deb *et al.* (2002) compared various multi-objective evolutionary algorithms and concluded as the Non-dominated Sorting Genetic Algorithm-II (NSGA-II) performed best in converging nearer to the true Pareto-optimal set. Therefore, this study applied the NSGA-II principle to solve the multi-objective reservoir operation problem in the Lake Tana Basin.

## **7.2. Methodology**

### **7.2.1. Description of the Reservoir System in the Lake Tana Basin**

In the Lake Tana Basin, some water resources project schemes (i.e., irrigation and hydropower development) are under construction. Construction of the Tana-Beles Hydropower project is completed which has a capacity of generating 460 MW by diverting approximately 2,985 Mm<sup>3</sup> water from the natural reservoir (i.e., Lake Tana) to Beles River through a 12 km long, and 7.1 m diameter tunnel (Salini and Mid-day, 2006; SMEC, 2008). The elevation difference between the Lake Tana and the Beles River

is 311 m. Furthermore, the Koga irrigation project has been completed, and some irrigation schemes (e.g., Gilgelabay, Gummera, Jemma, Megech, and Ribb irrigation) are planned on the main rivers flowing into the Lake Tana. Figure 7.1 presents the reservoirs system configurations in the Lake Tana Basin, in which all the irrigation and hydropower development activities that are expected to be operational shortly are considered.

The outflow from the Lake Tana (i.e., Blue Nile River) is regulated by the Chara-Chara Weir, in which seven gates are installed, over a 3 m range of water levels from 1784 to 1787 m above mean sea level. In between these Lake levels, the Lake active storage is 9100 Mm<sup>3</sup>. The total flow through the seven gates is 490 m<sup>3</sup>/s at full supply level in which the surface area of the Lake Tana is about 3156 Km<sup>2</sup>. The length and height of the Chara-Chara Weir are 700 m and 3 m, respectively. Figure 7.2 shows the Lake storage-elevation-surface area characteristics. An environmental impact assessment (EIA) were conducted by Bellier *et al.* (1997), to estimate the minimum flow requirements over the *Tis Issat* waterfall, which is a major tourist attraction in the area that situated downstream of the Chara-Chara Weir. The recommended monthly downstream flow (see Table 7.2) was considered as the minimum downstream release from the system.

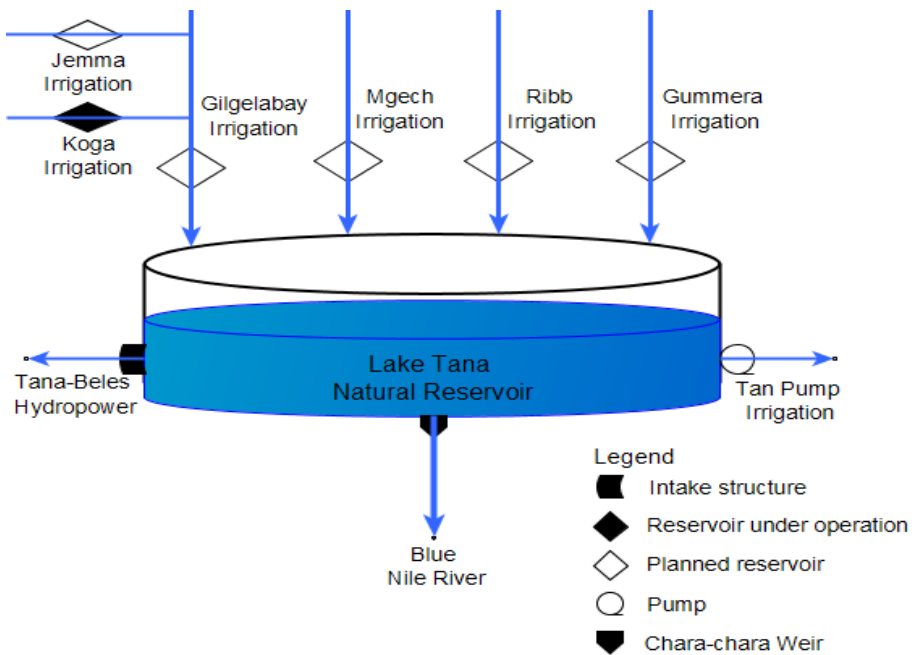


Figure 7.1. Schematic diagram of the Lake Tana Basin's reservoir model configuration

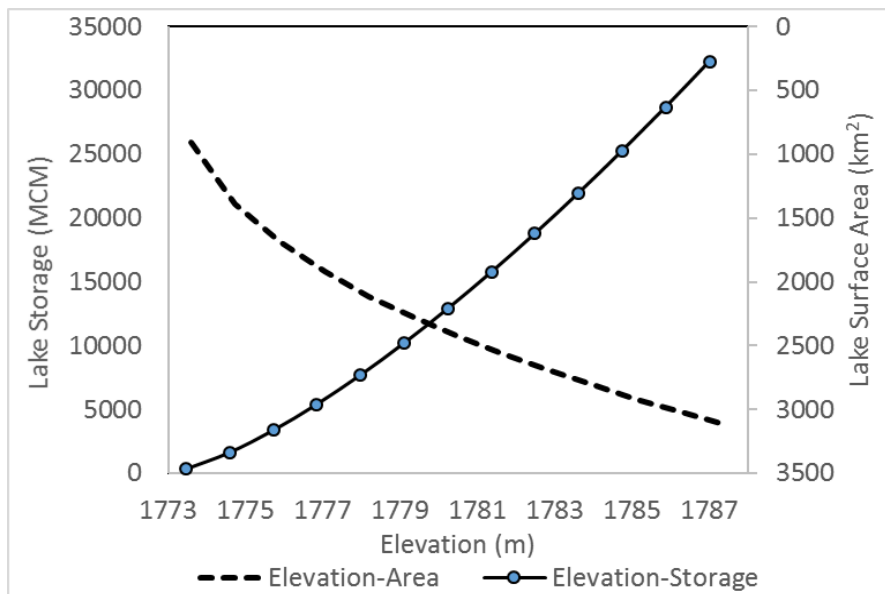


Figure 7.2. Elevation-Area & Elevation-Volume relationship of the Lake Tana reservoir

Table 7.1. Planned irrigation development in the Lake Tana Basin (Source: BCEOM 1998)

<b>Irrigation scheme</b>	<b>Irrigable area (ha)</b>	<b>Net water demand (Mm<sup>3</sup>)</b>	<b>Reservoir storage (Mm<sup>3</sup>)</b>
Gilgelabay	12852	88-121	563
Gummera	14000	98	59.7
Ribb	19925	146-187	233.7
Megech	7300	54-83	181.9
Jemma	7800	48	173
Koga	6000	52	78.5
Northeast Lake Tana Pump	5745	43-53	withdrawals from the Lake
Northwest Lake Tana Pump	6720	46	withdrawals from the Lake
Southwest Lake Tana Pump	5132	36	withdrawals from the Lake

Table 7.2. Recommended flow over the Tis Issat Falls from the Chara-Chara Weir (Source: Bellier et al., 1997)

<b>Month</b>	<b>Jan</b>	<b>Feb</b>	<b>Mar</b>	<b>Apr</b>	<b>May</b>	<b>Jun</b>	<b>Jul</b>	<b>Aug</b>	<b>Sep</b>	<b>Oct</b>	<b>Nov</b>	<b>Dec</b>
EIA flow (Mm <sup>3</sup> )	161	146	27	26	27	26	54	54	104	107	104	161

## 7.2.2. Mathematical Formulation of Model

The total number of 96 decision variables, which is equal to the dimension of the problem, should be solved by the formulated reservoir operation model. For this, two objectives (i.e. minimization of irrigation and hydropower deficits) and the optimization constraints are expressed as follows.

- i) Minimize sum of squared deviations of releases from demands for irrigation,

$$f_1 = \sum_{n=1}^7 \left[ \sum_{t=1}^{12} (D_{n,t} - R_{n,t})^2 \right] \quad (7.1)$$

where  $D_{n,t}$  is required demand for irrigation site  $n$  in period  $t$ ,  $R_{n,t}$  is irrigation release for demand site  $n$  in period  $t$ .

- ii) Minimize sum of squared deviations of releases from demands for hydropower

$$f_2 = \sum_{t=1}^{12} (D_{g,t} - R_{g,t})^2 \quad (7.2)$$

where  $R_{g,t}$  is release for hydropower in time  $t$ ,  $D_{g,t}$  is required demand to generate hydropower during period  $t$ .

The optimization is subjected to the following constraints:

a) Storage continuity

$$S_{n,(t+1)} = S_{n,t} + I_{n,t} + P_{n,t} - (R_{n,t} + E_{n,t} + DR_{n,t}) \quad (7.3)$$

$$\forall t = 1, 2, \dots, 12, \text{ and } \forall n = 1, 2, \dots, 8$$

where  $S_{n,t}$  is the initial storage volume of reservoir  $n$  in month  $t$ ,  $S_{n,(t+1)}$  is the initial storage volume of reservoir  $n$  in month  $t+1$ ,  $I_{n,t}$  is the inflow to reservoir  $n$  in month  $t$ ,  $E_{n,t}$  is the evaporation losses from reservoir  $n$  during month  $t$ ,  $DR_{n,t}$  is the downstream release from reservoir  $n$  in month  $t$ , and  $P_{n,t}$  is the areal rainfall at reservoir  $n$  in month  $t$ .

b) Storage limits

The lower and upper bounds on reservoir storage should be fixed based on the criteria for recreation, the minimum level for power generation, and flood control.

$$S_n^{min} \leq S_{n,t} \leq S_n^{max} \quad (7.4)$$

$$\forall t = 1, 2, \dots, 12, \text{ and } \forall n = 1, 2, \dots, 7$$

where  $S_n^{min}$  is the minimum active storage of reservoir  $n$ , and  $S_n^{max}$  is the maximum active storage of reservoir  $n$ .

c) Irrigation and hydropower demands

$$D_{n,t}^{min} \leq R_{n,t} \leq D_{n,t}^{max} \quad (7.5)$$

d) Downstream requirement

$$DR_{n,t} \geq DR_{n,t}^{min} \quad (7.6)$$

where  $DR_{n,t}^{min}$  is minimum flow required by downstream users,  $DR_{n,t}$  is downstream release from reservoir  $n$  during period  $t$ .

e) Spill

$$O_{n,t} = \max \begin{cases} S_{n,t} - S_{n,t}^{max} \\ \emptyset \end{cases} \quad (7.7)$$

where  $O_{n,t}$  is a spill from reservoir  $n$  during period  $t$

### 7.2.3. A Utopia Tracking Approach

All efficient solutions of the two objectives are standardized (and weighted to specify importance) and then summed to form a single overall fitness value for every set of efficient solutions along the Pareto front. Then the smallest value is considered as the utopia point (i.e. compromise solution). Mathematically, the procedures to identify this point is expressed as follows:

- Standardize all efficient solutions of objective 1 ( $f_1$ ), and objective 2 ( $f_2$ ),

$$f_{1,i}^{std} = \frac{f_{1,i} - \mu_1}{\sigma_1} \quad (7.8)$$

$$f_{2,i}^{std} = \frac{f_{2,i} - \mu_2}{\sigma_2} \quad (7.9)$$

- Sum absolute of the standardized values of the two objectives,

$$f_{1+2,i}^{std} = Abs(f_{1,i}^{std}) + Abs(f_{2,i}^{std}) \quad (7.10)$$

- Select the utopia point which is the minimum value among all possible solutions,

$$utopia\ point = \min(f_{1+2,i}^{std}) \quad (7.11)$$

where  $\mu_1$  and  $\mu_2$  represents the mean value of the efficient solution in objective 1 and 2, respectively;  $\sigma_1$  &  $\sigma_2$  represents the standard deviation value of the efficient solution in objective 1 and 2, respectively;  $f_{1,i}$  &  $f_{2,i}$  represents the value of the efficient solution in iteration  $i$  for objective 1 and 2, respectively.

#### 7.2.4. Method of Reflecting the Uncertainty of Inflows

The uncertainty of inflow was considered by developing the operation rule curve for the most similar years that have been clustered by using a neural clustering technique. Based on this, the historical inflows from 1995 to 2009 were considered to be clustered into four most similar groups for deriving the reservoir operating rule curve as follows:

- ✓ Cluster-I includes the inflows during the years of 1995, 1997, 2001, 2002, & 2004.

- ✓ Cluster-II includes the inflow during the years of 1998, 2000, 2003, 2005, 2007, & 2009.
- ✓ Cluster-III includes the inflow during the years of 1996, 2006, & 2008.
- ✓ Cluster-IV includes the inflow during the year of 1999.

The general procedure of reflecting the uncertainty of inflow into the reservoir operating rule is shown in Figure 7.3. A cross-validation technique is further implemented to improve the model's predictive performance. For this purpose, the reservoir forecasted inflows (as described in section 7.3.6) during the years of 2010, 2011, and 2012 were considered for cross-validating the derived operating rule. Figure 7.4 presents the total inflow, rainfall, and evaporation of the Lake Tana for all clusters.

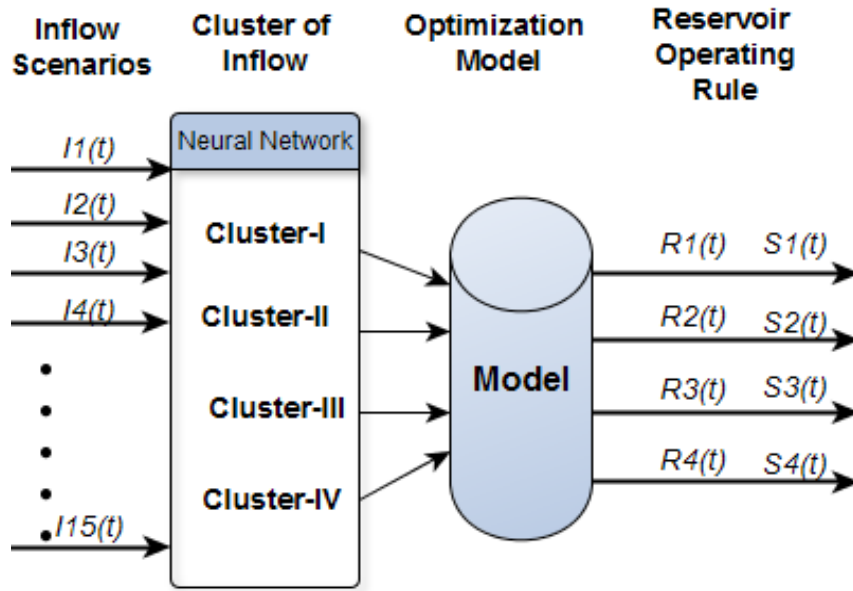


Figure 7.3. Method of reflecting the uncertainty of inflows in the reservoir operating rule where  $I_i(t)$  is the reservoir inflow,  $R_i(t)$  is the reservoir release, and  $S_i(t)$  is the reservoir active storage

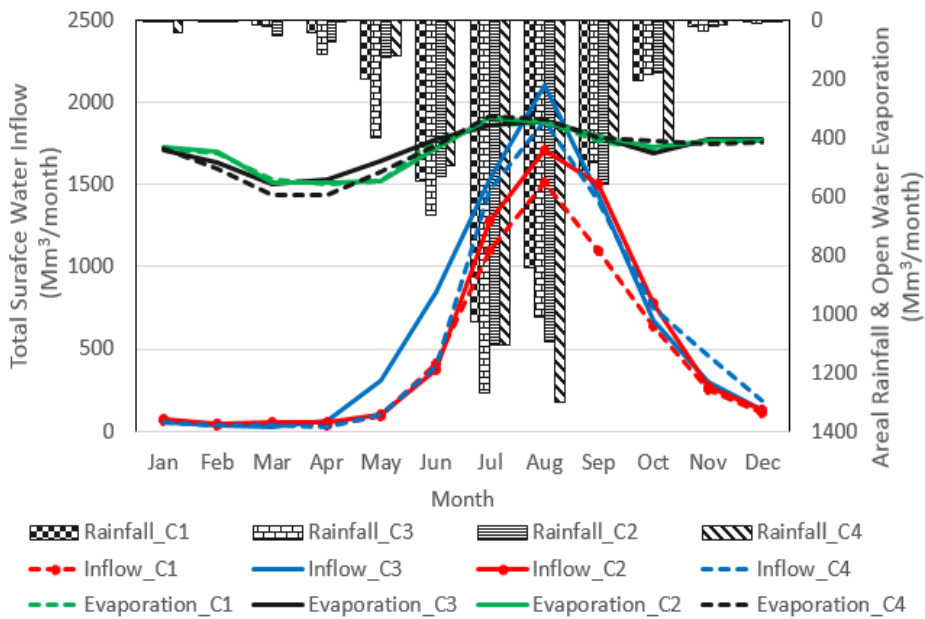


Figure 7.4. Monthly inflow, areal rainfall, and evaporation of the Lake Tana for the four clustered scenarios. (C1: cluster-I, C2: cluster-II, C3: cluster-III, and C4: cluster-IV)

### 7.2.5. Reservoir Performance

The vulnerability, volumetric reliability, and sum of the square deficit of reservoir release for meeting the demand were used as the reservoir system performance indices. The vulnerability is a measure of the likely damage of a failure event. The maximum vulnerability ( $V_{max}$ ) is a suitable indicator of reservoir performance (Kjeldsen and Rosbjerg, 2004).

$$V_{max} = \max\{v_j\} \quad (7.12)$$

where  $v_j$  is the maximum irrigation water deficit among all the continuous failure or unsatisfactory months.

Reliability is the probability of success and it can be computed on the basis of the period or volumetric. The period reliability is the probability that the system state lies in the set of satisfactory states. The volumetric reliability ( $r_v$ ) is the ratio of the volume of water supplied to the volume demanded (McMahon *et al.*, 2006).

$$r_v = V_s/V_d \quad (7.13)$$

where  $V_s$  is the volume of water supplied and  $V_d$  the volume of water demanded during a given period.

## **7.2.6. Reservoir Operating Rules Obtained by Multiple Regression**

### **Analysis**

Different linear multiple regression equations were tested for each cluster to express the monthly reservoir release in terms of the system state variables and monthly reservoir inflows. The reservoir release is regressed on the reservoir storage and reservoir inflow for each cluster. Standard multiple regression estimators were used to fit the parameters, and a t-student test was conducted to test whether the parameters are statistically different from zero.

## **7.2.7. Reservoir Inflow Forecasting**

The monthly inflow to the reservoir is not constant since it varies by month. Seasonality makes it so that the mean of the observations is not constant, but instead evolves according to a cyclical pattern. The monthly inflow to each reservoir possesses a seasonal component that repeats every 12 observations in a year. The autocorrelation of the monthly inflow to the Lake Tana is computed using the R function, `acf()`, which is given in Figure 7.5 with the lag in months. The zero lag has  $acf(0)=1$ , and as expected there is a periodic or cyclical pattern to the autocorrelation, with strong positive autocorrelation at intervals of 12 months and multiples thereof, and matching negative correlation at 6 months, 18 months etc. Hence, the

Seasonal Autoregressive Integrated Moving Average (SARIMA) model has been formulated to deal with seasonality.

Box *et al.* (1967) developed the class of multiplicative Seasonal Autoregressive, Integrated Moving Average (SARIMA) models to describe the series containing seasonal patterns with period  $S$ . It is written as follows:

$$ARIMA(p, d, q)(P, D, Q)_S \quad (7.14)$$

where  $(p, d, q)$  is the nonseasonal part of the model,  $(P, D, Q)_S$  is the seasonal part of the model and  $S$  is the number of periods per season. We use the uppercase notation for the seasonal parts of the model and the lowercase notation for the nonseasonal parts of the model.

In general the seasonal  $ARIMA(p, d, q)(P, D, Q)_S$  is written as:

$$\Phi(B^S)\phi(B)(1 - B^S)^D(1 - B)^d y_t = \Theta(B^S)\theta(B)\varepsilon_t \quad (7.15)$$

where

$$\Phi(B^S) = 1 - \Phi_1 B^S - \dots - \Phi_p B^{pS}$$

$$\phi(B) = 1 - \phi_1 B - \dots - \phi_p B^p$$

$$\Theta(B^S) = 1 + \Theta_1 B^S + \dots + \Theta_Q B^{QS}$$

$$\theta(B) = 1 + \theta_1 B + \dots + \theta_q B^q$$

$$B^n y_t = y_{t-n}$$

The notation  $B$  is the backward operator,  $p$  is the order of nonseasonal term,  $P$  is the order of seasonal term,  $d$  is the order of nonseasonal differencing,  $D$  is the order of seasonal differencing,  $q$  is the order of nonseasonal moving average term,  $Q$  is the order of seasonal moving average term,  $S$  is the seasonal length,  $\theta(B)$  is the nonseasonal moving average operator,  $\Theta(B)$  is the seasonal moving average operator,  $\phi(B)$  is the nonseasonal autoregressive operator, and  $\Phi(B)$  is the seasonal autoregressive operator,  $\varepsilon_t$  is the residuals (white noise series), and  $y_t$  is the output series.

The general procedure we followed were: 1) make correlograms (autocorrelation function and partial autocorrelation function), 2) fit the model, 3) find the residuals, 4) do the diagnostic test, if the residuals are independent and identically distributed (i.i.d.), then the fitted model is good otherwise, repeat the same process. 5) use the fitted model for forecasting.

The monthly inflow was partitioned into training period (i.e. 1995 – 2009), and test period (i.e. 2010 – 2012) to fit the seasonal ARIMA model. The Akaike Information Criterion (AIC) test was performed to compare the competing models. The Akaike information criterion (AIC) is a measure of the relative quality of statistical models for a given set of data. Given a collection of models for the data, AIC estimates the quality of each model, relative to each of the other models. Hence, AIC provides a means for model selection.

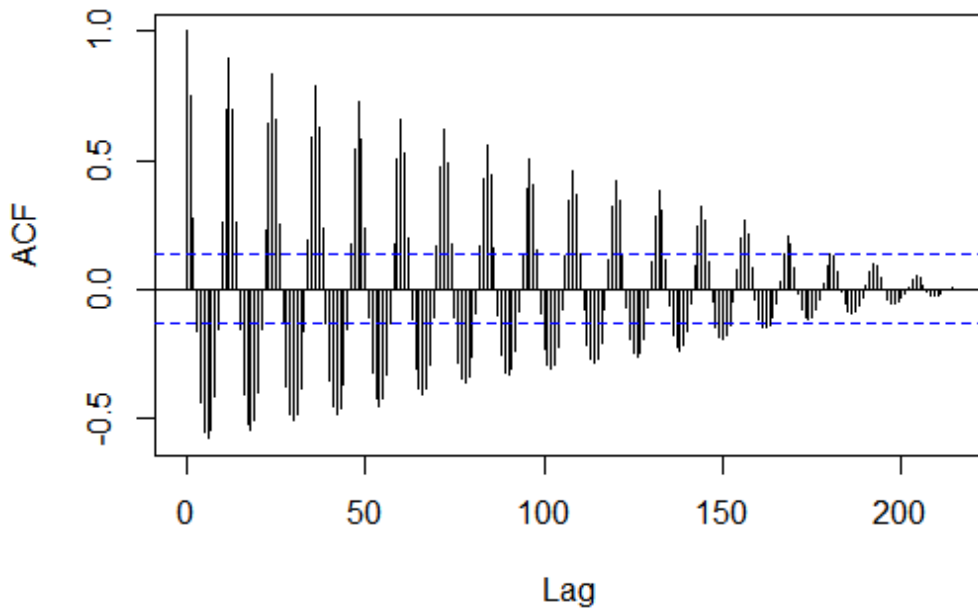


Figure 7.5. Autocorrelation function (acf) of the monthly inflow to the Lake Tana. The dotted horizontal line indicates a confidence interval for the acf value.

The AIC value of the model is given by:

$$AIC = 2k - 2\ln(L) \quad (7.16)$$

where  $L$  is the maximum value of the likelihood function for the model,  $k$  is the number of estimated parameters in the model. From a set of candidate models for the data, the preferred model is the one with the minimum AIC value.

The Ljung-Box test was used for the diagnostic test of the residuals. The hypothesis;  $H_0$ : the data are random and  $H_a$ : the data are not random. The test statistic is

$$Q_{LB} = n(n+2) \sum_{j=1}^h \frac{\rho^2(j)}{n-j} \quad (7.17)$$

where  $n$  is the sample size,  $\rho(j)$  is the autocorrelation at lag  $j$ , and  $h$  is the number of lags being tested.

The  $P$ -value approach involves determining likely or unlikely by determining the probability. If the  $P$ -value is small, say less than (or equal to)  $\alpha$ , then it is unlikely in which the null hypothesis is rejected in favor of the alternative hypothesis. And, if the  $P$ -value is large, say more than  $\alpha$ , then it is likely, in which the null hypothesis is not rejected.

### **7.3. Application**

The multi-objective genetic algorithm is applied to the Lake Tana Basin reservoir system to derive the operating policies for the multi-reservoir system in the basin and also to maximize the monthly release to the downstream users. This algorithm is used to generate different alternatives aiming to help the decision makers to make a proper decision. For this, four inflow scenarios into the Lake Tana reservoir system were considered to solve the formulated model, which are cluster-I, cluster-II, cluster-III, and cluster-IV of the historical inflow. The historical inflows for the period of 1995-2009 were considered to derive the reservoir operating rules, and the derived reservoir operating rules were validated by using the forecasted inflows for the period of 2010 – 2012. The derived operating rules were also applied to assess the climate change impact, that is under the three future climate scenarios of the 2020s, 2050s, and 2080s, on the reservoir operating rule policy.

Before fixing the population size of the genetic algorithm, a sensitivity analysis was performed. In the Multiobjective Genetic Algorithm (MOGA), the size of population and number of iterations play a vital role in obtaining optimal solutions for a given problem. Depending upon the problem nature and the number of decision variables involved in the problem, a suitable number of the population and iterations need to be selected for solving the problem. The MOGA parameters used to solve the reservoir operation

problem have been chosen after a thorough sensitivity analysis by varying each of the parameters. Based on this, a population size and maximum generation number of 1000 and 9600, respectively, are chosen to run the formulated model that gives better optimal fitness values of the two objective functions. The selected parameters for the genetic algorithm are tournament size of 2, reproduction crossover fraction of 0.8, constraint dependent mutation fraction, and heuristic crossover function with the ratio of 1.2.

Figure 7.6 presents a set of efficient solutions along the Pareto front for the four clustered inflow scenarios. The decision makers can choose one optimal solution among a set of efficient solutions along the Pareto front based on preferences. The optimal points were chosen in such a way that the highest net benefits can be achieved with respect to both objectives. For the selection of these optimal points, the utopia tracking approach which is discussed in section 7.3.2 was used. Based on this, the values of the objective function for irrigation (i.e. squared annual irrigation deficits) was found to be  $14.75 \text{ Mm}^3$ ,  $13.52 \text{ Mm}^3$ ,  $13.32 \text{ Mm}^3$ , and  $13.42 \text{ Mm}^3$  for cluster-I, cluster-II, cluster-III, and cluster-IV, respectively. On the other hand, the squared annual deviation for hydropower production was found to be  $61.84 \text{ Mm}^3$ ,  $53.25 \text{ Mm}^3$ ,  $42.16 \text{ Mm}^3$ , and  $54.61 \text{ Mm}^3$  for cluster-I, cluster-II, cluster-III, and cluster-IV, respectively. The minimum annual squared deviation of allocation from the demand for hydropower and irrigation was

found under cluster-III. The release policies for all irrigation and hydropower projects under cluster-III are provided in Figure 7.7 & 7.8, respectively, when the reservoir operator gives equal priority for the hydropower generation and meeting irrigation demands. Here it can be observed that there is high reliability in meeting all the demands (see Figure 7.10). With this reservoir operation policy, the minimum downstream release is also achieved. Figure 7.10 presents the volumetric reliability of all projects, in which all projects have a reliability of above 90%. The vulnerability index was found to be 429,121 m<sup>3</sup>/month, 808,203 m<sup>3</sup>/month, 939,846 m<sup>3</sup>/month, 1,121,599 m<sup>3</sup>/month, 938,969 m<sup>3</sup>/month, 379,837 m<sup>3</sup>/month, 1,041,624 m<sup>3</sup>/month and 5,760,000 m<sup>3</sup>/month for Gilgelabay, Gummera, Jemma, Koga, Megech, Ribb, Tana Pump irrigation, and Tana-Beles Hydropower projects, respectively. In general, the results revealed that the proposed projects demand is almost satisfied with the reservoir release policy that derived by the genetic algorithm.

Furthermore, the optimal reservoir releases derived from the genetic algorithm were regressed on the reservoir storage and the reservoir inflow for the four clusters. The reservoir inflows were partitioned into the training periods (i.e. 1995 – 2009) and test periods (i.e. 2010 – 2012), in which the data in the training periods were used to derive the regression equation, whereas the data in the test periods were used to validate the performance of the derived regression equation.

The derived regression equation (Equation 7.18) could be thus used to estimate the reservoir release at any time having the reservoir storage and inflow.

$$R_t(I_t, S_t) = a_1 + a_2 I_t + a_3 S_t \quad (7.18)$$

where  $I_t$  and  $S_t$  represent the reservoir inflow and reservoir storage, respectively,  $R_t$  is the reservoir release, and  $a_1, a_2, a_3$  represents the coefficients of the regression equation.

The regression coefficients given in Table 7.3 are derived from the total release of flow in the baseline inflow scenario, and the values of these coefficients for the future inflow scenarios under climate change are given in Table 7.6. The  $R^2$  value of the regression equation for the training periods was found to be 0.13 for cluster-I; 0.67 for cluster-II; 0.79 for cluster-III; and 0.62 for cluster-IV, respectively (see Table 7.3). The coefficients of regression equations were statistically different from zero based on a *t-student* test.

The derived reservoir release rules were also applied for the years of 2010, 2011, and 2012, in which the forecasted inflows to the reservoir were used. The `auto.arima(.)` function in r-programming was used to select the best seasonal ARIMA model via AIC criterion, and the best model was found to be ARIMA(1,0,0)(0,1,1)[12].

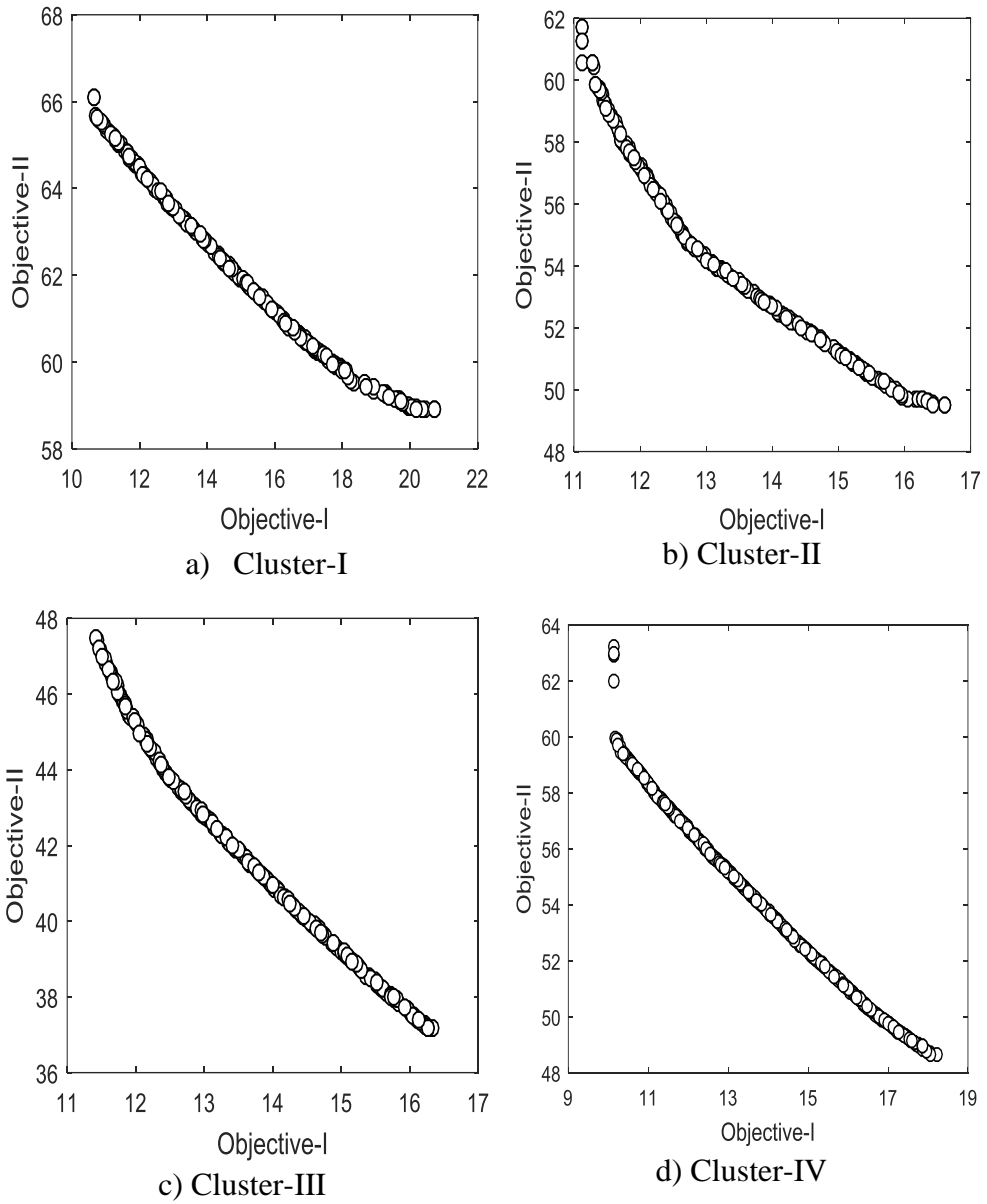


Figure 7.6. Pareto front, where the goal is to maximize both objectives: objective-I (irrigation) and objective-II (hydropower).

The selected SARIMA model can be expressed as follows:

$$(1 - \phi_1 B)(1 - B^{12})y_t = (1 + \theta_1 B^{12})\varepsilon_t \quad (7.19)$$

By solving for  $y_t$ , the equation becomes:

$$y_t = \phi_1 y_{t-1} + y_{t-12} - \phi_1 y_{t-13} + \varepsilon_t + \theta_1 \varepsilon_{t-1} \quad (7.20)$$

The best fit coefficients were found to be 0.456 and -0.797 for the nonseasonal autoregressive term and seasonal moving average term, respectively. By substituting the optimal coefficients into equation (7.20), the equation can be written as follows:

$$y_t = 0.456 * y_{t-1} + y_{t-12} - 0.456 * y_{t-13} + \varepsilon_t - 0.797 * \varepsilon_{t-1} \quad (7.21)$$

The forecasted inflow at a lead time of  $L$  months can be written as:

$$y_t(L) = 0.456[y_{t+L-1}] + [y_{t+L-12}] - 0.456[y_{t+L-13}] + [\varepsilon_{t+L}] - 0.797[\varepsilon_{t+L-1}] \quad (7.22)$$

The forecasted inflow is plotted with the historical inflow in the training period of the model in Figure 7.11. The accuracy of the model for the training and test period is performed. The mean absolute percentage error for the training and test periods was found to be 26.13%, and 30.01%, respectively.

The forecasting accuracy of the model was also checked using the performance indicator of RSR, NSE,  $R^2$ , and PBIAS, which were found to

be 0.15, 0.98, 0.97, and 7.49, respectively. The result showed that as the selected SARIMA model was the perfect model for forecasting the inflow to the Lake Tana natural reservoir. Figure 7.12 presents the forecasted inflow with a blue line, actual inflow with a black broken line, 80%, and 95% confidence intervals.

The diagnostic test for the model residual was performed based on Ljung-Box test, and the p-value was found to be 0.99, which is larger than the significant level  $\alpha$  of 0.05. Therefore, the null hypothesis is not rejected, in which the model residual is identically and independently distributed. The residual plot is provided in Figure 7.13. The performance of the derived reservoir release rules was also validated by comparing the optimal release that derived by using the actual inflow through a genetic algorithm and the release corresponding to the forecasted inflow which was estimated by using the derived multiple-linear regression equation 7.19. The validation result revealed that the predictive performance of the derived reservoir release rule was found to be satisfactory with NSE,  $R^2$ , RSR, PBIAS, and RMSE values presented in Table 7.4.

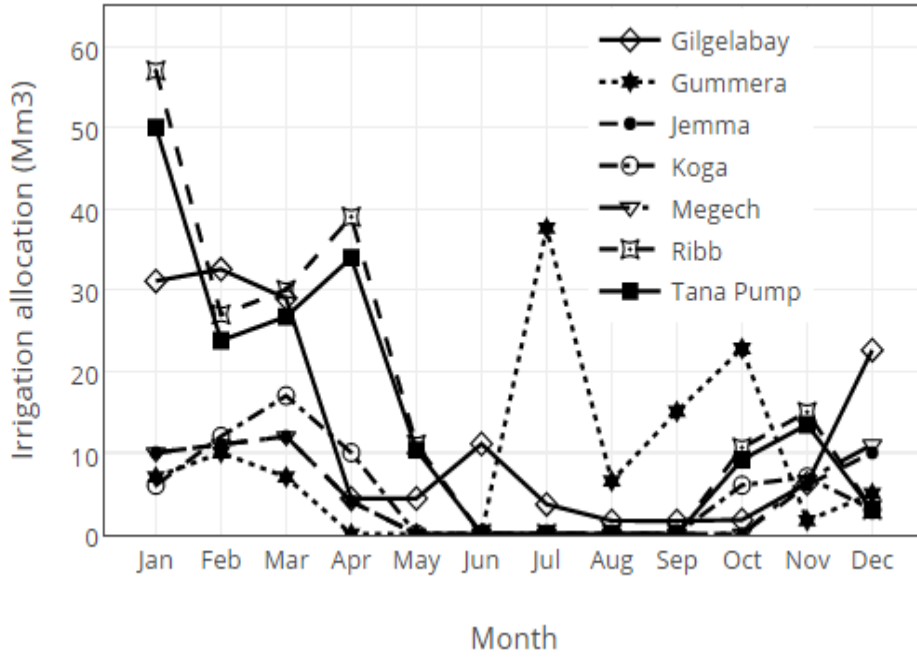


Figure 7.7. Reservoir release policies for each irrigation projects

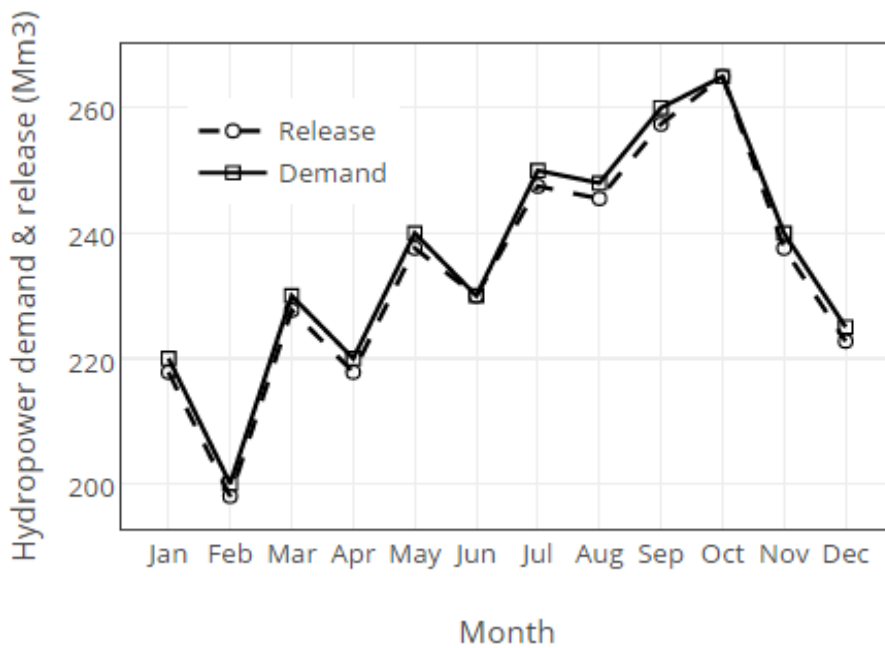


Figure 7.8. Reservoir release policies for Tana-Beles hydropower project

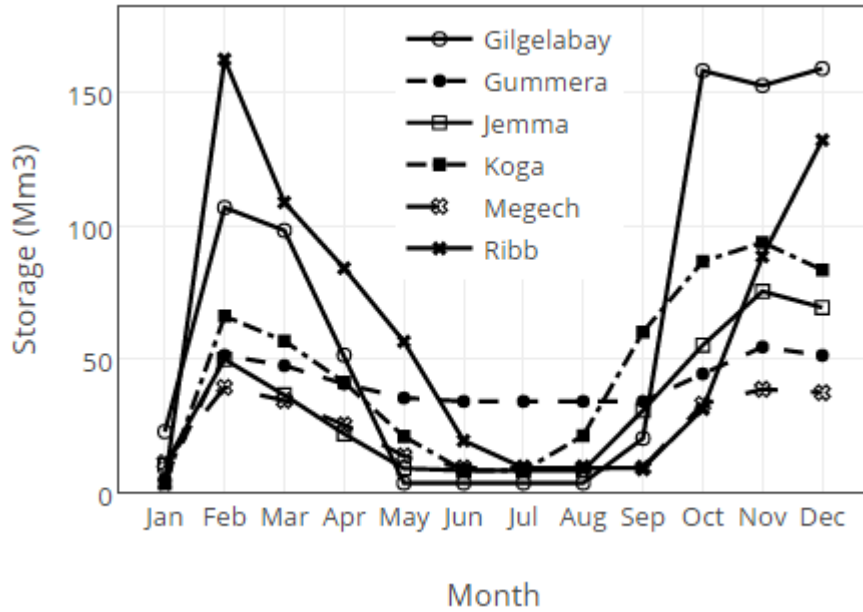


Figure 7.9. Individual reservoir storage curve under optimal reservoir policy

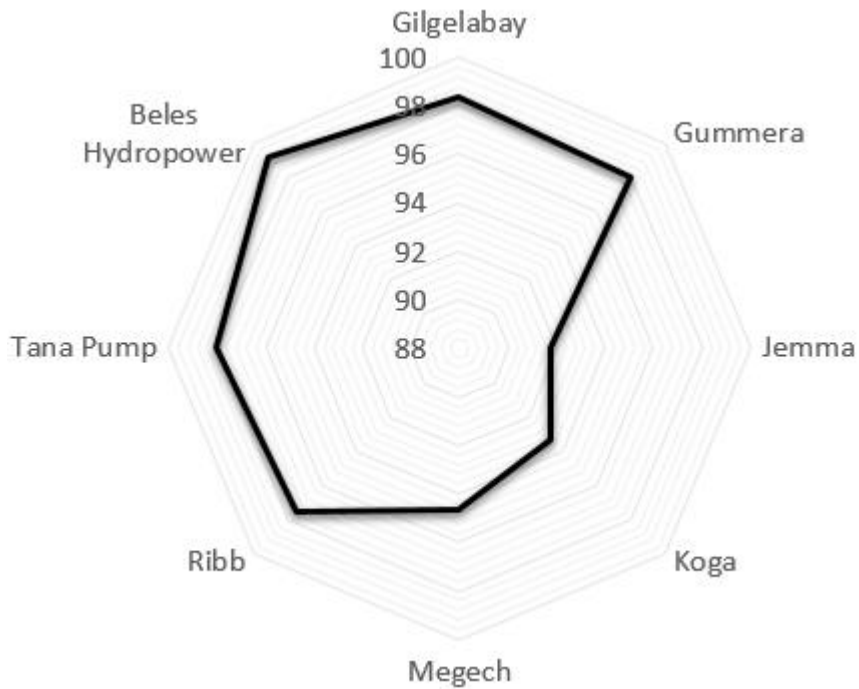


Figure 7.10. Volumetric reliability (%) of water resources projects in the LTB

The plot of the correlation matrix between the possible pairs of reservoir releases is presented in Figure 7.15, and their correlation coefficients are presented in Table 7.5. From the correlation matrix, it is clear that the release rule of cluster-II, cluster-III, and cluster-IV is strongly correlated, but these release rules are moderately correlated with the release rule of cluster-I. Therefore, one of the release rules from cluster-II, cluster-III, and cluster-IV with the release rule of cluster-I can be used to estimate the reservoir release at any time having the reservoir storage and inflow.

The monthly storages and the forecasted inflows in the year 2010, 2011, and 2012 were used to predict the monthly releases in the year 2010, 2011, and 2012, respectively, by using the multiple linear regression equations that derived for each cluster. On the other hand, the optimal monthly releases in the year 2010, 2011, and 2012 were estimated through the genetic algorithm by using the actual inflow scenarios.

In Table 7.5, and Figure 7.15, the notation R1, R2, R3, and R4 represents the predicted releases using the derived regression equation 7.18 for cluster-I, cluster-II, cluster-III, and cluster-IV, respectively, whereas R5 represents the optimal release obtained through the genetic algorithm by using the actual inflow to the reservoir.

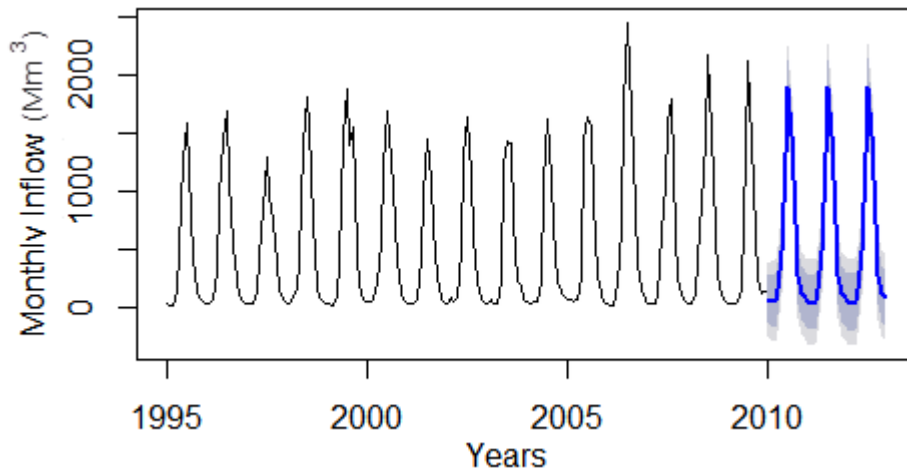


Figure 7.11. Monthly inflow series into the Lake Tana

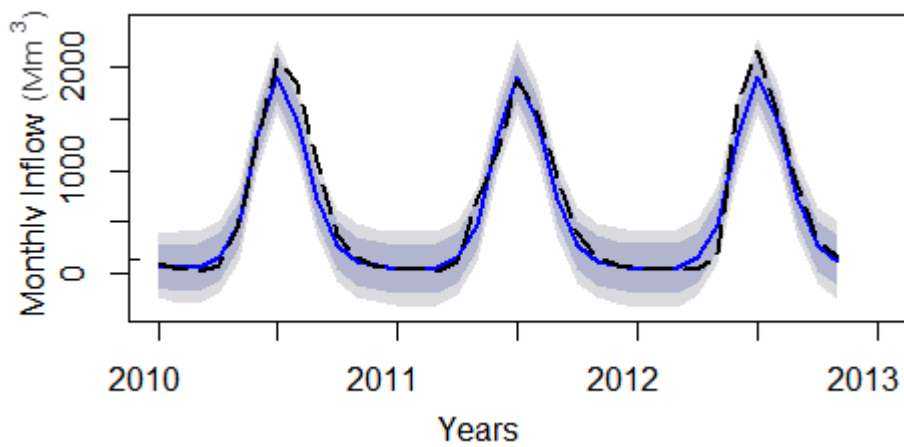


Figure 7.12. Plot of the forecasted inflow, actual inflow, 80% and 95% confidence interval

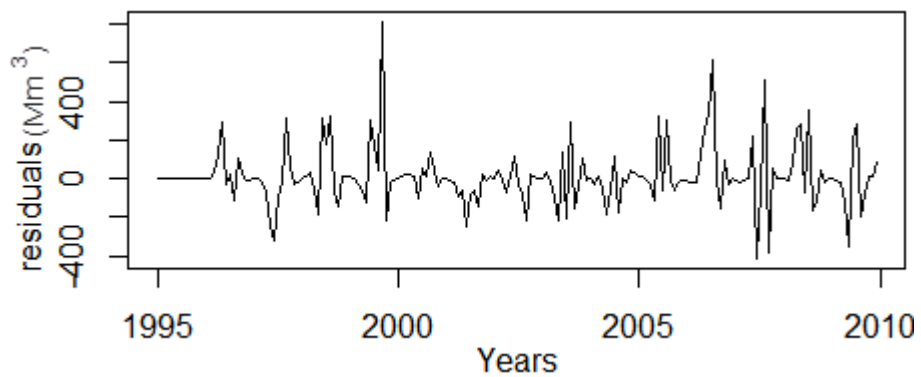


Figure 7.13. Plot of model residual

The derived reservoir release rules were also applied to the future inflow scenarios of the 2020s, 2050s, and 2080s by considering the changing climate under RCP2.6, RCP4.5, and RCP8.5. The results showed that the future inflow series into the Lake Tana would likely to improve the reliability of the proposed projects in the basin by 30%. The reservoir operation rule with and without considering the climate change impact revealed that the Lake level exceeds 1785 m above mean sea level (i.e. the minimum lake level required for navigation) for all development and inflow scenarios. Figure 7.16 shows the Lake Level for the four inflow scenarios (i.e. cluster-I, cluster-II, cluster-III, and cluster-IV) and Figure 7.17 presents the Lake level for the future time periods of 2020, 2050, and 2080 under RCP2.6, RCP4.5, and RCP8.5. The result showed that the climate change significantly improved the reliability of the reservoir systems in the Lake Tana Basin. Also, the result showed that the basin is likely to be vulnerable to the high floods in the 2080s under RCP8.5 inflow scenarios, in which the release from the Lake Tana reservoir was observed to be higher than the spillway capacity (Figure 7.18). The regression equations were also developed for the future total release from the Lake Tana in terms of the reservoir storage and reservoir inflow. Table 7.6 presents the coefficients and the performances of the regression equations for the future reservoir release.

Table 7.3. Coefficient values of the regression equation with their performance for the baseline inflow scenarios

Cluster	$a_1$	$a_2$	$a_3$	$R^2$
Cluster-I	956.40	0.14	-0.02	0.13
Cluster-II	-50.80	0.42	0.02	0.67
Cluster-III	-1112.00	0.52	0.05	0.79
Cluster-IV	-30.66	0.41	0.02	0.62

Table 7.4. Performance indices of the reservoir release rule for each cluster

Performance indices	Cluster-I	Cluster-II	Cluster-III	Cluster-IV
NSE	0.73	0.88	0.82	0.88
R2	0.46	0.61	0.64	0.61
RSR	0.52	0.34	0.42	0.34
PBIAS	30.25	5.67	31.82	4.09
RMSE	500.74	328.37	405.87	328.61

Table 7.5. Correlation coefficients between the possible pairs of release

	R1	R2	R3	R4	R5
R1	1.00	0.59	0.65	0.58	0.68
R2	0.59	1.00	<b>0.98</b>	<b>1.00</b>	0.78
R3	0.65	<b>0.98</b>	1.00	<b>0.98</b>	0.80
R4	0.58	<b>1.00</b>	<b>0.98</b>	1.00	0.78
R5	0.68	0.78	0.80	0.78	1.00

Table 7.6. Coefficient values & performance of the regression equation for the future inflow scenarios

Scenarios	Periods	Coefficients			Performance	
		$a_1$	$a_2$	$a_3$	$R^2$	RMSE
RCP2.6	2020	1127	0.49	-0.03	0.91	172
	2050	540.9	0.47	-0.006	0.81	267
	2080	-323.3	0.51	0.02	0.85	254
RCP4.5	2020	1381	0.37	-0.04	0.58	328
	2050	525	0.47	-0.004	0.84	240
	2080	-680.7	0.41	0.05	0.75	316
RCP8.5	2020	489.6	0.04	-0.003	0.03	186
	2050	850.4	0.47	-0.02	0.82	265
	2080	3696	0.91	-0.13	0.57	1463

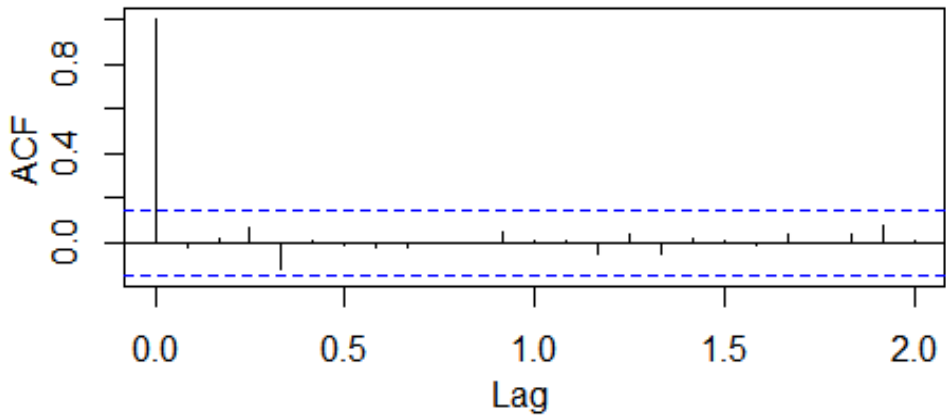


Figure 7.14. Autocorrelation function of the forecasting model

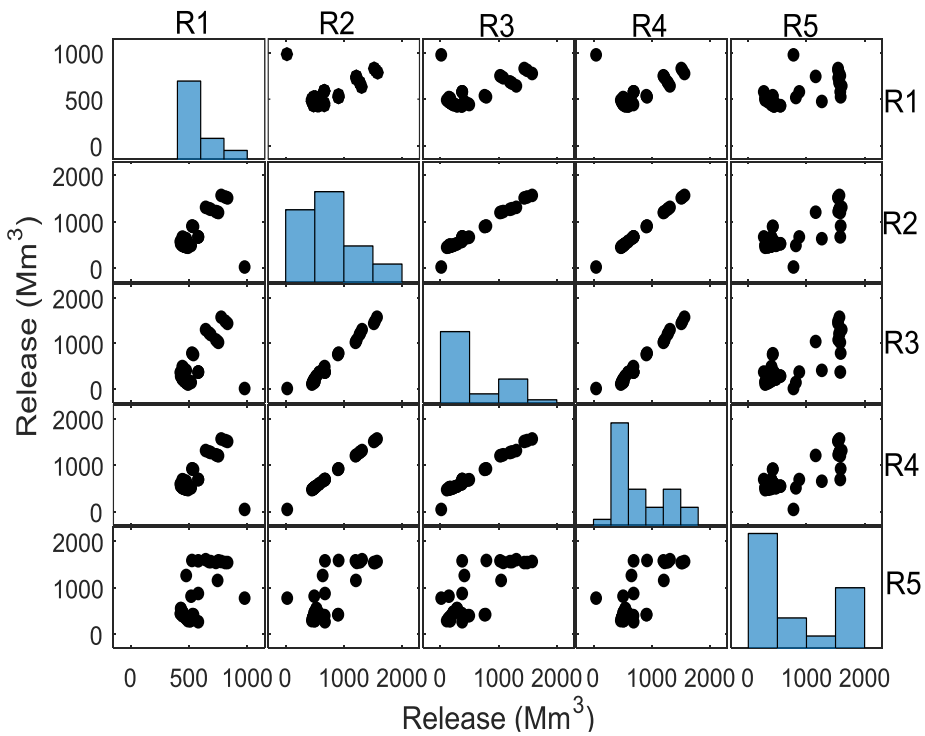


Figure 7.15. Correlation matrix between the possible reservoir releases

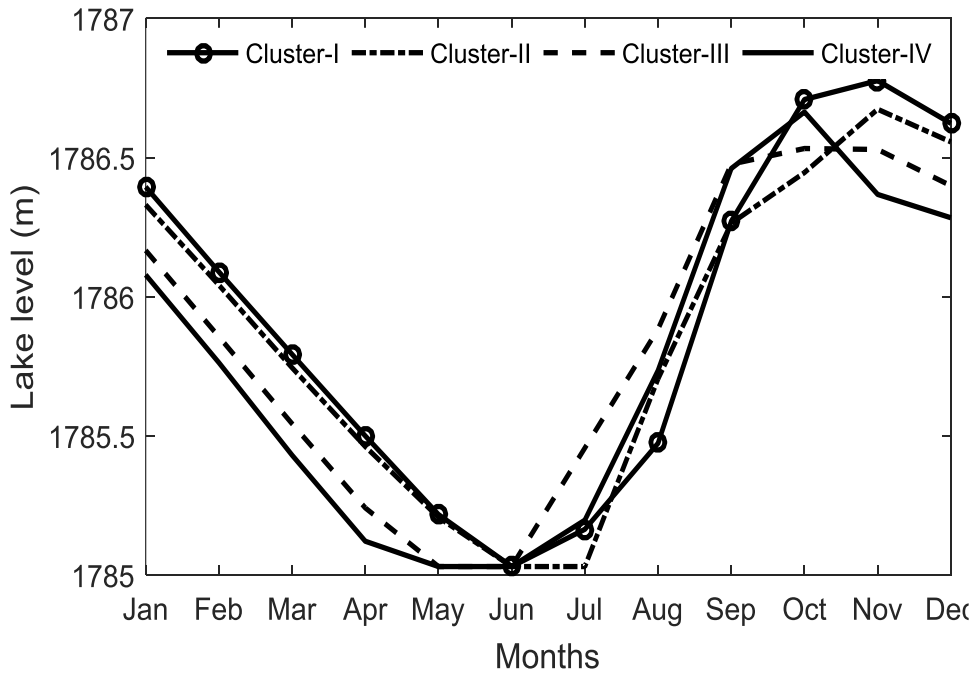


Figure 7.16. The monthly Lake level for the baseline scenario

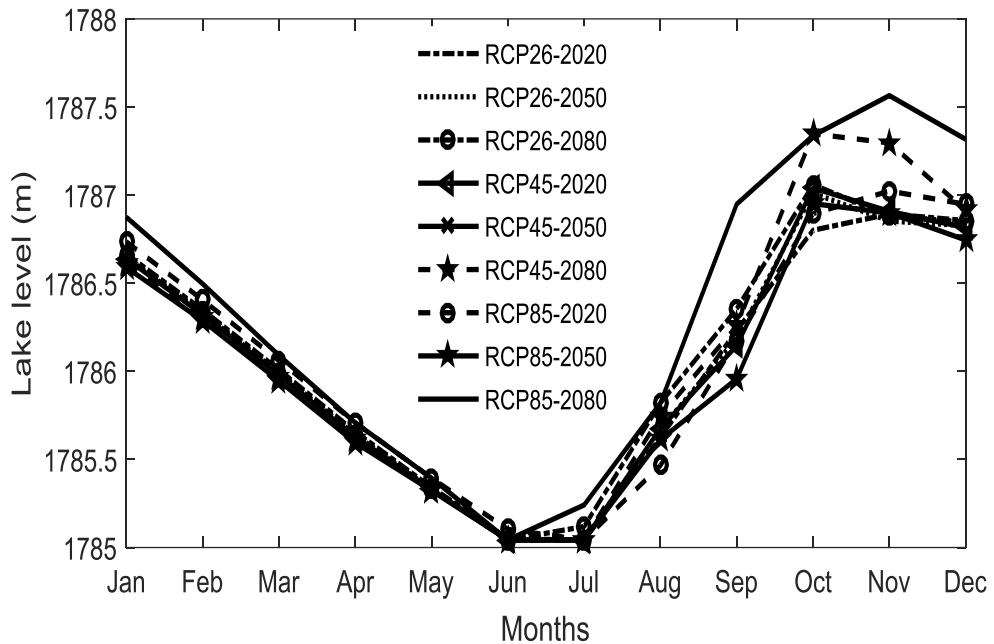


Figure 7.17. The monthly Lake level for future inflow scenarios

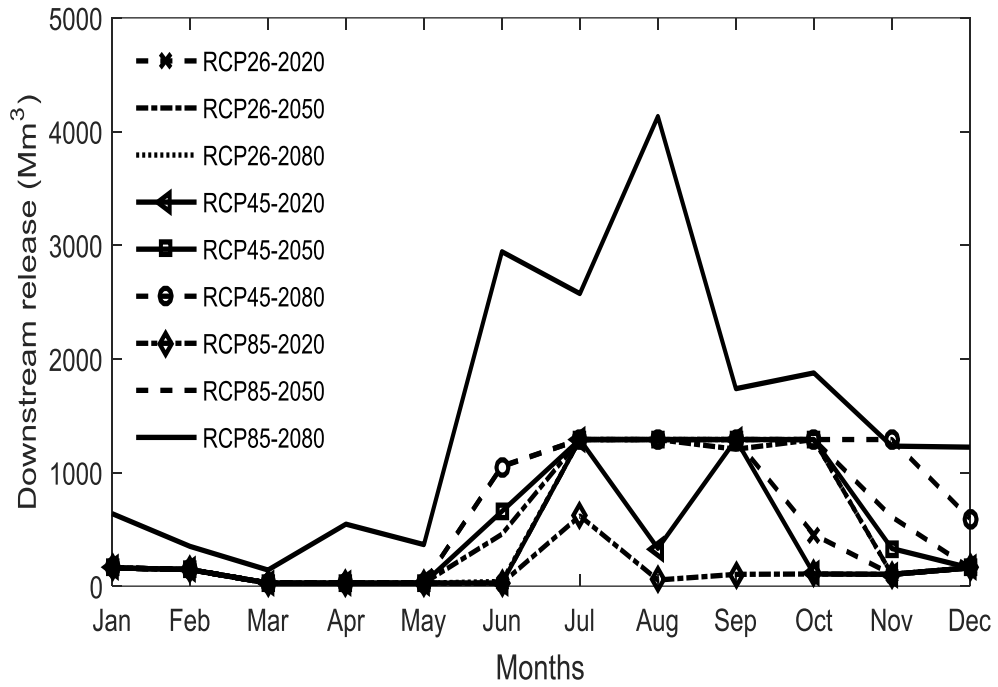


Figure 7.18. Downstream release from the basin for future inflow scenarios under climate change

## **7.4. Conclusions**

The MOGA approach was applied to the multi-reservoir systems in the Lake Tana Basin to derive operating policies of each reservoir. The main advantage of the MOGA approach is finding many Pareto optimal solutions in a single run, which is attractive and efficient that helps the decision maker to take proper decisions at different levels. For this, a non-dominated sorting genetic algorithm-II (NSGA-II) was used, which has a selection operator, elitism mechanism, and the crowded distance operator to obtain efficient solutions. This multi-objective model was formulated with irrigation and hydropower as two competing objectives. The NSGA-II model was applied for the four different inflow scenarios (i.e. cluster-I, cluster-II, cluster-III, & cluster-IV), and the corresponding Pareto optimal fronts were obtained through the formulated model. The model resulted in releases of more than 90% of the irrigation and hydropower demands. For flood protection, we maintained the minimum reservoir level at the beginning of the flood season by incorporating it into the formulated model. This type of reservoir operating policy is expected to be useful in real life implementation of reservoir operation. In general, demand coverage and reliability of above 90% were observed in all inflow scenarios. Regarding the Lake level, the mean monthly Lake levels exceed 1785 m above mean sea level (i.e. the minimum Lake level required for shipping) for all development and climate change scenarios.

# CHAPTER EIGHT

## 8. Conclusions and Future Study

### 8.1. Conclusions

It is always a good practice to identify a good model among the simple conceptual and complex hydrological models to accurately estimate the surface water resources potential of the Lake Tana Basin. Hence, this study compared two conceptual rainfall-runoff models (IHACRES, GR4J) to one physically based rainfall-runoff model (SWAT) concerning their performance to reproduce the observed discharge in both time and quantile domains. The comparison result showed that all three models captured the magnitudes and variabilities of the observed streamflow for the four gauging stations, and our results do not indicate that any of these hydrologic models is superior to the others for all sites or all measures of model performance. Therefore, the selected simple conceptual models (GR4J and IHACRES) perform comparably to a more complex model (SWAT) at a daily time-step. SWAT is considered to be the best model for the assessment of the surface water resources due to its benefit concerning the physical representation of the study basin. Furthermore, this study was also designed to accurately estimate the surface water resources of the ungauged catchments in the Lake Tana Basin. For this, the calibrated SWAT model parameters were transferred to the ungauged catchments by using the arithmetic mean, the

physical similarity, the spatial proximity, and the catchment runoff-response similarity which is originally proposed by this study. The performance of these four parameter transfer schemes were also compared to identify the best methods for modeling the ungauged catchments. The results showed that the catchment runoff-response similarity approach slightly improved the results obtained by the other three commonly used methods. Based on this parameter transfer approach, the mean annual surface water inflow to the Lake Tana from the ungauged catchments was found to be 2.61 Bm<sup>3</sup>/year which represents 41% of the total inflow from the gauged and ungauged catchments. The Statistical Downscaling Model was used to downscale the weather events corresponding to the three Representative Concentration Pathways (i.e. RCP2.6, RCP4.5, and RCP8.5) that used to explore the impacts of the climate change on the surface water resources of the Lake Tana Basin. The precipitation output of the SDSM was corrected for the bias in time and quantile-domains whereas the temperature was adjusted for the bias in time-domain only. The quantile-domain based bias correction performed much better than the time-domain based bias correction concerning the precipitation variability range. The quantile-based bias-corrected mean annual precipitation has shown a significant decrease by 14.93% at Ayikel station under RCP4.5; 0.87%, 5.54%, 20.21% in Gonder station under RCP2.6, RCP4.5, and RCP8.5, respectively, at Gonder weather station, whereas in all other stations it showed an increasing

magnitude in all RCPs and future time periods. The overall average changes in the maximum and minimum temperature showed values of 1.40 °C and 0.35 °C, respectively. The mean annual surface water inflow into the Lake Tana was also showed an increasing trend in all the future time periods and under all RCPs. The increase in the mean annual runoff can be beneficial to the improvement of agricultural productivity as well as to enhance the hydropower potential of the basin. However, the increases in temperature will also have a significant impact on the water balance of the reservoir in which open water evaporation will be higher. Therefore, the development of the reservoir operation rule for the Lake Tana Basin might be crucial for the better management of the surface water resources of the basin. Hence, a non-dominated sorting genetic algorithm-II (NSGA-II) was used to derive the operating policies of each reservoir in the Lake Tana Basin. This multi-objective model was formulated with irrigation and hydropower as two competing objectives, and the model was applied to the four different inflow scenarios (i.e. cluster-I, cluster-II, cluster-III, & cluster-IV). The model resulted in releases of more than 90% of the irrigation and hydropower demands. Concerning the Lake level, the mean monthly Lake levels exceed 1785 m above mean sea level (i.e. the minimum Lake level required for shipping) for all development and climate change scenarios.

## **8.2. Future Study**

In this study, a multi-criterion based model comparison was performed to identify the good hydrological model to accurately estimate the surface water resources of the Lake Tana Basin. The main limitation of this model comparison could be that the identification of the good hydrological model is not designed to be a comprehensive global assessment of water resources. Therefore, the performance of the three hydrological models should be tested in different climate zones to decide the best model for global water resources assessment among the simple and complex hydrological models. This study was also designed to understand the hydrological process of the basin under climate change. For this purpose, the precipitation and temperature were downscaled by using the Statistical Downscaling Model. The bias correction technique was applied to the downscaled climate data to minimize the biases between downscaled and observed data. The main drawback of the applied bias correction method is that the same correction algorithm applies to both current and future climate conditions. The consideration of time-dependent bias can be a good approach to solve this kind of issues for future study. We also recommend the use of different GCMs so as to cover the range of uncertainties related to GCMs. The other limitation of this study is that the land cover was considered constant throughout the simulation period. However, such an assumption can affect the projections of the streamflow in the basin.

## References

- Abbaspour, K.C. 2012. SWAT Calibration and Uncertainty Programs Manual Version 4, Department of Systems Analysis, Integrated Assessment and Modeling SIAM, Eawag. Swiss Federal Institute of Aquatic Science and Technology, Duebendorf, Switzerland.
- Ahn, S.; Jeong, J.H. & Kim, S.J. 2015. Assessing drought threats to agricultural water supplies under climate change by combining the SWAT and MODSIM models for the Geum River Basin, South Korea. *Hydrological Sciences Journal*. 10.1080/02626667.2015.1112905.
- Ajami, N.K.; Gupta, H.; Wagener, T. & Sorooshian, S. 2004. Calibration of a semi-distributed hydrologic model for streamflow estimation along a river system. *Journal of Hydrology*. 298 (1-4), 112-135.
- Allen, R.G.; Pereira, L.S.; Raes, D. & Smith, M. 1998. Crop Evapotranspiration. Guidelines for Computing Crop Water Requirements. FAO Irrigation and Drainage Paper 56, FAO, Rome.
- Andrews, F.T.; Croke, B.F.W. & Jakeman, A.J. 2011. An open software environment for hydrological model assessment and development. *Environ. Modell. Softw.* 26 (10), 1171-1185.
- Andréassian, V.; Perrin, C.; Berthet, L.; Moine, N.L.; Lerat, J.; Loumagne, C.; Oudin, L.; Mathevet, T.; Ramos, M.H. & Valéry, A. 2009. Crash

- tests for a standardized evaluation of hydrological models, *Hydrol. Earth. Syst. Sci.*, 13, 1757-1764.
- Anna M., Liliana P., Faycal B. & Marco F. 2014. Comparing calibrated parameter sets of the SWAT model for the Scandinavian and Iberian peninsulas. *Hydrological Sciences Journal*, 60 (5) 2015.
- Armstrong, J.S. 1989. Combining forecasts: The end of the beginning or the beginning of the end? *Int. J. Forecast.*, 5, 585–588.
- Arnold, J.G. & Fohrer, N. 2005. SWAT2005: current capabilities and research opportunities in applied watershed modeling. *Hydrological Processes*, 19(3), 563-572.
- Arnold, J.G.; Srinivasan, R.; Muttiah, R.S. & Williams, J.R. 1998. Large area hydrologic modeling and assessment—Part 1: Model development. *J. Am. Water Resour. Assoc.*, 34, 73-89.
- ASCE. 1993. Criteria for evaluation of watershed models. *J. Irrigation Drainage Eng.* 119(3): 429-442.
- Azari, M.; Moradi, H.R.; Saghafian, B. & Faramarzi, M. 2016. Climate change impacts on streamflow and sediment yield in the North of Iran. *Hydrological Sciences Journal*. 10.1080/02626667.2014.967695.
- Bastola, S.; Ishidaira, H. & Takeuchi, K. 2008. Regionalisation of hydrological model parameters under parameter uncertainty: A case

- study involving TOPMODEL and basins across the globe, *Journal of Hydrology*, 357, 188-206, doi:10.1016/j.jhydrol.2008.05.007.
- Bates, J. M. and Granger, C. W. J. 1969. The combination of forecasts. *Operational Research Quarterly*, Vol. 20, pp. 451-468.
- BCEOM (Egis Bceom International). 1999. Abbay River Basin Integrated Development Master Plan Project and Associates; Abbay Basin Integrated Development Master Plan Project; Phase 2, Section II, Vol. III: Water Resources: Part 1 – Climatology and Part 2 – Hydrology. Report to the Ministry of Water Resources: Ethiopia.
- Bellier C, Humphreys H, Kennedy R. & Donkin. 1997. Environmental Impact Assessment, Federal Republic of Ethiopia, Ministry of Water Resources medium scale hydropower plant study project Tis Abay II joint venture.
- Bergstrom S. & Graham L.P. 1998. On the Scale Problem in Hydrological Modelling. *Journal of Hydrology* 211: 253–265.
- Beven, K.J.; Calver, A. & Morris, E.M. 1987. Institute of Hydrology distributed model. Internal Report, Institute of Hydrology, Wallingford, Oxfordshire, UK.
- Beven, K.J. 1989. Changing ideas in hydrology - the case of physically based models. *Journal of Hydrology* 105, 157-172.

- Beven, K.J. 1997. Distributed Modeling in Hydrology. Application of the TOPMODEL concepts. Wiley, Chichester, 360p.
- Beven, K.J. 2000a. Rainfall-runoff modeling: The Primer. John Wiley and Sons, Chichester, U.K. pp. 360.
- Beyene, T.; Lettenmaier, D.P. & Kabat, P. 2010. Hydrologic impacts of climate change on the Nile River Basin: implications of the IPCC scenarios. *ClimaticChange* 100, 433–461.
- Bicknell, B.R.; Imhoff, J.C.; Kittle, J.L.; Donigian, A.S. & Johanson, R.C. 1997. Hydrological Simulation Program-Fortran, User's Manual for Version 11. US Environmental Protection Agency, National Exposure Research Laboratory, Athens, GA, EPA/600/R-97/080, 755p.
- Box, G.E.P.; Jenkins, G.M. & Bacon, D.W. 1967. Models for Forecasting Seasonal and Nonseasonal Time Series, in *Spectral Analysis of Time Series*, B. Harris, ed., John Wiley & Sons, Inc., New York.
- Box G.E.P. & Jenkins G.M. 1976. *Time Series Analysis: Forecasting and Control*. Holden-Day: San Francisco; 588 pp.
- Boyle, D.B.; Gupta, H.V.; Sorooshian, S.; Koren, V.; Zhang, Z. & Smith, M. 2001. Toward improved streamflow forecasts, value of semi-distributed modeling. *Water Resources Research* 37 (11), 2749–2759.

- Buser C.M.; Kunsch H.R.; Luthi D.; Wild M. & Schar C. 2009. Bayesian multi-model projection of climate: bias assumptions and interannual variability *Clim. Dynam.* 33 849–68
- Buttle, J.M. & Eimers, M.C. 2009. Scaling and physiographic controls on streamflow behaviour on the Precambrian Shield, south-central Ontario. *Journal of Hydrology*, 374 (3–4), 360–372.
- Cai, X.; Mckinney, D. & Lasdon, L.S. 2001. Solving nonlinear water management model using a combined genetic algorithm and linear programming approach. *Advanced Water Resources* 2 (6), 667–676.
- Carpenter, T.M. & Georgakos, K.P. 2001. Distributed model flow sensitivity to uncertainty in radar-rainfall input. IAHS Publ. no. 282. 2003.
- Caruso, B.S. 2000. Evaluation of low-flow frequency analysis methods. *Journal of Hydrology New Zealand*, 39: 19-47.
- Chang, Jian-Xia, Tao B., Qiang H. & Yang, Da-Wen. 2013. Optimization of water resources utilization by PSO-GA. *Water Resour Manage* 27: 3525-3540.
- Chang, L.C. & Chang, F.J. 2001. Intelligent control for modeling of real-time reservoir operation. *Hydrological Processes* 15 (9), 1621–1634.
- Chang, Y.T., Chang, L.C. & Chang, F.J. 2005. Intelligent control for modeling of real-time reservoir operation, part II: artificial neural

- network with operating rule curves. *Hydrological Processes* 19, 1431–1444.
- Chang, L.C. 2008. Guiding rational reservoir flood operation using penalty-type genetic algorithm. *Journal of Hydrology* 354, 65–74.
- Chen, L.; McPhee, J. & Yeh, W.W.G. 2007. A diversified multiobjective GA for optimizing reservoir rule curves. *Advances in Water Resources* 30 (5), 1082–1093.
- Chen, Y.H. & Chang, F.J. 2009. Evolutionary artificial neural networks for hydrological systems forecasting. *Journal of Hydrology* 367, 125–137.
- Cheng, C.T.; Zhao, M.Y.; Chau, K.W. & Wu, X.Y. 2006. Using genetic algorithm and TOPSIS for Xinanjiang model calibration with a single procedure. *Journal of Hydrology*, 316 (1-4), 129-140.
- Cheng, Q.; Koa, C.; Yuana, Y; Gea, Y. & Zhang, S. 2006. GIS modeling for predicting river runoff volume in ungauged drainages in the Greater Toronto Area, Canada. *Comput. Geosci.* , 32 (8), 1108–1119
- Chiu, Y.C.; Chang, L.C. & Chang, F.J. 2007. Using a hybrid genetic algorithm-simulated annealing algorithm for fuzzy programming of reservoir operation. *Hydrological Processes* 21, 3162–3172.
- Christensen, J.H.; Boberg, F.; Christensen, O.B. & Lucas-Picher, P. 2008. On the need for bias correction of regional climate change projections of temperature and precipitation. *Geophys. Res. Lett.* 35 (20), L20709.

- Chu J., Xia J., Xu C.Y. & Singh V. 2010. Statistical downscaling of daily mean temperature, pan evaporation and precipitation for climate change scenarios in Haihe River, China. *Theor Appl Climatol* 99 (1):149–161.
- Chu T.W. & Shirmohammadi A. 2004. Evaluation of the SWAT model's hydrology component in the piedmont physiographic region of Maryland. *Transactions of the American Society of Agricultural Engineers* 47: 1057–1073.
- Conway D. 1997. A water balance model of the Upper Blue Nile in Ethiopia. *Hydrological Sciences Journal* 42(2): 265–286.
- Conway D. 2005. The Climate and Hydrology of the Upper Blue Nile, Ethiopia. *Geographical Journal* 166:49-62
- Cooper, V.A; Nguyen, V.T.V. & Nicell, J.A. 1997. Evaluation of global optimization methods for conceptual rainfall-runoff model calibration. *Water Science Technology*, 36(5), 53-60.
- Covey C., AchutaRao K.M., Cubasch U., Jones P., Lambert S.J., Mann M.E., Phillips T.J. & Taylor K.E. 2003. An overview of results from the coupled model inter-comparison project. *Global Planet Change* 37 103–33.
- Croke B.F.W. & Jakeman A.J. 2004. A catchment moisture deficit module for the IHACRES rainfall–runoff model. *Environmental Modelling and Software* 19(1): 1–5.

- Croke, B.F.W, Merrittc, W.S. & Jakeman, A.J. 2004. A dynamic model for predicting hydrologic response to land cover changes in gauged and ungauged catchments. *Journal of Hydrology (Amsterdam)*, 291, 115–131.
- Cunderlik, M.J. 2003. Hydrologic model selection fort the CFCAS project: Assessment of Water Resources Risk and Vulnerability to Changing Climatic Conditions, Project Report I. University of Western Ontario, Canada.
- Dams, J.; Nossent, J.; Senbeta, T.B.; Willems, P. & Batelaan, O. 2015. Multi-model approach to assess the impact of climate change on runoff. *Journal of Hydrology. (Amst.)* 529: 1601-1616.
- Deb, K.; Pratap, A.; Agarwal, S. & Meyarivan, T. 2002. A Fast and Elitist Multi- Objective Genetic Algorithm: NSGA-II, *IEEE Transactions on Evolutionary Computation*, 6, 182–197.
- Devkota, L.P. & Gyawali, D.R. 2015. Impacts of climate change on hydrological regime and water resources management of the Koshi River Basin, Nepal. *Journal of Hydrology: Regional Studies*. 10.1016/j.ejrh.2015.06.023.
- Duan Q.Y., Gupta V.K. & Sorooshian S. 1993. Shuffled complex evolution approach for effective and efficient global minimization. *Journal of Optimization Theory and Applications* 76(3): 501–521

- Duan Q.Y, Sorooshian S. & Gupta V. 1992. Effective and efficient global optimization for conceptual rainfall–runoff models. *Water Resources Research* 28(4): 1015–1031.
- Duku, C.; Rathjens, H.; Zwart S.J. & Hein, L. 2015. Towards ecosystem accounting: A comprehensive approach to modeling multiple hydrological ecosystem services. *Hydrol. Earth Syst. Sci.* 10.5194/hess-19-4377-2015.
- Dye, P.J. & Croke, B.F.W. 2003. Evaluation of streamflow predictions by the IHACRES rainfall-runoff model in two South African catchments, *Environmental Modeling and Software* 18:705-712.
- Eberhart R.C. & Kennedy J. 1995. A new optimizer using particle swarm theory. In *Proceedings of the Sixth International Symposium on Micro Machine and Human Science*. Nagoya, Japan; 39–43.
- Edijatno, Nascimento, N.O., Yang, X., Makhlouf, Z., Michel, C. 1999. GR3J: a daily watershed model with three free parameters. *Hydrological Sciences Journal* 44(2), 263-277.
- Evans, J.P. & Jakeman, A.J. 1998. Development of a simple, catchment-scale, rainfall evapotranspiration-runoff. *Environmental Modeling & Software* 13 (1998) 385–393.
- Fi-John C, Li C. & Li-Chiu C. 2005. Optimizing the reservoir operating rule curves by genetic algorithms. *Hydrological Processes* 19:2277–2289.

- Fortin, J.P.; Turcotte, R.; Massicotte, S.; Moussa, R.; Fitzback, J. & Villeneuve, J.P. 2001. A Distributed Watershed Model Compatible with Remote Sensing and GIS Data II: Application to Chaudiere Watershed. *Journal of Hydrologic Engineering*, 6, 100-108.
- Gabriel, M.; Knightes, C.; Cooter, E. & Dennis, R. 2015. Evaluating relative sensitivity of SWAT-simulated nitrogen discharge to projected climate and land cover changes for two watersheds in North Carolina, USA. *Hydrological Processes*. 10.1002/hyp.10707.
- Gan, T.Y. & Biftu, G. F. 1996. Automatic calibration of conceptual rainfall-runoff models: optimization algorithms, catchment conditions, and model structure. *Water Resources Research*, 32(12), 3513-3524.
- Gassman P.W., Reyes M., Green C.H. & Arnold JG. 2007. The soil and water assessment tool: historical development, applications, and future directions. *Transactions ASABE* 50(4): 1212–1250.
- Gilbert R.O. 1987. *Statistical Methods for Environmental Pollution Monitoring*. Van Nostrand Reinhold: New York.
- Githui, F.; Thayalakumaran, T. & Selle, B. 2015. Estimating irrigation inputs for distributed hydrological modeling: A case study from an irrigated catchment in southeast Australia. *Hydrological processes*. 10.1002/hyp.10757.

- Goldberg D.E. 1989. Genetic algorithms in search, optimization and machine learning. Addison-Wesley, Reading.
- Goldstein, J.C. & Tarhule, A. 2015. Evaluating the impacts of climate change and switchgrass production on a semiarid basin. *Hydrological processes*. 10.1002/hyp.10159.
- Götzinger, J. & Bárdossy, A. 2007. Comparison of four regionalization methods for a distributed hydrological model. *Journal of Hydrology* 333, 374–384.
- Granger, C.W.J. & Newbold, P. 1977. *Forecasting economic time series*, Academic, New York.
- Grossman R., Seni G., Elder J., Agarwal N. & Liu H. 2010. *Ensemble Methods in Data Mining: Improving Accuracy Through Combining Predictions*. Morgan & Claypool.
- Grusson, Y.; X. Sun, S. Gascoin, S. Sauvage, S. Raghavan, F. Anctil & J.-M. Sacher-Perez. 2015. Assessing the capability of the SWAT model to simulate snow, snowmelt and streamflow dynamics over an alpine watershed. *Journal of Hydrology*. 531(Part 3): 574–588.
- Gupta HV, Sorooshian S, & Yapo PO. 1999. Status of automatic calibration for hydrologic models: Comparison with multilevel expert calibration. *Journal of Hydrologic Engineering* 4(2): 135–143.

- Guse, B., M. Pfannerstill, M. Strauch, D.E. Reusser, S. Ladtke, M. Volk, H. Gupta & N. Fohrer. 2015. On characterizing the temporal dominance patterns of model parameters and processes. *Hydrological Processes*. 10.1002/hyp.10764.
- Guttman, N.B. 1994. On the sensitivity of sample L-moments to sample size. *Journal of Climate*, 7(6):1026–1029.
- Guttman, N.B. 1998. Comparing the Palmer drought index and the Standardized Precipitation Index. *Journal of the American Water Resources Association*, 34(1):113–121.
- Hansen, D.P., W. Ye, A.J. Jakeman, R. Cooke, & P. Sharma. 1996. Analysis of the effect of rainfall and streamflow data quality and catchment dynamics on streamflow prediction using the rainfall-runoff model IHACRES, *Environmental Software*, 11:193-202.
- Hargreaves, G.H. & Z.A. Samani. 1985. Reference crop evapotranspiration from temperature. *Applied Engineering in Agriculture* 1:96-99.
- He, Y.; Bárdossy, A. & Zehe, E. 2011. A review of regionalisation for continuous streamflow simulation. *Hydrol. Earth Syst. Sci.*, 15 (11), 3539–3553.
- Hejazi MI, Cai X & Borah D. 2008. Calibrating a watershed simulation model involving human interference – an application of multi-objective genetic algorithms. *J Hydroinformatics* 10(1):97–111.

- Hesse, C.; Krysanova, V.; Stefanova, A.; ielecka M. & Domnin, D.A. 2015. Assessment of climate change impacts on water quantity and quality of the multi-river Vistula Lagoon catchment. *Hydrological Sciences Journal*. 10.1080/02626667.2014.967247.
- Heuvelmans, G.; Muys, B. & Feyen, J. 2006. Regionalization of the parameters of a hydrological model: Comparison of linear regression models with artificial neural nets, *Journal of Hydrology*, 319, 245-265, doi: 10.1016/j.jhydrol.2005.07.030.
- Horn, J.; Nafpliotis, N.; & Goldberg, D.E. 1994. A niched Pareto genetic algorithm for multiobjective optimization. *Proceedings of the First IEEE Conference on Evolutionary Computation*, Z. Michalewicz, 82-87.
- Huang J, Zhang J, Zhang Z, Xu C, Wang B, Yao J. 2011. Estimation of future precipitation change in the Yangtze River basin by using statistical downscaling method. *Stoch. Env Res Risk A* 25(6):781– 792.
- Huang, W.C., Yuan, L.C. 2004. A drought early warning system on real-time multireservoir operations. *Water Resources Research* 40 (6), W06401, doi: 10.1029/2003WR002910.
- Huang, W.C., Yuan, L.C., Lee, C.M. 2002. Linking genetic algorithms with stochastic dynamic programming to the long-term operation of a multireservoir system. *Water Resources Research* 38 (2), 401–409.

- Huber, W.C., & R.E. Dickinson. 1988. Storm Water Management Model User's Manual, Version 4. EPA/600/3-88/001a (NTIS PB88-23664/AS), Environmental Protection Agency, Athens, GA, 595p.
- Hurst, H. E.; Black, R. P. & Simaika, Y. M. 1959. Nile Basin: Vol. IX The hydrology of the Blue Nile and Atbara and of the Main Nile to Aswan, with some reference to projects. Cairo: General Organization for Government Printing Office.
- Iman RL, & Conover WJ. 1980. Small sample sensitivity analysis techniques for computer models, with an application to risk assessment. *Communications in Statistics: Theory and Methods* 17: 1749–1842.
- IPCC. 2007. Climate change. 2007. The physical sciences basis Contribution of Working Group 1 to the Fourth Assessment Report of the Intergovernmental Panel on Climate Change. (Cambridge: Cambridge University Press) p 966.
- IPCC. 2007. Climate Change. 2007. Synthesis Report. Contribution of Working Groups I, II and III to the Fourth Assessment Report of the Intergovernmental Panel on Climate Change. IPCC, Geneva, Switzerland, 104 pp.
- IPCC. 2011. Climate Change. 2011. IPCC Special Report on Renewable Energy Sources and Climate Change Mitigation. Prepared by Working Group III of the Intergovernmental Panel on Climate Change. Cambridge

University Press, Cambridge, United Kingdom and New York, NY, USA, 1075 pp.

IPCC. 2013. Climate change. 2013. the physical science basis Contribution of Working Group I to the Fifth Assessment Report of the Intergovernmental Panel on Climate Change. (Cambridge: Cambridge University Press).

Jakeman AJ, & Hornberger GM. 1993. How much complexity is warranted in rainfall–runoff model? *Water Resources Research* 29(8): 2637–2649.

Jeong, D. I., & Kim, Y. O. 2009. Combining single-value streamflow forecast—A review and guidelines for selecting techniques. *Journal of Hydrology*, 377(3–4), 284–299.

Jin, X., Xu, C. Y., Zhang, Q., & Chen, Y. D. 2009. Regionalization study of a conceptual hydrological model in Dongjiang basin, south China. *Quaternary Int.*, 208 (1–2), 129–137.

Kendall, M.G. 1975. *Rank Correlation Methods*. Charles Griffin, London.

Kennedy, J and Eberhart, R.C. 1995. Particle swarm optimization, in *Proceedings of IEEE International Conference on Neural Networks (ICNN '95)*, vol. 4, pp. 1942–1948, IEEE Service Center, Perth, Western Australia, November-December.

Kannan N, & Jeong J. 2011. An approach for estimating streamflow health using flow duration curves and indices of hydrologic alteration. EPA

region 6 water quality protection division U.S. Environmental Protection Agency: Dallas, TX.

Karlsson, I.B., T.O. Sonnenborg, J.C. Refsgaard, D. Trolle, C.D. Borgesen, J.E. Olesen, E. Jeppesen & K.H. Jensen. 2016. Combined effects of climate models, hydrological model structures and land use scenarios on hydrological impacts of climate change. *Journal of Hydrology*. 10.1016/j.jhydrol.2016.01.069.

Kebede S, Travi Y, Alemayehu T, & Marc V. 2006. Water Balance of Lake Tana and its Sensitivity to fluctuations in rainfall, Blue Nile Basin, Ethiopia. *Journal of Hydrology* 316: 233–247.

Kim, T., Heo, J.H., & Jeong, C.S. 2006. Multireservoir system optimization in the Han River Basin using multi-objective genetic algorithms. *Hydrological Processes* 20 (9), 2057–2075.

Kim, U., & Kaluarachchi, J.J. 2008. Application of parameter estimation and regionalization methodologies to ungauged basins of the Upper Blue Nile River Basin, Ethiopia. *Journal of Hydrology*. 362, 39–56.

Kim, Y.O.; Jeong, D. & Ko, I.H. 2006. Combining rainfall-runoff model outputs for improving ensemble streamflow prediction. *Journal Hydrologic Engineering*, 10.1061/(ASCE)1084-0699(2006)11:6(578), 578–588.

- Kite, G.W. 1995. The SLURP model, in *Computer Models of Watershed Hydrology*, edited by V. P. Singh, pp. 521 – 562, Water Resour. Publ., Highlands Ranch, Colo.
- Kjeldsen T.R., & Rosbjerg D. 2004. Choice of reliability, resilience and vulnerability estimators for risk assessments of water resources systems. *Hydrological Science Journal* 49(5), 755–767.
- Knowles, J.D. & Corne, D.W. 2000. Approximating the nondominated front using the Pareto archived evolution strategy. *Evolutionary Computation*, 8,149–172.
- Knudsen, J., Thomsen, A. & Refsgaard, J. C. 1986. WATBAL, A semi-distributed, physically based hydrological modeling system. *Nordic Hydrol.* 17, 347-362.
- Kokkonen, T.S.; Jakeman, A.J.; Young, P.C. & Koivusalo, H.J. 2003. Predicting daily flows in ungauged catchments: Model regionalization from catchment descriptors at the Coweeta Hydrologic Laboratory, North Carolina. *Hydrological Process.* 17, 2219-2238.
- Koren V, Reed S, Smith M, Zhang Z, & Seo D.J. 2004. Hydrology Laboratory Research Modeling System (HL-RMS) of the U.S. National Weather Service. *Journal of Hydrology* 291(3–4): 297–318.
- Kouwen, N. 2001. WATFLOOD/SPL9 Hydrological Model & Flood Forecasting System. University of Waterloo, 192 p.

- Krajewski W.F, Lakshimi V, Georgakakos K.P, & Jain S.C. 1991. A Monte Carlo study of rainfall sampling effect on a distributed catchment model. *Water Resources Research* 27(1): 119–128.
- Legates D.R, & McCabe G.J. 1999. Evaluating the use of “goodness-of-fit” measures in hydrologic and hydroclimatic model validation. *Water Resources Research* 35(1): 233–241.
- Le Moine, N. 2008. Le bassin versant de surface vu par le souterrain: une voie d’amélioration des performances et du réalisme des modèles pluie-débit?, PhD thesis, Université Pierre et Marie Curie, Paris, France, 348 pp., 2008.
- Lenderink, G.; Buishand, A. & Deursen, W.V. 2007. Estimates of future discharges of the river Rhine using two scenario methodologies: direct versus delta approach. *Hydrol. Earth Syst. Sci.* 11 (3), 1145–1159.
- Liang, X.; Lettenmaier, D.P.; Wood, E.F. & Burges, S.J. 1994. A simple hydrologically-based model of land surface water and energy fluxes for general circulation models. *Journal of Geophysical Research* 99(D7):14,415–14,428.
- Li, H.; Zhang, Y.; Chiew, F.H.S. & Shiguo, X. 2009. Predicting runoff in ungauged catchments by using Xinanjiang model with MODIS leaf area index. *Journal of Hydrology*, 370 (1–4), 155–162.

- Lindstrom, G.; Johansson, B.; Persson, M.; Gardelin, M. & Bergstrom, S. 1997. Development and test of the distributed HBV-96 hydrological model. *Journal of Hydrology*. 201, pp.272-288.
- Littlewood, I.G., and Marsh, T.J. 1996. A re-assessment of the monthly naturalised flow record for the River Thams at Kingston from 1883, and implications for the relative severity of historic droughts, *Regulated Rivers: Res. Manag.*, 12, 13-26.
- Liu J.P., Song M.R, Horton R.M. & Hu Y. 2013. Reducing spread in climate model projections of a September ice-free arctic P. *Natl. Acad. Sci. USA* 110 12571–6.
- Maidment, D.R. 1993. *Handbook of Hydrology*, McGraw-Hill
- Malagò, A., L. Pagliero, F. Bouraoui & M. Franchini. 2015. Comparing calibrated parameter sets of the SWAT model for the Scandinavian and Iberian Peninsulas. *Hydrological Sciences Journal*. 10.1080/02626667.2014.978332.
- Mann, H.B. 1945. Nonparametric Tests against Trend. *Econometrica* 13, 245-259.
- Markovic, D. & M. Koch. 2015. Stream response to precipitation variability: A spectral view based on analysis and modeling of hydrological cycle components. *Hydrological Processes*. 10.1002/hyp.10293.

- McKay MD. 1988. Sensitivity and uncertainty analysis using a statistical sample of input values. In *Uncertainty analysis*, Ronen Y (ed). CRC Press, Inc.: Boca Raton, FL; 145–186.
- McKay MD, Beckman RJ, & Conover WJ. 1979. A comparison of three methods for selecting values of input variables in the analysis of output from a computer code. *Technometrics* 21(2): 239–245.
- McKee, T. B., J. Nolan, & J. Kleist. 1993. The relationship of drought frequency and duration to time scales. Preprints, Eighth Conf. on Applied Climatology, Anaheim, CA, Amer. Meteor. Soc., 179 -184.
- McMahon T.A., Adeloye A.J., & Zhou S.L. 2006. Understanding performance measures of reservoirs. *Journal of Hydrology* 324(1–4), 359–382.
- Mechal, A., T. Wagner & S. Birk. 2015. Recharge variability and sensitivity to climate: The example of Gidabo River Basin, Main Ethiopian Rift. *Journal of Hydrology: Regional Studies*. 10.1016/j.ejrh.2015.09.001
- Mekonnen, B.A., K.A. Mazurek & G. Putz. 2016. Incorporating landscape depression heterogeneity into the Soil and Water Assessment Tool (SWAT) using a probability distribution. *Hydrological Processes*. 10.1002/hyp.10800.
- Merz, R.; & Blöschl, G. 2004. Regionalisation of catchment model parameters. *Journal of Hydrology*, 287, 95-123.

- Me, W., J.M. Abell & D.P. Hamilton. 2015. Effects of hydrologic conditions on SWAT model performance and parameter sensitivity for a small, mixed land use catchment in New Zealand. *Hydrol. Earth Syst. Sci...* 10.5194/hess-19-4127-2015.
- Michel, C., Perrin, C., Andréassian, V., Oudin, L. & Mathevet, T. 2006. Has basin-scale modeling advanced beyond empiricism? Large sample basin experiments for hydrological model parameterization: results of the model parameter experiment (MOPEX) pp. 108-116. IAHS Publication 307.
- Modrick T, & Georgakakos KP. 2006. Intercomparison of lumped versus distributed hydrologic model ensemble simulations on operational forecast scales. *Journal of Hydrology* 329: 174– 185.
- MoFED (Ministry of Finance and Economic Development). 2006. A plan for accelerated and sustained development to end poverty, (2005/06–2009/10), volume I. Addis Ababa, Ethiopia.
- Monteith JL. 1965. Evaporation and environment. The state and movement of water in living organisms, XIXth symposium. Cambridge University Press: Swansea, United Kingdom.
- Monteiro, J.A.E., M. Strauch, R. Srinivasan, K. Abbaspour & B. Gücker. 2015. Accuracy of grid precipitation data for Brazil: Application in river discharge modeling of the Tocantins catchment. *Hydrological Processes*. 10.1002/hyp.10708.

- Moss R.H, Edmonds JA, Hibbard KA, Manning MR, Rose SK, van Vuuren DP, Carter TR, Emori S, Kainuma M, Kram T, Meehl GA, Mitchell JF, Nakicenovic N, Riahi K, Smith SJ, Stouffer RJ, Thomson AM, Weyant JP, Wilbanks TJ. 2010. The next generation of scenarios for climate change research and assessment. *Nature* 463 747–56.
- Nascimento, N. O. 1995. *Appréciation à l'aide d'un modèle empirique des effets d'action anthropiques sur la relation pluie-débit à l'échelle du bassin versant*, Thèse de Doctorat thesis, 550 pp, CERGRENE/ENPC, Paris.
- Nash JE, & Sutcliffe JV. 1970. River flow forecasting through conceptual models part I—A discussion of principles. *Journal of Hydrology* 10(3): 282–290.
- Neitsch SL, Arnold JG, Kiniry JR, Williams JR, & King KW. 2005. *Soil and Water Assessment Tool (SWAT) Theoretical Documentation*. Grassland Soil and Water Research Laboratory, Blackland Research Center, Texas Agricultural Experiment Station, Texas Water Resources Institute, Texas Water Resources Institute: College Station, Texas; 506 pp.
- Neupane, R.P., J.D. White & S.E. Alexander. 2015. Projected Hydrologic changes in monsoon-dominated Himalaya Mountain basins with changing climate and deforestation. *Journal of Hydrology*. 10.1016/j.jhydrol.2015.03.048.

- Nicks AD, Gander GA. 1994. CLIGEN: a weather generator for climate inputs to water resource and other model. In Proceedings of the 5th International Conference on Computers in Agriculture. American Society of Agricultural Engineers, St. Joseph, MI, 3–94.
- Nigatu, Z.M., Rientjes, T. & Haile, A.T. 2016. Hydrological Impact Assessment of Climate Change on Lake Tana's Water Balance, Ethiopia. *American Journal of Climate Change*, 5, 27-37.
- Niraula, R., T. Meixner, & L.M. Norman. 2015. Determining the effect of model calibration on predicting relative/absolute changes in streamflow from LULC and climate changes. *Journal of Hydrology*. 10.1016/j.jhydrol.2015.01.007.
- Noilhan, J. & Planton, S. 1989. A simple parameterization of land surface processes for meteorological models. *Mon. Weather Rev.*, 117: 536-549.
- Oudin, L., Andréassian, V.C., Perrin, C., Michel, C., & Le Moine, N. 2008. Spatial proximity, physical similarity, regression and ungauged catchments: a comparison of regionalization approaches based on 913 French catchments. *Water Resources Research*. W03413.
- Oudin, L., Perrin, C., Mathevet, T., Andréassian, V., & Michel, C. 2006. Impact of biased and randomly corrupted inputs on the efficiency and the parameters of watershed models. *Journal of Hydrology (Amsterdam)*, 320, 62–83.

- Parajka, J., Merz, R., & Blöschl, G. 2005. A comparison of regionalization methods for catchment model parameters. *Hydrol. Earth Syst. Sci.*, 9, 157–171.
- Payan, J. L., Perrin, C., Andréassian, V. & Claude, M. 2008. How can man-made water reservoirs be accounted for in a lumped rainfall-runoff model? *Water Resources Research*, 44, 11 p.
- Perrin, C. 2000. Towards an improvement of a lumped rainfall-runoff model through a comparative approach (in french). Ph.D thesis, Université Joseph Fourier, Grenoble.
- Perrin C, Miche C, & Andréassian V. 2003. Improvement of a parsimonious model for streamflow simulation. *Journal of Hydrology* 279(1): 275–289.
- Ponce, V.M. 1989. *Engineering Hydrology. Principles and Practices*. Prentice Hall, 640p.
- Post, D.A.; & Jakeman, A.J. 1996. Relationships between catchment attributes and hydrological response characteristics in small Australian mountain ash catchments. *Hydrological Process*. 10, 877-892.
- Post, D.A.; & Jakeman, A.J. 1999. Predicting the daily streamflow of ungauged catchments in SE Australia by regionalising the parameters of a lumped conceptual rainfall-runoff model. *Ecol. Model.*, 123, 91-104

- Preiestly, C.H.B. & R.J. Taylor. 1972. On the assessment of surface heat flux and evapotranspiration using large-scale parameters. *Mon. weather. Rev.*100:81-92.
- Rajib, M.A. & V. Merwade. 2015. Improving soil moisture accounting and streamflow prediction in SWAT by incorporating a modified time-dependent SCS CN method. *Hydrological Processes*. 10.1002/hyp.10639.
- Rajib, M.A., V. Merwade & Z. Yu. 2016. Multi-objective calibration of a hydrologic model using spatially distributed remotely sensed/in-situ soil moisture. *Journal of Hydrology*, 10.1016/j.jhydrol.2016.02.037.
- Razavi, T. & Coulibaly, P. 2013. Streamflow Prediction in Ungauged Basins: Review of regionalization methods. *Journal Hydrologic Engineering* 18, 958–975.
- Reddy, M.J. & Kumar, D.N. 2006. Optimal reservoir operation using multi-objective evolutionary algorithm. *Water Resources Management* 20 (6), 861–878.
- Reed S, Koren V, Smith M, Zhang Z, Moreda F, & Seo DJ. 2004. Overall distributed model intercomparison project results. *Journal of Hydrology* 298: 27–60.

- Refsgaard, J.C. & Storm, B. 1995. MIKE SHE, in *Computer Models of Watershed Hydrology*, Singh, V.P., Ed., Water Resources Publications, Colorado, USA, p809-846.
- Refsgaard JC. 1997. Parameterisation, calibration and validation of distributed hydrological models. *Journal of Hydrology* 198: 69–97.
- Refsgaard JC, & Knudsen J. 1996. Operational validation and intercomparison of different types of hydrological models. *Water Resources Research* 32(7): 2189–2202.
- Richardson CW. 1981. Stochastic simulation of daily precipitation, temperature, and solar radiation. *Water Resources Research*. 17: 182–190.
- Rientjes, T.H.M.; Perera, B.U.J.; Haile, A.T.; Reggiani, P. & Muthuwatta, L.P. 2011. Regionalisation for lake level simulation – the case of Lake Tana in the Upper Blue Nile, Ethiopia. *Hydrol. Earth Syst. Sci.*, 15, 1167–1183, 2011.
- Rogelj J, Meinshausen M & Knutti R. 2012. Global warming under old and new scenarios using IPCC climate sensitivity range estimates. *Nat. Clim. Change* 2 248–53.
- Salini & Mid-day. 2006. *Environmental Impact Assessment for Beles multipurpose project*. Addis Ababa, Ethiopia: Ethiopia Electric and Power Corporation.

- Salzmann, N; Frei, C; Vidale, PL and Hoelzle, M. 2007. The application of Regional Climate Model output for the simulation of high-mountain permafrost scenarios. *Global Planet Change*, 56 (1–2), pp. 188–202.
- Samaniego, L., Bárdossy, A., & Kumar, R. 2010. Streamflow Prediction in ungauged catchments using copula-based dissimilarity measures. *Water Resources Research*, 46 (2), W02506.
- Samuel, J.; Coulibaly, P. & Metcalfe, R.A. 2011. Estimation of Continuous Streamflow in Ontario Ungauged Basins: Comparison of Regionalization Methods. *Journal of Hydrologic Engineering*, 2011, 16(5): 447-459.
- Santos, C.C., J.P. Nunes, A.T. Monteiro, L. Hein & J.P. Honrado. 2015. Assessing the effects of land cover and future climate conditions on the provision of hydrological services in a medium-sized watershed of Portugal. *Hydrological Processes*. 10.1002/hyp.10621.
- Sefton, C. E. M., & Howart, S. M. 1998. Relationships between dynamic response characteristics and physical descriptors of catchments in England and Wales. *Journal of Hydrology*. 211, 1–16.
- Sellami, H; La Jeunesse, I; Benabdallah, S; Baghdadi, N & Vanclooster, M. 2014. Uncertainty analysis in model parameters regionalization: a case study involving the SWAT model in Mediterranean catchments (Southern France). *Hydrol. Earth Syst. Sci.* p. 2393 - p. 2413. 10.5194/hess-18-2393-2014.

- Semenov M.A., Barrow E.M. 2002. LARS-WG, A Stochastic Weather Generator for Use in Climate Impact Studies, User Manual. [http://www.rothamsted.ac.uk/mas-models/download/LARS-WG Manual](http://www.rothamsted.ac.uk/mas-models/download/LARS-WG%20Manual).
- Setegn, S. G., D. Rayner, A. M. Melesse, B. Dargahi, & R. Srinivasan. 2011. Impact of climate change on the hydroclimatology of Lake Tana Basin, Ethiopia, *Water Resources Research*, 47, W04511.
- Setegn, S. G., R. Srinivasan, A. M. Melesse & Bijan Dargahi. 2009. SWAT model application and prediction uncertainty analysis in the Lake Tana Basin, Ethiopia. *Hydrological Process.* 24, 357–367. doi:10.1002/hyp.7457.
- Sevat E, & Dezetter A. 1991. Selection of calibration objective functions in the context of rainfall–runoff modeling in a Sudanese savannah area. *Hydrological Sciences Journal* 36(4): 307–330.
- Seyoum, W.M., A.M. Milewski & M.C. Durham. 2015. Understanding the relative impacts of natural processes and human activities on the hydrology of the Central Rift Valley Lakes, East Africa. *Hydrological Processes*. 10.1002/hyp.10490.
- Shah SMS, O’Connell PE, & Hosking JRM. 1996. Modelling the effects of spatial variability in rainfall on catchment response, 2, experiments with distributed and lumped models. *Journal of Hydrology* 175: 89–111.

- Shahin M. 1988. Hydrology of the Nile Basin. International Institute for Hydraulic and Environmental Engineering, Elsevier: the Netherlands.
- Shen, C. & Phanikumar, M.S. 2010. A process-based, distributed hydrologic model based on a large-scale method for surface-subsurface coupling. *Advances in Water Resources*, 33(12), 1524–1541. 10.1016/j.advwatres.2010.09.002.
- Singh J, Knapp HV, Arnold JG, & Demissie M. 2005. Hydrologic modelling of the Iroquois River watershed using HSPF and SWAT. *Journal of the American Water Resources Association* 41(2): 361–375.
- Smakhtin VY. 2001. Low flow hydrology: a review. *Journal of Hydrology* 240: 147–186.
- SMEC (Snowy Mountains Engineering Corporation). 2007. Hydrological Study of the Tana–Beles Subbasins, main report. Ministry of Water Resources: Addis Ababa, Ethiopia.
- Smith MB, Seo DJ, Koren VI, Reed SM, Zhang Z, Duan Q, Moreda F, & Cong S. 2004. The distributed model intercomparison project (DMIP): motivation and experiment design. *Journal of Hydrology* 298: 4–26.
- Spear RC, & Hornberger GM. 1980. Eutrophication in Peel Inlet, II, Identification of critical uncertainties via generalised sensitivity analysis. *Water Research* 14: 43–49.

- Srinivas, N. & Deb, K. 1994. Multiobjective optimization using nondominated sorting in genetic algorithms. *Evolutionary Computation*, 2(3), 221- 248.
- Stewart, I.T., D.L. Ficklin, C.A. Carrillo & R. McIntosh. 2015. 21st-century increases in the likelihood of extreme hydrologic conditions for the mountainous basins of the south-western United States. *Journal of Hydrology*. 10.1016/j.jhydrol.2015.07.043.
- Taylor K.E, Stouffer R.J & Meehl G.A. 2012. An overview of Cmp5 and the experiment design B. *Am. Meteorol. Soc.* 93 485–98.
- Teutschbein, C., & Seibert, J. 2010. Regional climate models for hydrological impact studies at the catchment scale: a review of recent modeling strategies. *Geogr. Compass* 4 (7), 834–860.
- Thiessen AH. 1911. Precipitation averages for large areas. *Monthly Weather Review* 39: 1082–1084.
- Tian, F., Y.H. Lu, B.J. Fu, Y.H. Yang, G. Qiu, C. Zang & L. Zhang. 2015. Effects of ecological engineering on water balance under two different vegetation scenarios in the Qilian Mountain, northwestern China. *Journal of Hydrology: Regional Studies*. 10.1016/j.ejrh.2015.11.015.
- Tung C, Hsu S, Liu C, & Li J. 2003. Application of the genetic algorithm for optimizing operation rules of the LiYuTan reservoir in Taiwan. *J Am Water Resour Assoc* 39(3):649–57.

- Uniyal, B., M.K. Jha & A.K. Verma. 2015. Parameter identification and uncertainty analysis for simulating streamflow in a river basin of Eastern India. *Hydrological Processes*. 10.1002/hyp.10446.
- U.S. Army Corps of Engineers. 2002. HEC-HMS Applications Guide, Hydrologic Engineering Center, Davis, CA.
- USBR (US Bureau of Reclamation). 1964. Land and Water Resources of the Blue Nile Basin. Main Report, United States Department of Interior Bureau of Reclamation, Washington, DC. US-ACE. 2003. HEC-HMS. URL.
- Van Griensven A, Meixner T, Grunwald S, Bishop T, Diluzio M, & Srinivasan R. 2006. A global sensitivity analysis tool for the parameters of multi-variable catchment models. *Journal of Hydrology* 324: 10–23.
- Van Vuuren, D.P.; Edmonds, J.; Kainuma, M.; Riahi, K.; Thomson, A.; Hibbard, K.; Hurtt, G.C.; Kram, T.; Krey, V.; Lamarque, J.F.; Masui, T.; Meinshausen, M.; Nakicenovic, N.; Smith, S.J.; & Rose, S.K. 2011. The representative concentration pathways: an overview. *Climatic Change*.109:5–31. doi 10.1007/s10584-011-0148-z.
- Vazquez-Amábile GG, & Engel BA. 2005. Use of SWAT to compute groundwater table depth and streamflow in the Muscatatuck River watershed. *Transactions of the American Society of Agricultural Engineers* 48(3): 991–1003.

- Vrugt, J.A.; Gupta, H.V.; Bouten, W. & Sorooshian, S. 2003. A Shuffled Complex Evolution Metropolis algorithm for optimization and uncertainty assessment of hydrologic model parameters. *Water Resources Research* 39(8): 1201, DOI: 10.1029/2002WR001642.
- Wagener, T.; Sivapalan, M.; Troch, P.; & Woods, R. 2007. Catchment Classification and Hydrologic Similarity, *Geography Compass*, 1, 901-931, doi: 10.1111/j.1749-8198.2007.00039.
- Wale A, Rientjes THM, Gieske ASM, & Getachew HA. 2009. Ungauged catchment contributions to Lake Tana's water balance. *Hydrologic Processes* 23: 3682–3693.
- Wambura, F.J.; Ndomba, P.M.; Kongo, V.; & Tumbo, S.D. 2015. Uncertainty of runoff projections under changing climate in Wami River subbasin. *Journal of Hydrology: Regional Studies*. 10.1016/j.ejrh.2015.05.013.
- Wang, J.; Hong, Y.; Li, L.; Gourley, J.J.; Yilmaz, K.; Khan, S.I.; Policelli, F.S.; Adler, R.F.; Habib, S.; Irwin, D.; Limaye, S.A.; Korme, T. & Okello, L. 2011. The Coupled Routing and Excess Storage (CREST) distributed hydrological model. *Hydrological Sciences Journal*, 56, 84-98.
- Wang, X., Y. Luo, L. Sun & Y. Zhang. 2015. Assessing the effects of precipitation and temperature on hydrological processes in a glacier-dominated catchment. *Hydrological Processes*. 10.1002/hyp.10538.

- Wang, Z.W.; Batelaan, O. and Smedt, F.D. 1997. A distributed model for water and energy transfer between soil, plants and atmosphere (WetSpa). *Phys. Chem. Earth*, Vol. 21, No. 3, pp. 189-193.
- Watson, B.M.; Ghafouri, M. & Selvalingam, S. 2003. Application of SWAT to model the water balance of the Woody Yaloak River catchment, Australia. 2nd International SWAT Conference, Bari Italy. TWRI Tech. Report 266: 94-110.
- Wilby R.L, Dawson C.W, & Barrow EM. 2002. SDSM—a decision support tool for the assessment of regional climate change impacts. *Environ Model Software* 17(2):145–157.
- Wilby R.L, Hay L.E, & Leavesley G.H. 1999. A comparison of downscaled and raw GCM output: implications for climate change scenarios in the San Juan River basin, Colorado. *Journal of Hydrology*, 225 (1–2):67–91.
- Wilby R.L, Whitehead P.G, Wade A.J, Butterfield D, Davis R.J, & Watts G. 2006. Integrated modeling of climate change impacts on water resources and quality in a lowland catchment: River Kennet, UK. *J Hydrol* 330(1–2):204–220.
- World Meteorological Organization (WMO). 2012. Standardized Precipitation Index User Guide, WMO-No. 1990. ISBN 978-92-63-11091-6.

- Xu, C.Y. 1999. From GCMs to river flow: a review of downscaling methods and hydrologic modeling approaches. *Progress in Physical Geography*, 23(2), 229-249.
- Yang, C.C.; Chang, L.C.; Yeh, C.H. & Chen, C.S. 2007. Multiobjective planning of surface water resources by multiobjective genetic algorithm with constrained differential dynamic programming. *Journal of Water Resources Planning and Management – ASCE* 133 (6), 499–508.
- Yapo, P.O.; Gupta, H.V. & Sorooshian, S. 1996. Automatic calibration of conceptual rainfall–runoff models: sensitivity to calibration data. *Journal of Hydrology* 181, 23–48.
- Ye, W., Bates, B.C.; Viney, N.R.; Sivapalan, M. & Jakeman, A.J. 1997. Performance of conceptual rainfall-runoff models in low-yielding ephemeral catchments. *Water Resources Research* 33(1): 153-166.
- Young, A.R. 2006. Streamflow simulation within UK ungauged catchments using a daily rainfall-runoff model. *Journal of Hydrology (Amsterdam)*, 320, 155–172.
- Zhang, L.; Nan, Z.; Yu, W. & Ge, Y. 2015. Modeling land-use and land-cover change and hydrological responses under consistent climate change scenarios in the Heihe River Basin, China. *Journal of Water Resources Management*. 10.1007/s11269-015-1085-9.

- Zhang, X.; Srinivasan, R.; Zhao, K. & Liew, M.V. 2008. Evaluation of global optimization algorithms for parameter calibration of a computationally intensive hydrologic model.
- Zhang, Z.Y.; Koren, V.; Smith, M.; Reed, S. & Wang, D. 2004. Use of next generation weather radar data and basin disaggregation to improve continuous hydrograph simulations. *Journal of Hydrologic Engineering* 9(2): 103–115.
- Zhuang, X.W.; Li, Y.P.; Huang, G.H. & Wang, X.Q. 2015. A hybrid factorial stepwise-cluster analysis method for streamflow simulation - a case study in north-western China. *Hydrological Sciences Journal*. 10.1080/02626667.2015.1125482.
- Zitzler, E.; Deb, K. & Thiele, L. 2000. Comparison of multiobjective evolutionary algorithms: Empirical results. *Evolutionary Computation*, 8(2), 173-195.

## **Appendices**

### **Appendix A. Hydrological Models**

#### **A.1. The Soil and Water Assessment Tool (SWAT)**

The SWAT model is a physically based continuous time-scale model, which operates on a daily time step by using the readily available inputs. The model is computationally efficient and capable of simulating a high level of spatial details by allowing the watershed to be divided into a large number of sub-watersheds. In the hydrologic module of the model, the surface runoff is estimated separately for each subbasin and routed to quantify the total surface runoff for the watershed. Runoff volume is commonly estimated from daily rainfall using modified SCS-CN method. The model needs several data inputs to represent watershed conditions which include: digital elevation model (DEM), land use, soils, and climate data. In SWAT, a watershed is divided into multiple sub-watersheds, which are then further subdivided into unique soil/land-use characteristics called hydrologic response units (HRUs). The water balance of each HRU in SWAT is represented by four storage volumes: snow, soil profile (0-2m), shallow aquifer (typically 2-20m), and deep aquifer (>20m). Flow generation, sediment yield, and non-point-source loadings from each HRU in a sub-

watershed are summed, and the resulting loads are routed through channels, ponds, and reservoirs to the watershed outlet.

Simulation of the hydrology of a watershed in SWAT is separated into two major divisions. The first division is the land phase of the hydrological cycle, which controls the amount of water, sediment, nutrient and pesticide loadings to the main channel in each subbasin. The land phase of the hydrological cycle is simulated by SWAT based on the water balance equation.

$$SW_t = SW_0 + \sum_{i=1}^t (R_{day} - Q_{surf} - E_a - w_{seep} - Q_{gw}) \quad (A.1)$$

where  $SW_t$  is the final water content (mm H<sub>2</sub>O),  $SW_0$  is the initial soil water content on day  $i$  (mm H<sub>2</sub>O),  $t$  is time (days),  $R_{day}$  is the amount of precipitation on day  $i$  (mm H<sub>2</sub>O),  $Q_{surf}$  is the amount of surface runoff on day  $i$  (mm H<sub>2</sub>O),  $E_a$  is the amount of evapotranspiration on day  $i$  (mm H<sub>2</sub>O),  $W_{seep}$  is the amount of water entering the vadose zone from the Soil profile on day  $i$ ,  $Q_{gw}$  is the amount of groundwater flow on day  $i$  (mm H<sub>2</sub>O).

The second division is the water or routing phase of the hydrological cycle which is the movement of water, nutrients, sediment and pesticides through the channel network of the watershed into the outlet. SWAT incorporated three methods to estimate potential evapotranspiration (PET): the Penman-Monteith method (Monteith, 1965), the Priestly-Taylor method (Priestly and Taylor, 1972) and the Hargreaves method (Hargreaves et al.,

1985). The Penman-Monteith method requires solar radiation, air temperature, relative humidity, and wind speed. The Priestley-Taylor method requires solar radiation, air temperature, and relative humidity. The Hargreaves method requires air temperature only.

Surface runoff occurs whenever the rate of water application to the ground surface exceeds the rate of infiltration. SWAT provides two methods for estimating surface runoff: the SCS curve number procedure (SCS, 1972) and the Green & Ampt infiltration method (1911). For this study, SCS curve number method has been selected based on the data availability. The SCS curve number equation is (SCS, 1972).

$$Q_{surf} = \frac{(R_{day} - I_a)^2}{(R_{day} - I_a + S)} \quad (A.2)$$

where  $Q_{surf}$  is the accumulated runoff or rainfall excess (mm H<sub>2</sub>O),  $R_{day}$  is the rainfall depth for the day (mm H<sub>2</sub>O),  $S$  is the retention parameter (mm H<sub>2</sub>O), &  $I_a$  is the initial abstractions which includes surface storage, interception, and infiltration prior to runoff (mm H<sub>2</sub>O).

The retention parameter varies spatially due to changes in soils, land use, management and slope and temporally due to changes in soil water content. The retention parameter is defined as:

$$S = 25.49 \left( \frac{1000}{CN} - 10 \right) \quad (A.3)$$

where  $CN$  is the curve number for the day.

The initial abstraction,  $I_a$  is commonly approximated as  $0.2S$  and Eqn. (A.2) becomes,

$$Q_{surf} = \frac{(R_{day} - 0.2S)^2}{(R_{day} + 0.8S)} \quad (A.4)$$

The runoff will only occur when  $R_{day} > I_a$ . The SCS curve number is a function of the soil's permeability, land use, and antecedent soil water conditions. SCS defines three antecedent moisture conditions: i) dry, ii) average moisture, and iii) wet. The moisture condition (i) curve number is the lowest value the daily curve number can assume in dry conditions. The curve number for moisture conditions (i) and (iii) can be calculated with the equation:

$$CN_1 = CN_2 - \frac{20(100 - CN_2)}{(100 - CN_2 + \exp[2.533 - 0.0636(100 - CN_2)])} \quad (A.5)$$

$$CN_3 = CN_2 \exp[0.00673(100 - CN_2)] \quad (A.6)$$

where  $CN1$  is the moisture condition (i) curve number,  $CN2$  is the moisture condition (ii) curve number, and  $CN3$  is the moisture condition (iii) curve number.

In SWAT, the retention parameter can be calculated by allowing the retention parameter to vary with the soil water content profile or by allowing the retention parameter to vary with accumulated plant evapotranspiration.

The following equation can be used to calculate the retention parameter when it varies with the soil profile water content:

$$S = S_{max} \left( 1 - \frac{SW}{[SW + \exp(w_1 - w_2 SW)]} \right) \quad (A.7)$$

where  $S$  is the retention parameter for a given day (mm),  $S_{max}$  is the maximum value the retention parameter can achieve on any given day (mm),  $SW$  is the soil water content of the entire profile excluding the amount of water held in profile at wilting point (mm H<sub>2</sub>O), and  $w_1$  and  $w_2$  are shape coefficients.

The following equation can be used to calculate the retention parameter when it varies with plant evapotranspiration:

$$S = S_{prev} + E_0 * \exp\left(\frac{-w_c S_{prev}}{S_{max}}\right) - R_{day} + Q_{surf} \quad (A.8)$$

where  $S$  is the retention parameter for a given day (mm),  $S_{prev}$  is the retention parameter for the previous day (mm),  $E_0$  is the potential evapotranspiration for the day (mm/day),  $w_c$  is the weighting coefficient used to calculate the retention coefficient for daily curve number,  $Q_{surf}$  is the surface runoff (mm H<sub>2</sub>O).

The initial value of the retention parameter can be defined as  $S = 0.9 * S_{max}$ .

The retention parameter can be modified using the following equation when the top soil layer is frozen:

$$S_{frz} = S_{max} [1 - \exp(-0.000862 * S)] \quad (A.9)$$

where  $S_{frz}$  is the retention parameter adjusted for frozen conditions (mm).

The curve number (CN) value adjusted for moisture content can be calculated as follows:

$$CN = \frac{25400}{(S + 254)} \quad (A.10)$$

The curve number can be adjusted based on the slope (Williams, 1995) as follows:

$$CN_{2s} = \left( \frac{CN_3 - CN_2}{3} \right) [1 - 2 * \exp(-13.86 * slope)] + CN_2 \quad (A.11)$$

where  $CN_{2s}$  is the moisture condition (ii) curve number adjusted for slope,  $CN_2$  and  $CN_3$  are the moisture condition (ii) & (iii) curve number for the default 5% slope, respectively, and the slope is the average fraction slope of the subbasin. In SWAT model, the adjustment of curve number based on a slope can be done prior to entering the curve numbers in the management input file.

SWAT uses a modified rational method to calculate the peak runoff rate.

The rational formula to compute the peak runoff rate is given by:

$$q_{peak} = \frac{C * i * A}{3.6} \quad (A.12)$$

where  $q_{peak}$  is the peak runoff rate ( $m^3/s$ ),  $C$  is the runoff coefficient,  $i$  is the rainfall intensity ( $mm/hr$ ),  $A$  is the subbasin area ( $km^2$ ), and 3.6 is a unit conversion factor.

This equation is based on the assumption that if a rainfall intensity  $i$  begins at time  $t = 0$  and continues indefinitely, the rate of runoff will increase until the time of concentration,  $t = t_{conc}$ , when the entire subbasin area is contributing to flow at the outlet. The time of concentration is calculated by summing the overland flow time (the time it takes for flow from the remotest point in the subbasin to reach the channel) and the channel flow time (the time it takes for flow in the upstream channels to reach the outlet):

$$t_{conc} = t_{ov} + t_{ch} \quad (A.13)$$

where  $t_{conc}$  is the time of concentration for a subbasin (hr),  $t_{ov}$  is the time of concentration for the overland flow (hr), and  $t_{ch}$  is the time of concentration for channel flow (hr).

The time of concentration for overland flow can be computed by;

$$t_{ov} = \frac{L_{slope}}{3600v_{ov}} \quad (A.14)$$

where  $L_{slope}$  is the subbasin slope length (m),  $v_{ov}$  is the overland flow velocity (m/s) and 3600 is a unit conversion factor.

The overland flow velocity can be computed by using the Manning's equation as given below:

$$v_{ov} = \frac{q_{ov}^{0.4} slope^{0.3}}{n^{0.6}} \quad (A.15)$$

where  $q_{ov}$  is the average overland flow rate ( $m^3/s$ ), the slope is the average slope of the subbasin (m/m), and  $n$  is the Manning's roughness coefficients for the subbasin.

The channel flow time of concentration can be computed by using the equation given below:

$$t_{ch} = \frac{L_c}{3.6v_c} \quad (A.16)$$

where  $L_c$  is the average flow channel length for the subbasin (km),  $v_c$  is the average velocity (m/s), and 3.6 is a unit conversion factor.

The average flow velocity ( $v_c$ ) can be computed by using the Manning's equation. The average channel flow length can be computed as follows:

$$L_c = \sqrt{L * L_{con}} \quad (A.17)$$

where  $L$  is the channel length from the most remot point to the subbasin outlet (km), and  $L_{con}$  is the distance along the channel to the subbasin centroid (km)

The runoff coefficient ( $C$ ) can be calculated using the following equation:

$$C = \frac{Q_{surf}}{R_{day}} \quad (A.18)$$

where  $Q_{surf}$  is the surface runoff (mm H<sub>2</sub>O) and  $R_{day}$  is the rainfall for the day (mm H<sub>2</sub>O)

The rainfall intensity can be computed using the equation:

$$i = \frac{R_{tc}}{t_{conc}} \quad (A.19)$$

where  $i$  is the rainfall intensity (mm/hr), and  $R_{tc}$  is the amount of rain falling during the time of concentration (mm H<sub>2</sub>O).

The amount of rain falling during the time of concentration is proportional to the amount of rain falling during the 24-hr period.

$$R_{tc} = \alpha_{tc} * R_{day} \quad (A.20)$$

where  $R_{tc}$  is the amount of rain falling during the time of concentration (mm H<sub>2</sub>O),  $\alpha_{tc}$  is the fraction of the daily rainfall that occurs during the time of concentration, and  $R_{day}$  is the amount of rain falling during the day (mm H<sub>2</sub>O).

SWAT estimates the fraction of rain falling in the time of concentration ( $\alpha_{tc}$ ) as a function of the fraction of daily rain falling in the half-hour of highest intensity rainfall ( $\alpha_{0.5}$ ).

$$\alpha_{tc} = 1 - \exp[2 * t_{conc} * \ln(1 - \alpha_{0.5})] \quad (A.21)$$

Now, the modified rational formula that used to estimate the peak runoff rate can be given by:

$$q_{peak} = \frac{\alpha_{tc} * Q_{surf} * Area}{3.6 * t_{conc}} \quad (A.22)$$

In the large subbasin with a time of concentration greater than one day, only a portion of surface runoff will reach the main channel on the day it is generated. SWAT incorporates a surface runoff storage to lag a portion of the surface runoff release to the main channel. The amount of surface runoff release to the main channel can be computed by using:

$$Q_{surf} = (Q'_{surf} + Q_{stor,i-1}) \left( 1 - \exp \left[ \frac{-surlag}{t_{conc}} \right] \right) \quad (A.23)$$

where  $Q_{surf}$  is the amount of surface runoff discharged to the main channel (mm H<sub>2</sub>O),  $Q'_{surf}$  is the amount of surface runoff generated in the subbasin (mm H<sub>2</sub>O),  $Q_{stor,i-1}$  is the surface runoff stored or lagged from the previous day (mm H<sub>2</sub>O),  $surlag$  is the surface runoff lag coefficient, and  $t_{conc}$  is the time of concentration for the subbasin (hrs).

The routing phase is the second division of hydrological cycle which can be defined as the movement of water, sediments, etc. through the channel network of the watershed to the outlet. Water is routed through the channel network using the variable storage routing method or the Muskingum River routing method. For a given reach segment, storage routing is based on the continuity equation:

$$\Delta V_{stored} = V_{in} - V_{out} \quad (A.24)$$

where  $V_{in}$  is the volume of inflow during the time step (m<sup>3</sup> water),  $V_{out}$  is the volume of outflow during the time step (m<sup>3</sup> water), and  $\Delta V_{storage}$  is the change in volume of storage during the time step (m<sup>3</sup> water).

This equation can also be detailed as follows:

$$V_{storage,2} - V_{stored,1} = \Delta t \left( \frac{q_{in,1} + q_{in,2}}{2} \right) - \Delta t \left( \frac{q_{out,1} + q_{out,2}}{2} \right) \quad (A.25)$$

where  $\Delta t$  is the length of the time step (s),  $q_{in,1}$  is the inflow rate at the beginning of the time step ( $\text{m}^3/\text{s}$ ),  $q_{in,2}$  is the inflow rate at the end of the time step ( $\text{m}^3/\text{s}$ ),  $q_{out,1}$  is the outflow rate at the beginning of the time step ( $\text{m}^3/\text{s}$ ),  $q_{out,2}$  is the outflow rate at the end of the time step ( $\text{m}^3/\text{s}$ ),  $V_{storage,1}$  is the storage volume at the beginning of the time step ( $\text{m}^3$  water), and  $V_{storage,2}$  is the storage volume at the end of the time step ( $\text{m}^3$  water).

Travel time is computed by dividing the volume of water in the channel by the flow rate.

$$TT = \frac{V_{storage}}{q_{out}} = \frac{V_{storage,1}}{q_{out,1}} = \frac{V_{storage,2}}{q_{out,2}} \quad (\text{A.26})$$

where  $TT$  is the travel time (s),  $V_{storage}$  is the storage volume ( $\text{m}^3$  water), and  $q_{out}$  is the discharge rate ( $\text{m}^3/\text{s}$ ).

Groundwater balance in SWAT model is calculated by assuming two layers of aquifers. SWAT partitions groundwater into a shallow, unconfined aquifer and a deep-confined aquifer and it simulates two aquifers in each subbasin. The shallow aquifer is an unconfined aquifer that contributes to flow in the main channel or reach of the subbasin. The deep aquifer is a confined aquifer. Water that enters the deep aquifer is assumed to contribute to stream flow somewhere outside of the watershed (Arnold et al., 1993). The water balance for a shallow aquifer in SWAT is calculated with:

$$aq_{sh,i} = aq_{sh,i-1} + w_{rchrg} - Q_{gw} - w_{deep} - w_{pump,sh} \quad (A.27)$$

where  $aq_{sh,i}$  is the amount of water stored in the shallow aquifer on day  $i$  (mm),  $aq_{sh,i-1}$  is the amount of water stored in the shallow aquifer on day  $i-1$  (mm),  $w_{rchrg}$  is the amount of recharge entering the aquifer on day  $i$  (mm),  $Q_{gw}$  is the groundwater flow, or base flow, into the main channel on day  $i$  (mm),  $w_{revap}$  is the amount of water moving into the soil zone in response to water deficiencies on day  $i$  (mm),  $w_{deep}$  is the amount of water percolating from the shallow aquifer into the deep aquifer on day  $i$  (mm), and  $w_{pump,sh}$  is the amount of water removed from the shallow aquifer by pumping on day  $i$  (mm).

The water balance for the deep aquifer is:

$$aq_{dp,i} = aq_{dp,i-1} + w_{deep} - w_{pump,dp} \quad (A.28)$$

where  $aq_{dp,i}$  is the amount of water stored in the deep aquifer on day  $i$  (mm),  $aq_{dp,i-1}$  is the amount of water stored in the deep aquifer on day  $i-1$  (mm),  $w_{deep}$  is the amount of water percolating from the shallow aquifer into the deep aquifer on day  $i$  (mm), and  $w_{pump,dp}$  is the amount of water removed from the deep aquifer by pumping on day  $i$  (mm).

## A.2. The IHACRES Model

IHACRES is an acronym for "Identification of Unit Hydrographs And Component flow from Rainfall, Evaporation and Streamflow data." IH is also an acronym for the Institute of Hydrology (now the Centre for Ecology and Hydrology, Wallingford, UK) and CRES is an acronym of Centre for Resource and Environmental Studies, Australian National University. The original IHACRES model is described in a paper by authors from these two institutions (Jakeman *et al.*, 1990). The power law relationship between the soil moisture index and the effective rainfall was applied by the study Ye *et al.* (1997), and Evans and Jakeman (1998) revised it using the Catchment Moisture Deficit (CMD) concept.

IHACRES-CMD requires three sets of time series data. These are observed rainfall in mm, temperature (daily maximum) in degrees Celsius or potential evapotranspiration (PET) in mm, and observed streamflow for calibration. IHACRES-CMD is a continuous rainfall-runoff model used to generate estimates of runoff from rainfall and temperature (or PET) data. Each time step the CMD is calculated as:

$$M[t] = M[t - 1] - p[t] + E[t] + U[t] \quad (\text{A.29})$$

where  $t$  is the time step,  $M$  is the CMD,  $P$  is rainfall,  $E$  is actual evapotranspiration (ET),  $U$  is drainage (effective rainfall). Units are millimeters per time step. The minimum value of  $M$  is 0, which means that

the catchment is fully saturated, while a value greater than 0 indicates that there is a moisture deficit.

The effective rainfall (drainage) is assumed to be an instantaneous, linear function of the CMD given by:

$$\frac{dU}{dP} = 1 - \min\left(1, \frac{M}{d}\right) \quad (\text{A.30})$$

where  $d$  is a flow threshold parameter. If the CMD is greater than the threshold, no flow is produced.

The resulting equations for  $M_f$  is given by:

$$M_f = \begin{cases} M_{t-1} \exp\left(-\frac{P_t}{d}\right), & \text{if } M_{t-1} < d \\ d \exp\left[-\left(P_t - \frac{(M_{t-1} - d)}{d}\right)\right], & \text{if } d \leq M_{t-1} < d + P_t \\ M_{t-1} - P_t, & \text{if } M_{t-1} \geq d + P_t \end{cases} \quad (\text{A.31})$$

where  $d$   $M_{t-1}$  is the CMD value for the previous time step, and  $M_f$  is an interim value of CMD, which is the value before evapotranspiration loss is accounted.

Effective rainfall is given by:

$$U_t = P_t - M_{t-1} + M_f \quad (\text{A.32})$$

The actual evapotranspiration is calculated as follows:

$$E[t] = eT[t] \exp\left(2\left(1 - \frac{M_f[t]}{g}\right)\right) \quad (\text{A.33})$$

where  $T$  is the temperature,  $M_f$  is the value of the CMD before taking into account ET losses, and  $e$  is a temperature to PET conversion factor.

If PET data is used as input data,  $e$  should be fixed as 1 (Case for this study). The parameter  $g$  represents the value of the CMD above which the ET rate will begin to decline due to insufficient water availability for plant transpiration and it is given by:

$$g = fd \quad (\text{A.34})$$

where  $f$  is a parameter represents the plant stress threshold as a fraction of the flow threshold,  $d$ . It controls the amount of actual evapotranspiration (large  $f$  value indicates deeper roots of plant and more actual evapotranspiration) and is related to the drying of the catchment.

Effective rainfall is routed through two parallel unit hydrograph storages to translate and attenuate the effective rainfall into Streamflow. In Figure 4, the top storage represents quick flow while the bottom storage represents the slow flow. The sum of the slow and quick unit hydrographs gives the total Streamflow. The linear unit hydrograph module has three to five parameters depending on the number of stores. The configuration of two stores is given as follows:

$$Q_t = Q_t^q + Q_t^s \quad (\text{A.35})$$

$$Q_t^q = -\alpha_q Q_{t-1}^q + \beta_q U_t \quad (\text{A.36})$$

$$Q_t^s = -\alpha_s Q_{t-1}^s + \beta_s U_t \quad (\text{A.37})$$

where  $Q$  is the discharge,  $Q^q$  is quick flow,  $Q^s$  is slow flow,  $\alpha_q$  and  $\alpha_s$  are parameters for the recession rate of quick and slow flow, respectively, and  $\beta_q$  and  $\beta_s$  are parameters for the peak response of quick and slow flow, respectively.

The parameters for the quick and slow flows stores can be expressed in terms of time constants, and relative volumes of quick and slow flow as follows:

$$\tau_q = \frac{-\Delta}{\ln(-\alpha_q)} \quad (\text{A.38})$$

$$\tau_s = \frac{-\Delta}{\ln(-\alpha_s)} \quad (\text{A.39})$$

$$v_q = 1 - v_s = \frac{\beta_q}{1 + \alpha_q} = 1 - \frac{\beta_s}{1 + \alpha_s} \quad (\text{A.40})$$

where  $\tau_q$  and  $\tau_s$  are the recession time constants for quick and slow flows, respectively,  $v_q$  and  $v_s$  is the proportion of quick and slow flow from the total flow, respectively, and  $\Delta$  is the time step. The  $v_q$  value is calculated using  $v_s$ , hence a two linear storage modules have three parameters.

### **A.3. The GR4J Model**

The GR4J model is a rainfall–runoff model that is based on four free parameters: X1, the maximum capacity of the production store (mm); X2, the groundwater exchange coefficient (mm); X3, the maximum capacity of the routing store (mm); and X4, the time peak ordinate of hydrograph unit UH1 (day). The production store (X1) is storage at the surface of the soil that holds rainfall. Evapotranspiration and percolation occur in this store. The storage capacity depends on the types of soil in the river basin. Low porosity in the soil can increase the size of the production store. The groundwater exchange coefficient (X2) is a function of groundwater exchange, which influences the routing store. When X2 has a negative value, water infiltrates to the depth of the aquifer; when it has a positive value, water exits the aquifer for storage. Routing Storage (X3) is the amount of water that can be stored in soil porosity. The value of X3 depends upon the type and the humidity of the soil. The time peak (X4) is the time when the ordinate peak of the flood hydrograph is created during GR4J modeling. The ordinate of this hydrograph is generated based on runoff, where 90% of the flow is a slow flow that infiltrates into the ground, and 10% of the flow is a fast flow along the soil surface. The mathematical details provided below follow the presentation of the model made by Perrin *et al.* (2003).

- **Determination of net rainfall ( $P_n$ ) and potential evapotranspiration ( $E$ )**

The first operation is the subtraction of  $E$  from  $P$  to determine either a net rainfall  $P_n$  or a net evapotranspiration capacity  $E_n$ . In GR4J, this operation is computed as if there were an interception storage of zero capacity.  $P_n$  and  $E_n$  are computed with the following equations:

$$(P \geq E) \text{ then } (P_n = P - E) \text{ and } (E_n = 0) \quad (\text{A.41})$$

otherwise

$$(P_n = 0) \text{ and } (E_n = E - P) \quad (\text{A.42})$$

- **Production store**

This store can be considered as a soil moisture accounting (SMA) store. In case  $P_n$  is not zero, a part  $P_s$  of  $P_n$  fills the production store. It is determined as a function of the level  $S$  in the store as follows:

$$P_s = \frac{x_1 \left( 1 - \left( \frac{S}{x_1} \right)^2 \right) \tanh \left( \frac{P_n}{x_1} \right)}{1 + \frac{S}{x_1} \tanh \left( \frac{P_n}{x_1} \right)} \quad (\text{A.43})$$

where  $X_l$  (mm) is the maximum capacity of the production store. In the case where  $E_n$  is not zero, the evaporation from the store ( $E_s$ ) is calculated using the level  $S$  in the store as follows:

$$E_s = \frac{S \left(2 - \frac{S}{x_1}\right) \tanh\left(\frac{E_n}{x_1}\right)}{1 + \left(1 - \frac{S}{x_1}\right) \tanh\left(\frac{E_n}{x_1}\right)} \quad (\text{A.44})$$

The level  $S$  in the production store is then updated with:

$$S = S - E_s + P_s \quad (\text{A.45})$$

Note that  $S$  can never exceed  $X_l$ .

A percolation leakage  $Perc$  from the production store is then calculated as a power function of the reservoir content:

$$Perc = S \left\{ 1 - \left[ 1 + \left( \frac{4S}{9x_1} \right)^4 \right]^{-1/4} \right\} \quad (\text{A.46})$$

$Perc$  is always lower than  $S$ . the percolation does not contribute much to the stream flow and is interesting mainly for low flow simulation. The reservoir content becomes:

$$S = S - Perc \quad (\text{A.47})$$

#### - *Linear routing with unit hydrographs*

The total quantity  $P_r$  of water that reaches the routing functions is given by:

$$P_r = Perc + (P_n - P_s) \quad (\text{A.48})$$

$P_r$  is divided into two flow components: 90 % of  $P_r$  is routed by a unit hydrograph  $UH1$  and then a non-linear routing store, and the remaining 10% of  $P_r$  is routed by a single unit hydrograph  $UH2$ . Both unit hydrographs

( $UH1$ , and  $UH2$ ) depend on the same time parameter  $X_4$  expressed in days. However,  $UH1$  has a time base of  $X_4$  days whereas  $UH2$  has a time base of  $2X_4$  days.  $X_4$  can take real values and is greater than 0.5 days. In their discrete form, unit hydrographs  $UH1$  and  $UH2$  have  $n$  and  $m$  ordinates, respectively, where  $n$  and  $m$  are the smallest integers exceeding  $X_4$  and  $2X_4$ , respectively. This means that the water is staggered into  $n$  unit hydrograph inputs for  $UH1$  and  $m$  inputs for  $UH2$ . The ordinates of both unit hydrographs are derived from the corresponding S-curves (cumulative proportion of the input with time) denoted by  $SH1$  and  $SH2$ , respectively.  $SH1$  is defined along time  $t$  by:

$$\text{For } t \leq 0, SH1(t) = 0$$

$$\text{For } 0 < t < x_4, SH1(t) = \left(\frac{t}{x_4}\right)^{5/2}$$

$$\text{For } t \geq x_4, SH1(t) = 1$$

$SH2$  is similarly defined by:

$$\text{For } t \leq 0, SH2(t) = 0$$

$$\text{For } 0 < t < x_4, SH2(t) = \frac{1}{2} \left(\frac{t}{x_4}\right)^{5/2}$$

$$\text{For } x_4 < t < 2x_4, SH2(t) = 1 - \frac{1}{2} \left(2 - \frac{t}{x_4}\right)^{5/2}$$

$$\text{For } t \geq 2x_4, SH2(t) = 1$$

$UH1$  and  $UH2$  ordinates are then calculated by:

$$UH1(j) = SH1(j) - SH1(j - 1) \tag{A.49}$$

$$UH2(j) = SH2(j) - SH2(j - 1) \quad (A.50)$$

where  $j$  is an integer. If  $0.5 \leq X4 \leq 1$ ,  $UH1$  has a single ordinate equal to one and  $UH2$  has only two ordinates.

At each time-step, the outputs  $Q_0$  and  $Q_1$  of the two unit hydrographs correspond to the discrete convolution products are given by:

$$Q_1(k) = 0.1 \sum_{j=1}^m UH2(j) * Pr(k - j + 1) \quad (A.51)$$

$$Q_0(k) = 0.9 \sum_{j=1}^1 UH1(j) * Pr(k - j + 1)$$

- *Catchment groundwater exchange*

A groundwater exchange term  $F$  that acts on both flow components is then calculated as:

$$F = x_2 \left( \frac{R}{x_3} \right)^{7/2} \quad (A.52)$$

where  $R$  is the level in the routing store,  $X3$  its reference capacity and  $X2$  the water exchange coefficient.  $X2$  can be either positive in case of water imports, negative for water exports or zero when there is no water exchange. The higher the level in the routing store, the larger the exchange.

- *Nonlinear routing store*

The level in the nonlinear routing store is updated as follows:

$$R = \max(0; R + Q_9 + F) \quad (\text{A.53})$$

The outflow  $Q_r$  of the nonlinear routing store is calculated as:

$$Q_r = R \left\{ 1 - \left[ 1 + \left( \frac{R}{x_3} \right)^4 \right]^{-1/4} \right\} \quad (\text{A.54})$$

The level in the nonlinear routing store becomes:

$$R = R - Q_r \quad (\text{A.55})$$

- *Total streamflow*

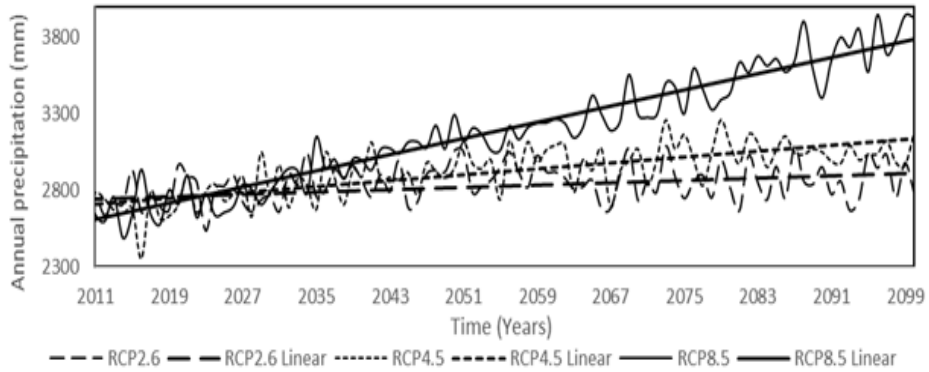
The outflow  $Q_1$  of UH2 is subject to the same water exchange F to give the flow component  $Q_d$  as follows:

$$Q_d = \max(0; Q_1 + F) \quad (\text{A.56})$$

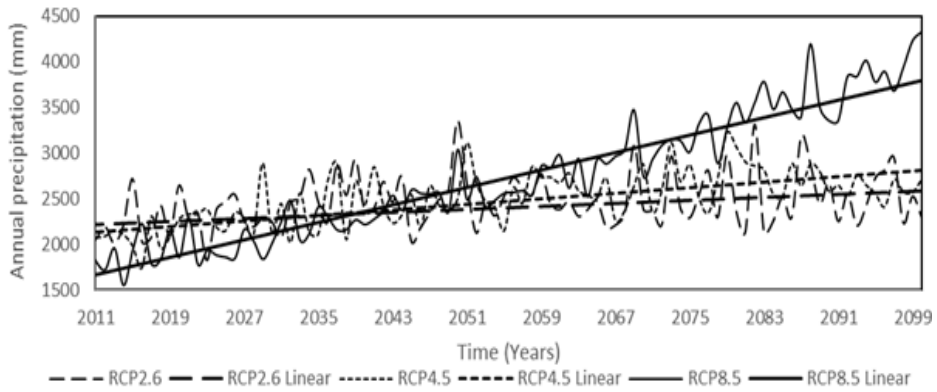
Total outflow Q is finally obtained by:

$$Q = Q_r + Q_d \quad (\text{A.57})$$

## Appendix B. List of Figures

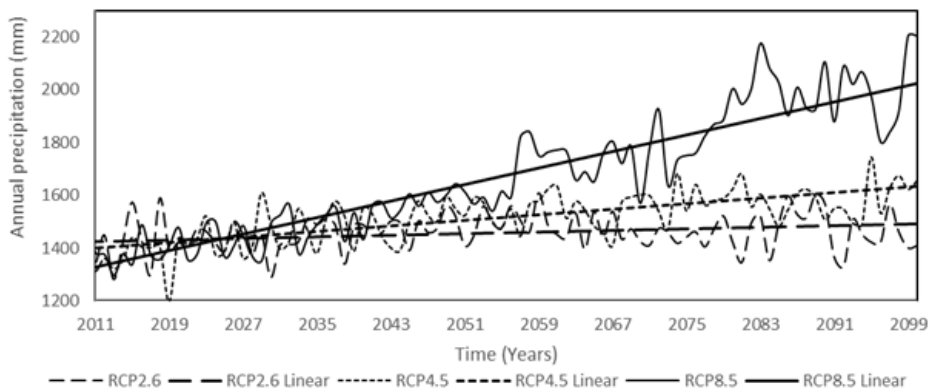


a) Time-domain based bias-corrected precipitation in Enjibara

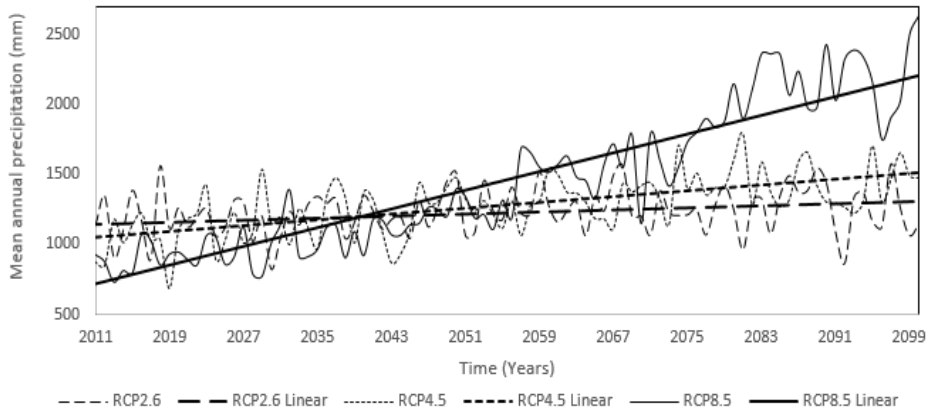


b) Quantile-domain based bias-corrected precipitation in Enjibara

Figure B.1. Pattern of future annual precipitation in Enjibara

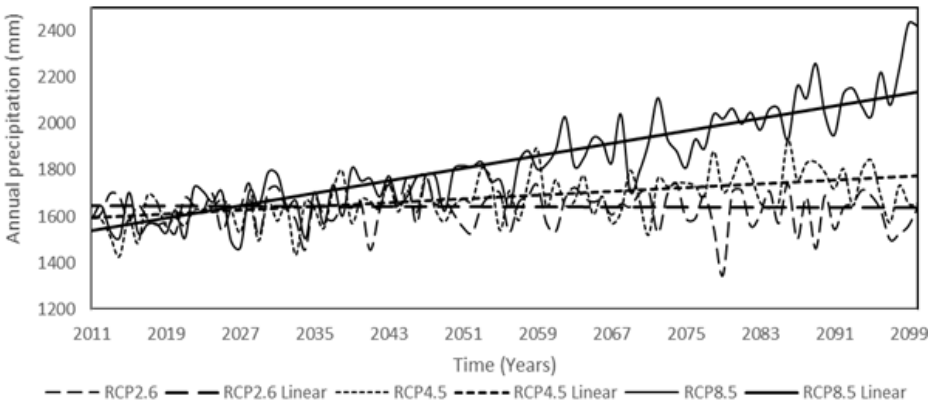


a) Time-domain based bias-corrected precipitation in Gonder

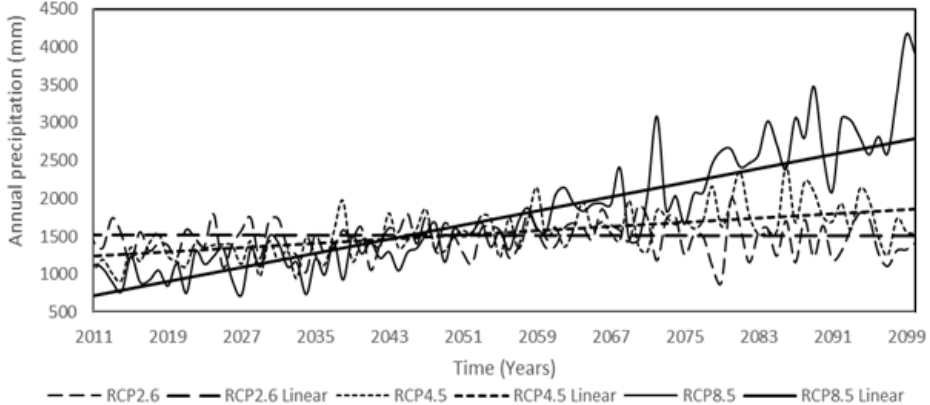


b) Quantile-domain based bias-corrected precipitation in Gonder

Figure B.2. Pattern of future annual precipitation in Gonder



a) Time-domain based bias-corrected precipitation in Woreta



b) Quantile-domain based bias-corrected precipitation in Woreta

Figure B.3. Pattern of future annual precipitation in Woreta

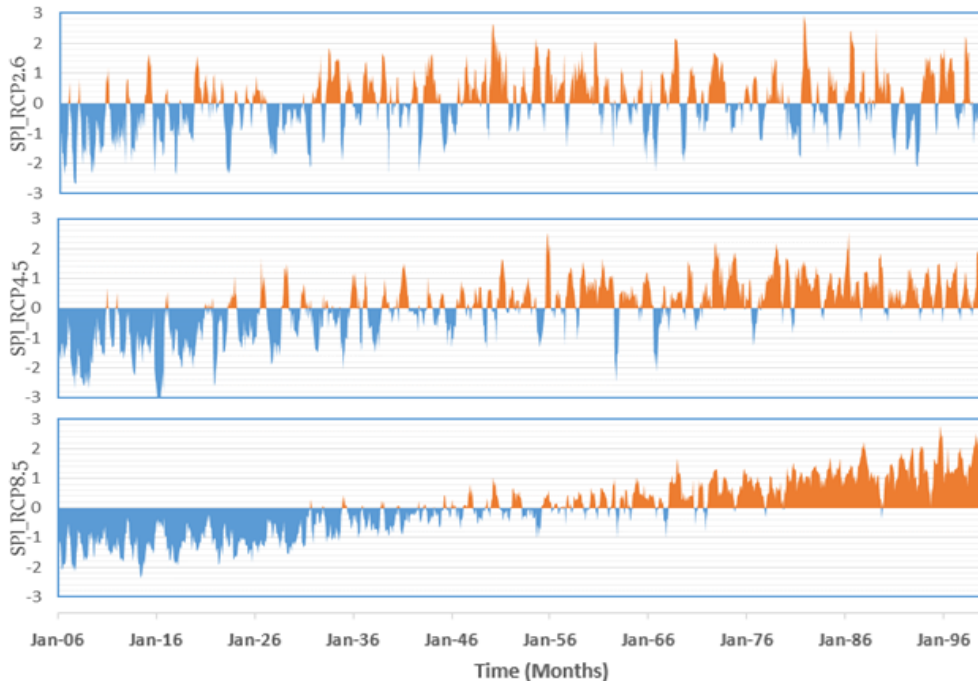


Figure B.4. Time series plot of 6-month standard precipitation index in Enjibara

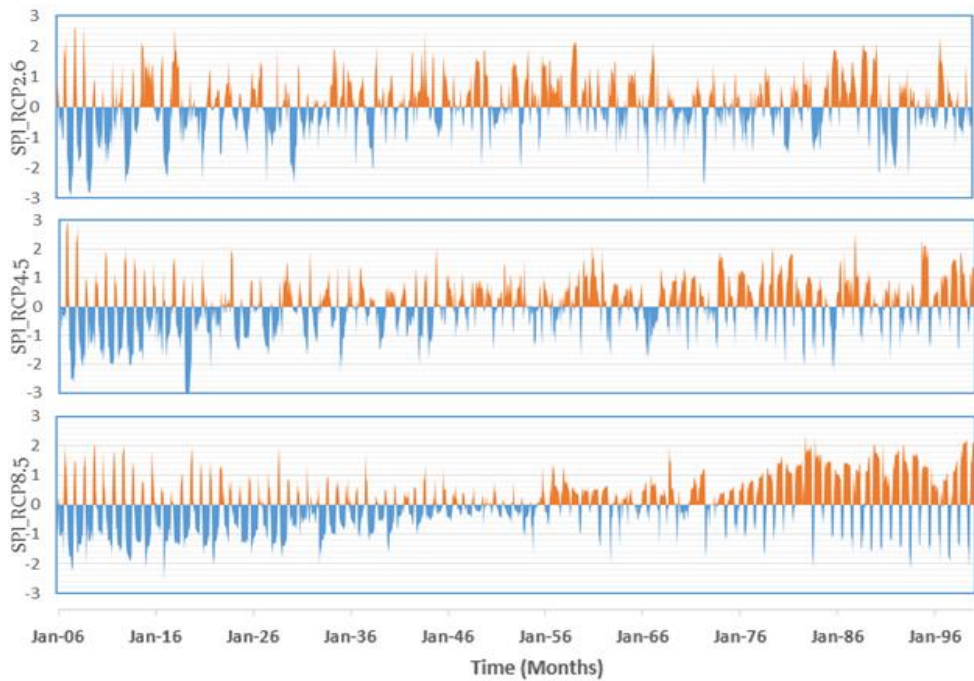


Figure B.5. Time series plot of 6-month standard precipitation index in Gonder

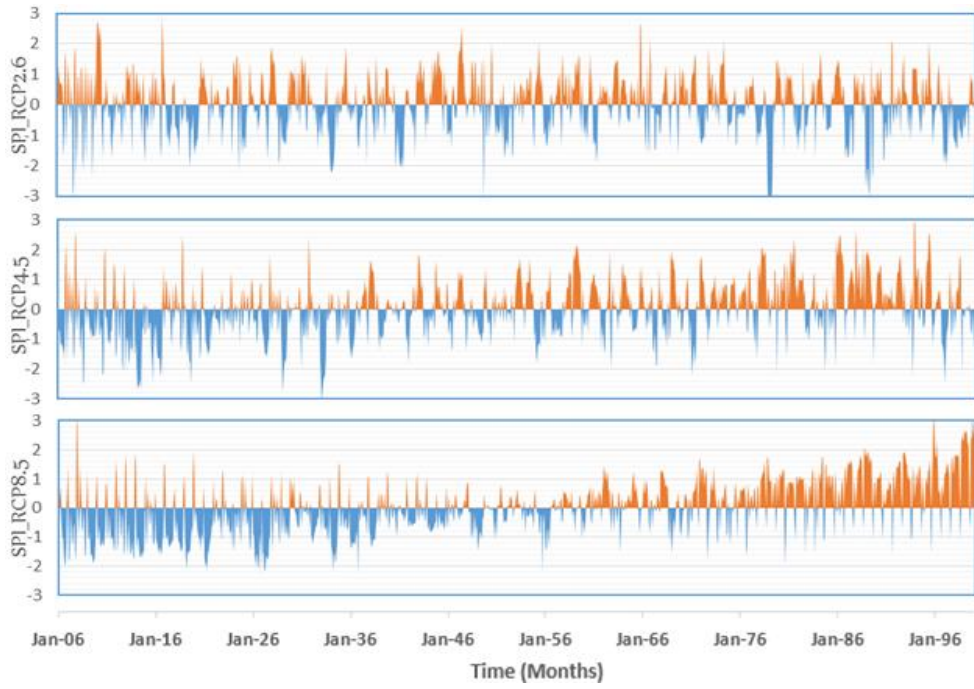


Figure B.6. Time series plot of 6-month standard precipitation index in Woreta

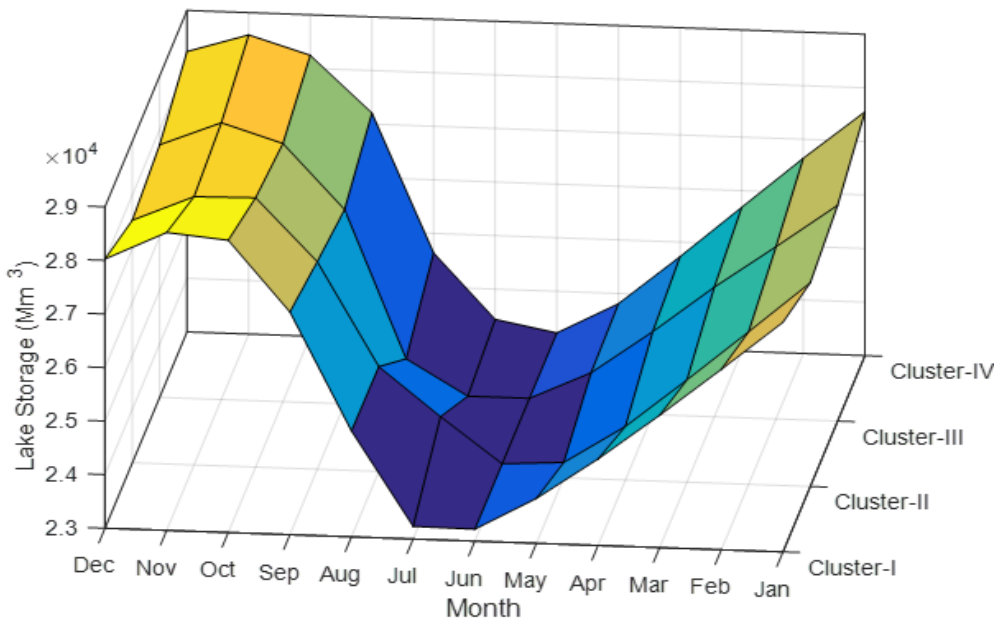


Figure B.7. Monthly storages of the Lake Tana for the four baseline inflow scenarios

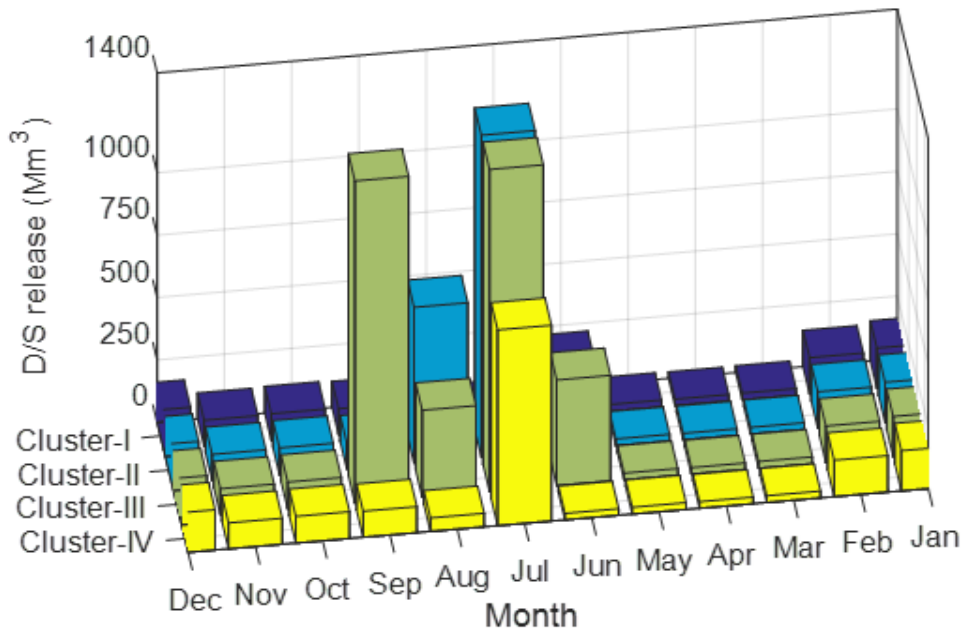


Figure B.8. Monthly downstream release from the Lake Tana for all baseline inflow scenarios

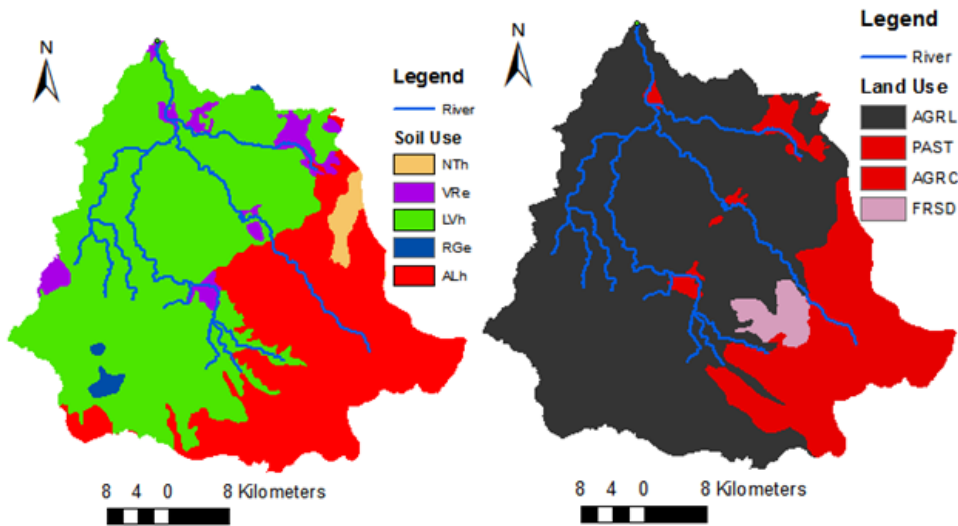


Figure B.9. Soil and land use map of the Gilgelabay reservoir catchment

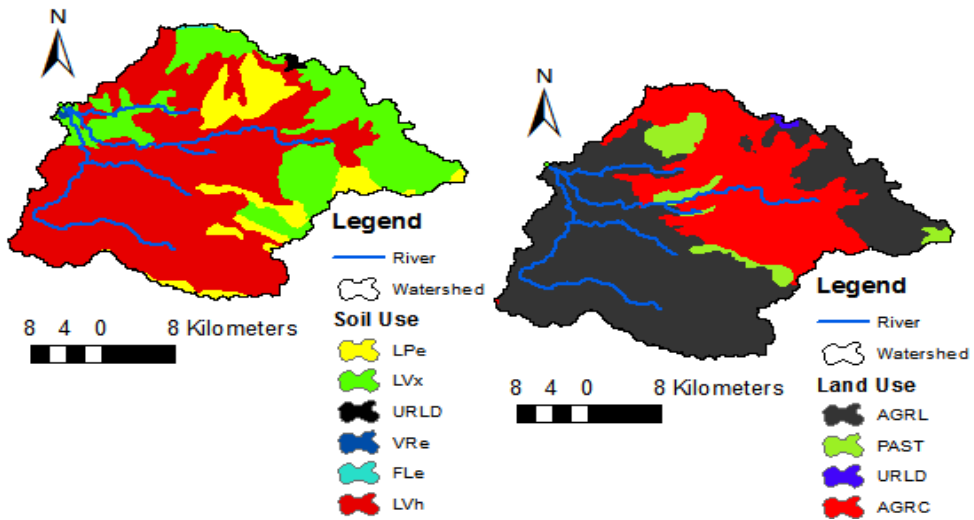


Figure B.10. Soil and land use map of the Gummera reservoir catchment

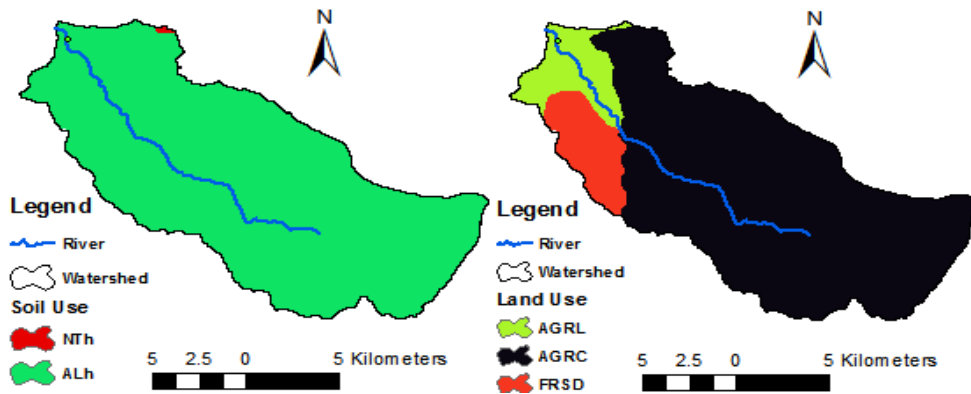


Figure B.11. Soil and land use map of the Jemma reservoir catchment

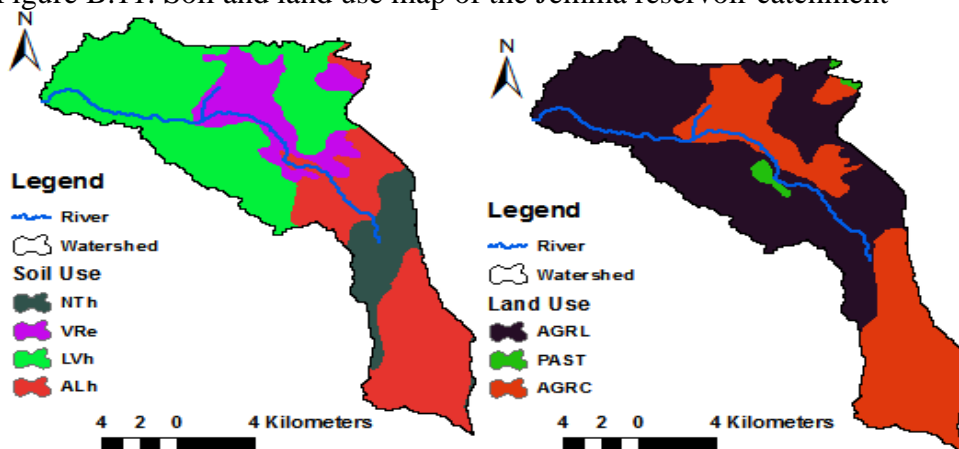


Figure B.12. Soil and land use map of the Koga reservoir catchment

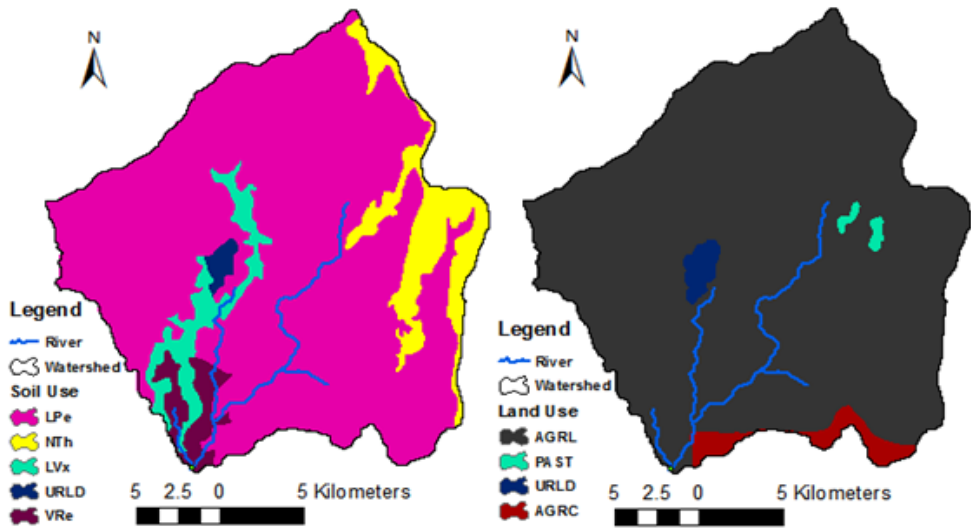


Figure B.13. Soil and land use map of the Megech reservoir catchment

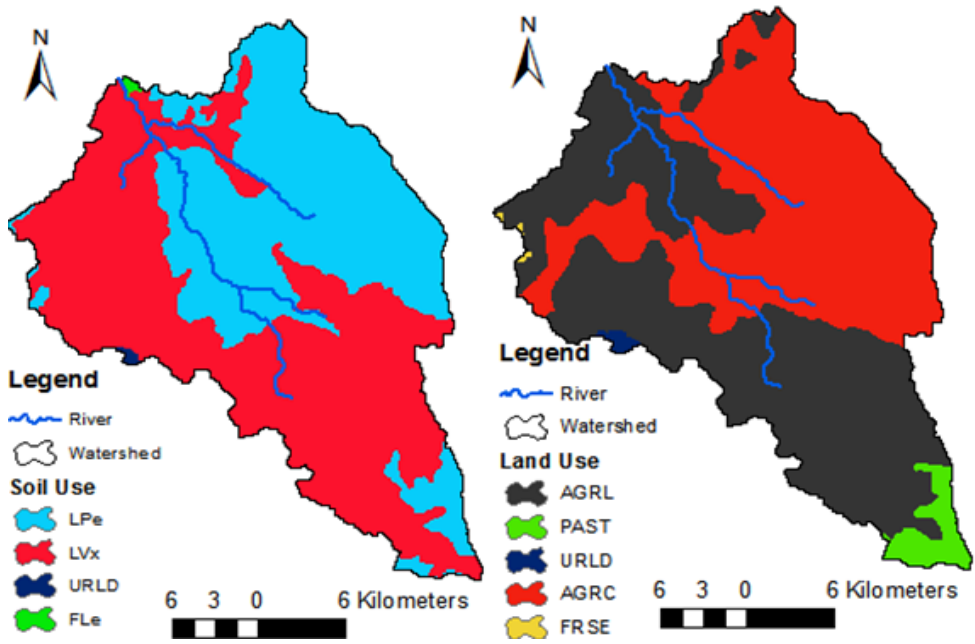


Figure B.14. Soil and land use map of the Ribb reservoir catchment

## Appendix C. List of Tables

Table C.1. The performance of the individual and combined rainfall-runoff model outputs.

Combination Method	Model	Gilgelabay	Gummera	Megech	Ribb
		RMSE			
<b>Individual Model</b>	M1	35.53	32.81	17.76	15.71
	M2	45.22	32.47	16.69	14.22
	M3	43.22	30.75	16.21	22.52
<b>Simple Average</b>	M1+M2	37.15	31.10	16.83	11.97
	M1+M3	36.61	30.76	16.65	15.22
	M2+M3	43.88	31.04	16.34	16.32
	M1+M2+M3	38.60	30.61	16.50	13.37
<b>Variance Covariance</b>	M1+M2	35.41	31.11	16.71	11.93
	M1+M3	35.38	30.49	16.30	15.46
	M2+M3	43.17	30.71	16.21	15.88
	M1+M2+M3	37.84	30.59	16.50	12.55
<b>Sum of squared error</b>	M1+M2	36.43	31.10	16.82	11.94
	M1+M3	36.18	30.69	16.63	15.35
	M2+M3	43.85	31.00	16.34	16.27
	M1+M2+M3	37.84	30.59	16.50	12.55
<b>Time varying</b>	M1+M2	36.77	31.10	16.87	11.91
	M1+M3	36.50	30.67	16.70	15.85
	M2+M3	43.84	31.00	16.33	16.50
	M1+M2+M3	38.30	30.59	16.54	13.77
<b>Artificial Neural Network</b>	M1+M2	33.18	29.08	17.21	13.39
	M1+M3	32.47	29.01	16.36	11.93
	M2+M3*	38.78	28.89	<b>16.01</b>	12.10
	M1+M2+M3*	<b>31.73</b>	<b>28.55</b>	16.26	<b>11.06</b>

\*Indicates the best combination, RMSE=root mean square error, M1=SWAT model output, M2= GR4J model output, and M3=IHACRES model output.

Table C.2. Monthly average water balance values of the LTB for the baseline scenario (1995-2012).

<b>Month</b>	<b>Rain (mm)</b>	<b>Surface flow (mm)</b>	<b>Lateral Flow (mm)</b>	<b>Water Yield (mm)</b>	<b>Evapotranspiration (mm)</b>	<b>Potential evapotranspiration (mm)</b>
<b>Jan</b>	14.16	1.29	0.60	40.82	30.45	71.63
<b>Feb</b>	4.88	0.18	0.43	32.34	31.44	72.34
<b>Mar</b>	16.46	1.22	0.37	30.96	49.14	80.88
<b>Apr</b>	30.31	2.47	0.30	27.28	52.83	78.88
<b>May</b>	92.19	14.07	0.30	35.85	48.06	75.83
<b>Jun</b>	211.31	44.93	0.45	65.77	37.62	51.01
<b>Jul</b>	386.77	106.62	1.09	138.03	37.18	46.67
<b>Aug</b>	365.64	103.17	1.85	154.2	35.67	46.38
<b>Sep</b>	195.27	48.09	1.96	108.76	42.92	60.96
<b>Oct</b>	79.86	17.95	1.58	77.94	44.49	71.05
<b>Nov</b>	19.52	3.00	1.11	54.88	38.14	68.48
<b>Dec</b>	6.61	1.66	0.82	47.82	33.24	71.54
<b>Total</b>	1422.98	344.65	10.86	814.65	481.18	795.65

Table C.3. Monthly average water balance values of the LTB for the future scenario under RCP2.6 in quantile-domain (2011-2100).

<b>Month</b>	<b>Rain (mm)</b>	<b>Surface flow (mm)</b>	<b>Lateral Flow (mm)</b>	<b>Water Yield (mm)</b>	<b>Evapotranspiration (mm)</b>	<b>Potential evapotranspiration (mm)</b>
<b>Jan</b>	59.17	35.53	0.69	47.82	35.16	106.96
<b>Feb</b>	11.85	5.70	0.59	10.98	38.23	108.59
<b>Mar</b>	0.12	0.00	0.57	4.13	69.94	127.00
<b>Apr</b>	3.87	0.01	0.46	2.30	76.07	133.07
<b>May</b>	6.85	0.00	0.43	1.47	57.17	128.29
<b>Jun</b>	238.89	29.87	0.56	30.10	48.34	64.72
<b>Jul</b>	543.15	165.69	0.55	183.22	49.88	61.16
<b>Aug</b>	321.57	88.96	2.21	181.39	49.47	63.47
<b>Sep</b>	287.23	99.07	2.11	215.80	52.81	76.14
<b>Oct</b>	65.33	6.45	1.59	115.80	50.62	93.89
<b>Nov</b>	3.17	0.60	1.05	65.35	39.65	98.80
<b>Dec</b>	3.37	0.45	0.83	33.27	33.59	99.15
<b>Total</b>	1544.57	432.33	11.64	891.63	600.93	1161.24

Table C.4. Monthly average water balance values of the LTB for the future scenario under RCP4.5 in quantile-domain (2011-2100).

<b>Month</b>	<b>Rain (mm)</b>	<b>Surface flow (mm)</b>	<b>Lateral Flow (mm)</b>	<b>Water Yield (mm)</b>	<b>Evapotranspiration (mm)</b>	<b>Potential evapotranspiration (mm)</b>
<b>Jan</b>	90.44	62.46	0.71	73.85	35.80	107.27
<b>Feb</b>	24.64	15.33	0.64	26.27	39.18	108.66
<b>Mar</b>	0.29	0.00	0.63	6.70	70.65	127.08
<b>Apr</b>	5.65	0.03	0.50	3.32	76.13	133.42
<b>May</b>	5.62	0.00	0.45	1.99	57.61	129.83
<b>Jun</b>	277.84	48.17	0.60	48.18	48.81	65.50
<b>Jul</b>	522.51	157.99	1.63	180.51	49.53	61.22
<b>Aug</b>	303.63	81.34	2.24	173.48	50.13	64.78
<b>Sep</b>	311.85	118.95	2.13	232.66	53.62	77.85
<b>Oct</b>	86.33	12.65	1.64	123.49	50.43	92.91
<b>Nov</b>	7.17	2.14	1.09	70.18	39.84	98.69
<b>Dec</b>	29.60	9.21	0.86	44.09	33.82	98.09
<b>Total</b>	1665.57	508.27	13.12	984.72	605.55	1165.30

Table C.5. Monthly average water balance values of the LTB for the future scenario under RCP8.5 in quantile-domain (2011-2100).

<b>Month</b>	<b>Rain (mm)</b>	<b>Surface flow (mm)</b>	<b>Lateral Flow (mm)</b>	<b>Water Yield (mm)</b>	<b>Evapotranspiration (mm)</b>	<b>Potential evapotranspiration (mm)</b>
<b>Jan</b>	1.42	0.00	0.72	16.64	71.72	126.76
<b>Feb</b>	13.57	1.57	0.58	7.50	75.00	133.79
<b>Mar</b>	4.07	0.00	0.51	4.07	57.93	132.60
<b>Apr</b>	148.39	123.57	0.76	157.98	37.20	108.33
<b>May</b>	121.89	107.96	0.75	124.8	41.47	109.17
<b>Jun</b>	362.57	100.85	0.67	101.57	48.74	68.08
<b>Jul</b>	474.74	148.82	1.73	178.00	50.38	63.04
<b>Aug</b>	1000.26	625.92	0.93	646.2	30.81	96.54
<b>Sep</b>	389.69	174.52	2.12	277.92	54.27	78.66
<b>Oct</b>	279.59	76.42	2.23	162.18	52.21	68.94
<b>Nov</b>	172.37	48.53	1.73	163.93	48.88	89.56
<b>Dec</b>	9.21	2.25	1.20	81.09	0.15	98.45
<b>Total</b>	2977.77	1410.41	13.93	1921.88	568.76	1173.92

Table C.6. Monthly average water balance values of the LTB for the future scenario under RCP2.6 in time-domain (2011-2100).

<b>Month</b>	<b>Rain (mm)</b>	<b>Surface flow (mm)</b>	<b>Lateral Flow (mm)</b>	<b>Water Yield (mm)</b>	<b>Evapotranspiration (mm)</b>	<b>Potential evapotranspiration (mm)</b>
<b>Jan</b>	10.92	2.16	0.96	22.57	37.59	100.91
<b>Feb</b>	21.01	3.97	0.86	12.04	37.73	87.02
<b>Mar</b>	33.41	1.25	0.79	7.91	61.68	91.88
<b>Apr</b>	49.59	1.70	0.83	10.33	61.42	84.26
<b>May</b>	139.10	4.21	0.85	15.86	50.27	69.95
<b>Jun</b>	309.91	48.87	1.30	74.71	48.71	57.63
<b>Jul</b>	384.60	82.03	2.12	167.18	49.14	59.42
<b>Aug</b>	365.96	81.56	2.50	215.81	46.71	57.70
<b>Sep</b>	229.02	40.02	2.46	190.43	49.75	66.22
<b>Oct</b>	100.11	5.75	2.04	136.66	45.33	67.04
<b>Nov</b>	22.28	0.31	1.50	83.81	38.88	70.72
<b>Dec</b>	7.13	0.79	1.17	46.46	36.31	88.38
<b>Total</b>	1673.04	272.62	17.38	983.77	563.52	901.13

Table C.7. Monthly average water balance values of the LTB for the future scenario under RCP4.5 in time-domain (2011-2100).

<b>Month</b>	<b>Rain (mm)</b>	<b>Surface flow (mm)</b>	<b>Lateral Flow (mm)</b>	<b>Water Yield (mm)</b>	<b>Evapotranspiration (mm)</b>	<b>Potential evapotranspiration (mm)</b>
<b>Jan</b>	17.07	5.86	1.01	27.07	37.92	100.92
<b>Feb</b>	28.41	8.10	0.93	18.05	38.55	88.39
<b>Mar</b>	38.10	2.85	0.85	11.87	63.91	95.74
<b>Apr</b>	46.58	2.30	0.89	13.97	63.27	90.49
<b>May</b>	144.73	4.63	0.88	18.04	51.51	74.70
<b>Jun</b>	318.14	53.34	1.36	79.56	48.96	58.03
<b>Jul</b>	387.75	84.41	2.20	170.57	48.51	59.24
<b>Aug</b>	377.36	89.20	2.57	224.10	46.77	57.99
<b>Sep</b>	243.23	46.32	2.53	199.27	50.02	66.97
<b>Oct</b>	107.46	7.86	2.11	142.47	45.23	66.98
<b>Nov</b>	24.38	0.41	1.55	87.02	39.33	71.72
<b>Dec</b>	8.20	0.41	1.21	48.25	36.74	88.70
<b>Total</b>	1741.41	305.69	18.09	1040.24	570.72	919.87

Table C.8. Monthly average water balance values of the LTB for the future scenario under RCP8.5 in time-domain (2011-2100).

Month	Rain (mm)	Surface flow (mm)	Lateral Flow (mm)	Water Yield (mm)	Evapotranspiration (mm)	Potential evapotranspiration (mm)
Jan	52.86	36.50	1.11	61.74	38.18	99.71
Feb	65.08	36.26	1.06	52.82	40.77	91.02
Mar	49.96	8.78	0.96	23.85	66.93	101.09
Apr	46.47	4.82	1.02	22.68	65.81	101.10
May	160.44	9.51	0.95	26.63	52.72	79.70
Jun	338.86	67.08	1.46	95.10	49.34	58.88
Jul	393.50	91.23	2.34	179.07	47.91	58.76
Aug	411.75	114.62	2.68	249.07	47.25	58.58
Sep	295.71	73.76	2.67	232.35	50.64	68.83
Oct	131.91	14.94	2.28	159.31	45.13	67.93
Nov	57.11	10.53	1.71	105.4	40.19	73.23
Dec	26.11	6.24	1.32	62.39	37.45	89.12
<b>Total</b>	<b>2029.76</b>	<b>474.27</b>	<b>19.56</b>	<b>1270.41</b>	<b>582.32</b>	<b>947.95</b>

Table C.9. Annual average water balance values of the LTB for the all scenario.

Basin Water Balance Component	Water balance component values (mm)						
	Baseline period (1995-2012)	Quantile-domain			Time-domain		
		RCP2.6 (2011-2100)	RCP4.5 (2011-2100)	RCP8.5 (2011-2100)	RCP2.6 (2011-2100)	RCP4.5 (2011-2100)	RCP8.5 (2011-2100)
<b>Rainfall</b>	1422.90	1544.30	1665.00	2974.40	1673.70	1741.90	2029.30
<b>Surface runoff</b>	344.65	432.18	507.88	1407.48	272.72	305.69	473.62
<b>Lateral flow</b>	10.85	12.65	13.10	13.92	17.38	18.06	19.55
<b>Groundwater (shallow aquifer)</b>	435.46	423.30	439.22	476.05	658.46	679.98	737.03
<b>Groundwater (deep aquifer)</b>	22.92	23.07	23.88	25.77	35.24	36.37	39.37
<b>Revap shallow aquifer</b>	11.12	14.89	14.94	15.05	11.21	11.44	11.83
<b>Deep aquifer recharge</b>	22.92	23.06	23.91	25.87	35.25	36.40	39.42
<b>Total aquifer recharge</b>	458.39	461.26	478.18	517.32	704.93	727.91	788.48
<b>Total water yield</b>	813.85	891.20	984.07	1918.50	983.80	1040.11	1269.45
<b>Percolation out of soil</b>	459.07	461.27	478.31	517.87	704.95	728.01	788.82
<b>Evapotranspiration</b>	480.40	600.00	604.50	611.00	562.70	569.80	581.40
<b>Potential evapotranspiration</b>	793.80	1158.50	1162.50	1171.10	898.80	917.50	945.50

## Abstract in Korean

개발과 기후변화 시나리오에 따른 블루 나일강 상류의 지표수  
영향 평가 및 최적 관리 방안 도출

By

Getachew Tegegne Damtew

Department of Civil and Environmental Engineering

College of Engineering

Graduate School of Seoul National University

Advisor: Professor Kim, Young-Oh

본 연구의 목적은 기후 변화 시나리오가 Lake Tana 유역의 지표 수자원에 미치는 영향을 평가하고 최적의 수자원 관리 방안을 제시하는데 있다. Lake Tana 유역의 수자원 평가를 위해서는 최적의 수문 모형 선정이 우선적으로 필요하지만, 이 유역에 대한 수문 모형 비교 연구는 아직 진행되지 않고 있다. 본 연구는 Lake Tana 유역내 4 개의 주요 계측유역을 대상으로 두 개의 개념모형(GR4J, IHACRES)과 하나의 준분포형 물리모형(SWAT)을 적용하여 일 유량을 모의하고, 시계열 및 분위 수 모의에 대한 관측 유량과의 비교를 통해

각 모형의 수행 능력을 평가하였다. 유량 시계열 모의 비교에서의 최적 모형은 수자원의 관리 및 실시간 운영에 사용될 수 있는 반면에, 유량 분위 수 비교에서의 최적 모형은 계획 및 기후 변화 영향 평가에 사용될 수 있다. 선택된 수문 모형의 보정된 매개변수는 산술 평균, 물리적 유사성, 공간 근접성 및 유출-반응 유사성 접근법을 사용하여 미계측유역에 사용되었다. 이 연구에서 제안된 유출-반응 유사성 접근법은 미계측유역에서의 지표 수자원 추정에 가장 좋은 수행 결과를 보였다. 또한 기후변화가 수문 과정에 미치는 영향에 대한 이해는 대상 유역의 미래 수자원 계획 및 관리에 매우 중요하므로 본 연구에서는 적절한 통계적 상세화기법을 사용하여 선택된 수문 모형에 세 가지 대표 온실가스 시나리오 (RCP 2.6, RCP 4.5 및 RCP 8.5)를 적용하였다. 마지막으로, 본 연구는 Lake Tana 유역의 진행 중이거나 계획된 수자원 프로젝트에 지표 수자원을 최적으로 분배하기 위하여 Multi-Objective Genetic Algorithm (MOGA)을 이용한 최적화 모형을 개발하였고, 모의 결과 관측 및 미래 유량 시나리오에

있어서 관개 및 수력발전 수요의 90% 이상이 충족 되었다. 최적화 결과는 Lake Tana 호수의 수위가 모든 기후변화 시나리오에 있어서 운영에 필요한 최소 수준(즉, 1,785m)를 초과함을 나타낸다.

Keywords: Climate Change, Lake Tana Basin, Reservoir Operation, Ungauged Catchment Modeling, Water Resources Assessment

Student Number: 2013-31302